

Report 3

FACILITY FORM 802

N64-33290

(ACCESSION NUMBER)

181

(PAGES)

NASA CR 5-9245

(NASA CR OR TMX OR AD NUMBER)

(THRU)

1

(CODE)

09

(CATEGORY)

## FLUX SWITCHING IN MULTIPATH CORES

Prepared for:

JET PROPULSION LABORATORY  
4800 OAK GROVE DRIVE  
PASADENA, CALIFORNIA

CONTRACT 950095  
UNDER NASw-6  
FINAL REPORT

By: D. NITZAN V. W. HESTERMAN

STANFORD RESEARCH INSTITUTE

MENLO PARK, CALIFORNIA

\*SRI

### OTS PRICE

XEROX \$ 5.00

MICROFILM \$ 1.25



June 1964

Report 3

## FLUX SWITCHING IN MULTIPATH CORES

*Prepared for:*

JET PROPULSION LABORATORY  
4800 OAK GROVE DRIVE  
PASADENA, CALIFORNIA

CONTRACT 950095  
UNDER NASw-6  
FINAL REPORT

*By:* D. NITZAN V. W. HESTERMAN

*SRI Project 3696*

*Approved:* D. R. BROWN, MANAGER  
COMPUTER TECHNIQUES LABORATORY

J. D. NOE, DIRECTOR  
ENGINEERING SCIENCES DIVISION

Copy No. 92

## ABSTRACT

33290 over

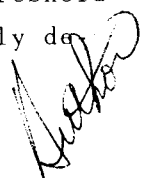
The parabolic inelastic switching model  $\dot{\phi} = \dot{\phi}_p(F)\eta(\phi)$ , where  $\dot{\phi}_p(F)$  is the peak  $\dot{\phi}$  of a step- $F$  switching, is improved by replacing the parabola  $\eta = 1 - (\phi/\phi_s)^2$  by the parabola  $\eta = 1 - [(2\phi + \phi_s - \phi_d)/(\phi_s + \phi_d)]^2$ , in which  $\phi_d$  is the  $\phi$  value on the static  $\phi(F)$  curve. Additional models are proposed for the initial elastic and inelastic  $\phi$  spikes of step- $F$  switching. Using Burroughs' Extended ALGOL-60 language, a computer PROCEDURE was written for computing  $\dot{\phi}(F, \phi)$  from the improved inelastic switching model. Computer ALGOL-60 programs, which use the  $\dot{\phi}(F, \phi)$  PROCEDURE, were written for the numerical solutions of the following magnetic-circuit problems: (a) For an unloaded core, switched by  $MMF$  drives of various shapes, compute  $\dot{\phi}(t)$  and  $\phi(t)$ ; (b) For a core switched by step- $F$  and ramp- $F$  drives and loaded by various combinations of  $R$ ,  $L$ ,  $C$ , and a diode, compute  $\dot{\phi}(t)$ ,  $\phi(t)$ ,  $F(t)$ , and the loading current  $i_L(t)$ ; and (c) For a core-diode shift register with a single ONE, compute the loop currents and  $\dot{\phi}(t)$ ,  $\phi(t)$ , and  $F(t)$  of the transmitter, the receiver and the receiver of the previous stage during the switching time; compute also the flux-gain curves and back ZERO flux transfer *vs.* the transmitted flux. The agreement between the computed and the experimental results is approximately within  $\pm 10$  percent, and in many cases even better. It was found that switching parameters proportional to  $\dot{\phi}_p$  are lower for ramp- $F$  than step- $F$  switching, and that computation accuracy is not sacrificed if the time element  $\Delta t$  is below about 2 percent of the switching time.

The flux switching properties of a partially demagnetized core in response to a rectangular TEST pulse were investigated. The partially demagnetized state is obtained by first switching the core to negative remanence,  $\phi = -\phi_r$ , and then partially setting it to  $\phi = \phi_{ps}$  with a rectangular  $MMF$  pulse of duration  $T_{ps}$ . The switching properties are measured as a function of three parameters:  $\phi_{ps}$ ,  $T_{ps}$ , and the period of time,  $T_b$ , from the end of the partial setting to the beginning of the TEST pulse. The switching properties of each partially set state are determined by means of three types of measurements: (1) static  $\phi(F)$  curves,

(2)  $\dot{\phi}(t)$  waveforms, and (3)  $\dot{\phi}_p(F)$  curves. The experimental data for a positive TEST pulse were similar to the results of a previous report [Tech. Report 5, Contract Nonr 2712(00)] for a different ferrite material. Switching from a partially set state can be described by the same parabolic model used for switching from  $\phi = -\phi_r$ , except that a new parameter,  $\phi_c$ , has to be included in  $\eta$ . The parabolic model then becomes

$$\dot{\phi} = \lambda(F - F_0'')^\nu \{1 - [(2\phi + 2\phi_c + \phi_s - \phi_d)/(\phi_s + 2\phi_c + \phi_d)]^2\} .$$

In addition, the value of  $\lambda$  is significantly lowered by partial setting (e.g., about 40 percent for  $\phi_{ps} = -\frac{1}{2}\phi_r$ ), and  $F_0''$  was lowered a small amount for small  $T_{ps}$  (e.g., decreased about 10 percent for  $\phi_{ps} = -\frac{1}{2}\phi_r$  and  $T_{ps} = 0.5 \mu\text{sec}$ ). In contrast to the results for a positive TEST pulse, a negative TEST pulse results in a static  $\phi(F)$  curve having a lower threshold and less rounding in the upper knee, and  $\dot{\phi}(t)$  waveforms not accurately describable by the parabolic model.





# CONTENTS

---

ABSTRACT . . . . .	iii
LIST OF ILLUSTRATIONS . . . . .	vii
LIST OF SYMBOLS. . . . .	ix
ACKNOWLEDGEMENTS . . . . .	xvii
PREFACE. . . . .	xix
 I INTRODUCTION. . . . .	 1
II COMPUTATION OF FLUX SWITCHING IN MAGNETIC CIRCUITS. . . . .	5
A. Improved Flux Switching Models. . . . .	5
1. Limitations of the Model $\dot{\phi} = \dot{\phi}_p [1 - (\phi/\phi_s)^2]$ . . . . .	5
2. Static- $\phi(F)$ -Limited Parabolic Model . . . . .	6
3. Initial Spike Models. . . . .	10
4. Effects of Core Thickness . . . . .	12
5. Summary . . . . .	15
B. Computer Program for the Parabolic $\dot{\phi}(F, \phi)$ Model . . . . .	16
1. Introduction. . . . .	16
2. PROCEDURE for Computing $\dot{\phi}(F, \phi)$ . . . . .	16
3. Summary . . . . .	21
C. Unloaded Core . . . . .	22
1. Experiment. . . . .	22
2. Computation . . . . .	25
3. Manual Computation of Initial Spikes. . . . .	29
4. Experimental and Computed Results . . . . .	29
5. Discussion. . . . .	33
6. Summary . . . . .	39
D. Loaded Core . . . . .	39
1. Experiment. . . . .	39
2. Computation . . . . .	41
3. Experimental and Computed Results . . . . .	46
4. Discussion. . . . .	46
5. Summary . . . . .	54
E. Core-Diode Shift Register . . . . .	55
1. Operation . . . . .	55
2. Analysis. . . . .	57
3. Computation . . . . .	60

# CONTENTS

4. Computed and Experimental Results . . . . .	68
5. Discussion . . . . .	69
6. Summary . . . . .	75
F. Conclusions . . . . .	77
III FLUX SWITCHING FROM A PARTIALLY-SET STATE . . . . .	81
A. Description of Experiments . . . . .	81
1. Introduction . . . . .	81
2. Experimental Set-up . . . . .	82
B. Curves of $\phi(F)$ . . . . .	87
1. Experiment . . . . .	87
2. Results . . . . .	88
3. Discussion . . . . .	89
C. Waveform of $\dot{\phi}(t)$ . . . . .	93
1. Introduction . . . . .	93
2. Comparison of $\dot{\phi}(t)$ and $\text{Sech}^2$ Function . . . . .	95
3. Effects of Varying $T_{ps}$ . . . . .	99
4. Effects of Varying $\phi_{ps}$ . . . . .	104
5. Summary . . . . .	106
D. Curves of $\dot{\phi}_p(F)$ . . . . .	107
1. Introduction . . . . .	107
2. Effects of Varying $T_{ps}$ . . . . .	108
3. Effects of Varying $\phi_{ps}$ . . . . .	118
4. Effects of Varying $T_b$ . . . . .	118
5. Summary . . . . .	124
E. Discussion and Conclusions . . . . .	125
APPENDIX A COMPUTER PROGRAM FOR PROCEDURE $\dot{\phi}(F, \phi, \phi_d, \dot{\phi}')$ . . . . .	131
APPENDIX B COMPUTER PROGRAMS FOR PROCEDURES $\text{MIN}(A, B)$ , $\text{MAX}(A, B)$ , MIN3(A, B, C), AND $\text{IA}(T)$ . . . . .	137
APPENDIX C COMPUTER PROGRAM FOR UNLOADED-CORE FLUX SWITCHING . . . . .	141
APPENDIX D COMPUTER PROGRAM FOR LOADED-CORE FLUX SWITCHING . . . . .	147
APPENDIX E COMPUTER PROGRAM FOR CORE-DIODE SHIFT REGISTER . . . . .	155
REFERENCES . . . . .	165
INDEX . . . . .	167

## ILLUSTRATIONS

Fig. 1	Step $F$ Flux Switching . . . . .	7
Fig. 2	Two Parabolic $\eta(\phi)$ Plots . . . . .	8
Fig. 3	Graphical Relations Among $\phi_d(F)$ , $\phi_p(F)$ , and $\phi(\phi)$ . . . . .	9
Fig. 4	Models for Initial Elastic and Inelastic $\phi$ Spikes . . . . .	11
Fig. 5	Division of a Thick Leg into Thin Leg Elements . . . . .	13
Fig. 6	Waveforms of Drive MMF . . . . .	24
Fig. 7	Experimental and Computed $\phi(t)$ Waveforms of Core E-6 Switching with No Load and Step- $F$ Drive . . . . .	30
Fig. 8	Experimental and Computed $\phi(t)$ Waveforms of Core E-6 Switching with No Load and Variable- $F$ Drive . . . . .	31
Fig. 9	Experimental and Computed $\phi(t)$ Waveforms of Core J-1 Switching with No Load . . . . .	32
Fig. 10	Variations of $\phi$ vs. $F$ of Core E-6 Switching with No Load and Step- $F$ Drive (Corresponding to Fig. 7) . . . . .	34
Fig. 11	Recomputed $\phi$ Waveforms of Cores E-6 and J-1 Switching with No Load and Ramp- $F$ Drive Using Lower Values of $\lambda$ and $\rho_p$ . . . . .	36
Fig. 12	Variation of $\phi$ vs. $F$ of Core E-6 Switching with No Load and Ramp- $F$ Drive [corresponding to Recomputed $\phi(t)$ in Fig. 11(a)] . . . . .	37
Fig. 13	Effect of $\Delta t$ on Computed $\phi(t)$ Waveform (of Core J-1 Switching with No Load and Step- $F$ Drive of 1.938 amp-turn) . . . . .	38
Fig. 14	Flux Switching in a Loaded Core . . . . .	39
Fig. 15	Experimental (Solid Line) and Computed (Dashed Line) $\phi(t)$ and $i_L(t)$ Waveforms of Core J-1 Switching with Load and Step- $F$ Drive . . . . .	48
Fig. 16	Experimental (Solid Line) and Computed (Dashed Line) $\phi(t)$ and $i_L(t)$ Waveforms of Core J-1 Switching with Load and Ramp- $F$ Drive . . . . .	50
Fig. 17	Variations of $\phi$ vs. $F$ of Core J-1 Switching with Load and Step- $F$ Drive (corresponding to Fig. 15) . . . . .	52
Fig. 18	Variations of $\phi$ vs. $F$ of Core J-1 Switching with Load and Ramp- $F$ Drive (corresponding to Fig. 16) . . . . .	53
Fig. 19	Core-Diode Shift-Register Circuit . . . . .	56
Fig. 20	Equivalent Circuit for Core-Diode Shift Register . . . . .	58
Fig. 21	Experimental and Computed Time Variables in a Core-Diode Shift Register with a single ONE ( $I_A = 1.18$ ampere) . . . . .	70
Fig. 22	Variations of $\phi_T(F_T)$ and $\phi_R(F_R)$ in a Core-Diode Shift Register (corresponding to Fig. 21) . . . . .	72
Fig. 23	Flux-Gain Curves of a Core-Diode Shift Register with a Single ONE . . . . .	73
Fig. 24	Back Flux Transfer in a Core-Diode Shift Register with a Single ONE . . . . .	74
Fig. 25	Experimental Time Variables in a Core-Diode Shift Register with Single-ONE and All-ONE Information Patterns . . . . .	76

# ILLUSTRATIONS

Fig. 26	Partial Switching Experiment . . . . .	84
Fig. 27	Configuration of Core and Windings . . . . .	85
Fig. 28	Circuit for Measuring Flux Changes . . . . .	87
Fig. 29	700- $\mu$ sec $\phi(F)$ Curves of Core I-3 . . . . .	88
Fig. 30	700- $\mu$ sec $\phi(F)$ Curves of Core I-4 . . . . .	90
Fig. 31	Effect of $\phi_c$ on $\dot{\phi}(\phi)$ . . . . .	94
Fig. 32	Comparison of $\dot{\phi}(t)$ to $\text{sech}^2$ Function . . . . .	96
Fig. 33	$\dot{\phi}(t)$ of Core I-3 . . . . .	98
Fig. 34	Effects of $T_{ps}$ on $\dot{\phi}(t)$ of Core I-4 . . . . .	100
Fig. 35	Effects of $T_{ps}$ on $\dot{\phi}(t)$ of Core I-3 . . . . .	101
Fig. 36	$\phi_c$ vs. $F_{ps}$ . . . . .	102
Fig. 37	Effects of $\Delta\phi_{ps}$ on $\dot{\phi}(t)$ . . . . .	105
Fig. 38	$\dot{\phi}_p(+F)$ of Core I-4 with $T_{ps}$ as a Parameter . . . . .	109
Fig. 39	$\dot{\phi}_p(+F)$ of Core I-3 . . . . .	110
Fig. 40	$\log \dot{\phi}_p$ vs. $\log (F - F_0'')$ of (ORE I-4 . . . . .	112
Fig. 41	$F_0''$ , $\lambda$ , and $\nu$ vs. $T_{ps}$ for a Positive TEST Pulse . . . . .	113
Fig. 42	$\dot{\phi}_p(-F)$ of Core I-4 with $T_{ps}$ as a Parameter . . . . .	116
Fig. 43	$F_0''$ , $\lambda$ , and $\nu$ vs. $T_{ps}$ for a Negative TEST Pulse . . . . .	117
Fig. 44	$\dot{\phi}_p(+F)$ with $\phi_{ps}$ as a Parameter . . . . .	119
Fig. 45	$F_0''$ , $\lambda$ , and $\nu$ vs. $\phi_{ps}$ . . . . .	120
Fig. 46	Effect of $T_b$ on $\dot{\phi}_p(F)$ . . . . .	122
Fig. 47	$F(t)$ for $T_b = 0$ . . . . .	125
Fig. 48	A Sketch of $F_0''(\phi, F_{ps})$ . . . . .	128

# TABLES

Table I	Dimensions and Switching Parameters of Cores E-6 and J-1 . . . . .	23
Table II	MMF Drives Applied to Unloaded Cores . . . . .	24
Table III	Loads and Drives Applied to Core J-1 . . . . .	40
Table IV	Dimensions of Cores I-3 and I-4 . . . . .	83

## LIST OF SYMBOLS

<u>Symbol</u>	<u>Definition</u>	<u>Reference</u>
$A$	Cross-sectional area of a leg	Rep. 1, Fig. 19
$B$	Flux density	
$B_r$	Maximum residual $B$	Rep. 2, Fig. 2
$B_s$	Saturation $B$	
$\dot{B}$	Time rate of change of $B$	
$\dot{B}_p$	Peak $\dot{B}$	Rep. 1, Fig. 17
$C$	Capacitance	Fig. 14
$C_i$	Parameter in a model for initial inelastic $\dot{\phi}$ spike	Eq. (8)
$E_k$	Parameter in a model for a junction diode	Eq. (55)
$e_d$	Voltage across a junction diode, not including $iR$ drop	Eq. (55)
$F$	MMF	
$F_B$	MMF at boundary between nonlinear and linear regions of $\dot{\phi}_p(F)$	cf. $H_B = F_B/l$ , Rep. 2, Fig. 15
$F_c$	Coercive $F$	Fig. 1
$F_D$	Amplitude of drive MMF	Fig. 6
$F_d^n$	Static $F$ threshold	Fig. 1
$F_k$	Coefficient in the expression for $\phi_c$	Eq. (96) and Fig. 36
$F_R$	MMF of a receiver core in a shift register	Eq. (76)
$F_T$	MMF of a transmitter core in a shift register	Eq. (75)
$F_0$	MMF threshold obtained by extrapolating linear $\dot{\phi}_p(F)$ to $F$ axis	cf. $H_0 = F_0/l$ , Rep. 2, Fig. 15

# SYMBOLS

<u>Symbol</u>	<u>Definition</u>	<u>Reference</u>
$F''_0$	Dynamic $F$ threshold	Fig. 3
$F_{1B}$	Average static $F$ threshold from $\phi = -\phi_r$ to $\phi \approx -0.6 \phi_r$	p. 58
$F_{12}$	Boundary between first and second regions of computed static $\phi(F)$ curve, i.e., $H_{th} l_i$	Rep. 2, pp. 6 and 28
$F_{23}$	Boundary between second and third regions of computed static $\phi(F)$ curve, i.e., $H_{th} l_o$	Rep. 2, pp. 6 and 28
$\dot{F}$	Time rate of change of $F$	
$G$	Flux gain, $\Delta\phi_R/\Delta\phi_T$	Rep. 1, pp. 67-70
$H$	Magnetic field	
$H_a$	Parameter in the hyperbolic model for static $B_c(H)$	Rep. 2, Eq. (10) and Fig. 2
$H_B$	$H$ at boundary between linear and non-linear regions of $\dot{B}_p(H)$	Rep. 2, Fig. 15
$H_c$	Coercive $H$	Rep. 2, Eq. (14) and Fig. 2
$H_n$	Parameter in the hyperbolic model for static $B_u(H)$	Rep. 2, Eq. (11) and Fig. 2
$H_q$	Parameter in the hyperbolic model for static $B_u(H)$	Rep. 2, Eq. (11) and Fig. 2
$H_{th}$	Static $H$ threshold	Rep. 2, Eq. (12) and Fig. 2
$H_0$	$H$ threshold, obtained by extrapolating linear $\dot{B}_p(H)$ to $H$ axis	Rep. 2, Eq. (24) and Fig. 15
$H''_0$	Dynamic $H$ threshold	Rep. 2, Eq. (83) and Fig. 15
$h$	Height of a leg (or core)	Rep. 1, Fig. 19
$I_A$	Amplitude of ADVANCE current in a shift register	Fig. 21(a)
$ID$	Inside diameter of a toroid	

SYMBOLS

<u>Symbol</u>	<u>Definition</u>	<u>Reference</u>
$I_D$	Amplitude of drive current	Fig. 6
$I_0$	Saturation current in a model for a junction diode	Eq. (55)
$i_A$	ADVANCE current in a shift register	Fig. 20
$i_B$	Back loop current in a shift register	Fig. 20
$i_D$	Drive current	Fig. 14
$i_F$	Forward loop current in a shift register	Fig. 20
$i_L$	Load current	Fig. 14
$j$	Index for a leg element in a thick leg	Fig. 5, Eqs. (9)-(22)
$j$	Index of iteration in a numerical solution e.g., p. 27 of variables for each $n$ th $\Delta t$ , e.g., $\phi_{n(j)}$ , $\dot{\phi}_{n(j)}$ , $q_{n(j)}$ , $\dot{q}_{n(j)}$ , $\phi_{n(j-1)}$ , $\dot{\phi}_{n(j-1)}$ , etc.	
$j$	Index for a stage in a shift register	Fig. 19
$L$	Inductance	Fig. 14
$l$	Leg length	Fig. 5
$l^{av}$	Average $l$ , i.e., $(l_i + l_o)/2$	
$l_i$	Length of the short edge of a leg	Fig. 5
$l_o$	Length of the long edge of a leg	Fig. 5
$N$	Number of turns	
$N_A$	Number of turns of ADVANCE winging in a shift register	Fig. 19
$N_c$	Number of turns of load winding	Fig. 14
$N_D$	Number of turns of drive winding	Fig. 14
$N_R$	Number of turns of input winding of a receiver core in a shift register	Fig. 19
$N_T$	Number of turns of output winding of a transmitter core in a shift register	Fig. 19

# SYMBOLS

<u>Symbol</u>	<u>Definition</u>	<u>Reference</u>
$n$	Number of leg elements in a thick leg	Fig. 5
$n$	Index number for a time element $\Delta t$ and the associated variables, e.g., $\phi_n$ , $\dot{\phi}_n$ , $q_n$ , $\dot{q}_n$ , $\ddot{q}_n$ , $i_{Dn}$ , $i_{An}$ , $\phi_{n-1}$ , $\dot{\phi}_{n-1}$ , etc.	e.g., p. 27
$OD$	Outside diameter of a toroid	
$q$	Electric charge	p. 41
$\dot{q}$	Load current, $i_L = dq/dt$	p. 41
$\ddot{q}$	Time rate of change of load current	p. 41
$R$	Resistance	
$R_d$	Forward resistance of a diode	pp. 57-58
$R_L$	Load resistance	Fig. 14
$R_{\ell}$	Coupling-loop resistance in a shift register	p. 58
$r_i$	Inside radius of a toroid	
$r_o$	Outside radius of a toroid	
$T_b$	Time between end of PARTIAL-SET pulse and beginning of TEST pulse	Fig. 26
$T_f$	Fall time of a drive pulse	Figs. 6(c) and (d)
$T_h$	Constant- $F$ time of a drive pulse	Fig. 6(d)
$T_{ps}$	Duration of PARTIAL-SET pulse	Fig. 26
$T_r$	Rise time of a drive pulse	Fig. 6
$t$	Time	
$t_p$	Peak time of $\dot{\phi}$	Fig. 1
$t_0$	Time for beginning of inelastic switching when $F = F''_0$	Figs. (1) and (4)
$V_d$	Bias voltage of junction-diode model	p. 57; Fig. 20



SYMBOLS

<u>Symbol</u>	<u>Definition</u>	<u>Reference</u>
$V_1$	Abbreviation for $(\phi_s - \phi_r)/[(l_o - l_i)H_a]$	Eq. (28)
$V_2$	Abbreviation for $[(\phi_s + \phi_r)H_q] [(l_o - l_i)H_n]$	Eq. (29)
$w$	Width of a leg	Fig. 5
$\Delta \dot{q}$	Change in $\dot{q}$	Eq. (71)
$\Delta t$	Small time increment used in computation of time variables	<i>e.g.</i> , p. 27
$\Delta w$	Width of leg element	Fig. 5
$\Delta \phi$	Change of $\phi$	
$\Delta \phi_B$	$\Delta \phi$ of a receiver core of a previous stage in a shift register	p. 60
$\Delta \phi_{ps}$	$\Delta \phi$ caused by PARTIAL-SET pulse	Fig. 26
$\Delta \phi_R$	$\Delta \phi$ of a receiver core in a shift register	p. 60
$\Delta \phi_T$	$\Delta \phi$ of a transmitter core in a shift register	p. 60
$\Delta \phi_\epsilon$	Elastic $\Delta \phi$	Rep. 1, pp. 18-21
$\Delta \phi'$	Initial $\Delta \phi$ not accounted for by parabolic model for inelastic switching	Eq. (95)
$\epsilon_i$	Coefficient of elastic switching of initial $\dot{\phi}$ spike	Eqs. (5), (6), and (7)
$\zeta$	Coefficient of inelastic $\dot{B}$	Rep. 2, Eq. (24)
$\zeta_p$	Peak $\zeta$	Rep. 2, Eq. (82)
$\eta$	Flux-form factor in parabolic model for $\dot{\phi}$	Eq. (1) and Fig. (2)
$\kappa$	Coefficient of inelastic $\dot{B}$ in nonlinear $\dot{B}_p(H)$ region	Rep. 2, p. 38
$\lambda$	Coefficient of inelastic $\dot{\phi}$ in nonlinear $\phi_p(F)$ region	Rep. 2, Eq. (91)
$\mu_0$	$\mu$ of vacuum (air)	Rep. 1, p. 23
$\nu$	Power coefficient of inelastic $\dot{B}$ in nonlinear $B_p(H)$ region	Rep. 2, p. 38
$\rho$	Coefficient of inelastic $\dot{\phi}$	

# SYMBOLS

<u>Symbol</u>	<u>Definition</u>	<u>Reference</u>
$\rho_i$	Coefficient of inelastic initial $\dot{\phi}$ spike	Eq. (8)
$\rho_p$	Peak $\rho$	Rep. 2, p. 39
$\bar{\rho}$	Average $\rho$	Rep. 2, pp. 17-19
$\tau_i$	Time constant for decaying initial in-elastic $\dot{\phi}$ spike	Eq. (8)
$\tau_s$	Switching time	
$\phi$	Magnetic flux	
$\phi_B$	$\phi$ of a receiver core of a previous stage in a shift register	Fig. 20
$\phi_c$	Parameter in parabolic model for inelastic switching from partially set state	Eq. 92 and Figs. 31 and 36
$\phi_d$	$\phi$ value on a static $\phi(F)$ curve	Fig. 1
$\phi_p$	$\phi$ at $t = t_p$ when $\dot{\phi} = \dot{\phi}_p$	Fig. 1
$\phi_R$	$\phi$ of a receiver core in a shift register	Fig. 20
$\phi_{R0}$	Initial $\phi_R$	
$\phi_r$	Maximum residual $\phi$	Fig. 1
$\phi_s$	Saturation $\phi$	p. 8
$\phi_T$	$\phi$ of a transmitter core in a shift register	Fig. 20
$\phi_{T0}$	Initial $\phi_T$	p. 63
$\phi'_d$	$d\phi_d/dF$	p. 18; Eq. (31) or (33) or (35)
$\dot{\phi}$	Time rate of change of $\phi$	
$\dot{\phi}_B$	$\dot{\phi}$ of a receiver core in a previous stage in a shift register	Fig. 20
$\dot{\phi}_p$	Peak $\dot{\phi}$	Eq. (2); Fig. 1
$\dot{\phi}_R$	$\dot{\phi}$ of a receiver core in a shift register	Fig. 20
$\dot{\phi}_T$	$\dot{\phi}$ of a transmitter core in a shift register	Fig. 20

# SYMBOLS

<u>Symbol</u>	<u>Definition</u>	<u>Reference</u>
$\dot{\phi}_{\epsilon i}$	Elastic component of initial $\dot{\phi}$ spike	Eqs. (5) and (6); Fig. 4
$\dot{\phi}_{\rho i}$	Inelastic component of initial $\dot{\phi}$ spike	Eq. 8; Fig. 4
$\dot{\phi}_{\rho i 0}$	Initial value of $\dot{\phi}_{\rho i}$ at $t = T_r$	Eq. (8); Fig. 4
$\dot{\phi}_0$	Initial value of $\dot{\phi}$ obtained from parabolic model for inelastic switching	p. 99
$\dot{\phi}'$	$\partial \dot{\phi} / \partial F$	Eq. (41)
$\dot{\phi}'_p$	$d \dot{\phi}_p / dF$	p. 18; Eq. (37) or (39)
$\dot{\phi}'_R$	$\partial \dot{\phi}_R / \partial F_R$	p. 61
$\dot{\phi}'_T$	$\partial \dot{\phi}_T / \partial F_T$	p. 61

## ACKNOWLEDGEMENTS

---

The computer programs in this report have been written by David F. Fraser. The helpful comments made by David R. Bennion are gratefully acknowledged.

## PREFACE

---

In the previous two reports on this project, Contract 950095 under NASw-6, SRI Project 3696, we were primarily concerned with the characteristics of flux switching, and proposed several models for certain types of switching. In this report, we have continued to investigate this subject, with two objectives in mind: to study the physical properties of magnetic flux switching in ferrites by means of flux-switching models, and to apply these models to the solutions of engineering problems in magnetic circuits.

Switching models have been investigated for two cases of initial flux state:  $|\phi| = \phi_r$  (residual saturation state), and  $|\phi| < \phi_r$  (partially set state). In the first case, which is much easier to handle than the second case, we have improved the parabolic inelastic switching model, and have proposed additional models for the beginning of step- $F$  switching. The second case presents a much more difficult problem because of the multitude of factors that affect collection, classification, and interpretation of experimental data of flux switching from a partially set state. The experimental data accumulated so far have been restricted to partially set states reached from  $\phi = -\phi_r$  by various time-limited step- $F$  pulses. By processing these data for different ferrite materials, certain switching properties have been encountered consistently enough to justify the first attempts of flux-switching modeling.

A large portion of the work to be described in this report covers the area of application of the improved parabolic model to numerical analysis of magnetic circuit problems. All of the computations have been performed on a digital computer, using the international programming language ALGOL-60. A computer was used not only because the switching model is too complex to be handled manually, but also because of the low cost and ease of extension to similar problems, once a proper program has been written and debugged. For this reason, this report includes detailed descriptions of the methods of computations and the computer programs for solving magnetic-circuit problems. It is hoped that inclusion of this detailed information would help others in using digital computers for solving similar problems.

The work of this report can be utilized in many practical magnetic circuits involving toroidal cores. Primarily, however, this work serves as a preliminary step towards the use of switching models in numerical solutions of engineering problems in magnetic circuits involving multipath cores. This, perhaps, explains why the words "multipath cores" are included in the title of this report.

## I INTRODUCTION

This is a third report covering the subject of flux switching in multipath magnetic cores. This subject has been studied in the past three years under the sponsorship of Jet Propulsion Laboratory, Pasadena, California. Before reporting on the last year's work, we wish to summarize the work of the first two years of the project.

The work of the first year is covered in a report <sup>1\*</sup> entitled "Flux Switching in Multipath Cores--Report 1" (hereinafter referred to as Report 1). The work can be classified into three categories:

- (1) Survey of the U. S. and foreign literature on magnetic multipath cores
- (2) Organization of the material on magnetics in the files of Stanford Research Institute
- (3) Theoretical and experimental work on flux switching phenomena.

The topics included in Report 1 are summarized as follows:

*Section I—Flux-Switching Characteristics.* The equivalence between toroidal and multipath cores is explained by introducing the leg model. An elementary description of domain growth and flux density in ferrite material is followed by discussing the static  $\phi(F)$  loops of toroidal and multipath cores. A distinction is then made between the mechanisms of elastic and inelastic switching. Models for elastic and inelastic switching, and their representation by electrical circuit analogue, are proposed. Additional published thin-ring static and dynamic models are surveyed. Finally, the measurement and application of time-limited  $\phi(F)$  curves are described.

*Section II—Flux Transfer.* The asymmetrical and symmetrical setting characteristics associated with a multipath core are reviewed and analyzed. All-magnetic flux-transfer schemes, of resistance and nonresistance types, are described and compared in terms of speed and drive range of operation.

---

\* References are listed at the end of the report.

*Section III--Geometry Effects.* The literature on flux division in a three-leg Laddie is reviewed. Flux unsetting and oversetting, which result from excessive drives on outer minor legs, are analyzed qualitatively, and conclusions are drawn relative to multipath-core shaping in order to improve the  $\phi(F)$  squareness, the signal-to-noise ratio, and the property of flux clipping. Crude models for legs in series and in parallel are proposed.

*Section IV--Flux Pattern.* Analog-to-digital conversion of flux-pattern representation is assisted by using an arrow model. A distinction is made between domains and domain-like zones in ferrite cores in order to describe the flux pattern of set and cleared multipath cores. The literature on pole distribution in toroidal and multipath cores is reviewed.

*Section V--Literature Survey.* The literature on multipath cores is listed, classified, and frequently annotated. Most of the U. S. patents that make use of multipath cores are also listed.

The work of the second year is covered in a report<sup>2</sup> entitled "Flux Switching in Multipath Cores--Report 2" (hereinafter referred to as Report 2). The topics included in Report 2 are summarized as follows:

*Section I--Calculations.* Hyperbolic models for  $B(H)$  are used to calculate a static  $\phi(F)$  curve. The limitations of a leg model are discussed, and  $\rho$  (inelastic switching coefficient) of a tapered leg is calculated. Average values of  $\rho$  of a constant-width leg and a tapered leg are calculated as a function of the amount of flux switching. The parabolic inelastic switching model is applied in the calculation of flux division of a three-leg saturable core, which is coupled to a resistive load.

*Section II--Experimentation.* Experimental observations associated with toroidal cores are discussed, including the effect of time rate of flux switching on the static  $\phi(F)$  curve, testing of disks with large OD/ID ratio, and  $\phi(\phi)$  of a thin ring driven by variable-amplitude step MMF. Switching in a core with a re-entrant shape is discussed, and geometry considerations are applied to the fabrication of nonsaturable and saturable three-leg cores. A test procedure is given for the determination of core parameters by measuring static  $\phi(F)$  and  $\phi_p(F)$ . Flux



division experiments are performed, using a nonsaturable core and a saturable core; the results of the latter are then compared with calculated plots. The unsettling effect, caused by overdriving an outer minor leg, is investigated experimentally and discussed.

The work of this last year is covered in this report in two main divisions: Section II discusses the application of improved switching models in machine computation of flux switching in three types of magnetic circuits; and Section III discusses the study of the flux switching properties from a partially set core.

## II COMPUTATION OF FLUX SWITCHING IN MAGNETIC CIRCUITS

Two major topics are described in this section: improved switching models; and the application of a computer to the numerical solutions of magnetic circuit problems. In Part A, the parabolic model for inelastic switching is modified, and new models are proposed for the initial  $\dot{\phi}$  spikes of step- $F$  switching. In Part B, a computer program is written for the modified parabolic model. This program is then used inside other computer programs for computing the flux switching of an unloaded core (Part C), a core loaded by various types of load (Part D), and a core-diode shift register (Part E).

### A. IMPROVED FLUX SWITCHING MODELS

#### 1. LIMITATIONS OF THE MODEL $\dot{\phi} = \dot{\phi}_p [1 - (\phi/\phi_s)^2]$

Our inelastic flux switching model (see Report 2, pp. 8 and 40) has so far been of the following form:

$$\dot{\phi} = \dot{\phi}_p \eta \quad (1)$$

where  $\dot{\phi}_p$  is the peak  $\dot{\phi}$ , expressed as

$$\dot{\phi}_p = \begin{cases} 0 & \text{if } F \leq F_0'' \\ \lambda(F - F_0'')^\nu & \text{if } F_0'' \leq F \leq F_B \\ \rho_p(F - F_0) & \text{if } F_B \leq F \end{cases} \quad (2)$$

and where

$$\eta = 1 - \left( \frac{\phi}{\phi_s} \right)^2 \quad (3)$$

This switching model has the following limitations:

- (1) The model assumes that  $F$ , if not time limited, is of sufficient magnitude to complete the switching of flux from  $-\phi_r$  to  $+\phi_s$ . The model is, therefore, inadequate

to describe switching that ends at  $\phi$  below  $\phi_s$ ; that is, for example, if the  $F$  value is near or below the "knee" of the static  $\phi(F)$  curve.

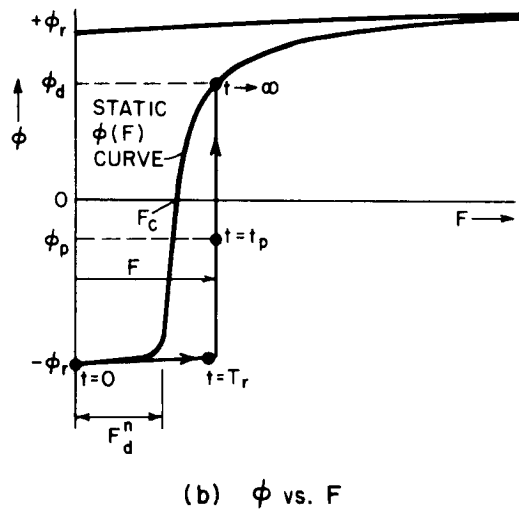
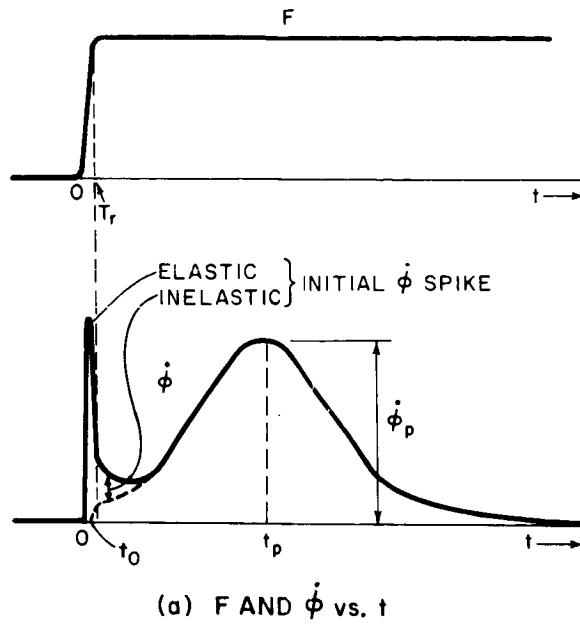
- (2) According to Eqs. (1) and (3), if  $F$  is constant in time, then  $\phi$  reaches its peak value,  $\phi_p$ , at  $\phi = 0$ . This agrees with experimental data only if the condition stated in (1) is fulfilled, i.e., if the value of  $F$  is high enough to switch  $\phi$  to positive saturation. Figures 20 and 21(a) of Report 2 indicate that for  $F$  values below the static  $\phi(F)$  "knee,"  $\phi$  reaches peak at  $\phi = \phi_p$ , where  $\phi_p < 0$ , and that the smaller the value of  $F$  is, the lower (algebraically)  $\phi_p$  is.
- (3) Equations (1) through (3) are completely invalid to describe slow switching caused by a low  $F$  value which varies between the static threshold value  $F_d^n = H_{th} l_i$  and around the coercive MMF  $F_c \approx H_c(l_i + l_o)/2$  (see Report 2, pp. 4-6 and 72-75). For such low-drive switching, and if  $F$  is a step function, then, to a good approximation,  $\phi(t)$  has an exponentially decaying waveform.
- (4) Equations (1) through (3) are based on the assumption that the leg is relatively thin. This is evident from Report 2, pp. 39 and 40, where the effect of leg thickness on the variations of  $H$  and  $B$  in the leg cross section are assumed negligible. For relatively thick cores, this effect is not negligible.

We shall now attempt to improve our inelastic switching model by correcting the drawbacks outlined above, one step at a time.

## 2. STATIC- $\phi(F)$ -LIMITED PARABOLIC MODEL

First, let us assume that the leg is relatively thin and that  $F$  is larger than  $F_c$ , but not large enough to switch  $\phi$  to positive saturation. Under this assumption, we need to consider only Items (1) and (2) in the above discussion in order to improve the inelastic parabolic switching model, Eqs. (1) through (3).

Consider the flux switching caused by essentially a step  $F$ , as shown in Fig. 1. Two initial  $\phi$  spikes are distinguished before  $\phi(t)$  proceeds essentially as a  $\text{sech}^2$  function of time, in accordance with the parabolic switching model (cf. Report 1, pp. 27 and 28): an elastic high  $\phi$  spike during the rise time of  $F$ , followed by an inelastic decaying  $\phi$  spike. These initial  $\phi$  spikes may affect the flux switching described by the modified parabolic model, because  $\eta$  is a function of  $\phi$ . We shall examine these spikes in more detail later (pp. 10-12).



RA-3696-210

FIG. 1 STEP-F FLUX SWITCHING

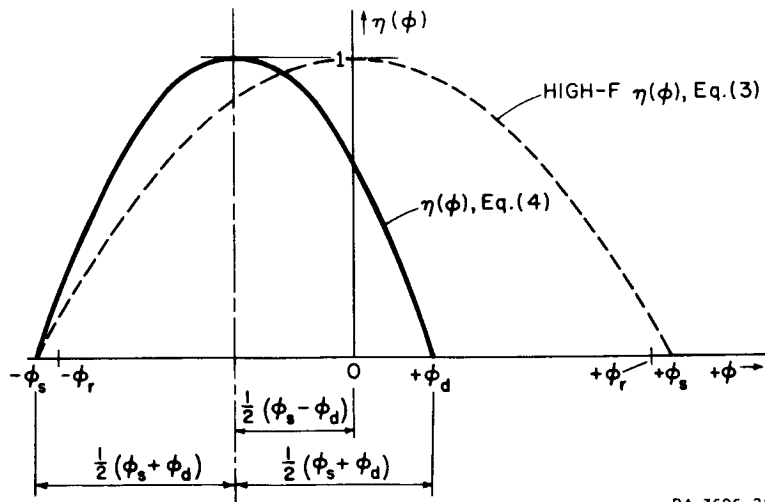
After the initial inelastic  $\dot{\phi}$  spike has decayed to a negligible value,  $\dot{\phi}(t)$  may be described quite well by a  $\text{sech}^2$  function of time. At  $t = t_p$ ,  $\dot{\phi}$  reaches its peak value,  $\dot{\phi}_p$ . The corresponding flux level,  $\phi_p$ , is negative. The flux switching continues and, by definition of static  $\phi(F)$  curve,  $\phi \rightarrow \phi_d$  as  $t \rightarrow \infty$ , where  $(\phi_d, F)$  is a point on the static  $\phi(F)$  curve of the leg. For a given value of  $F$ , we may calculate  $\phi_d$  quite accurately

from the static  $\varphi(F)$  model suggested on pp. 5-6 of Report 2, by substituting the value of  $F$  into Eq. (17) or Eq. (18) of Report 2.

Based on the observations associated with Fig. 1, we conclude that Eqs. (1) and (2) are still valid, but  $\eta$ , in Eq. (3), must be modified to include the following features: first, the final flux should be the  $\phi$  value corresponding to the  $F$  value on the static  $\varphi(F)$  curve; second,  $\phi_p$  (the  $\phi$  value corresponding to  $\dot{\phi} = \dot{\phi}_p$ ) is negative and its algebraic value should decrease as  $F$  decreases. A modified parabolic model that satisfies these two requirements is suggested:

$$\eta = 1 - \left( \frac{2\phi + \phi_s - \phi_d}{\phi_s + \phi_d} \right)^2 \quad (4)$$

The improvement in this expression for  $\eta$ , compared with the one in Eq. (3), allows us now to remove the artificial distinction between  $\phi_s$  and  $\phi_{s,s}$  (or  $B_s$  and  $B_{s,s}$ ) that was introduced in Report 2 (see p. 3 of Report 2) in order to get a better agreement with experimental data. A plot of the modified  $\eta$  vs.  $\phi$ , Eq. (4), is compared with  $\eta$  vs.  $\phi$  of Eq. (3) in Fig. 2. Both  $\eta(\phi)$  plots are parabolas, and in both cases,  $\eta = 0$  at  $\phi = -\phi_s$ . However, in the modified expression for  $\eta$ , Eq. (4), the axis of symmetry is at  $\phi = -(\phi_s - \phi_d)/2$ , rather than at  $\phi = 0$ , and the second value of  $\phi$  for which  $\eta = 0$  is  $\phi_d$ , rather than  $+\phi_s$ . In fact, Eq. (3) may be regarded as



RA-3696-211

FIG. 2 TWO PARABOLIC  $\eta(\phi)$  PLOTS

Thus, the switching model expressed by Eqs. (1), (2), and (4) overcomes the drawbacks of our previous model, which are listed under Items (1) and (2) above. The modified model, referred to as “static- $\phi(F)$ -limited parabolic model,” is summarized graphically in Fig. 3 by tracing the switching behavior caused by three values of  $F$ , i.e.,  $F_1$ ,  $F_2$ , and  $F_3$ .

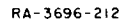


FIG. 3 GRAPHICAL RELATIONS AMONG  $\phi_d(F)$ ,  $\dot{\phi}_p(F)$ , AND  $\dot{\phi}(\phi)$

### 3. INITIAL SPIKE MODELS

We shall now examine the elastic and inelastic initial  $\dot{\phi}$  spikes in Fig. 1, which result from an applied  $F$  of a short rise time,  $T_r$ , and a constant amplitude,  $F_D$ .

#### a. ELASTIC $\dot{\phi}_i$ SPIKE

The elastic initial  $\dot{\phi}$  spike, denoted by  $\dot{\phi}_{\epsilon_i}$ , occurs chiefly during the rise time of  $F$ . The peak of this spike is reached near  $t = T_r/2$ , when  $\dot{F}$  is maximal. This is in agreement with the elastic switching model proposed on p. 23 of Report 1; *i.e.*,

$$\dot{\phi}_{\epsilon_i} = \epsilon_i \dot{F} \quad (5)$$

where  $\epsilon_i$  is the elastic switching coefficient. To a good approximation,  $\epsilon_i = d\Delta\phi_\epsilon/dF$ . The value of  $\epsilon_i$  may be calculated from Eq. (34) on p. 23 of Report 1, except that instead of  $a$  we use here, as on p. 3 of Report 2, the symbol  $H_a$ . Since  $F$  is relatively low, the term  $\mu_0 \ln(l_o/l_i)$  in Eq. (34) of Report 1 may be neglected. Furthermore, since  $\phi_s = B_s hw$ , Eq. (34) of Report 1 is reduced to the following:

$$\epsilon_i = \frac{\phi_s - \phi_r}{(l_o - l_i)H_a} \left[ \ln \left( \frac{H_a l_o - F}{H_a l_i - F} \right) + F \left( \frac{1}{H_a l_i - F} - \frac{1}{H_a l_o - F} \right) \right] \quad (6)$$

In order to evaluate  $\epsilon_i$ ,  $F \cong F_D/2$  should be substituted in Eq. (6). However, in most practical cases,  $F_D \ll H_a l_i$ , so that  $\epsilon_i$  is hardly affected by  $F$ , and Eq. (6) is reduced to

$$\epsilon_i \cong \frac{\phi_s - \phi_r}{(l_o - l_i)H_a} \ln \left( \frac{l_o}{l_i} \right) \quad (7)$$

This expression is identical with the expression for  $\epsilon_{s0}$  in Eq. (35) of Report 1 (p. 23) if, in the latter expression,  $\mu_0$  is neglected relative to  $(B_s - B_r)/H_a$ .

Detailed  $\dot{\phi}$  waveforms during and past the rise time of the applied  $F$  are shown in Fig. 4 by expanding the time scale of Fig. 1(a). To avoid ambiguity, the rise time  $T_r$  is defined as the time during which  $F$  rises to  $0.95F_D$ . Near  $t = T_r$ , there is a sudden change in the flux-switching

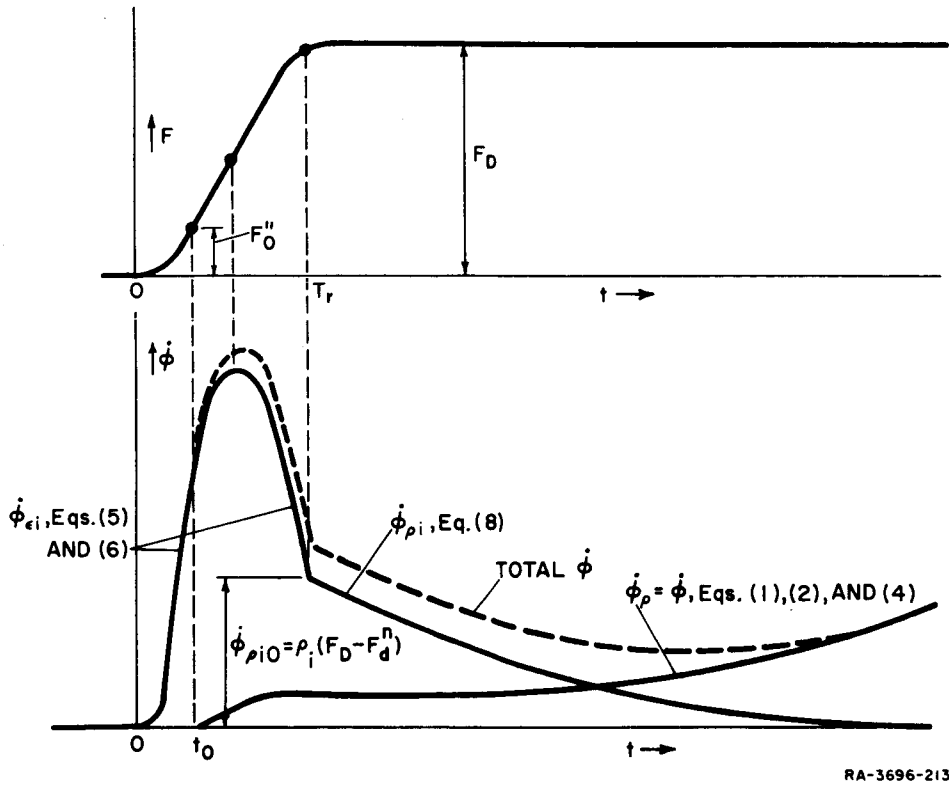


FIG. 4 MODELS FOR INITIAL ELASTIC AND INELASTIC  $\dot{\phi}$  SPIKES

mechanism. This change involves a transition from the elastic  $\dot{\phi}_{ei}$  spike to a decaying inelastic  $\dot{\phi}_{\rho i}$  spike, to be discussed next.

b. INELASTIC  $\dot{\phi}_i$  SPIKE

The inelastic  $\dot{\phi}_{\rho i}$  spike appears to decay exponentially with a time constant  $\tau_i$  from an initial value  $\dot{\phi}_{\rho i 0}$  at  $t = T_r$ . The initial excess drive-MMF responsible for this inelastic switching is  $(F_D - F_d^n)$ , where  $F_d^n$  is the minimum static threshold (cf. Fig. 1). As an approximation,  $\tau_i$  is inversely proportional to  $(F_D - F_d^n)$ , and  $\dot{\phi}_{\rho i 0}$  is proportional to  $(F_D - F_d^n)$ . Thus, the inelastic  $\dot{\phi}_{\rho i}$  may be described by the function

$$\dot{\phi}_{\rho i} = \dot{\phi}_{\rho i 0} e^{-[(t-T_r)/\tau_i]} = \rho_i (F_D - F_d^n) e^{-(t-T_r)(F_D - F_d^n)/C_i} \quad (8)$$

where  $\rho_i$  and  $C_i$  are constants in time.

At present, we can only speculate about the physical mechanism of the  $\dot{\phi}_{\rho i}$  spike. If  $F_D$  is not too high, the value  $\rho_i (F_D - F_d^n)$  has been reached by elastic domain-wall motion during the rise time. Referring



to Fig. 4, note that the rising  $\dot{\phi}_\rho$ , which is described by the parabolic model in Eqs. (1), (2), and (4), is distinguished from the decaying  $\dot{\phi}_{\rho i}$ , Eq. (8). These inelastic  $\dot{\phi}$  waveforms seem to result from different mechanisms of domain-wall motion. The inelastic  $\dot{\phi}$  described by the parabolic model of Eqs. (1), (2), and (4) results from domain-wall motion which is accompanied by domain collisions. The random distributions of the velocity and collision of these domains appear to be the cause for the bell-shaped  $\dot{\phi}$  waveform. On the other hand,  $\dot{\phi}_{\rho i}$ , Eq. (8), arises from the motion of those walls that do not collide with one another. The motion of each of these domain walls terminates when the wall is obstructed by an energy hill of a high slope. The exponentially decaying waveform of  $\dot{\phi}_{\rho i}$  results from the random distribution of the distance from the first energy hill to the obstructing energy hill. Initially (at  $t = T_r$ ), all walls move, so that  $\dot{\phi}_{\rho i}$  is maximal. As more and more walls are obstructed,  $\dot{\phi}_{\rho i}$  decreases and finally disappears. The higher the initial excess MMF ( $F_D - F_d^n$ ) is, the smaller is the number of noncolliding walls (more precisely, the smaller is their total area); hence,  $\rho_i$  should decrease as  $F_D$  increases. Furthermore, the higher ( $F_D - F_d^n$ ) is, the faster is the motion of these domain walls; this explains why  $\tau_i = C_i / (F_D - F_d^n)$  and  $\dot{\phi}_{\rho i 0} = \rho_i (F_D - F_d^n)$  in Eq. (8). Typically, for  $F_D$  value larger than the coercive force  $F_c$ ,  $\tau_i$  is much smaller than the switching time.

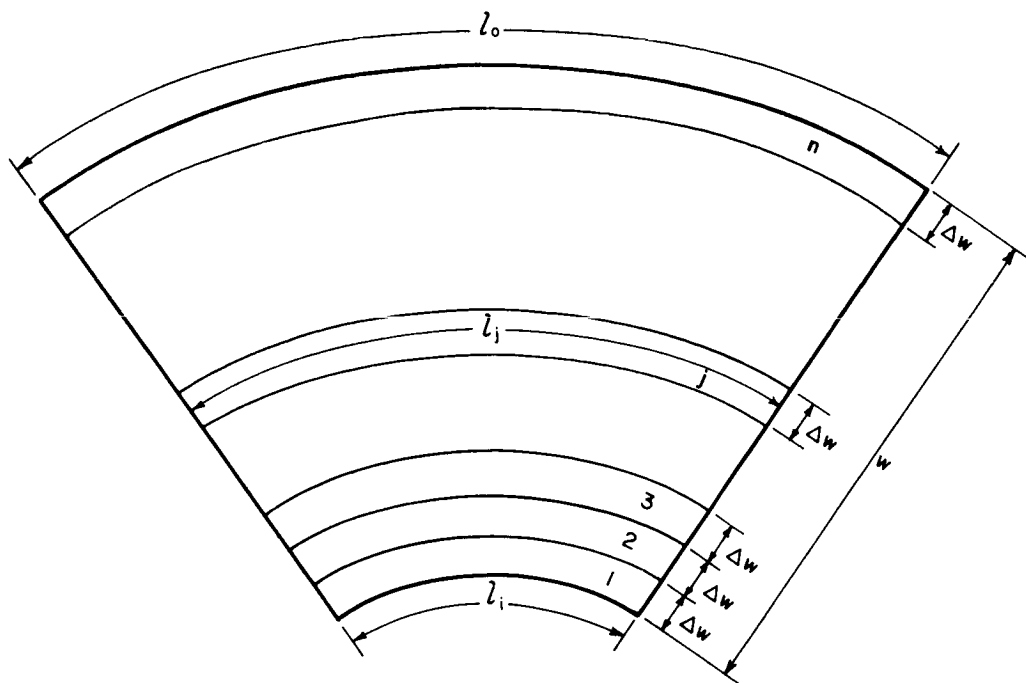
Better understanding of the flux switching phenomena associated with the initial  $\dot{\phi}$  spikes requires further investigation.

#### 4. EFFECTS OF CORE THICKNESS

The switching models described so far, except for the static  $\phi(F)$  model of Report 2, ignore the variation of  $H$  and  $B$  in the leg cross section. For cores with wide legs, this variation is not negligible. Integration of the function  $\dot{B} = \dot{B}_p \cdot \eta(B)$  [which corresponds to Eq. (1)] over the leg cross section cannot be expressed in a closed form. We have, therefore, to resort to numerical integration.

In Fig. 5, a leg of width  $w$  is divided into  $n$  thin leg elements, each having a width  $\Delta w = w/n$ . Consider an arbitrary  $j$ th leg element whose average length is  $l_j$ . Substituting  $x = [j - (1/2)]\Delta w$  into Eq. (26) of Report 1, we find that

$$l_j = l_i - \frac{l_o - l_i}{2n} + \frac{l_o - l_i}{n} j \quad (9)$$



RA-3696-214

FIG. 5 DIVISION OF A THICK LEG INTO THIN LEG ELEMENTS

The cross-sectional area of the  $j$ th leg element is, simply,

$$A_j = \frac{wh}{n} \quad (10)$$

The switching parameters of the  $j$ th leg element are determined from the expression on pp. 39 and 40 of Report 2. Following Eqs. (91), (92), (88), and (89) of Report 2,

$$\lambda_j = \kappa \frac{A_j}{(l_j)^\nu} \quad (11)$$

$$F''_{0j} = H''_0 l_j \quad (12)$$

$$\rho_{pj} = \zeta_p \frac{A_j}{l_j} \quad (13)$$

and

$$F_{0j} = H_0 l_j \quad (14)$$

Similarly,

$$F_{Bj} = H_B l_j \quad (15)$$

Following Eq. (2), and since  $F$  is common to all leg elements,

$$\dot{\phi}_{pj} = \begin{cases} 0 & \text{if } F \leq F''_{0j} \\ \lambda_j (F - F''_{0j})^\nu & \text{if } F''_{0j} \leq F \leq F_{Bj} \\ \rho_{pj} (F - F_{0j}) & \text{if } F_{Bj} \leq F \end{cases} \quad (16)$$

The function  $\phi_{dj}$  vs.  $F$  [i.e., the static  $\phi(F)$  curve of the  $j$ th leg element] may be determined from Eqs. (16), (17), and (18) of Report 2 (in which  $B_{ss}$  is replaced by  $B_s$ ) by letting

$$l_{ij} = l_i + \frac{l_o - l_i}{n} (j - 1) \quad (17)$$

and

$$l_{oj} = l_i + \frac{l_o - l_i}{n} j \quad (18)$$

Note that  $l_{ij}/l_{oj}$  increases with  $j$ , thus having a minimum value (worst case) for  $j = 1$ . An alternative method of determining  $\phi_{dj}(F)$ , which is simpler but less accurate, is based on treating the original hyperbolic model for static  $B(H)$  curve, given on pp. 3 and 4 of Report 2, as the static  $\phi(F)$  curve of a leg element. This method is justified if  $n \gg l_o/l_i$  since, under this condition,  $l_{ij} \approx l_{oj}$  [Eqs. (17) and (18)] for the worst case of  $j = 1$ . Thus, if  $F \leq H_{th} l_j$ , then

$$\phi_{dj} = -A_j \left( B_r + \frac{B_s - B_r}{1 - \frac{H_a l_j}{F}} \right) \quad (19)$$

and if  $H_{th} l_j \leq F$ , then

$$\phi_{dj} = A_j \left[ -B_r + (B_s + B_r) \frac{F - H_q l_j}{F - H_n l_j} \right] \quad (20)$$

where  $H_{th}$  is expressed in Eq. (12) of Report 2. Applying Eq. (4) to a leg element whose flux is  $\phi_j$ ,

$$\eta_j = 1 - \left( \frac{2\phi_j + \phi_{sj} - \phi_{dj}}{\phi_{sj} + \phi_{dj}} \right)^2 \quad (21)$$

where  $\phi_{sj} = \phi_s/n = B_s h w/n$ .

Combining Eqs. (16) and (21), the over-all  $\dot{\phi}$  is the following summation:

$$\dot{\phi} = \sum_{j=1}^n \dot{\phi}_{pj} \cdot \eta_j \quad (22)$$

The material switching parameters associated with  $\dot{\phi}_{pj}$  (i.e.,  $\kappa$ ,  $H_0''$ ,  $\nu$ ,  $\zeta_p$ ,  $H_0$ , and  $H_B$ ) and the ones associated with  $\eta_j$  (i.e.,  $B_r$ ,  $B_s$ ,  $H_a$ ,  $H_q$ , and  $H_n$ ) have been used in the expressions above. These parameters can be determined from experimental  $\dot{\phi}_p(F)$  and  $\phi_d(F)$  curves of an ultrasonically cut, thin, ferrite ring of the same material as the core under investigation. The error introduced by this method stems from the fact that the ultrasonic cut can cause a change in the strain conditions. This error may be decreased by refiring the thin ring under the conditions of the original firing. An alternative method, which is more practical, is to calculate the material parameters from experimental  $\phi_d(F)$  and  $\dot{\phi}_p(F)$  curves of the actual core under investigation. Here, a cut-and-try method, (or a more straightforward method) may be employed in correlating between the measured static  $\phi_d(F)$  curve and Eqs. (16), (17), and (18) of Report 2, and between the measured  $\dot{\phi}_p(F)$  curve and Eq. (22).

## 5. SUMMARY

The parabolic inelastic switching model  $\dot{\phi} = \dot{\phi}_p \eta$  is modified by replacing the parabola  $\eta = 1 - (\phi/\phi_s)^2$  by a shifted parabola,  $\eta = 1 - [(2\phi + \phi_s - \phi_d)/(\phi_s + \phi_d)]^2$ , in which, for a given  $F$  value,  $\phi_d$  is the  $\phi$  value on the static  $\phi(F)$  curve. Switching models are proposed for the initial  $\dot{\phi}$  spikes caused by a step MMF,  $F_D$ , with a short rise time,  $T_r$ : the elastic component,  $\dot{\phi}_{ei} = \epsilon_i \dot{F}$ , where  $\epsilon_i \approx [\ln(l_o/l_i)](\phi_s - \phi_r)/[(l_o - l_i)H_a]$ , and the inelastic component  $\dot{\phi}_{pi} = \rho_i(F_D - F_d^n) \exp[-(t - T_r)(F_D - F_d^n)/C_i]$ , where  $\rho_i$  and  $C_i$  are constants, and  $F_d^n$  is the threshold of the static  $\phi(F)$  curve. The effect of core thickness on the  $\phi$  waveform is taken into

account by dividing the leg into  $n$  thin leg elements, calculating  $\dot{\phi}_j = \dot{\phi}_p \eta_j$  of each  $j$ th leg element according to its length  $l_j = l_i - (l_o - l_i)/(2n) + j(l_o - l_i)/n$ , and summing, i.e.,  $\dot{\phi} = \sum_{j=1}^n \dot{\phi}_j$ .

## B. COMPUTER PROGRAM FOR THE PARABOLIC $\dot{\phi}(F, \phi)$ MODEL

### 1. INTRODUCTION

Practical application of the switching models of Part A to magnetic circuits requires the use of digital computers. Until a few years ago, such a use was too complicated for routine engineering problems. However, the development of simpler programming languages, such as ALGOL and FORTRAN, together with a compiler program that translates these languages to a machine language, has changed the situation considerably. An engineer who is unfamiliar with machine language can now program his own problems with little difficulty. In this report we shall use the Burroughs extended version<sup>3,4</sup> of the international language ALGOL 60 (which stands for ALGORITHMIC Language, 1960 revision).

An important feature of ALGOL 60 is the ability to write a special program, called PROCEDURE, within the main program (the comparable special program in the FORTRAN language is called a FUNCTION subprogram). The main program may include several PROCEDURES, each of which is identified by its own name. A PROCEDURE has a set of input and output parameters, each of which is called by a different name, or identifier. When a PROCEDURE is declared, these identifiers are listed (in parentheses) following the PROCEDURE'S name. At any place in the main program where there is a need for the execution of one of these special programs, all that is needed to do is to call the name of the corresponding PROCEDURE and to assign values (or identifiers that are used in the main program) to the input and output parameters in the order of their appearance in the original declaration. A program of any computational process that has to be executed repeatedly (in one or more than one program) will be written as a PROCEDURE. A process of this nature is the computation of  $\dot{\phi}$  as expressed by the parabolic model in Eqs. (1), (2), and (4). The corresponding PROCEDURE will be used later in solving magnetic circuit problems.

### 2. PROCEDURE FOR COMPUTING $\dot{\phi}(F, \phi)$

#### a. INPUT AND OUTPUT

In Eq. (1),  $\dot{\phi}$  is given as a product of  $\dot{\phi}_p$  and  $\eta$ . Following Eq. (2),  $\dot{\phi}_p$  is a function of  $F$ ; following Eq. (4), and since  $\phi_d$  is a

function of  $F$ ,  $\eta$  is a function of both  $F$  and  $\phi$ . We may thus express Eqs. (1), (2), and (4) formally as

$$\dot{\phi} = \dot{\phi}(F, \phi) \quad . \quad (23)$$

We now wish to write a PROCEDURE for computing the relations expressed by Eq. (23). The input parameters of the  $\dot{\phi}$  PROCEDURE are  $F$  and  $\phi$ . In addition to  $\dot{\phi}$  itself, we wish to have  $\phi_d$  and  $\partial\dot{\phi}/\partial F$  (which is denoted by  $\dot{\phi}'$ ) as output parameters for the following reasons. Following Eqs. (1) and (4),  $\phi_d$  must be computed in order to compute  $\dot{\phi}$ . We might then as well declare  $\phi_d$  to be an output parameter, and thus be able to plot the calculated static  $\phi(F)$  curve. The output parameter  $\dot{\phi}'$  will be used in the solution of magnetic circuit problems, using the method of successive Newton's approximations, as we shall see later in Parts D and E.

#### b. CORE PARAMETERS

In addition to  $F$  and  $\phi$ , the core parameters must be provided in order to compute  $\dot{\phi}(F, \phi)$ . These include the parameters,  $l_i$ ,  $l_o$ ,  $\phi_r$ ,  $\phi_s$ ,  $H_a$ ,  $H_q$  and  $H_n$  for computing  $\eta$  [from Eq. (4)], and the parameters  $\lambda$ ,  $F_0''$ ,  $\nu$ ,  $\rho_p$ ,  $F_0$ , and  $F_B$  for computing  $\dot{\phi}_p$  [from Eq. (2)].

In order to be able to use the same  $\dot{\phi}(F, \phi)$  PROCEDURE for different cores, the values of the core parameters will be given in the main program rather than inside the PROCEDURE.

The six parameters appearing in Eq. (2) may be determined by driving the core under study with a step-MMF of variable amplitude,  $F$  and plotting  $\dot{\phi}_p$  versus  $F$ . The values of  $\rho_p$  and  $F_0$  can be determined easily and quite accurately from the plot of  $\dot{\phi}_p$  vs.  $F$  on linear graph paper. (Determination of the value of  $F_B$  from the same plot is less accurate.) On the other hand, the values of  $\lambda$ ,  $F_0''$ , and  $\nu$  are best determined from the plot of  $\dot{\phi}_p$  vs.  $F$  on log-log paper. However, the two expressions for  $\dot{\phi}_p$  in Eq. (2), as well as their derivatives with respect to  $F$ , should be equal at  $F = F_B$ . These requirements result in the following two constraints on the six parameters appearing in Eq. (2):

$$\nu = \frac{F_B - F_0''}{F_B - F_0} \quad (24)$$

and

$$\lambda = \frac{\rho_p}{\nu(F_B - F_0'')^{\nu-1}} \quad (25)$$

It is, therefore, concluded that only four independent parameters are needed in order to compute  $\dot{\phi}_p$  vs.  $F$ . One might, therefore, be inclined to have the two remaining parameters be computed by the computer itself. This practice may be valid in special cases, but not in general.

Bearing in mind that the constraints in Eqs. (24) and (25) must be satisfied, we shall nevertheless continue to use six parameters in computing  $\dot{\phi}_p$ , for the following reason: In fitting Eq. (2) to the measured  $\dot{\phi}_p(F)$  curve, two different portions of the curve are used to determine the parameters  $\rho_p$ ,  $F_0$ , and  $F_B$  and the parameters  $\lambda$ ,  $\nu$ , and  $F_0''$ . Such a fit is never perfect. In fitting Eq. (2) to one of these portions, three of the six parameters are determined. Because of the constraints in Eqs. (24) and (25), we are free to select only one additional parameter. This may result in a rather poor fit between Eq. (2) and the other portion of the measured  $\dot{\phi}_p(F)$  plot. In order to get an *over-all* best fit, we wish to have the freedom to adjust any one of the six parameters. Therefore, we shall not state *a priori* which four of the six parameters should be determined independently and leave the other two parameters to be computed unmonitored inside the PROCEDURE or in the main program.

#### c. SEQUENCE OF COMPUTATION

It can be seen from Eqs. (1), (2), and (4) that  $\dot{\phi}'$  includes the terms  $\phi_d' = d\phi_d/dF$  and  $\dot{\phi}_p' = d\dot{\phi}_p/dF$ . Computation of  $\dot{\phi}$  and  $\dot{\phi}'$  vs.  $F$  and  $\phi$  is preceded by computation of  $\phi_d$  and  $\phi_d'$  and computation of  $\dot{\phi}_p$  and  $\dot{\phi}_p'$ . The details of this computation are described as follows.

Computation of  $\phi_d$  and  $\phi_d'$  vs.  $F$  follows Eqs. (16), (17), and (18) of Report 2, except for one simplification: The threshold field  $H_{th}$ , of Eq. (12) in Report 2, is replaced by  $H_q$ , which is very close to  $H_{th}$ . For example, on p. 74 of Report 2,  $H_{th} = 36.03$  ampere-turns, where  $H_q = 36.00$  ampere-turns. In computing  $\phi_d$  and  $\phi_d'$  vs.  $F$ , the following terms are independent of  $F$ , and hence may be computed only once, if only one core is involved in the main program:

$$F_{12} = H_q l_i \quad (26)$$

$$F_{23} = H_q l_o, \quad (27)$$

$$V_1 = \frac{\phi_s - \phi_r}{(l_o - l_i)H_a}, \quad (28)$$

and

$$V_2 = \frac{(\phi_s + \phi_r)H_q}{(l_o - l_i)H_n}. \quad (29)$$

Here  $F_{12}$  and  $F_{23}$  serve to determine whether either Eq. (16) or Eq. (17) or Eq. (18) of Report 2 is valid, and  $V_1$  and  $V_2$  are merely abbreviations. Computation of  $\phi_d$  and  $\phi'_d$  vs.  $F$  is, therefore, as follows: If  $F \leq F_{12}$ , then

$$\phi_d = V_1 F \ln \left( \frac{F - H_a l_o}{F - H_a l_i} \right) - \phi_r \quad (30)$$

and

$$\phi'_d = V_1 \left[ \ln \left( \frac{F - H_a l_o}{F - H_a l_i} \right) + F \left( \frac{1}{F - H_a l_o} - \frac{1}{F - H_a l_i} \right) \right]; \quad (31)$$

if  $F_{12} < F \leq F_{23}$ , then

$$\phi_d = V_2 \left[ \frac{F}{H_q} - l_i + F \left( \frac{1}{H_n} - \frac{1}{H_q} \right) \ln \left( \frac{1 - \frac{H_n}{H_q}}{1 - \frac{H_n l_i}{F}} \right) \right] - \phi_r \quad (32)$$

and

$$\phi'_d = V_2 \left\{ \frac{1}{H_q} + \left( \frac{1}{H_n} - \frac{1}{H_q} \right) \left[ \ln \left( \frac{F \left( 1 - \frac{H_n}{H_q} \right)}{F - H_n l_i} \right) - \frac{H_n l_i}{F - H_n l_i} \right] \right\}; \quad (33)$$

and if  $F_{23} < F$ , then

$$\phi_d = V_2 \left[ l_o - l_i + F \left( \frac{1}{H_n} - \frac{1}{H_q} \right) \ln \left( \frac{F - H_n l_o}{F - H_n l_i} \right) \right] - \phi_r \quad (34)$$



and

$$\phi_d' = V_2 \left( \frac{1}{H_n} - \frac{1}{H_q} \right) \left[ \ln \left( \frac{F - H_n l_o}{F - H_n l_i} \right) + F \frac{H_n (l_o - l_i)}{(F - H_n l_o)(F - H_n l_i)} \right] \quad (35)$$

Using Eq. (2), computation of  $\dot{\phi}_p$  and  $\dot{\phi}_p'$  is as follows:  
If  $F \leq F_0''$ , then  $\dot{\phi}_p = 0$  and  $\dot{\phi}_p' = 0$ ; otherwise, if  $F_0'' < F \leq F_B$ , then

$$\dot{\phi}_p = \lambda (F - F_0'')^\nu \quad (36)$$

and

$$\dot{\phi}_p' = \lambda \nu (F - F_0'')^{\nu-1} \quad ; \quad (37)$$

and if  $F_B < F$ , then

$$\dot{\phi}_p = \rho_p (F - F_0) \quad (38)$$

and

$$\dot{\phi}_p' = \rho_p \quad . \quad (39)$$

Having thus computed  $\dot{\phi}_d$ ,  $\dot{\phi}_d'$ ,  $\dot{\phi}_p$ , and  $\dot{\phi}_p'$ , we finally compute the values of  $\dot{\phi}$  and  $\dot{\phi}'$ , using Eqs. (1) and (4) as follows:

$$\dot{\phi} = \dot{\phi}_p \left[ 1 - \left( \frac{2\phi + \phi_s - \phi_d}{\phi_s + \phi_d} \right)^2 \right] \quad (40)$$

and

$$\dot{\phi}' = \left[ 1 - \left( \frac{2\phi + \phi_s - \phi_d}{\phi_s + \phi_d} \right)^2 \right] \dot{\phi}_p' + 4\dot{\phi}_p \frac{(2\phi + \phi_s - \phi_d)(\phi + \phi_s)}{(\phi_s + \phi_d)^3} \phi_d' \quad (41)$$

For practical reasons, switching is assumed to be terminated when  $\phi$  approaches  $\phi_d$  to within, say,  $0.001\phi_r$ .

#### d. OUTLINE FOR COMPUTER PROGRAM

The actual PROCEDURE for computing  $\dot{\phi}(F, \phi)$  is given in Appendix A, together with some explanatory remarks. The outline of this PROCEDURE is as follows:

- (1) Declare all the identifiers to be used in the PROCEDURE, in accordance with the rules of the ALGOL-60 language.
- (2) Compute (only once\*)  $F_{12}$ ,  $F_{23}$ ,  $V_1$  and  $V_2$ , using Eqs. (26) through (29).
- (3) Compute  $\phi_d$  and  $\phi'_d$ , using Eqs. (30) through (35).
- (4) Compute  $\dot{\phi}_p$  and  $\dot{\phi}'_p$ , using Eqs. (36) through (39).
- (5) Compute  $\dot{\phi}$  and  $\dot{\phi}'$ , using Eqs. (40) and (41). If  $\phi$  approaches  $\phi_d$  to within  $0.001\phi_r$ , let  $\dot{\phi} = 0$ .

e. INITIAL  $\dot{\phi}$  SPIKES

The computation described so far is based on the parabolic model for inelastic switching. The elastic and inelastic initial  $\dot{\phi}$  spike models, Eqs. (5) and (8), could have been added with no difficulty. However, we have not included these models here for three reasons: first, the model for  $\dot{\phi}_{\rho i}$ , Eq. (8), appears to be suitable for a step drive only; second, manual computation of  $\phi_{\epsilon i}$  and  $\dot{\phi}_{\rho i}$  is quite simple; and third, the initial spikes should be investigated more thoroughly before being included formally in the  $\dot{\phi}(F, \phi)$  PROCEDURE. Further investigation of the initial spikes (including the writing of a computer program for their models) will be made in future. Similarly, the validity and efficiency of Eqs. (9) through (22) in describing the effects of core thickness on the  $\dot{\phi}$  waveform will also be investigated.

f. APPLICATION

We now wish to apply the actual  $\dot{\phi}(F, \phi)$  PROCEDURE (cf. Appendix A) to various magnetic circuit problems. We shall start with an unloaded core (Part C), proceed with a core loaded by different types of load (Part D), and end up with the problem of a single ONE transfer in a core-diode shift register (Part E).

### 3. SUMMARY

A PROCEDURE for computing  $\dot{\phi}(F, \phi)$ , based on the modified parabolic model for inelastic switching, was written in the Burroughs' Extended ALGOL-60 computer-programming language. In addition to the input parameters  $F$  and  $\phi$ , the values of the switching parameters are fed into this

---

\* If two or more cores are involved in the main program,  $F_{12}$ ,  $F_{23}$ ,  $V_1$ , and  $V_2$  should either be treated as core parameters or be computed each time the PROCEDURE is called.

PROCEDURE from the main program. The output of the  $\dot{\phi}(F, \phi)$  PROCEDURE includes  $\phi_d$  and  $\dot{\phi}' = \partial \dot{\phi} / \partial F$  as well as  $\dot{\phi}$ .

### C. UNLOADED CORE

Improved flux switching models have been proposed in Part A. We now wish to describe the application of these models to the computation of  $\dot{\phi}(t)$  of different unloaded cores with various drive conditions, and to compare the results with experimental data.

#### 1. EXPERIMENT

Two toroidal ferrite cores of considerably different dimensions and material properties were employed in a no-load experiment. The first core was a thin ring of  $OD/ID = 1.06$ , which had been cut ultrasonically from a 1/2-inch-diameter, Telemeter Magnetics T-5, ferrite disk. This core is referred to as Core E-6, following its designation in Report 2, pp. 55-58. The second core was a commercial switch core of  $OD/ID = 1.61$  (Lockheed 145SC1, 145-mil  $OD$ , 90-mil  $ID$ ), which will be referred to as Core J-1. The dimensions, switching parameters, and material parameters of the two cores are given in Table I. Note that only half of the parameters in Table I, such as the ones marked by asterisks (\*), are needed for the  $\dot{\phi}(F, \phi)$  PROCEDURE. The other half are included in Table I only for possible future reference.

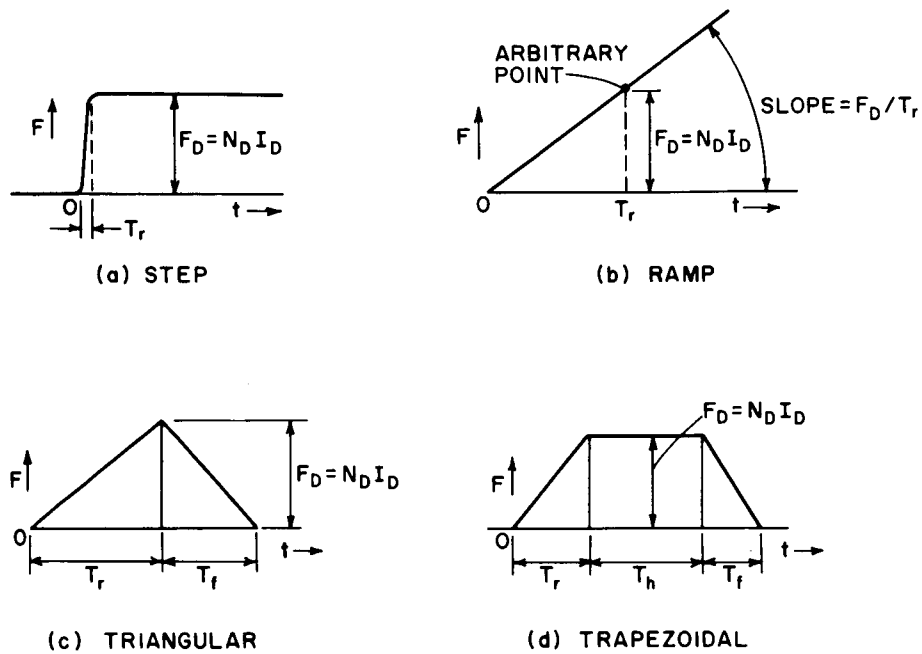
Each of the two cores was driven by step-MMF drives (actually, with a rise time of 50 nanoseconds) and ramp-MMF drives. In addition, Core E-6 was driven by triangular and trapezoidal drives. The shapes of the various drives and the definitions of their parameters are shown in Fig. 6. For the step drive, the rise time  $T_r$  is defined as the time during which  $F$  reaches 95 percent of  $F_D$ ;  $T_r$  is much smaller than the switching time,  $\tau_s$ . For the ramp drive, the slope is defined in terms of an arbitrary  $F$  value,  $F_D$ , and the corresponding  $t$  value,  $T_r$ . The purpose of this definition is to enable us to write a single expression for  $F$  in the computer program of both the step-drive and ramp-drive cases. The various MMF drive cases for the two cores are summarized in Table II.

The temperature was regulated to  $29 \pm 0.5^\circ\text{C}$  for Core E-6 and  $30 \pm 0.5^\circ\text{C}$  for Core J-1. Oscillograms of  $\dot{\phi}(t)$  for the various drive cases of Table II were photographed. These results will be compared later with the corresponding computed curves.

Table I

DIMENSIONS AND SWITCHING PARAMETERS OF CORES E-6 AND J-1  
(Parameters marked by \* are needed in the  $\phi(F, \phi)$  PROCEDURE, Appendix A.)

PARAMETER	CORE E-6	CORE J-1
	Telemeter Magnetics T-5 Ultrasonically Cut	Lockheed SC1 Commercial
	29 $\pm$ 0.5°C	30 $\pm$ 0.5°C
$r_o/r_i$	1.06	1.61
$r_o$ (mm)	3.75	1.84
$r_i$ (mm)	3.53	1.143
$h$ (mm)	0.688	1.778
$w$ (mm)	0.216	0.70
* $l_i$ (mm)	22.19	7.18
* $l_o$ (mm)	23.54	11.58
$l^{av}$ (mm)	22.86	9.38
$A$ (mm <sup>2</sup> )	0.1486	1.244
* $\phi_r$ (maxwells)	3.45	31.0
* $\phi_s$ (maxwells)	3.73	33.48
* $H_a$ (amp-turns/meter)	230.0	250.0
* $H_q$ (amp-turns/meter)	35.0	26.0
* $H_n$ (amp-turns/meter)	30.0	22.5
* $\lambda$ (ohm/turn <sup><math>\nu+1</math></sup> amp <sup><math>\nu-1</math></sup> )	0.069	1.64
* $F_0''$ (amp-turn)	0.95	0.27
* $\nu$	1.31	1.43
* $\rho_p$ (ohms/turn <sup>2</sup> )	0.112	2.27
* $F_0$ (amp-turn)	1.45	0.55
* $F_B$ (amp-turns)	3.00	1.2
$B_r$ (wb/meter <sup>2</sup> )	0.232	0.249
$B_s$ (wb/meter <sup>2</sup> )	0.251	0.269
$\kappa$ (ohms/turn <sup><math>\nu+1</math></sup> amp <sup><math>\nu-1</math></sup> meter <sup><math>2-\nu</math></sup> )	3,250	2,612
$H_0''$ (amp-turns/meter)	41.6	28.8
$\zeta_p$ (ohms/turn <sup>2</sup> meter)	17,230	17,116
$H_0$ (amp-turns/meter)	63.9	58.6
$H_B$ (amp-turns/meter)	131.2	128.0



RA-3696-215

FIG. 6 WAVEFORMS OF DRIVE MMF

Table II  
MMF DRIVES APPLIED TO UNLOADED CORES

MMF DRIVE SHAPE	CORE E-6				CORE J-1	
	$F_D$ (amp-turns)	$T_r$ ( $\mu\text{sec}$ )	$T_h$ ( $\mu\text{sec}$ )	$T_f$ ( $\mu\text{sec}$ )	$F_D$ (amp-turns)	$T_r$ ( $\mu\text{sec}$ )
Step	1.1	0.05	--	--	0.60	0.05
Step	1.2	0.05	--	--	0.975	0.05
Step	1.7	0.05	--	--	1.938	0.05
Step	2.7	0.05	--	--	--	--
Ramp	4.16	1.164	--	--	1.20	1.40
Triangular	3.277	0.90	0.0	1.12	--	--
Trapezoidal	2.923	0.68	0.4	0.82	--	--

## 2. COMPUTATION

### a. METHOD OF COMPUTATION

The parabolic model for the inelastic  $\dot{\phi}$ , Eqs. (1), (2), and (4), has been formally expressed in Eq. (23) as  $\dot{\phi}(F, \phi)$ . However, since  $F$  is a function of time, an alternative expression for  $\dot{\phi}$  is

$$\dot{\phi} = f(t, \phi) \quad (42)$$

Here,  $t$  is an independent variable and  $\phi$  is a dependent variable. Since Eq. (42) is a nonlinear differential equation, the solution of this equation will be obtained numerically.

There are several known ways to solve a differential equation numerically. The method to be used here (referred to as Method II by Milne<sup>5</sup>) is (briefly) as follows. Starting from an initial time,  $t_0$ , we divide time  $t$  into small  $\Delta t$  intervals, and denote the values of  $F$ ,  $\dot{\phi}$ , and  $\phi$  at time  $t_n = t_0 + n\Delta t$  by  $F_n$ ,  $\dot{\phi}_n$ , and  $\phi_n$ , respectively. Suppose that the values of  $\phi_{n-2}$ ,  $\dot{\phi}_{n-2}$ ,  $\phi_{n-1}$ , and  $\dot{\phi}_{n-1}$  have been determined. We now wish to compute  $\phi_n$  and  $\dot{\phi}_n$ . Two formulas are considered for computing an approximate value of  $\phi_n$ :

$$\phi_n = \phi_{n-2} + 2\Delta t \dot{\phi}_{n-1} \quad (43)$$

and

$$\phi_n = \phi_{n-1} + \Delta t \frac{\dot{\phi}_n + \dot{\phi}_{n-1}}{2} \quad (44)$$

Starting from a known value of  $\phi$ ,  $\phi_n$  in Eq. (43) is obtained by using  $\dot{\phi}_{n-1}$ , which is the slope of  $\phi(t)$  at the *average time*  $t_{n-1} = (t_n + t_{n-2})/2$ ; on the other hand,  $\phi_n$  in Eq. (44) is obtained by using  $(\dot{\phi}_n + \dot{\phi}_{n-1})/2$ , that is, the *average slope* of  $\phi(t)$ . Using Taylor's series, it can be shown<sup>5</sup> that Eq. (43) is more accurate than the relation  $\phi_n = \phi_{n-1} + \Delta t \dot{\phi}_{n-1}$ , but is less accurate than Eq. (44). We, therefore, prefer to use Eq. (44), but since  $\dot{\phi}_n$  is unknown to start with, we shall use Eq. (43) only to obtain an initial approximation for  $\phi_n$ , and then proceed to use Eq. (44) in an iterative manner. Alternative formulas,<sup>5</sup> which are slightly more exact than Eqs. (43) and (44), will not be used here because of the increased complexity of computation.

b. BEGINNING OF SWITCHING

In order to save computation time,  $n = 0$  corresponds to the beginning of flux switching (i.e., to  $t = t_0$ ), when  $F$  reaches  $F_0''$ . Since  $F \approx N_D I_D t / T_r$ , then,

$$t_0 \approx \frac{T_r F_0''}{N_D I_D} \quad (45)$$

Note that Eq. (45) holds also for what is essentially a step drive, i.e., a constant-amplitude drive with a short rise time.

c. TIME INCREMENT AND APPROXIMATE SWITCHING TIME

The length of the time increment  $\Delta t$  depends on the switching time  $\tau_s$ . The shorter  $\tau_s$  is, the shorter must  $\Delta t$  be. In order to determine  $\Delta t$ , we shall compute  $\tau_s$  corresponding to  $\Delta\phi = 2\phi_r$  very crudely, and assume that  $\Delta t$  is proportional to  $\tau_s$ —for example,  $\tau_s/500$ . An approximate value of  $\tau_s$  is obtained by equating  $2\phi_r$  to the time integral of  $\dot{\phi} \approx \bar{\rho}(F - F_0'')$ , in which  $\bar{\rho} \approx 0.6\rho_p$  (see Report 2, p. 21). The use of  $F_0''$  instead of  $F_0$  is needed for drives with amplitudes below  $F_0$ . Such a step is justified for two reasons: first, the value of the computed  $\tau_s$  need not be exact at all; second, the resulting value of  $\tau_s$  is smaller than the value obtained by using  $F_0$  (although this amounts to longer computation time, the accuracy of computation can only be improved because of smaller values of  $\Delta t$ ). For a step drive  $F_D = N_D I_D$ , the time integration of  $\dot{\phi}$  and  $0.6\rho_p(F - F_0'')$  from  $t = 0$  to  $t = \tau_s$  gives

$$\tau_{s, \text{step}} \approx \frac{\phi_r}{0.3 \rho_p (N_D I_D - F_0'')} \quad (46)$$

For a ramp drive,  $F = N_D I_D t / T_r$ . The time integration of  $\dot{\phi}$  and  $0.6\rho_p(F - F_0'')$  from  $t = t_0$ , Eq. (45), to  $t = \tau_s$  gives

$$\tau_{s, \text{ramp}} \approx \sqrt{\frac{\phi_r T_r}{0.15 \rho_p N_D I_D}} \quad (47)$$

d. DRIVE CURRENT VS. TIME

From Fig. 6(a), the essentially step-drive current may be described by the function

$$i_D = I_D \cdot \min \left( \frac{t}{T_r}, 1 \right) \quad (48)$$

For computational purposes, Eq. (48) may also be used to describe a ramp-drive current, Fig. 6(b), during switching time, provided that  $T_r > \tau_s$ . From Fig. 6(d), the trapezoidal drive may be described by the function

$$i_D = I_D \cdot \min \left( \frac{t}{T_r}, 1, \frac{T_r + T_h + T_f - t}{T_f} \right) \quad (49)$$

For a triangular drive, Fig. 6(c), we simply let  $T_h = 0$  in Eq. (49).

PROCEDURES for *min* functions of two and three variables, such as appear in Eqs. (48) and (49), as well as for a *max* function of two variables, are given in Appendix B.

e. SEQUENCE OF COMPUTATION

When the initial switching time,  $t_0$ , and the time increment,  $\Delta t$ , have been determined, the time of any  $n$ th  $\Delta t$ ,  $t_n = t_{n-1} + \Delta t$ , is used to determine  $i_{Dn}$  and, hence, also  $F_n = N_D i_{Dn}$ . Computation of  $\phi_n$  and  $\dot{\phi}_n$  is performed in one or more iterations, not counting the initial approximation. Each iteration is denoted by a subscript  $j$  in parentheses. The initial approximation ( $j = 0$ ) for  $\phi_n$  is obtained by using Eq. (43):

$$\phi_{n(0)} = \phi_{n-2} + 2\Delta t \dot{\phi}_{n-1} \quad (50)$$

For  $j = 1, 2, \dots$ ,  $\dot{\phi}_{n(j)}$  and  $\phi_{n(j)}$  are computed by using Eqs. (23) and (44), respectively:

$$\dot{\phi}_{n(j)} = \dot{\phi}[F_n, \phi_{n(j-1)}] \quad (51)$$

and

$$\phi_{n(j)} = \phi_{n-1} + \Delta t \frac{\dot{\phi}_{n(j)} + \dot{\phi}_{n-1}}{2} \quad (52)$$



Application of Eqs. (51) and (52) is continued until the change in  $\phi_n$  or  $\dot{\phi}_n$  from one iteration to the next is negligible. (In practice, one or two iterations are sufficient). The final values of  $\dot{\phi}_n$  and  $\phi_n$  are recorded, and  $t$  is advanced by  $\Delta t$  in order to compute  $\dot{\phi}_{n+1}$  and  $\phi_{n+1}$  in a similar manner. The computation is terminated when  $\phi = 0$ .

The number of iterations for each  $\Delta t$  is counted. If this number exceeds, say, 10, we may assume that the computation of  $\phi_n$  has either converged too slowly or has diverged. Because of the latter possibility, the initial approximation, Eq. (50), should be restored and corrected only once, before proceeding to the next  $\Delta t$ .

#### f. OUTLINE FOR COMPUTER PROGRAM

The actual computer program for the no-load case is given in Appendix C. The outline of this program is as follows:

- (1) Declare all identifiers, input-output lists and formats, and PROCEDURES to be used in the program, in accordance with the rules of the ALGOL-60 language.
- (2) Read in the core and drive parameters, and set initial values for all of the variables.
- (3) Compute the following:
  - (a) An approximate switching time,  $\tau_s$ , using Eq. (46) for a step drive, or Eq. (47) for a ramp drive
  - (b) The time increment,  $\Delta t$  (e.g.,  $\Delta t = 0.002\tau_s$ )
  - (c) The time for beginning of switching,  $t_0$ , using Eq. (45).
- (4) Starting from  $n = 1$ , for each  $n$ th  $\Delta t$  during switching:
  - (a) Compute  $t_n = t_{n-1} + \Delta t$ ,  $i_{Dn}$  [using Eq. (48) for a step or a ramp drive, or Eq. (49) for a triangular or a trapezoidal drive], and  $F_n = N_D i_{Dn}$ .
  - (b) Use Eq. (50) for an initial approximation of  $\phi_n$ , and Eqs. (51) and (52) for an iterative solution of  $\phi_n$  and  $\dot{\phi}_n$ , until the change in  $\phi$  is negligible. If the number of iterations reaches nine, restore the initial approximation, and perform only a single correction, before proceeding to the next  $\Delta t$ .

- (5) Print output ( $t$ ,  $\dot{\phi}$ ,  $\phi$ ,  $\phi_d$ ,  $F$ , and number of iterations), say once every  $25 \Delta t$ 's.
- (6) Stop computation when  $\ddot{\phi} = 0$ .

This computer program was applied to compute  $\dot{\phi}(t)$  in all the cases listed in Table II, p. 24.

### 3. MANUAL COMPUTATION OF INITIAL SPIKES

The elastic and inelastic initial  $\dot{\phi}$  spikes were computed manually for the four step-drive cases of Core E-6 listed in Table II.

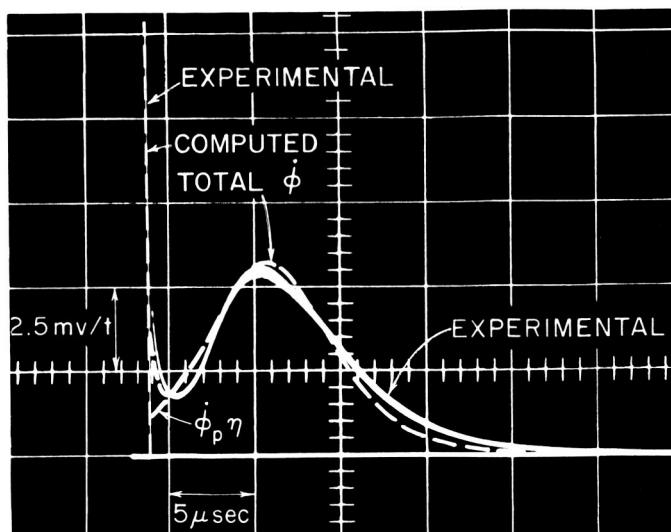
The elastic  $\dot{\phi}$  was computed from Eqs. (5) and (7). Substituting the values of the core parameters  $\phi_s$ ,  $\phi_r$ ,  $H_a$ ,  $l_o$ , and  $l_i$  (see Table I) into Eq. (7),  $\epsilon_i$  was found to be equal to  $5.25 \cdot 10^{-10}$  ohm second/turn<sup>2</sup>. Since exact details of the slope of  $F(t)$  during its rise time were lacking, the peak of  $F$  was assumed to be approximately equal to  $F_D/T_r$ . Thus, for  $F_D = 1.1, 1.2, 1.7$ , and  $2.7$  amp-turns, the peak values of  $\dot{\phi}_{\epsilon i}$  were found to be 12.83, 14.00, 19.84, and 30.50 millivolts/turn, respectively.

The inelastic  $\dot{\phi}$  spike was computed from Eq. (8), in which  $F_d^n = H_q l_i = 0.775$  amp-turn,  $\rho_i \cong 0.01$  ohm/turn<sup>2</sup>, and  $C_i = 0.14$  amp-turn-microsecond. The values of  $\rho_i$  and  $C_i$  were obtained by correlating Eq. (8) and the difference between the experimental  $\dot{\phi}$  oscillograms and the  $\dot{\phi}$  curves computed by using the  $\dot{\phi}(F, \phi)$  PROCEDURE. Following the relations  $\dot{\phi}_{\rho i 0} = \rho_i (F_D - F_d^n)$  and  $\tau_i = C_i / (F_D - F_d^n)$ , it was found that for  $F_D = 1.1, 1.2, 1.7$ , and  $2.7$  amp-turns,  $\dot{\phi}_{\rho i 0} = 3.25, 4.25, 9.25$ , and  $19.25$  millivolts/turn, and that  $\tau_i = 0.431, 0.329, 0.151$ , and  $0.0727$  microsecond, respectively.

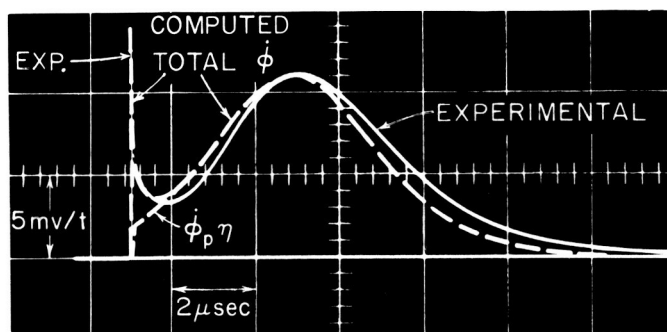
The total  $\dot{\phi}$  was obtained by adding  $\dot{\phi}_{\epsilon i}$  and  $\dot{\phi}_{\rho i}$  to the main  $\dot{\phi}_\rho$  computed by the  $\dot{\phi}(F, \phi)$  PROCEDURE. Using Eq. (45), the time  $t_0$  at which the main  $\dot{\phi}_\rho$  starts to rise is 0.0431, 0.0396, 0.0279, and 0.0176 microsecond for  $F_D = 1.1, 1.2, 1.7$ , and  $2.7$  amp-turns, respectively.

### 4. EXPERIMENTAL AND COMPUTED RESULTS

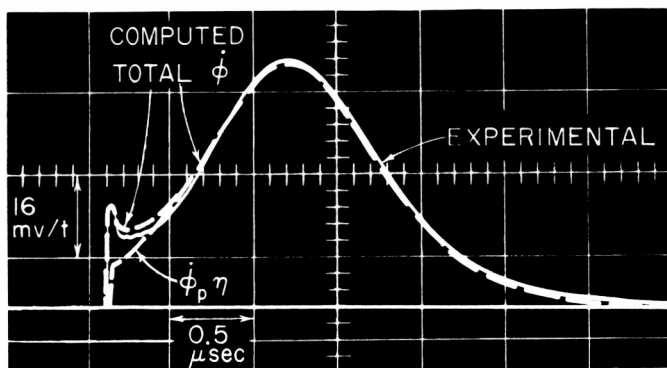
Experimental and computed curves of  $\dot{\phi}$  vs.  $t$  for the unloaded cores are compared in Figs. 7 through 9. Except for Fig. 8, the experimental curves are photographs of the original oscillograms. The computed curves were traced manually from curves that were first computed on a Burroughs B-5000 computer, and later plotted automatically on a CalComp, Model 570, plotter.



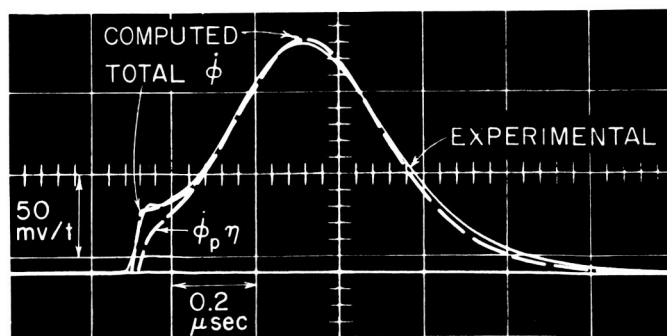
(a)  $F_D = 1.1$  amp-turn



(b)  $F_D = 1.2$  amp-turn



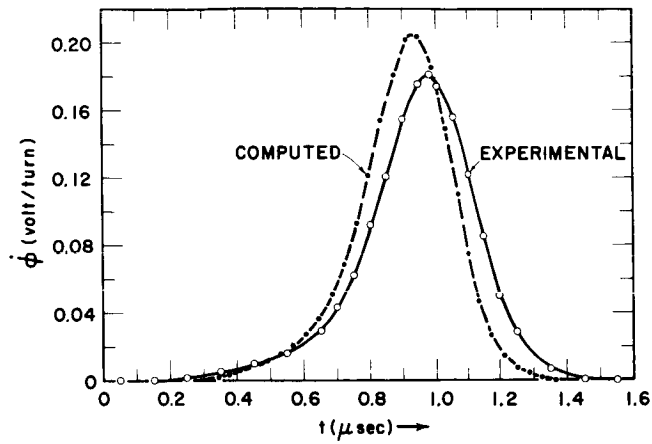
(c)  $F_D = 1.7$  amp-turn



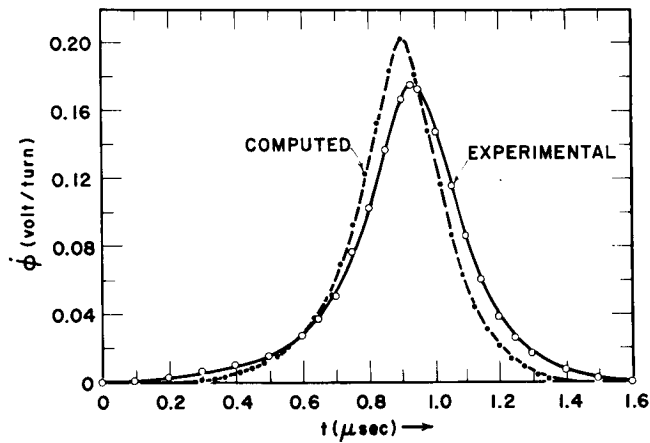
(d)  $F_D = 2.7$  amp-turns

RB-3696-216

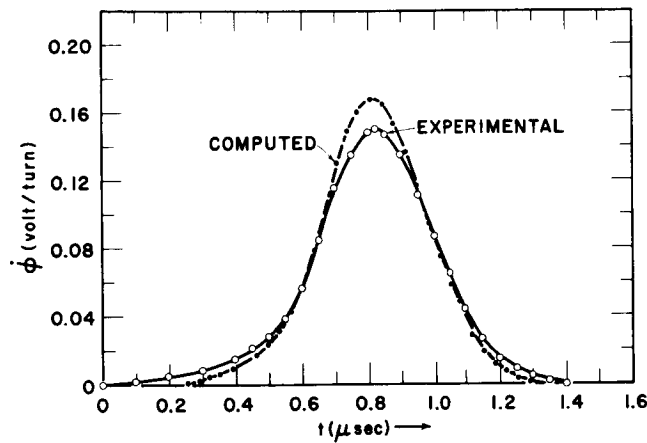
FIG. 7 EXPERIMENTAL AND COMPUTED  $\dot{\phi}(t)$  WAVEFORMS OF CORE E-6 SWITCHING WITH NO LOAD AND STEP-F DRIVE  
 $T_r = 0.05 \mu\text{sec}$



- (a) RAMP MMF  
 $F_D = 4.16$  amp-turns  
 $T_r = 1.164 \mu\text{sec}$



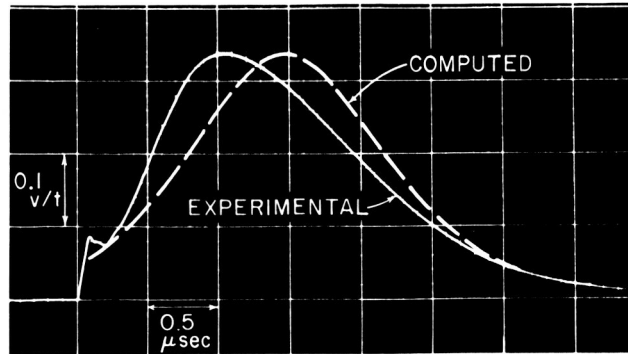
- (b) TRIANGULAR MMF  
 $F_D = 3.277$  amp-turns  
 $T_r = 0.9 \mu\text{sec}$   
 $T_f = 1.12 \mu\text{sec}$



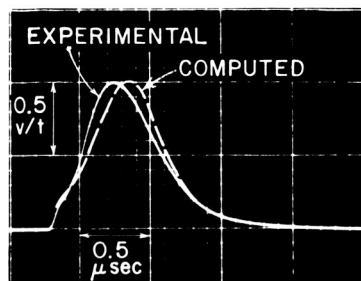
- (c) TRAPEZOIDAL MMF  
 $F_D = 2.923$  amp-turns  
 $T_r = 0.68 \mu\text{sec}$   
 $T_h = 0.4 \mu\text{sec}$   
 $T_f = 0.82 \mu\text{sec}$

RD-3696-217

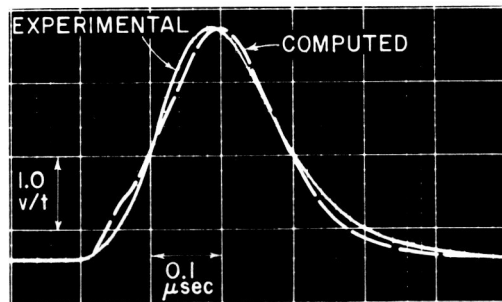
FIG. 8 EXPERIMENTAL AND COMPUTED  $\dot{\phi}(t)$  WAVEFORMS OF CORE E-6 SWITCHING WITH NO LOAD AND VARIABLE-F DRIVE



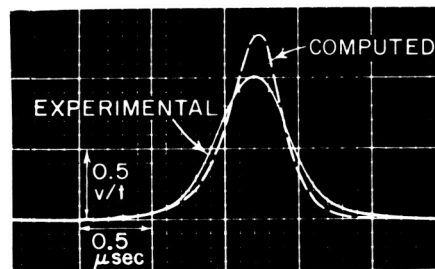
(a) STEP MMF  
 $F_D = 0.6$  amp-turn



(b) STEP MMF  
 $F_D = 0.975$  amp-turn



(c) STEP MMF  
 $F_D = 1.938$  amp-turn



(d) RAMP MMF  
 $F_D = 1.2$  amp-turn  
 $T_r = 1.4$   $\mu$ sec

RA-3696-218

FIG. 9 EXPERIMENTAL AND COMPUTED  $\dot{\phi}(t)$  WAVEFORMS OF CORE J-1 SWITCHING WITH NO LOAD  
For Step-F Drive,  $T_r = 0.05$   $\mu$ sec

The results for Core E-6 are compared in Fig. 7 for four values of step drive, and in Fig. 8 for ramp, triangular, and trapezoidal drives. The experimental elastic initial spikes in the first two cases of step drive, Figs. 7(a) and (b), have been retouched because the original traces were too faint to be reproduced photographically. Unfortunately, these  $\dot{\phi}_{\epsilon i}$  spikes are masked by the computed spikes as a result of the time scale. Compared with the computed peak values of 12.83 and 14.00 millivolts/turn, the experimental values are 12.3 and 17 millivolts/turn for  $F_D = 1.1$  and 1.2 amp-turn, respectively. In each of the cases of Fig. 7, the manually computed elastic and inelastic initial  $\dot{\phi}$  spikes have been added to the main  $\dot{\phi}(t)$  plot that had been computed on a computer.

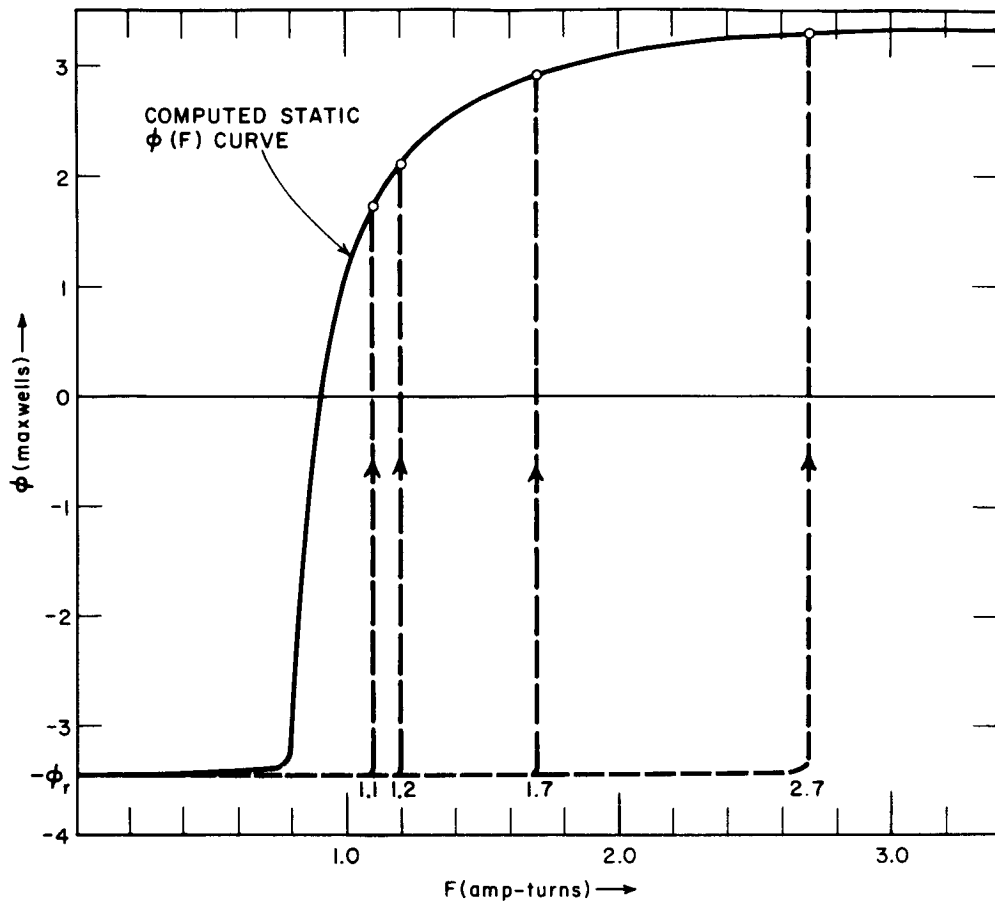
The results of Core J-1 are compared in Fig. 9 for three values of step drive and a single ramp drive. The computed  $\dot{\phi}(t)$  waveforms do not include the initial  $\dot{\phi}$  spikes.

On the average,  $\Delta t$  was 0.065 percent of the *actual* switching time. The over-all computation time for all the cases above was about 5 minutes, including 50 seconds of compiling time. When no automatic plotting was involved, the computation time was about 4 minutes, including 20 seconds of compiling time.

## 5. DISCUSSION

### a. STEP-DRIVE RESULTS

The variation of  $\phi$  vs.  $F$  of Core E-6 during switching is shown in Fig. 10 for each of the step- $F$  cases, superimposed on the static  $\phi(F)$  curve. Referring to Fig. 7, we see that the agreement between the computed and the experimental  $\dot{\phi}(t)$  waveforms becomes worse as  $F$  decreases below the  $F$  values around the "knee" of the static  $\phi(F)$  curve. A similar comparison for  $F = 1.0$  amp-turn (not shown in this report) indicates that the computed  $\dot{\phi}(t)$  is too low, and, consequently, the computed switching time is too long. Although there is no doubt that the parabolic model for inelastic switching has been improved considerably by replacing Eq. (3) by Eq. (4), there is a need for further improvements in the model for  $F$  values below  $F_c$ . Combining  $\dot{\phi}_{\epsilon i}$  and  $\dot{\phi}_{\rho i}$ , Eqs. (5) and (8), in the  $\dot{\phi}(F, \phi)$  PROCEDURE could have improved the results for the following reason. The manually computed elastic and inelastic initial spikes have simply been added to the main  $\dot{\phi}$  plot, whose machine computation was based on Eqs. (1), (2), and (4). A source of error in the over-all  $\dot{\phi}$  might have been caused by ignoring the



RB-3696-219

FIG. 10 VARIATIONS OF  $\phi$  vs.  $F$  OF CORE E-6 SWITCHING WITH NO LOAD AND STEP- $F$  DRIVE (Corresponding to Fig. 7)

contribution of  $\dot{\phi}_{\epsilon i}$  and  $\dot{\phi}_{\rho i}$  to the change in the total  $\phi$  in the computation of the main  $\dot{\phi}$ . This type of error can be remedied with no difficulty by including the expressions for  $\dot{\phi}_{\epsilon i}$  and  $\dot{\phi}_{\rho i}$ , Eqs. (5) and (8), in the  $\dot{\phi}(F, \phi)$  PROCEDURE. Such an improvement will be undertaken after the models for the initial  $\dot{\phi}$  spikes are established more soundly.

Comparing Figs. 7 and 9, we see that although for both Core E-6 and Core J-1 the disagreement between experimental and calculated  $\dot{\phi}(t)$  increases as  $F$  decreases, this disagreement is more pronounced in the case of Core J-1. This result is caused by the difference in the ratio of outside diameter (OD) to inside diameter (ID): The OD/ID ratio of Core E-6 is 1.06, whereas the OD/ID ratio of Core J-1 is 1.61 (cf. Table I). As explained in Part A-4, Eqs. (1), (2), and (4) are valid if the core is

not too thick. Application of Eqs. (9) through (22) will no doubt improve the agreement between calculated and experimental  $\dot{\phi}(t)$  of Core J-1.

#### b. RAMP-DRIVE RESULTS

A comparison between computed and experimental  $\dot{\phi}(t)$  waveform of Core E-6 in the case of a ramp drive is shown in Fig. 8(a). A similar comparison for Core J-1 is shown in Fig. 9(d). In both cases, the computed peak value of  $\dot{\phi}$  is higher than the experimental value. The difference is about 12 percent for Core E-6, and about 30 percent for Core J-1. It is evident from these comparisons that the values of  $\lambda$  and  $\rho_p$ , which have been obtained from measuring  $\dot{\phi}_p$  vs.  $F$  in the case of a step-drive switching, are too high for ramp-drive switching. Two problems remain to be solved: First, why are the values of  $\lambda$  and  $\rho_p$  of a ramp-drive switching smaller than the values of  $\lambda$  and  $\rho_p$  of a step-drive switching? Second, how are the values of  $\lambda$  and  $\rho_p$  affected by the slope of  $F(t)$ ? The first problem is discussed in Sec. III-E in connection with switching from a partially-set state. The second problem will be investigated in the near future.

Let us now repeat the computation of  $\dot{\phi}(t)$  for the ramp-drive cases of both cores, using lower values of  $\lambda$  and  $\rho_p$ . Following Eq. (25),  $\lambda$  and  $\rho_p$  are proportional, and hence both should be decreased by the same percentage. Experimental points of  $\dot{\phi}(t)$  of Cores E-6 and J-1, taken from the data of Figs. 8(a) and 9(d), and the newly computed curves are compared in Fig. 11. In Fig. 11(a),  $\dot{\phi}(t)$  of Core E-6 has been recomputed, using values of  $\lambda$  and  $\rho_p$  which are 25 percent lower than in Table I, and shifted to the left by 0.04 microsecond in order to align the maximum points of  $\dot{\phi}$ . In Fig. 11(b),  $\dot{\phi}(t)$  of Core J-1 has been recomputed using values of  $\lambda$  and  $\rho_p$  which are 30 percent lower than in Table I, and shifted to the left by 0.25 microsecond. The agreement between computed and experimental  $\dot{\phi}(t)$  is certainly better than in Figs. 8(a) and 9(d).

Having obtained a reasonable agreement between computed and experimental  $\dot{\phi}(t)$ , we can now use the computed  $\phi(t)$  and  $F(t)$  in order to plot the variation of  $\phi(F)$  during the switching time in the case of a ramp drive. Such a plot is shown in Fig. 12 for Core E-6.

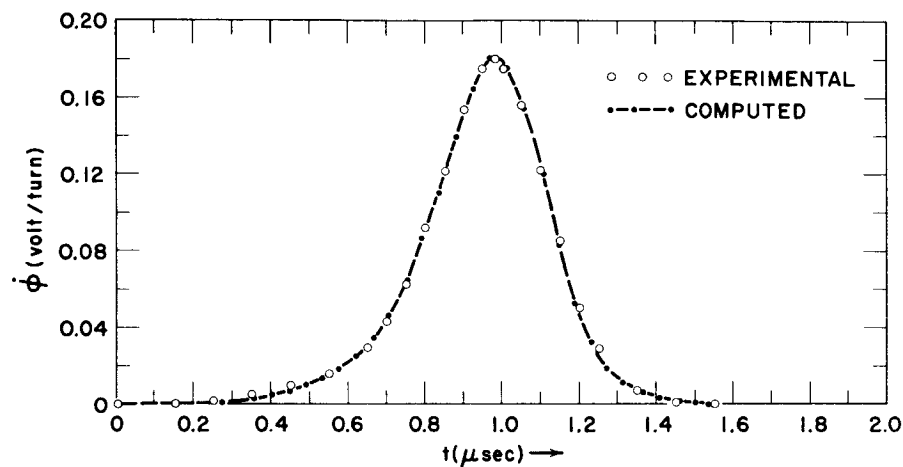
#### c. EFFECT OF $\Delta t$

The nonlinear differential equation  $\dot{\phi} = f(t, \phi)$ , Eq. (42), has been solved numerically, using a small time interval  $\Delta t$  in the solution.

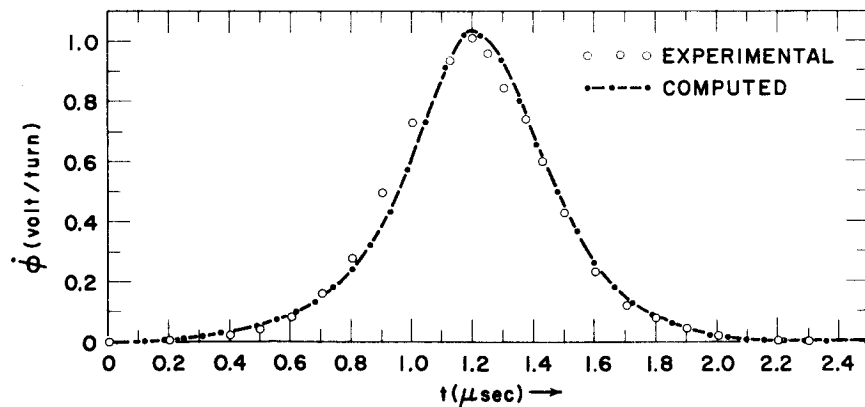


One may ask how small  $\Delta t$  should be, in view of the fact that the value of  $\Delta t$  affects both the accuracy and the cost of computation.

The smaller  $\Delta t$  is, the more accurate the results are. Furthermore, there is an upper bound on  $\Delta t$ , below which convergence is guaranteed.<sup>5</sup> A practical way to determine the value of  $\Delta t$  is to repeat the computation, starting from a low value of  $\Delta t$ , for increasing values of  $\Delta t$ , and select the largest value of  $\Delta t$  above which the results change noticeably. The effect of  $\Delta t$  on the accuracy of the computed results was tested by using different values of  $\Delta t$  in the computation of  $\dot{\phi}(t)$  for the case of a step drive of  $F_D = 1.938$  amp-turn, applied to Core J-1, Fig. 9(c). Compared



(a) CORE E-6,  $\lambda$  AND  $\rho_p$  75% OF STEP-F VALUES



(b) CORE J-1,  $\lambda$  AND  $\rho_p$  70% OF STEP-F VALUES

RC-3696-220

FIG. 11 RECOMPUTED  $\dot{\phi}$  WAVEFORMS OF CORES E-6 AND J-1 SWITCHING WITH NO LOAD AND RAMP-F DRIVE USING LOWER VALUES OF  $\lambda$  AND  $\rho_p$

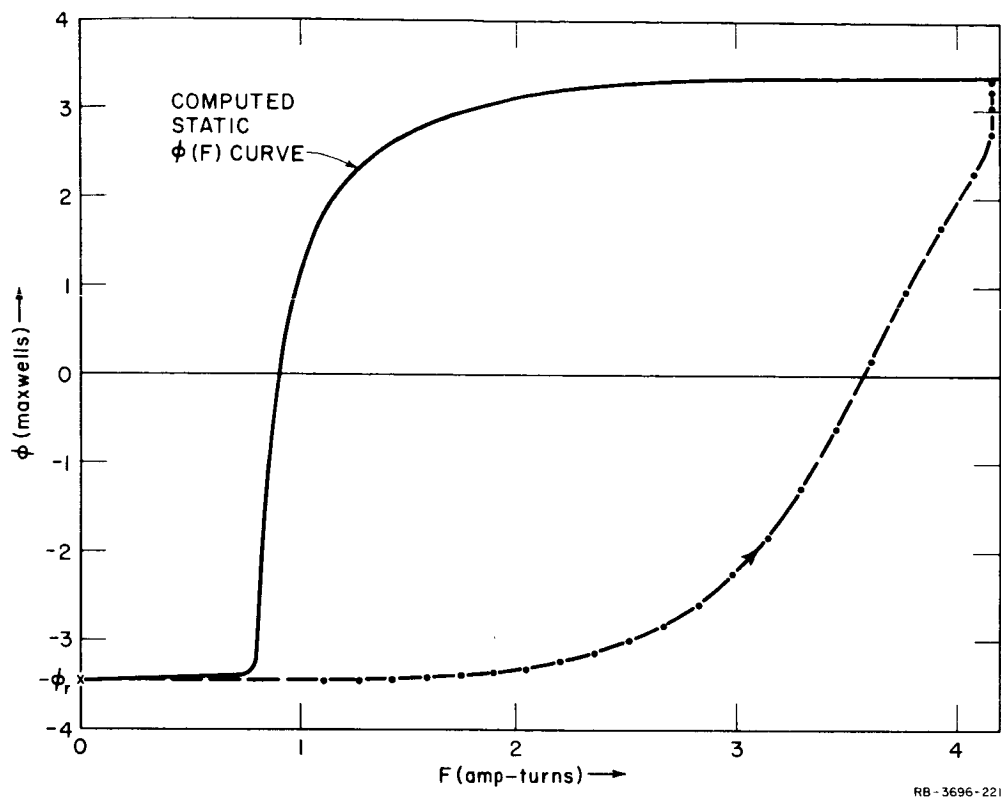
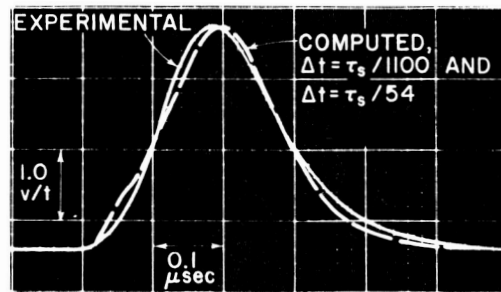
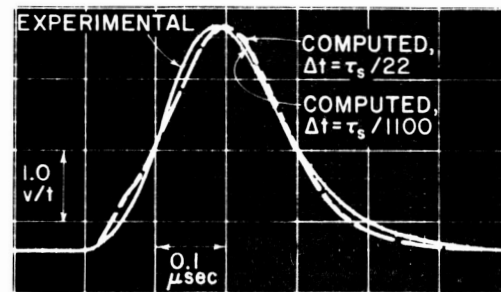


FIG. 12 VARIATION OF  $\phi$  vs.  $F$  OF CORE E-6 SWITCHING WITH NO LOAD AND RAMP- $F$  DRIVE [Corresponding to Recomputed  $\dot{\phi}(t)$  in Fig. 11(a)]

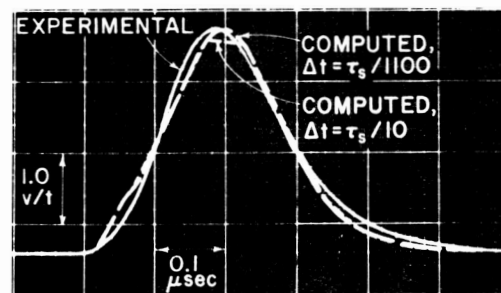
with the actually computed value of switching time  $\tau_s$  [not the approximated value, which is based on Eq. (46)], the following values of  $\Delta t/\tau_s$  were used:  $1/2200$ ,  $1/440$ ,  $1/220$ ,  $1/108$ ,  $1/54$ ,  $1/22$ , and  $1/10$ . No noticeable change in the computed  $\dot{\phi}(t)$  waveform was observed as  $\Delta t/\tau_s$  increased from  $1/2200$  to  $1/54$ . This result is demonstrated in Fig. 13(a) by superimposing the computed and automatically plotted  $\dot{\phi}(t)$ , using  $\Delta t/\tau_s = 1/54$ , on the experimental  $\dot{\phi}(t)$  and the manually-traced computed  $\dot{\phi}(t)$  of Fig. 9(c), using  $\Delta t/\tau_s = 1/1100$ . Similar comparisons with the experimental and computed waveforms of Fig. 9(c) are made in Figs. 13(b) and 13(c) for  $\Delta t/\tau_s = 1/22$  and  $1/10$ , respectively. Note that the broken lines in the last two cases, which result from automatic line plotting, could be smoothed out manually, and thus yield a better agreement with experimental data. However, even after smoothing, a small difference could be detected as compared to plots using  $\Delta t/\tau_s$  of  $1/54$  or lower. We conclude from this discussion that  $\Delta t$  should be below 2 percent of the switching time.



(a)  $\Delta t/\tau_s = 1/54$



(b)  $\Delta t/\tau_s = 1/22$



(c)  $\Delta t/\tau_s = 1/10$

RA-3696-222

FIG. 13 EFFECT OF  $\Delta t$  ON COMPUTED  $\dot{\phi}(t)$  WAVEFORM  
(of Core J-1 Switching with No Load and Step-F Drive of 1.938 amp-turn)

The smaller  $\Delta t$  is, the higher is the cost of computation. If the compiling time is relatively small, and if the output printing is performed at a constant frequency, then the computation time is essentially inversely proportional to  $\Delta t$ .

## 6. SUMMARY

Two toroidal cores of different materials and different ratios of outside to inside diameter were switched unloaded by MMF drives of various amplitude and shape, and oscillograms of  $\dot{\phi}(t)$  were photographed. A program for computing  $\dot{\phi}(t)$  numerically was written, using, in addition to the  $\dot{\phi}(F, \phi)$  PROCEDURE, the relation  $\phi_n \approx \phi_{n-2} + 2\Delta t \dot{\phi}_{n-1}$  as a first approximation and the relation  $\phi_n \approx \phi_{n-1} + \Delta t(\dot{\phi}_n + \dot{\phi}_{n-1})/2$  for an iterative solution during each time-element,  $\Delta t$ . Comparisons between experimental and computed  $\dot{\phi}(t)$  waveforms show good agreement if, for a step  $F$ , the value of  $F$  lies in the "wing" of the static  $\phi(F)$  curve, and if, for a ramp  $F$ , the values of  $\lambda$  and  $\rho_p$  obtained from a step- $F$  test are reduced by 25 to 30 percent.

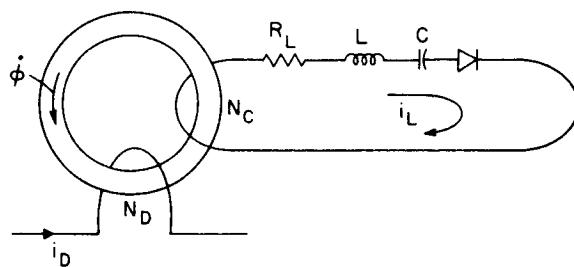
## D. LOADED CORE

The  $\dot{\phi}$  PROCEDURE of Part B, which is based on the parabolic model for inelastic switching [Eqs. (1), (2), and (4)], has been applied in Part C to compute  $\dot{\phi}$  vs.  $t$  in various drive conditions of unloaded core. We now wish to apply this model to the computation of flux switching in loaded cores. The loads include various combinations of a resistance, an inductance, a capacitance, and a semiconductor diode.

### 1. EXPERIMENT

Only Core J-1 (Lockheed 145SC1; 145-mil OD, 90-mil ID) was used in this experiment. The geometry and switching parameters of this core may be found in Table I, p. 23.

The circuit for a general case of a driven loaded core in this experiment is shown in Fig. 14, which serves to define



RA-3696-223

FIG. 14 FLUX SWITCHING IN A LOADED CORE

the symbols for the circuit parameters. The following six types of load were included in the experiment:

- (1) A resistance
- (2) A resistance and a diode
- (3) A resistance and an inductance
- (4) A resistance and a capacitance
- (5) A resistance, an inductance, and a capacitance
- (6) A resistance, an inductance, a capacitance, and a diode.

In each of Cases (2) through (6), all of the components were connected in series.

For each of these load cases, the core was driven by an essentially step-MMF drive and by a ramp-MMF drive, while the temperature was kept at  $30 \pm 0.5^\circ\text{C}$ . The amplitude of the step drive and the slope of the ramp drive varied among the various load cases. The circuit data for the various cases of load and drive used in the experiment are given in Table III.

Oscillograms of  $\dot{\phi}(t)$  and the load current  $i_L(t)$  were recorded for each of the twelve cases in Table III. The data from these oscillograms will be compared later with the corresponding computed results.

Table III  
LOADS AND DRIVES APPLIED TO CORE J-1

MMF DRIVE			LOAD				
Effective Shape	$N_D I_D$ (amp-turns)	$T_r$ ( $\mu\text{sec}$ )	$N_c$	$R_L$ (ohm)	$L$ ( $\mu\text{hy}$ )	$C$ ( $\mu\text{f}$ )	Diode
Step	1.76	0.10	1	1.1	--	--	--
Step	2.74	0.10	2	0.1	--	--	1N3604
Step	1.54	0.10	2	1.58	1.00	--	--
Step	2.78	0.10	2	1.1	--	0.552	--
Step	2.28	0.10	2	0.131	0.38	0.253	--
Step	1.80	0.10	2	0.131	0.38	0.253	1N3604
Ramp	3.887	1.30	1	1.1	--	--	--
Ramp	5.00	1.40	2	0.1	--	--	1N3604
Ramp	3.40	1.60	2	1.58	1.00	--	--
Ramp	4.00	1.35	2	1.1	--	0.552	--
Ramp	4.55	1.40	2	0.131	0.38	0.253	--
Ramp	3.40	1.40	2	0.131	0.38	0.253	1N3604

## 2. COMPUTATION

### a. MMF AND LOOP EQUATIONS

Computation of  $\dot{\phi}$  in a loaded core is more complicated than in an unloaded core because of an additional variable, *i.e.*, the load current,  $i_L$ . As shown in Fig. 14, the net MMF acting on the core is

$$F = N_D i_D - N_c i_L \quad (53)$$

The loop equation is

$$N_c \dot{\phi} = \frac{1}{C} \int_0^t i_L dt' + R i_L + L \frac{di_L}{dt} + e_d \quad (54)$$

Here,  $R = R_L + R_d$ , where  $R_L$  is the load resistance (including the winding resistance), and  $R_d$  is the internal resistance of the diode. The voltage developed across the diode, excluding the voltage drop  $i_L R_d$ , is denoted by  $e_d$ . Following a well-known expression for the forward characteristic of a *p-n* junction diode,<sup>6</sup>

$$e_d = E_k \ln \left( \frac{i_L}{I_0} + 1 \right) \quad (55)$$

where  $I_0$  and  $E_k$  are constants. Theoretically,<sup>6</sup>  $I_0$  is the diode saturation current, and  $E_k = kT/e$ , where  $k$  is Boltzman's constant,  $e$  is the charge of an electron, and  $T$  is the absolute temperature. In practice,  $E_k$  is found to be higher than  $kT/e$ . Let us consider the forward characteristic at 30°C of the silicon diode IN3604, which is used in four of the cases listed in Table III. The values  $R_d = 0.74$  ohm,  $I_0 = 2.7 \cdot 10^{-6}$  ampere, and  $E_k = 0.0833$  volt (rather than the theoretical value of  $kT/e = 0.0261$  volt) have been found to yield a good fit to the experimental data in the current range between 0.05 and 0.6 ampere, where  $i_L$  is very influential.

### b. METHODS OF COMPUTATION

Since  $i_L$  appears in an integral form in Eq. (54), let us make the following substitutions:

$$\int_0^t i_L dt = q; \quad i_L = \dot{q}; \quad \frac{di_L}{dt} = \ddot{q}$$

Since  $i_d$  is a function of time, substitution of Eq. (53) into the function  $\dot{\phi}(F, \phi)$  given by Eqs. (1), (2), and (4) results in a relation that is formally expressed as

$$\dot{\phi} = f_1(t, \phi, \dot{q}) \quad (56)$$

Similarly, Eq. (54) may be expressed formally as

$$\ddot{q} = f_2(t, q, \dot{q}, \dot{\phi}) \quad (57)$$

Equations (56) and (57) are two simultaneous differential equations of the first and second order, respectively, in which  $t$  is an independent variable, and  $\phi$  and  $q$  are dependent variables. The solutions to these equations could be obtained numerically, using only Eqs. (43) and (44) in a fashion similar to that used for the solution of Eq. (42), provided that the computation process is convergent. For the various load cases under investigation, convergence has been achieved if the load is sufficiently inductive. However, in other cases, it has been found that a supplementary method has to be employed in order to prevent the build-up of computational oscillations. (Reducing  $\Delta t$  may, perhaps, help, but the resulting long computation time is too costly.) Newton's method of successive approximations has been found to be very useful in eliminating these diverging computational oscillations. According to this method, the root  $x$  of a function  $f(x) = 0$  may be found within a specified accuracy by starting from an initial guess, and successively approaching its true value every  $j$ th cycle, following the relation

$$x_j = x_{j-1} - \frac{f(x_{j-1})}{f'(x_{j-1})} \quad (58)$$

where  $f'(x) = df(x)/dx$ .

Newton's method of successive approximation, Eq. (58), is slightly modified if the convergence to the correct solution is too slow. Usually, such a slow convergence is also oscillatory. Thus, if after a certain number of iterations the prescribed condition for convergence has not been satisfied, Eq. (58) is modified by taking only *half* of the change in  $x$ , i.e.,

$$x_j = x_{j-1} - 0.5 \frac{f(x_{j-1})}{f'(x_{j-1})} \quad (58a)$$

Substituting the expression for  $e_d$ , Eq. (55), into the loop equation, Eq. (54), we get

$$f(\dot{q}) = \frac{1}{C} q + R\dot{q} + L\ddot{q} + E_k \ln \left( \frac{\dot{q}}{I_0} + 1 \right) - N_c \dot{\phi} = 0 \quad (59)$$

Treating  $x$  as  $\dot{q}$ , Eq. (58) may now be applied in order to solve Eq. (59) for  $\dot{q}$ . Differentiating the expression in Eq. (59) with respect to  $\dot{q}$ , we get

$$f'(\dot{q}) = \frac{df(\dot{q})}{d\dot{q}} \cong \frac{1}{C} \frac{\dot{q}}{\dot{q}} + R + L \frac{\ddot{q}}{\dot{q}} + \frac{E_k}{\dot{q} + I_0} + N_c^2 \dot{\phi}' \quad (60)$$

where  $\dot{\phi}' = \partial \dot{\phi} / \partial F$  and where  $F = N_D i_D - N_c \dot{q}$ , Eq. (53).<sup>\*</sup> It is now clear that the computation program for  $\dot{\phi}'$  is included in the  $\dot{\phi}$  PROCEDURE for such an application, as in Eq. (60).

#### C. SEQUENCE OF COMPUTATION

Computation of  $t_0$ ,  $\tau_s$ , and  $i_D$  is performed by using the governing relations in the no-load case, Eqs. (45) through (48). Since the actual switching time is longer than the  $\tau_s$  of an unloaded core, a lower bound on the accuracy of computation due to the length of  $\Delta t$  is thus guaranteed.

Suppose that the values of the following variables have been computed:

$$\begin{aligned} \phi_{n-2}, \quad \dot{\phi}_{n-2}, \quad q_{n-2}, \quad \dot{q}_{n-2}, \quad \ddot{q}_{n-2} \\ \phi_{n-1}, \quad \dot{\phi}_{n-1}, \quad q_{n-1}, \quad \dot{q}_{n-1}, \quad \ddot{q}_{n-1} \end{aligned}$$

---

<sup>\*</sup> To be exact,

$$\frac{d\dot{\phi}}{d\dot{q}} = \frac{\partial \dot{\phi}}{\partial F} \frac{dF}{d\dot{q}} + \frac{\partial \dot{\phi}}{\partial \phi} \frac{d\phi}{d\dot{q}} = \frac{dF}{d\dot{q}} \left( \frac{\partial \dot{\phi}}{\partial F} + \frac{\partial \dot{\phi}}{\partial \phi} \frac{d\phi}{dF} \right),$$

where  $dF/d\dot{q} = -N_c$  [See Eq. (53)],  $\partial \dot{\phi} / \partial F = \dot{\phi}'$ , Eq. (41), and, following Eqs. (1) and (4),

$$\frac{\partial \dot{\phi}}{\partial \phi} = -4 \dot{\phi}_p \frac{2\phi + \phi_s - \phi_d}{(\phi_s + \phi_d)^2}$$

The expression in Eq. (60) is only an approximation for  $df(\dot{q})/d\dot{q}$ , because of the omission of the term  $N_c^2 (\partial \dot{\phi} / \partial \phi) (d\phi/dF)$ . Although this term could have been included in Eq. (60), such an inclusion would not guarantee faster convergence. In fact, it turned out that omitting this term improved the convergence for those cases in Table III where no inductance was included in the load, and hardly affected the convergence for the cases where an inductance was involved. The problem of whether to include or to omit the term  $(\partial \dot{\phi} / \partial \phi) (d\phi/dF)$ , relative to  $\dot{\phi}'$ , requires further examination.



We shall now describe the sequence of computation in order to solve for  $\phi_n$ ,  $\dot{\phi}_n$ ,  $q_n$ ,  $\dot{q}_n$ , and  $\ddot{q}_n$  numerically.

As an initial ( $j = 0$ ) approximation for  $\phi_n$ ,  $\dot{q}_n$ , and  $q_n$ , we use the form of Eqs. (43) and (44) as follows:

$$\phi_{n(0)} = \phi_{n-2} + 2\Delta t \dot{\phi}_{n-1} \quad (61)$$

$$\dot{q}_{n(0)} = \dot{q}_{n-2} + 2\Delta t \ddot{q}_{n-1} \quad (62)$$

and

$$q_{n(0)} = q_{n-1} + \Delta t \frac{\dot{q}_{n(0)} + \dot{q}_{n-1}}{2} \quad (63)$$

Computation of the variables now proceeds in one or more iterations, each of which is designated by Subscript  $j$ , until the change in these variables is negligible. For  $j = 1, 2, \dots$ , computation in each cycle is performed in the following order: Following Eqs. (53), (23), and (55),

$$F_{n(j)} = N_D i_{Dn} - N_c \dot{q}_{n(j-1)} \quad (64)$$

$$\dot{\phi}_{n(j)} = \dot{\phi} [F_{n(j)}, \phi_{n(j-1)}] \quad (65)$$

and

$$e_{dn(j)} = E_k \ln \left( \frac{\dot{q}_{n(j-1)}}{I_0} + 1 \right) \quad (66)$$

If  $\Delta t$  is small enough, to a good approximation,

$$\ddot{q}_{n(j)} = \frac{\dot{q}_{n(j-1)} - \dot{q}_{n-1}}{\Delta t} \quad (67)$$

Using Eq. (44),

$$\phi_{n(j)} = \phi_{n-1} + \Delta t \frac{\dot{\phi}_{n(j)} + \dot{\phi}_{n-1}}{2} \quad (68)$$

Using Eqs. (59) and (60),

$$f_{n(j)} = R \dot{q}_{n(j-1)} - N_c \dot{\phi}_{n(j)} + e_{dn(j)} + \frac{1}{C} q_{n(j-1)} + L \ddot{q}_{n(j)} \quad (69)$$

and

$$f'_{n(j)} = R + N_c^2 \dot{\phi}'_{n(j)} + \frac{E_k}{\dot{q}_{n(j-1)} + I_0} + \frac{\dot{q}_{n(j-1)}}{C \ddot{q}_{n(j)}} + L \frac{\ddot{q}_{n(j)} - \ddot{q}_{n-1}}{\dot{q}_{n(j-1)} - \dot{q}_{n-1}} \quad (70)$$

Note that in Eq. (70), the term  $[\ddot{q}_{n(j)} - \ddot{q}_{n-1}]/[\dot{q}_{n(j-1)} - \dot{q}_{n-1}]$  approximates the term  $\ddot{q}/\dot{q}$  in Eq. (60). Following Eq. (58),

$$\Delta \dot{q}_{n(j)} = - \frac{f_{n(j)}}{f'_{n(j)}} \quad (71)$$

and

$$\dot{q}_{n(j)} = \dot{q}_{n(j-1)} + \Delta \dot{q}_{n(j)} \quad (72)$$

If a diode is present in the loop,  $\dot{q}_{n(j)} \geq 0$ . Following Eq. (44),

$$q_{n(j)} = q_{n-1} + \Delta t \frac{\dot{q}_{n(j)} + \dot{q}_{n-1}}{2} \quad (73)$$

If  $|\Delta \dot{q}_{n(j)}|$  is larger than, say,  $0.001 |\dot{q}_{n(j)}|$ , then it is assumed that convergence has not been achieved and application of Eqs. (64) through (73) is repeated. A failure to converge within, say, nine iterations is handled in the same way as in the no-load case, i.e., the initial approximation is restored and corrected only once before proceeding to the next  $\Delta t$ . The final values of the variables are recorded, and a similar computation is performed for the next  $\Delta t$ . The computation is terminated when  $\dot{\phi} = 0$ .

#### d. OUTLINE FOR COMPUTER PROGRAM

The actual computer program for the various cases of a loaded core is given in Appendix D. The outline of this program is as follows:

- (1) Declare all identifiers, input-output lists and formats, and PROCEDURES to be used in the program, in accordance with the rules of the ALGOL-60 language.
- (2) Read in the core and circuit parameters, and set initial values for all of the variables.
- (3) Compute the following:
  - (a) The total loop resistance
  - (b) An approximate value of  $\tau_s$ , using Eq. (46) for a step drive or Eq. (47) for a ramp drive
  - (c) The time increment  $\Delta t$ , e.g.,  $\Delta t = 0.005 \tau_s$
  - (d) The time for beginning of switching,  $t_0$ , using Eq. (45).

- (4) Starting from  $n = 1$ , for each  $n$ th  $\Delta t$  during switching, compute the following:
  - (a) The time  $t_n = t_{n-1} + \Delta t$  and the drive current  $i_{Dn}$  [Eq. (48)]
  - (b) Initial approximations for  $\phi_n$ ,  $\dot{q}_n$ , and  $q_n$ , using Eqs. (61), (62), and (63)
  - (c) The values of  $F_n$ ,  $\dot{\phi}_n$ ,  $e_{dn}$ ,  $\ddot{q}_n$ ,  $\phi_n$ ,  $\Delta\dot{q}_n$ ,  $\dot{q}_n$ , and  $q_n$  in an iterative fashion, until the change in  $\dot{q}_n$  is negligible, e.g., until  $|\Delta\dot{q}_n| \leq 0.001|\dot{q}_n|$  (if the number of iterations reaches nine, restore the values of the initial approximation, and perform only a single correction before proceeding with the next  $\Delta t$ ).
- (5) Print output ( $t$ ,  $i_D$ ,  $\dot{\phi}$ ,  $\phi$ ,  $\phi_d$ ,  $F$ ,  $\dot{q}$ ,  $e_d + \dot{q}R_d$ , and number of iterations), say once every 10  $\Delta t$ 's.
- (6) Stop computation when  $\dot{\phi} = 0$ .

### 3. EXPERIMENTAL AND COMPUTED RESULTS

Experimental and computed plots of  $\dot{\phi}$  and  $i_L$  vs.  $t$  for the various cases of load are compared in Fig. 15 for the step drive, and in Fig. 16 for the ramp drive. The experimental curves are photographs of the original oscillograms. The computed curves were traced manually from curves that were first computed on a Burroughs B-5000 computer, and later plotted automatically on a CalComp, Model 570, plotter.

On the average  $\Delta t$  was 0.087 percent of the actual switching time. The over-all computation time for all twelve cases was around 5 minutes, including 51 seconds of compiling time. If no automatic plotting was involved, the computation time was reduced to 4 minutes, including 21 seconds of compiling time.

### 4. DISCUSSION

#### a. VARIATION OF $F$

The agreement between the computed and the experimental results seems, in general, to be slightly better in the cases of applied step drive, Fig. 15, than in the cases of applied ramp drive, Fig. 16. In comparing computed and experimental  $\dot{\phi}(t)$  and  $i_L(t)$  waveforms, it should be recalled that some of the core parameters used in the computation have been determined by applying a step  $F$  to an unloaded core and measuring  $\dot{\phi}_p$ . Although in Fig. 15 the *applied* MMF was a step  $F$ , the *net* MMF was not constant in either time or flux. Similarly, the net  $F$  in any one of the

ramp-drive cases of Fig. 16 was not proportional to time. The variation of  $F$  during the flux-switching time is, of course, load dependent, as is clear from Eq. (53). The variation of computed  $\phi(F)$  in each of the step-drive cases, Fig. 15, is shown in Fig. 17, and the variation of computed  $\phi(F)$  in each of the ramp-drive cases, Fig. 16, is shown in Fig. 18. Note that these  $\phi(F)$  plots correspond to the switching time only. In all the step-drive cases, the  $\phi(F)$  operating point moves along an S-shaped path. A similar path is traversed by the  $\phi(F)$  operating point in the ramp-drive cases, except that the S-shape is less pronounced. Note that flux switching caused by MMF that drops in time is an opposite case to the case of a ramp- $F$  switching for the following reason. We have seen in Part C that for ramp- $F$  switching, the values of  $\lambda$  and  $\rho_p$  are smaller than the corresponding values for a step- $F$  switching. One might, therefore, expect the values of  $\lambda$  and  $\rho_p$  for the case of switching with a monotonically decreasing  $F$  to be larger than those of a step- $F$  switching. This conclusion, whether correct or incorrect, cannot be drawn from the results of Figs. 15 through 18. In order to answer this question, further investigation, including the study of flux switching under a decaying  $F$  with no load, is needed.

#### b. WAVEFORM SHAPES

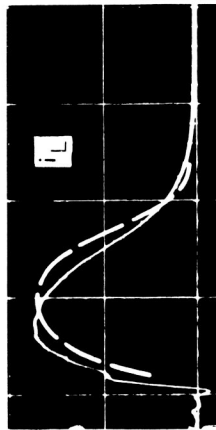
It can be seen from Figs. 15 and 16 that, in some cases [such as in Fig. 15(c)], there is good agreement between the *shape* of the computed waveform and that of the experimental  $\dot{\phi}(t)$  waveform, although there is some disagreement in amplitudes. Disagreement may also arise from any error in measuring the values of the load components. Note that the fluctuations in the  $i_L$  waveform of Fig. 15(b) appear to be noise.

#### c. INITIAL $\dot{\phi}$ SPIKES

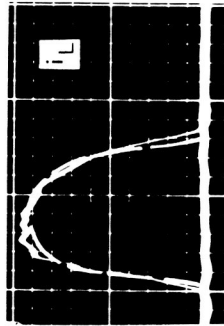
The initial  $\dot{\phi}(t)$  spikes have not been included in the computation. The omission of these spikes is evident in Figs. 15(b) and 15(d), where the experimental  $\dot{\phi}(t)$  is higher than the computed  $\dot{\phi}(t)$  at the outset of switching. Before the initial  $\dot{\phi}$  spikes are added to the computation, we should investigate the effect of elastic switching in the case of an unloaded core that is driven by a rising  $F(t)$  or a falling  $F(t)$ .

#### d. $\phi(F)$ PLOT AND SWITCHING RATE

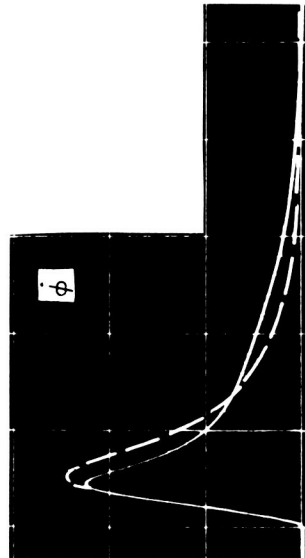
Referring to Figs. 17 and 18, note that in each load case, the time intervals between any two adjacent points, derived from the computed



(a)  $N_D I_D = 1.76$  amp-turn;  
 $N_c = 1$ ;  $R_L = 1.1 \Omega$



(b)  $N_D I_D = 2.74$  amp-turns;  
 $N_c = 2$ ;  $R_L = 0.1 \Omega$ , 1N3604 Diode

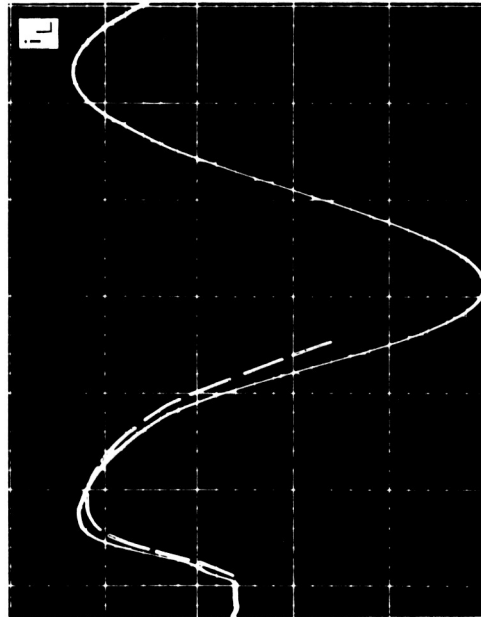
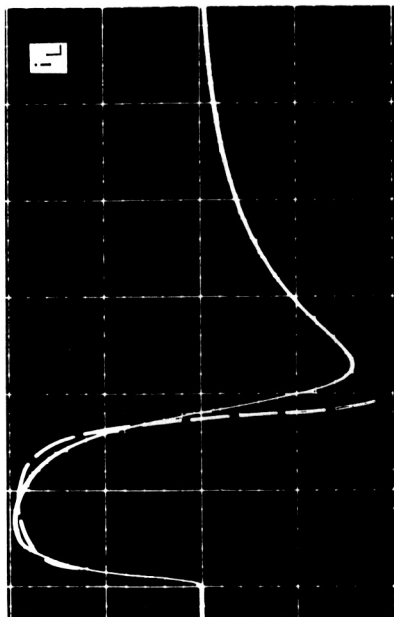
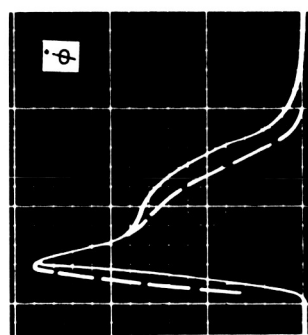
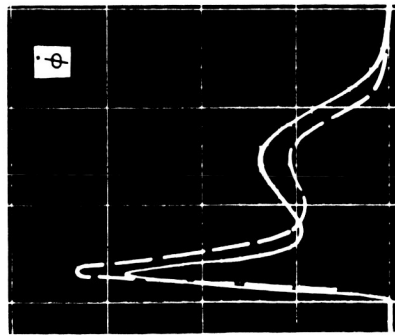
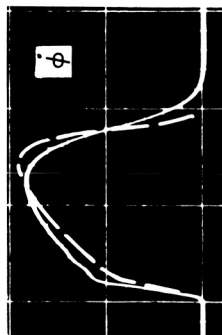


(c)  $N_D I_D = 1.54$  amp-turn;  
 $N_c = 2$ ;  $R_L = 1.58 \Omega$ ,  $L = 1.00 \mu\text{hy}$

RB-3696-224A

FIG. 15 EXPERIMENTAL (Solid Line) AND COMPUTED (Dashed Line)  $\dot{\phi}(t)$  AND  $i_L(t)$  WAVEFORMS OF CORE J-1 SWITCHING WITH LOAD AND STEP-F DRIVE

Time scale  $= 0.5 \mu\text{sec}/\text{major div.}$ ;  $i_L$  scale  $= 0.5 \text{ ampere}/\text{major div.}$ ,  
 $\dot{\phi}$  scale  $= 0.5 (\text{volt}/\text{turn})/\text{major div.}$ ;  $T_r = 0.1 \mu\text{sec.}$



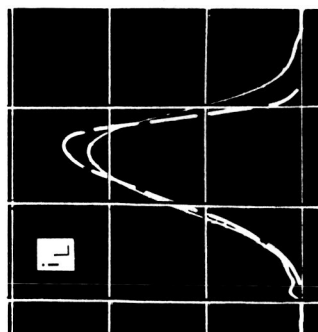
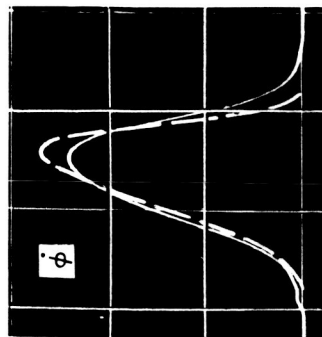
(d)  $N_D I_D = 2.78$  amp-turns;  
 $N_c = 2$ ;  $R_L = 1.1 \Omega$ ,  $C = 0.552 \mu\text{f}$

(e)  $N_D I_D = 2.28$  amp-turns;  
 $N_c = 2$ ;  $R_L = 0.131 \Omega$ ,  $L = 0.38 \mu\text{hy}$   
 $C = 0.253 \mu\text{f}$

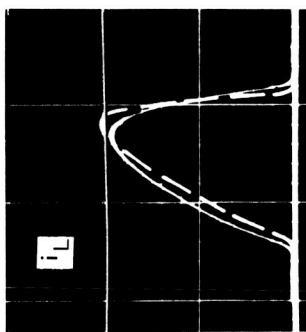
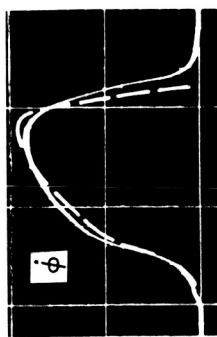
(f)  $N_D I_D = 1.80$  amp-turns;  
 $N_c = 2$ ;  $R_L = 0.131 \Omega$ ,  $L = 0.38 \mu\text{hy}$   
 $C = 0.253 \mu\text{f}$ , 1N3604 Diode

RB - 3696 - 224B

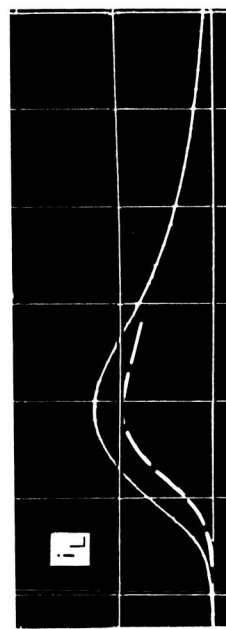
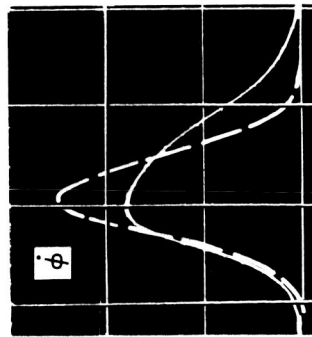
FIG. 15 Concluded



(a)  $N_D I_D = 3.887$  amp-turns;  $T_r = 1.30 \mu\text{sec}$   
 $N_c = 1$ ;  $R_L = 1.1 \Omega$



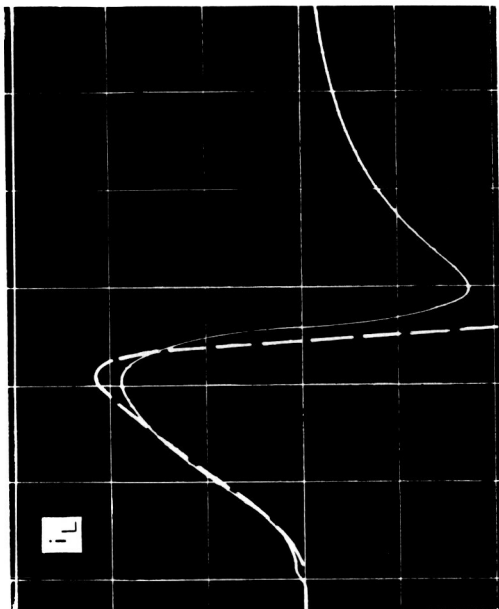
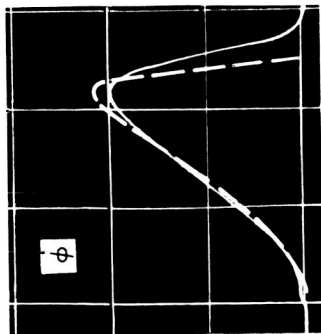
(b)  $N_D I_D = 5.00$  amp-turns;  $T_r = 1.40 \mu\text{sec}$   
 $N_c = 2$ ;  $R_L = 0.1 \Omega$ , 1N3604 Diode



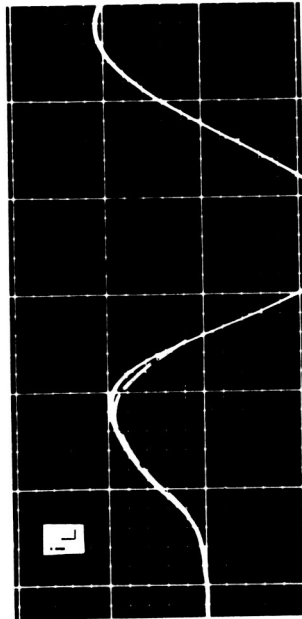
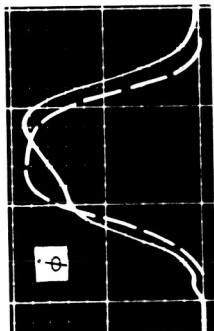
(c)  $N_D I_D = 3.40$  amp-turns;  $T_r = 1.60 \mu\text{sec}$   
 $N_c = 2$ ;  $R_L = 1.58 \Omega$ ,  $L = 1.00 \mu\text{H}$

RB-3696-225A

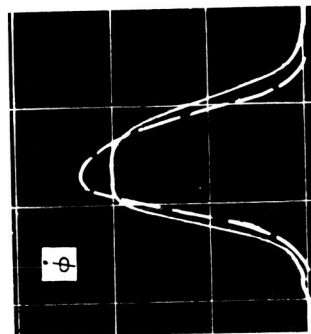
FIG. 16 EXPERIMENTAL (Solid Line) AND COMPUTED (Dashed Line)  $\dot{\phi}(t)$  AND  $i_L(t)$  WAVEFORMS OF CORE J-1 SWITCHING WITH LOAD AND RAMP-F DRIVE  
 Time scale =  $0.5 \mu\text{sec}/\text{major div.}$ ;  $i_L$  scale =  $0.5$  ampere/major div., except  
 $\dot{\phi}$  scale =  $0.5$  (volt/turn)/major div.;  $1.0$  ampere/major div. for (e).



(d)  $N_D I_D = 4.00$  amp-turns;  $T_r = 1.35 \mu\text{sec}$   
 $N_c = 2$ ;  $R_L = 1.1 \Omega$ ,  $C = 0.552 \mu\text{f}$



(e)  $N_D I_D = 4.55$  amp-turns;  $T_r = 1.40 \mu\text{sec}$   
 $N_c = 2$ ;  $R_L = 0.131 \Omega$ ,  $L = 0.38 \mu\text{hy}$   
 $C = 0.253 \mu\text{f}$

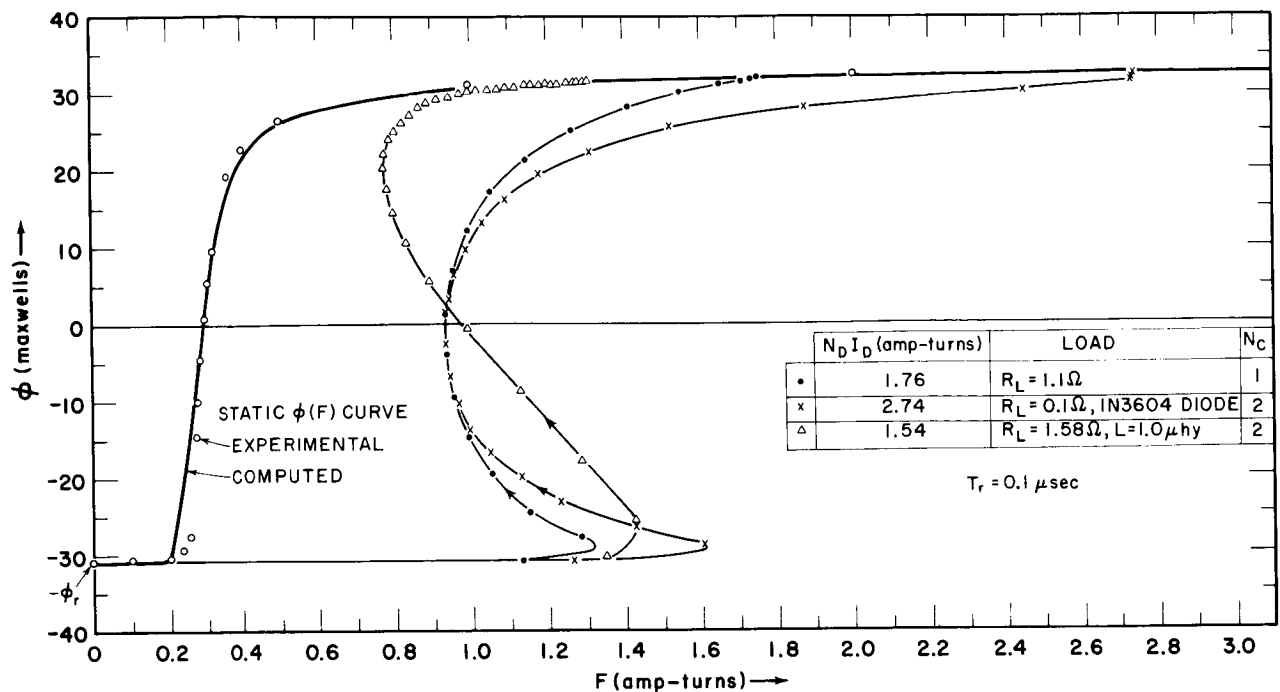


(f)  $N_D I_D = 3.40$  amp-turns;  $T_r = 1.40 \mu\text{sec}$   
 $N_c = 2$ ;  $R_L = 0.131 \Omega$ ,  $L = 0.38 \mu\text{hy}$   
 $C = 0.253 \mu\text{f}$ , 1N3604 Diode

RB-3696-225B

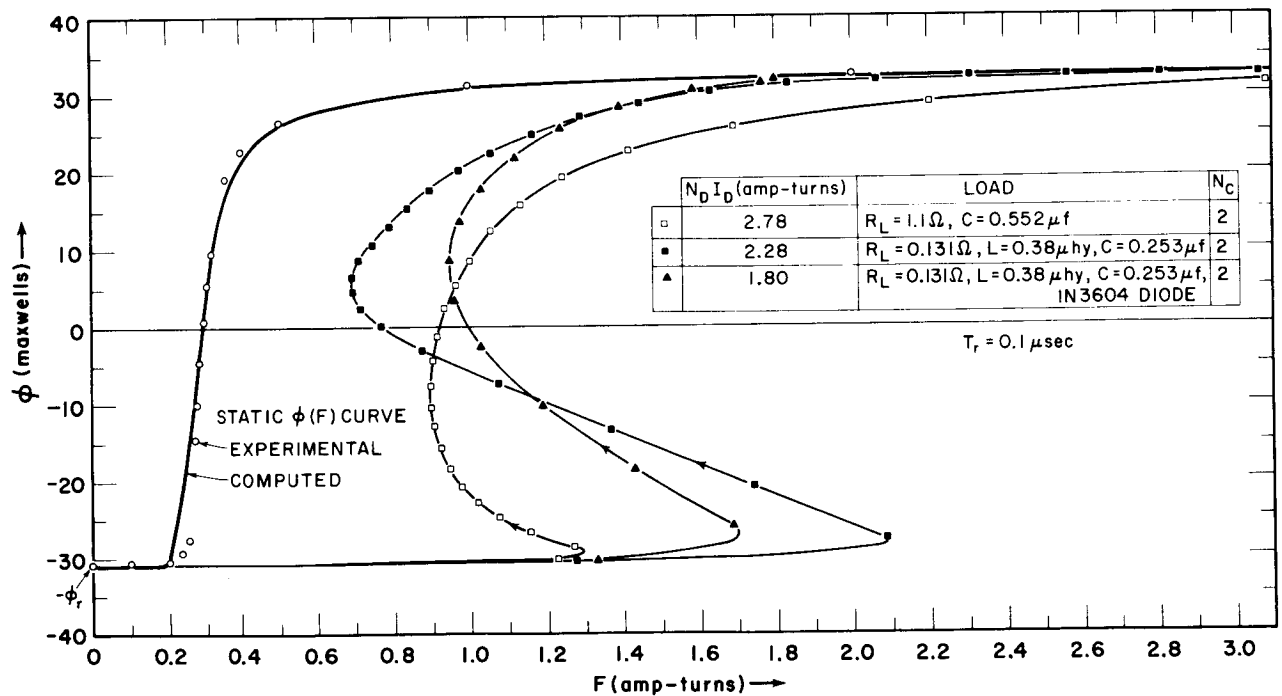
FIG. 16 Concluded





(a) R, R-DIODE, AND R-L LOADS

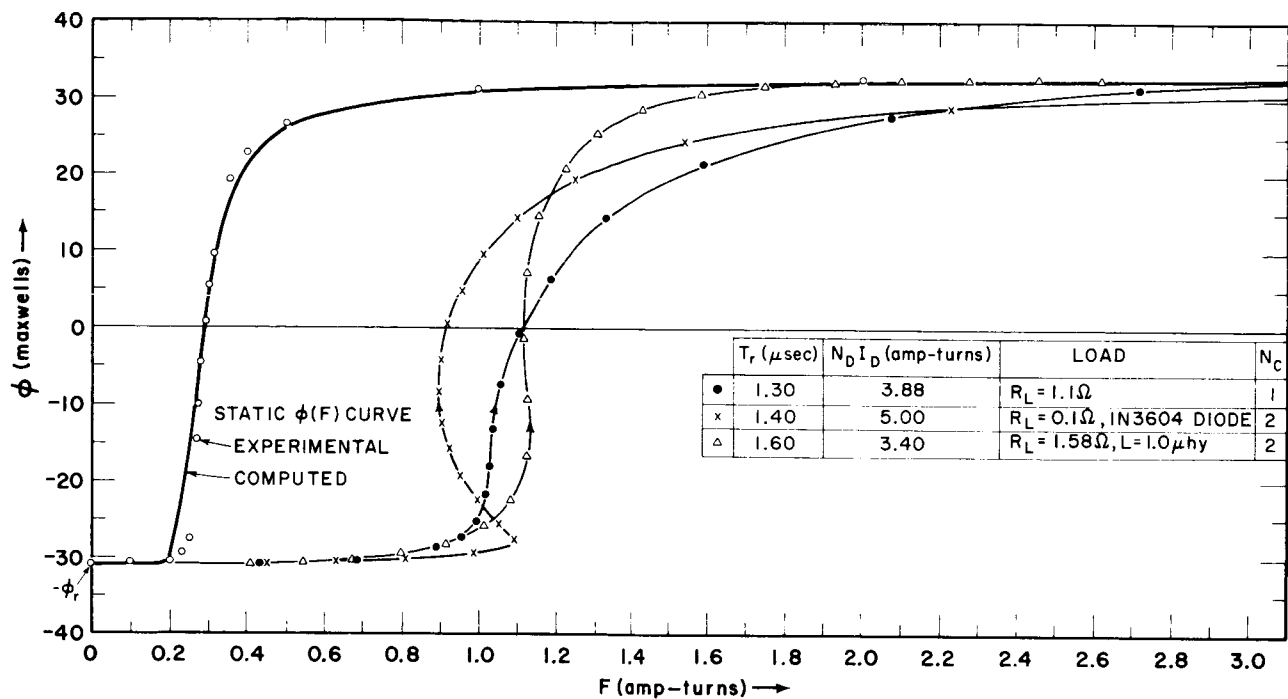
RC-2696-226



(b) R-C, R-L-C, AND R-L-C-DIODE LOADS

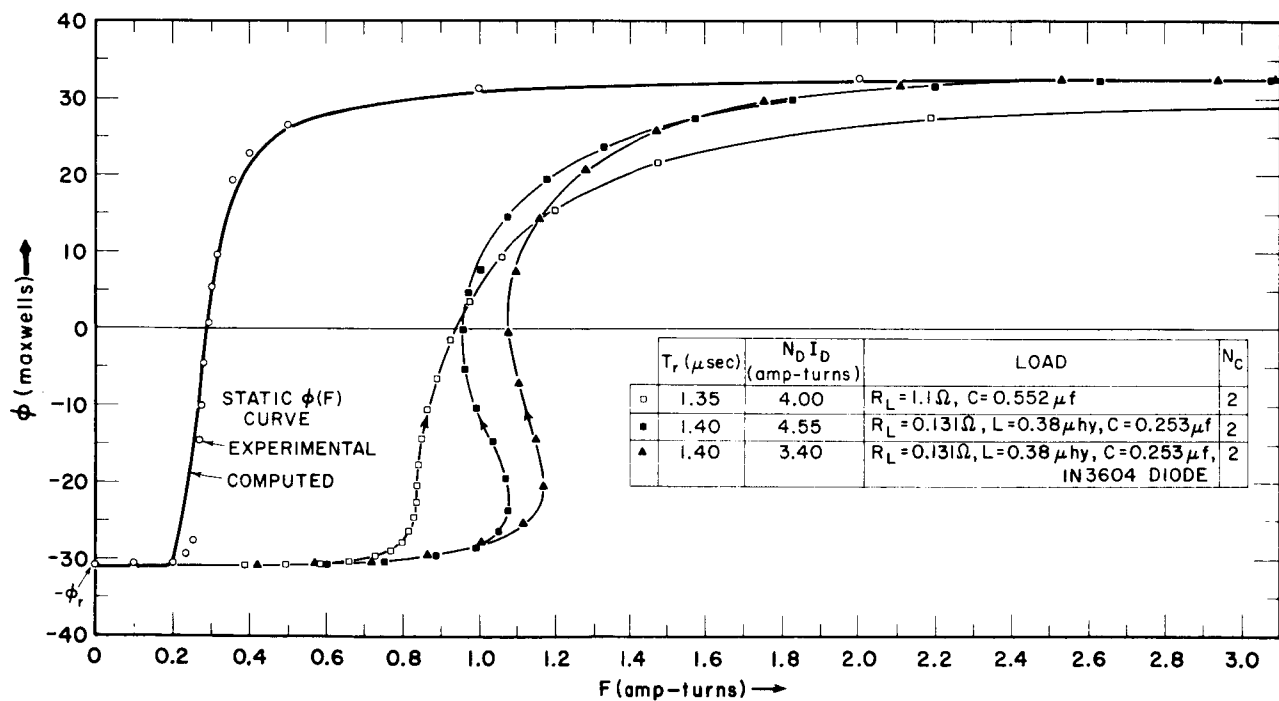
RC-3696-226A

FIG. 17 VARIATIONS OF  $\phi$  vs.  $F$  OF CORE J-1 SWITCHING WITH LOAD AND STEP-F DRIVE (Corresponding to Fig. 15)



(a) R, R-DIODE, AND R-L LOADS

RC-3696-227



(b) R-C, R-L-C, AND R-L-C-DIODE LOADS

RC-3696-227A

FIG. 18 VARIATIONS OF  $\phi$  vs.  $F$  OF CORE J-1 SWITCHING WITH LOAD AND RAMP-F DRIVE (Corresponding to Fig. 16)

results, are constant. However, this fixed time interval may vary among the different cases. Bearing in mind that time appears as a parameter in the  $\phi(F)$  plots in Figs. 17 and 18, note how flux switching takes place in each of the load cases. For the  $R$ - $L$  load [Fig. 17(a)],  $\dot{\phi}(t)$  has a long tail before  $\dot{\phi}$  reaches zero, because the  $\phi(F)$  operating point approaches the static  $\phi(F)$  curve with low excess MMF. On the other hand, for the  $R$ - $C$  load [Fig. 17(b)],  $\dot{\phi}(t)$  falls to zero rapidly, because the excess MMF is relatively high. These observations agree with the computed  $\dot{\phi}(t)$  waveforms in Figs. 15(c) and 15(d).

#### e. INDUCTIVE AND CAPACITIVE LOADS

The effects of the inductive and the capacitive loads shown in Figs. 17 and 18 (discussed above) are typical. An inductive load tends to sustain the load current which, in turn, opposes mainly the latter part of the flux switching. On the other hand, if the load is capacitive, at some instant after  $\phi$  peaks, the capacitor charge becomes large enough to reverse the load current, thus causing the flux switching to become faster compared with a no-load case. The net effect is that  $\dot{\phi}$  peaks early during the switching time for an inductive load, and late during the switching time for a capacitive load [cf. Figs. 15(c) and 15(d)].

#### f. POST-SWITCHING $i_L$

In each of the cases of Figs. 15(d), 15(e), 16(d), and 16(e), the load includes a capacitor, but no diode. In these cases, the load current becomes negative (and helps the drive current to complete the flux switching, as explained above). After switching is terminated, the load current decays exponentially for the  $R$ - $C$  load, and continues to oscillate for the  $R$ - $L$ - $C$  load. Computation of  $i_L$  after the flux switching is terminated is similar to that of a simple linear network, and was omitted from Figs. 15 and 16.

### 5. SUMMARY

A commercial core, loaded by six different combinations of  $R$ ,  $L$ ,  $C$ , and a silicon diode, was first switched by a step drive, and then by a ramp drive. In each case, oscillograms of  $\dot{\phi}(t)$  and load current  $i_L$  (or  $\dot{q}$ ) were photographed. A program for computing  $\dot{\phi}(t)$ ,  $\phi(t)$ ,  $\dot{q}(t)$ , diode voltage, and other time variables, was written, using, in addition to the  $\phi(F, \phi)$  PROCEDURE, the relations

$$\phi_n \approx \phi_{n-2} + 2\Delta t \dot{\phi}_{n-1}, \quad \dot{\phi}_n \approx \dot{\phi}_{n-2} + 2\Delta t \ddot{\phi}_{n-1}, \quad \text{and}$$

$$q_n \approx q_{n-1} + \Delta t (\dot{q}_n + \dot{q}_{n-1})/2$$

as initial approximations, and Newton's equation

$$\dot{q}_{n(j)} = \dot{q}_{n(j-1)} - [f_{n(j)}/f'_{n(j)}]$$

for an iterative solution of the loop equation,  $f = 0$ , during each  $\Delta t$ . Comparisons between experimental and computed  $\dot{\phi}(t)$  and load current waveforms are made in Figs. 15 and 16; in most cases the agreement is within  $\pm 10$  percent. The effect of the load on the net MMF is the formation of an S-shape  $\phi(F)$  path of switching, which is more pronounced for a step drive than for a ramp drive.

## E. CORE-DIODE SHIFT REGISTER

So far, the  $\dot{\phi}$  model [Eqs. (1), (2), and (4)] has been applied to a single core: an unloaded core in Part C, and a loaded core in Part D. We now wish to apply this model to the analysis of one stage of a core-diode shift register. First, the time variables during the switching time will be computed. Second, the flux-gain curves (see Report 1, pp. 67-70) and the ZERO  $\Delta\phi$  will be computed versus  $\Delta\phi_T$  for various amplitudes of drive current.

### 1. OPERATION

#### a. TRANSFER OF INFORMATION

A core-diode shift register circuit is shown in Fig. 19.\* This is a two-clock circuit, in which information in the form of flux change is transferred from left to right. Let us review briefly the bistable operation of this circuit.

Consider the ADVANCE  $O \rightarrow E$  clock phase, during which Core  $O_j$  is a transmitter and Core  $E_j$  is a receiver. [Core  $E_{j-1}$  is a receiver in the previous,  $(j-1)$ th stage.] Assume that Core  $O_j$  is initially either in a

---

\* This particular circuit was selected because this shift register is used in Jet Propulsion Laboratory's Ranger spacecraft.

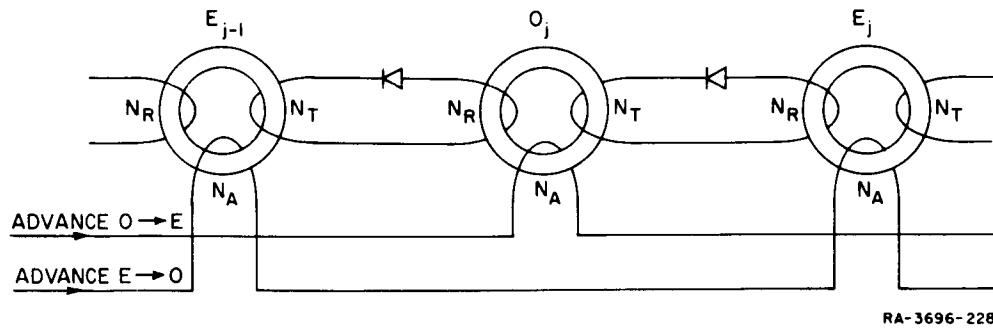


FIG. 19 CORE-DIODE SHIFT-REGISTER CIRCUIT

ZERO ( $\phi = -\phi_r$ ) state or in a ONE ( $\phi = +\phi_r$ ) state, and that Core  $E_j$  and Core  $E_{j-1}$  are initially in a ZERO, or CLEAR, state. An ADVANCE  $O \rightarrow E$  current pulse is applied through a winding with  $N_A$  turns, and drives Core  $O_j$  toward negative saturation. If Core  $O_j$  is initially in a ZERO state, only elastic flux switching results, and the forward loop current is too small to change the state of Core  $E_j$ . On the other hand, if Core  $O_j$  is initially in a ONE state, the resulting inelastic flux switching generates a forward loop current, which is high enough to switch Core  $E_j$  to positive saturation. The back voltage, appearing across the  $N_R$  turns of Core  $O_j$ , should appear primarily across the conducting diode, to prevent spurious setting of Core  $E_{j-1}$  in case the latter receives a ZERO. During the next ADVANCE  $E \rightarrow O$  clock phase, the cores interchange functions: all of the  $E$  cores are transmitters and all of the  $O$  cores are receivers.

#### b. RANGE OF ADVANCE CURRENT

The range of the ADVANCE current (*i.e.*, the tolerance on its amplitude  $I_A$ ) for bistable operation is determined by the following considerations. At the lower boundary of  $I_A$  (that is,  $I_A^{\min}$ ), a ONE drops to ZERO. As discussed on pp. 67-72 of Report 1, at this point the flux gain  $G = \Delta\phi_R/\Delta\phi_T$  vs.  $\Delta\phi_T$  is tangent to the horizontal straight line,  $G = 1$ . The worst case of a ONE dropout (*i.e.*, the maximum value of  $I_A^{\min}$ ) corresponds to a single ONE in the register.

The maximum value of  $I_A$  (that is  $I_A^{\max}$ ), is determined by the back loop current which may cause a cumulative ZERO buildup to ONE during successive clock phases. The worst case of a ZERO buildup (*i.e.*, the minimum value of  $I_A^{\max}$ ) corresponds to a single ZERO in the register.

If the rise time of the drive current were short compared with the switching time of either core, the range of ADVANCE current would be very poor because of a ZERO build-up resulting from a back transfer. This drawback has been overcome by making the drive-current pulse  $i_A(t)$  have a relatively long rise time. The lower the time rate of rise of  $i_A$  is, the lower is the back current  $i_B$ , and hence the smaller is the amount of spurious flux switching in the preceding core. The portion of flux switching taking place while  $i_A(t)$  is not constant in time increases as  $I_A$  increases, until at a certain value of  $I_A$ , all switching is performed under a ramp drive. If  $I_A$  is increased beyond this value, switching terminates during the rise of  $i_A(t)$ , and any further rise of  $i_A(t)$  after switching is completed has no significant effect.

## 2. ANALYSIS

### a. OBJECTIVES

The core-diode shift register circuit will now be analyzed for the case of a transfer of a single ONE in the register. A single ONE is selected as a worst case because no other information pattern in the register can have a lower flux gain. The objective of this analysis is two-fold: first, we wish to compute the variation with time of  $\dot{\phi}$  and  $\phi$  of each core, as well as the loop currents; second, we wish to compute the flux gain  $\Delta\phi_R/\Delta\phi_T$  versus  $\Delta\phi_T$ , as well as the undesired back flux transfer, for different values of load current.

### b. ASSUMPTIONS

The analysis is simplified by the following assumptions:

- (1) The forward characteristic of the diode is represented by a resistance,  $R_d$ , and a constant voltage,  $V_d$ , in series. This equivalent circuit is an alternative representation of the diode function used in Part D, p. 41. (Note that for a given diode, the values of  $R_d$  in the two models are different.) Although less accurate, this alternative model involves parameters that are easier to determine.
- (2) The loop inductance,  $L_\ell$ , is ignored. This assumption is justified by the fact that  $L_\ell di/dt$  is negligible compared with the total  $iR$  drop in the loop.

- (3) During the transfer of a ONE from Core  $O_j$  to Core  $E_j$ , while Core  $E_{j-1}$  receives a ZERO, the back-loop current rises to  $F_{1B}/N_T$ , which is slightly above  $F_d^n/N_T$  (see Fig. 1), and is clamped to this value while a permissible amount of flux is switching spuriously in Core  $E_{j-1}$ . This assumption is justified primarily because of the low rate of switching in Core  $E_{j-1}$  and also because of the lack of any better model for such slow switching.

### c. BASIC EQUATIONS

Based on Assumptions (1) and (2) above, the equivalent circuit for the core-diode shift register of Fig. 19 during the transfer of a single ONE from Core  $O_j$  to Core  $E_j$  would be as shown in Fig. 20. Here,

$$R = R_\ell + R_d \quad (74)$$

where  $R_\ell$  is the inherent loop resistance, and  $R_d$  is the diode resistance.

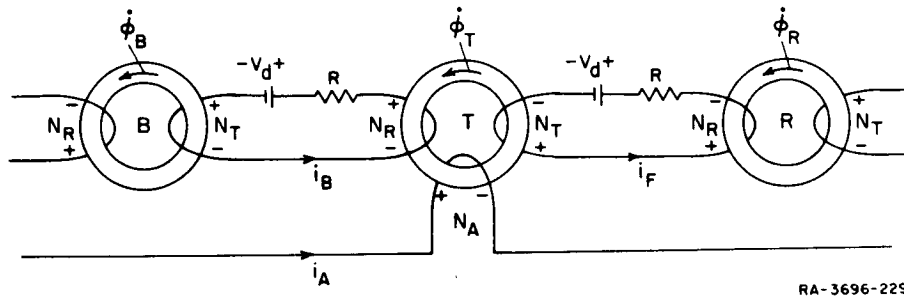


FIG. 20 EQUIVALENT CIRCUIT FOR CORE-DIODE SHIFT REGISTER

Note that Cores  $E_j$ ,  $O_j$ , and  $E_{j-1}$  have been renamed in accordance with their functions:  $R$  (for Receiver),  $T$  (for Transmitter), and  $B$  (for Back receiver). The ADVANCE  $O \rightarrow E$  current pulse is designated by  $i_A$ , and the forward and backward loop currents are designated by  $i_F$  and  $i_B$ , respectively.

Comparing Figs. 20 and 19, note that  $\dot{\Phi}_T$  and  $\dot{\Phi}$  of Core  $O_j$  during ADVANCE  $O \rightarrow E$  are opposite in direction. This change in the reference of  $\dot{\Phi}$  of the transmitter (but not of the receiver) has been introduced in order to be able to use the same  $\dot{\Phi}(F, \phi)$  PROCEDURE in the computation program for both the receiver and the transmitter.

The net amounts of MMF acting on Cores  $T$ ,  $R$ , and  $B$  are as follows:

$$F_T = N_A i_A - N_T i_F - N_R i_B \quad (75)$$

$$F_R = N_R i_F \quad (76)$$

and

$$F_B = N_T i_B \quad (77)$$

Using Eqs. (1), (2), and (4),  $\dot{\phi}_T$  and  $\dot{\phi}_R$  are expressed formally in the following two differential equations:

$$\dot{\phi}_T = \dot{\phi}(F_T, \phi_T) \quad (78)$$

and

$$\dot{\phi}_R = \dot{\phi}(F_R, \phi_R) \quad (79)$$

By inspection of Fig. 20, the two loop equations are

$$N_T \dot{\phi}_T = N_R \dot{\phi}_R + i_F R + V_d \quad (80)$$

and

$$N_R \dot{\phi}_T = N_T \dot{\phi}_B + i_B R + V_d \quad (81)$$

Based on Assumption (3), if  $i_B \lesssim F_{1B}/N_T$ , then  $\dot{\phi}_B = 0$ , and if  $\dot{\phi}_B \neq 0$ , then  $i_B \cong F_{1B}/N_T$ . Therefore, Eq. (81) contains only two unknowns:  $\dot{\phi}_T$  and either  $i_B$  or  $\dot{\phi}_B$ . The seven unknowns  $\dot{\phi}_T$ ,  $\dot{\phi}_R$ ,  $F_T$ ,  $F_R$ ,  $F_B$ ,  $i_F$ , and  $i_B$  (or  $\dot{\phi}_B$ ) can thus be calculated from Eqs. (75) through (81). Note, however, that it is trivial to reduce this set of seven equations into a set of four equations, two of which are differential, and four unknowns:  $\dot{\phi}_T$ ,  $\dot{\phi}_R$ ,  $i_F$ , and  $i_B$  (or  $\dot{\phi}_B$ ).

#### d. MODES OF OPERATION

Equations (75) through (81) are general in the sense that some of the terms may or may not be equal to zero, as we shall see next. For ease in analysis, we divide the operation during the switching time into the following three modes:

*Mode 1*— $\dot{\phi}_T \leq V_d/N_T$ . During the first mode of operation, the bias voltage across the diode,  $V_d$ , is not exceeded by the induced voltage  $N_T \dot{\phi}_T$ , and hence  $i_F = 0$  and  $\dot{\phi}_R = 0$ . Furthermore, because of the requirement for unity flux gain and the fact that there is an inherent flux loss



in the coupling loop,  $N_T$  must exceed  $N_R$ . As a result, also  $N_R \dot{\phi}_T < V_d$ , and hence,  $i_B = 0$  and  $\dot{\phi}_B = 0$ . In other words, Core  $T$  is being switched unloaded.

*Model 2*— $V_d/N_T < \dot{\phi}_T \leq V_d/N_R$ . During the second mode of operation,  $\dot{\phi}_T$  is high enough to unblock only the forward diode; thus,  $i_F > 0$ ,  $i_B = 0$ , and  $\dot{\phi}_B = 0$ . As long as  $i_F \leq F_0''/N_R$ ,  $\dot{\phi}_T$ ,  $i_F$ , and  $F_T$  may be calculated from Eqs. (75), (78), and (80), in which  $i_B = 0$  and  $\dot{\phi}_R = 0$ . If the forward loop current exceeds  $F_0''/N_R$ , Core  $R$  is switching, and  $\dot{\phi}_T$ ,  $\dot{\phi}_R$ ,  $i_F$ ,  $F_T$ , and  $F_R$  are calculated from Eqs. (75), (76), (78), (79), and (80), in which  $i_B = 0$ .

*Model 3*— $V_d/N_R < \dot{\phi}_T$ . During the third mode of operation,  $\dot{\phi}_T$  is high enough to unblock both diodes; that is,  $i_F > 0$  and  $i_B > 0$ . Recalling the condition that either  $0 < i_B < F_{1B}/N_T$  and  $\dot{\phi}_B = 0$ , or  $i_B \approx F_{1B}/N_T$  and  $\dot{\phi}_B \neq 0$ , note that all of the time variables in Eqs. (75) through (81) are positive and can be solved for.

Since  $\dot{\phi}_T$  rises and falls smoothly during the switching time, the modes occur in the following sequence during that time: Mode 1, Mode 2, Mode 3, Mode 2, Mode 1.

Using Eqs. (78) and (79), as we solve for  $\dot{\phi}_T(t)$  and  $\dot{\phi}_R(t)$ , we also solve for  $\phi_T(t)$  and  $\phi_R(t)$ . Also, as we solve for  $\dot{\phi}_B(t)$ , we may evaluate  $\phi_B(t)$ . Knowing the initial values of  $\phi_T$ ,  $\phi_R$ , and  $\phi_B$ , we may thus evaluate at the end of switching the net changes  $\Delta\phi_T$ ,  $\Delta\phi_R$ , and  $\Delta\phi_B$ . Hence, the flux gain

$$G = \frac{\Delta\phi_R}{\Delta\phi_T} \quad (82)$$

can be calculated. The major drawback of this calculation is the use of inadequate models in describing flux switching from a partially set ("soft") state. The properties of this type of switching are discussed in detail in Section III. When models that describe these properties more completely are established, we shall be able to calculate  $G$  more accurately.

### 3. COMPUTATION

#### a. METHOD OF COMPUTATION

Determination of the time increment  $\Delta t$  for the purpose of solving Eqs. (75) through (81) numerically is different from the determination of  $\Delta t$  for a loaded core in two respects: first,  $\tau_s$  is estimated more

accurately by considering the load on the transmitter; second, the  $n$ th  $\Delta t$  is a certain percentage, say 1 percent, of either  $\tau_s$  or  $2\phi_r/\dot{\phi}_{n-1}$ , whichever is smaller. This alternative way of determining  $\Delta t$  leads to a higher accuracy of computation when  $\dot{\phi}$  is relatively high. However, with  $\Delta t$  being a variable, we cannot use Eqs. (43) and (44), and must instead use the less-accurate approximation

$$\phi_n = \phi_{n-1} + \Delta t \dot{\phi}_{n-1} \quad (83)$$

As in the case of the loaded core, we resort to Newton's method of successive approximation, Eq. (58), in order to overcome the problem of diverging oscillations in the numerical solution of  $i_F$ . Also, if the convergence is slow, after a certain number of iterations, the modified Newton's method of approximation, Eq. (58a), is used instead of Eq. (58). Compared with the case of a loaded core, an additional improvement in the use of these methods is made. Here, Eq. (58) or (58a) is applied to solve for either  $x = i_F$  or  $x = \dot{\phi}_T$ , whichever yields a faster convergence.

Writing  $f$  instead of  $f(x)$ , following Eq. (80),

$$f = N_T \dot{\phi}_T - N_R \dot{\phi}_R - R i_F - V_d = 0 \quad (84)$$

During Mode 2,  $F_T = N_A i_A - N_T i_F$  and  $F_R = N_R i_F$ . Differentiating Eq. (84) with respect to  $i_F$  gives

$$f'_A \equiv \frac{df}{di_F} \approx -(N_T^2 \dot{\phi}'_T + N_R^2 \dot{\phi}'_R + R) \quad (85)$$

where  $\dot{\phi}'_T = \partial \dot{\phi}_T / \partial F_T$  and  $\dot{\phi}'_R = \partial \dot{\phi}_R / \partial F_R$ . Differentiating Eq. (84) with respect to  $\dot{\phi}_T$  gives

$$f'_B \equiv \frac{df}{d\dot{\phi}_T} \approx N_T + \frac{R + N_R^2 \dot{\phi}'_R}{N_T \dot{\phi}'_T} \quad (86)$$

Equations (85) and (86) also hold in Mode 3 if  $i_B = F_{1B}/N_T = \text{constant}$ , in which case,  $\dot{\phi}_B > 0$ . However, if  $\dot{\phi}_B = 0$ , then  $i_B$  is a function of time, varying between 0 and  $F_{1B}/N_T$ , and the differentiation of  $f$ , Eq. (84), should include the contribution due to  $i_B$ . Using Eqs. (75), (80), and (81), we get

$$F_T = N_A i_A + \frac{N_R}{R} \left(1 - \frac{N_R}{N_T}\right) V_d - \left(N_T + \frac{N_R^2}{N_T}\right) i_F - \frac{N_R^3}{N_T R} \dot{\phi}_R \quad (87)$$

Under this condition, differentiation of Eq. (84) with respect to  $i_F$  gives

$$f'_A \equiv \frac{df}{di_F} \approx - \left[ \left( N_T^2 + N_R^2 + \frac{N_R^4 \dot{\phi}_R'}{R} \right) \dot{\phi}_T' + N_R^2 \dot{\phi}_R' + R \right] \quad (88)$$

and differentiation of Eq. (84) with respect to  $\dot{\phi}_T$  gives

$$f'_B \equiv \frac{df}{d\dot{\phi}_T} \approx N_T + \frac{N_T(R + N_R^2 \dot{\phi}_R')}{\dot{\phi}_T' \left( N_T^2 + N_R^2 + \frac{N_R^4 \dot{\phi}_R'}{R} \right)} \quad (89)$$

Thus, if  $|f'_A| < (R/N_T)|f'_B|$ , then  $f'_B$  should be used in order to solve Eq. (84) for  $\dot{\phi}_T$ ; otherwise,  $f'_A$  should be used in solving Eq. (84) for  $i_F$ . This provision of a choice between  $f'_A$  and  $f'_B$  is effective if  $\dot{\phi}_T(t)$  and  $i_F(t)$  do not peak at the same time.

Following the previous analysis, the computation is performed in each mode of operation separately. Mode selection for an  $n$ th  $\Delta t$  is determined initially by comparing the value of  $\dot{\phi}_{T(n-1)}$  with  $V_d/N_T$  and  $V_d/N_R$ . For a given  $\Delta t$ , the results of normal computation must satisfy the following two conditions before proceeding to a new  $\Delta t$ :

- (1) Computation of  $i_F$  or  $\dot{\phi}_T$  has converged.
- (2) The resulting value of  $\dot{\phi}_{Tn}$  falls in the same mode of operation that is initially assumed.

Regardless of whether convergence has been achieved or not, if Condition (2) has not been satisfied for a given  $\Delta t$ , the resulting values of the time variables are disregarded, except for  $\dot{\phi}_T$  which is used only to determine in what mode of operation the computation of these variables should begin all over again. Following actual circuit behavior, such mode switching may only occur between Modes 1 and 2 or between Modes 2 and 3; switching between Modes 1 and 3 is forbidden. This restriction will also help to dampen any computational oscillations due to improper selection of mode of operation. Just in case the switching from mode to mode becomes oscillatory, the executions of mode switching should be limited to

a certain number, e.g., six. In this case, computation is assumed to have failed to converge, and should be registered as such. Another case for which convergence is assumed to have failed is when Condition (2) is satisfied, but Condition (1) is not satisfied in a single mode within a certain number of iterations, e.g., twenty.

#### b. COMPUTER PROGRAM

A computer program for the core-diode shift register is given in Appendix E, and is based on the following steps:

- (1) Declare all identifiers (core parameters, circuit parameters, time variables, etc.), input-output lists and formats, and PROCEDURES to be used in the program, in accordance with the rules of the ALGOL-60 language.
- (2) Set initial values for the core and circuit parameters.

The following steps are performed for various values of  $I_A$ , each of which is repeated for various values of initial transmitter flux,  $\phi_{T0}$ :

- (3) Set initial values for all time variables.
- (4) Compute an approximate value for  $\tau_s$ , using the relation\*

$$\tau_s \approx \frac{(\phi_r - \phi_{T0}) \left( \frac{N_T^2}{R + 0.6\rho_p N_R^2} + \frac{N_R^2}{R} + \frac{1.67}{\rho_p} \right)}{N_A I_A - F_0 + \frac{N_T(V_d - 0.6\rho_p N_R F_0)}{R + 0.6\rho_p N_R^2} + \frac{V_d N_R}{R}} \quad (90)$$

- (5) Compute the initial time  $t_0$ , at which  $N_A i_A$  reaches  $F_0''$  and switching starts.

The following steps are performed for every  $\Delta t$  during the switching time:

---

\* Equation (90) is obtained by applying the rough approximations  $\dot{\phi}_T \approx \bar{\rho}(F_T - F_0)$  and  $\dot{\phi}_R \approx \bar{\rho}(F_R - F_0)$ , where  $\bar{\rho} \approx 0.6\rho_p$ , to Eqs. (75), (76), (80), and (81), and from the relation  $\Delta\phi_T = \phi_r - \phi_{T0}$ .

- (6) Compute a time increment, using the relation

$$\Delta t_n = 0.005 \min [\tau_s, (\phi_r - \phi_{T0}) / |\dot{\phi}_{T(n-1)}|],$$

and then compute  $t_n = t_{n-1} + \Delta t_n$ .

- (7) Compute  $i_{An} = i_A(t_n)$ , where  $i_A(t)$  is a separate PROCEDURE for the drive current, given in Appendix B.
- (8) Compute a first approximation for  $i_{Fn}$ , using a relation similar to Eq. (83), i.e.,

$$i_{Fn(0)} = i_{F(n-1)} + \Delta t \frac{\Delta i_{F(n-1)}}{\Delta t_{n-1}}.$$

- (9) Using the  $\dot{\phi}_T$  value,\* select the mode of operation according to the following criteria:

If  $\dot{\phi}_T \leq V_d/N_T$ , then go to Mode 1.

If  $V_d/N_T < \dot{\phi}_T \leq V_d/N_R$ , then go to Mode 2.

If  $V_d/N_R < \dot{\phi}_T$ , then go to Mode 3.

The computation proceeds in only one of the following three modes.†

- (10) Compute in the one of the following modes selected in Step 9:

- (a) Mode 1—Compute the following:

$$\Delta i_{Fn} = i_{Fn} = i_{Bn} = 0$$

$$F_{Rn} = 0$$

$$F_{Tn} = N_A i_{An}$$

$$\dot{\phi}_{Tn} = \dot{\phi}[F_{Tn}, \phi_{T(n-1)}]$$

$$\dot{\phi}_{Rn} = \dot{\phi}[F_{Rn}, \phi_{R(n-1)}] = 0$$

$$\phi_{Tn} = \phi_{T(n-1)} + \Delta t_n \dot{\phi}_{Tn}$$

$$\phi_{Rn} = \phi_{R(n-1)}.$$

\* Initially,  $\dot{\phi}_T = \dot{\phi}_{T(n-1)}$ . In case Condition (2) has not been satisfied,  $\dot{\phi}_T$  is equal to the last iterative value of  $\dot{\phi}_{T(j)}$ .

† Iterative variables in each mode are designated by  $(j-1)$  or  $(j)$ , depending upon whether their values have been computed during the previous iteration or during the present iteration. Values computed for the second time within one iteration are denoted by prime, e.g.,  $(j-1')$  or  $(j')$ . For simplicity, the subscript  $n$  is deleted, e.g.,  $\dot{\phi}_{Tn(j)}$  is abbreviated to  $\dot{\phi}_{T(j)}$ .

If  $\dot{\phi}_{Tn} = 0$  and  $\phi_{Tn} > 0$ ,\* then discontinue computation.

If  $\dot{\phi}_{Tn} > V_d/N_T$ , then go to Mode 2.

- (b) Mode 2—If convergence has not been achieved, within five iterations, use Eq. (58a) instead of Eq. (58). Compute the following:

$$\begin{aligned} i_{Bn} &= 0 \\ F_{T(j)} &= N_A i_{An} - N_T i_{F(j-1)} \\ F_{R(j)} &= N_R i_{F(j-1)} \\ \dot{\phi}_{T(j)} &= \dot{\phi}[F_{T(j)}, \phi_{T(j-1)}] \\ \dot{\phi}_{R(j)} &= \dot{\phi}[F_{R(j)}, \phi_{R(j-1)}] \\ \phi_{T(j)} &= \phi_{T(n-1)} + \Delta t_n \dot{\phi}_{T(j)} \\ \phi_{R(j)} &= \phi_{R(n-1)} + \Delta t_n \dot{\phi}_{R(j)} \\ f_{(j)} &= N_T \dot{\phi}_{T(j)} - N_R \dot{\phi}_{R(j)} - R i_{F(j-1)} - V_d \\ f'_{A(j)} &= -(N_T^2 \dot{\phi}'_{T(j)} + N_R^2 \dot{\phi}'_{R(j)} + R) \\ f'_{B(j)} &= N_T + [(R + N_R^2 \dot{\phi}'_{R(j)})/N_T \dot{\phi}'_{T(j)}] \end{aligned}$$

If  $|f'_{A(j)}| < (R/N_T) |f'_{B(j)}|$ , then

$$\begin{aligned} \Delta \dot{\phi}_{T(j)} &= -f_{(j)}/f'_{B(j)} \\ \dot{\phi}_{T(j')} &= \dot{\phi}_{T(j)} + \Delta \dot{\phi}_{T(j)} \\ \Delta i_{F(j)} &= N_T \dot{\phi}_{T(j')}/R \\ i_{F(j)} &= [N_T \dot{\phi}_{T(j')} - N_R \dot{\phi}_{R(j)} - V_d]/R \end{aligned}$$

If  $|\Delta \dot{\phi}_{T(j)}| > 0.001 |\dot{\phi}_{(j')}|$  and the number of iterations is less than 20, repeat the computation steps of Mode 2.

---

\* The provision of  $\phi_T > 0$  allows computation for  $-\phi_r \leq \phi_{T0} \leq 0$  to continue in case the point  $(F''_0, \phi_{T0})$  is inside the static  $\phi(F)$  loop.

If  $|f'_{A(j)}| \geq (R/N_T)|f'_{B(j)}|$ , then

$$\Delta i_{F(j)} = -f_{(j)}/f'_{A(j)}$$

$$i_{F(j)} = i_{F(j-1)} + \Delta i_{F(j)}$$

If  $|\Delta i_{F(j)}| > 0.001|i_{F(j)}|$  and the number of iterations is less than 20, repeat the computation steps of Mode 2.

If  $V_d/N_T \geq \dot{\phi}_T$  or  $\dot{\phi}_T > V_d/N_R$ , then reset the final  $i_{F(j)}$  to  $i_{F(n-1)}$ , and go to Step (9).

(c) Mode 3—If convergence has not been achieved, within five iterations, use Eq. (58a) instead of Eq. (58). Compute the following:

$$F_{R(j)} = N_R i_{F(j)}$$

$$\dot{\phi}_{R(j)} = \dot{\phi}[F_{R(j)}, \phi_{R(j-1)}]$$

$$\Delta i_{B(j)} = \max \{0, \min [(N_R \dot{\phi}_{T(j-1)} - V_d)/R, F_{1B}/N_T] \} - i_{B(j-1)}$$

$$i_B = i_{B(j-1)} + \begin{cases} \Delta i_{B(j)} & \text{if the number of iterations is less than 5} \\ 0.5 \Delta i_{B(j)} & \text{otherwise} \end{cases}$$

$$F_{T(j)} = N_A i_{An} - N_T i_{F(j-1)} - N_R i_{B(j)}$$

$$\dot{\phi}_{T(j)} = \dot{\phi}[F_{T(j)}, \phi_{T(j-1)}]$$

$$\phi_{T(j)} = \phi_{T(n-1)} + \Delta t_n \dot{\phi}_{T(j)}$$

$$\phi_{R(j)} = \phi_{R(n-1)} + \Delta t_n \dot{\phi}_{R(j)}$$

$$f_{(j)} = N_T \dot{\phi}_{T(j)} - N_R \dot{\phi}_{R(j)} - R i_{F(j-1)} - V_d$$

$$f'_{A(j)} = \begin{cases} -[N_T^2 \dot{\phi}'_{T(j)} + N_R^2 \dot{\phi}'_{R(j)} + R] & \text{if } i_{B(j)} = F_{1B}/N_T \\ -\left[ \left( N_T^2 + N_R^2 + \frac{N_R^4 \dot{\phi}'_{R(j)}}{R} \right) \dot{\phi}'_{T(j)} + N_R^2 \dot{\phi}'_{R(j)} + R \right] & \text{otherwise} \end{cases}$$

$$f'_{B(j)} = \begin{cases} N_T + \frac{R + N_R^2 \dot{\phi}'_{R(j)}}{N_T \dot{\phi}'_{T(j)}} & \text{if } i_{B(j)} = F_{1B}/N_T \\ N_T + N_T \frac{R + N_R^2 \dot{\phi}'_{R(j)}}{\dot{\phi}'_{T(j)} \left[ N_T^2 + N_R^2 + \frac{N_R^4 \dot{\phi}'_{R(j)}}{R} \right]} & \text{otherwise} \end{cases}$$

If  $|f'_{A(j)}| < (R/N_T) |f'_{B(j)}|$ , then

$$\Delta \dot{\phi}_{T(j)} = -f_{(j)}/f'_{B(j)}$$

$$\dot{\phi}_{T(j')} = \dot{\phi}_{T(j)} + \Delta \dot{\phi}_{T(j)}$$

$$\Delta i_{F(j)} = N_T \Delta \dot{\phi}_{T(j)}/R$$

$$i_{F(j)} = [N_T \dot{\phi}_{T(j)} - N_R \dot{\phi}_{R(j)} - V_d]/R$$

If  $|\Delta \dot{\phi}_{T(j)}| > 0.001 |\dot{\phi}_{T(j)}|$  and the number of iterations is less than 20, repeat the computation steps of Mode 3.

If  $|f'_{A(j)}| \geq (R/N_T) |f'_{B(j)}|$ , then

$$\Delta i_{F(j)} = -f_{(j)}/f'_{A(j)}$$

$$i_{F(j)} = i_{F(j-1)} + \Delta i_{F(j)}$$

If  $|\Delta i_{F(j)}| > 0.001 |i_{F(j)}|$  and the number of iterations is less than 20, repeat the computation steps of Mode 3.

If  $V_d/N_R \geq \dot{\phi}_T$ , then reset the final  $i_{F(j)}$  to  $i_{F(n-1)}$ , and go to Mode 2.

(11) Compute  $\dot{\phi}_B$  and  $\phi_B$

$$\dot{\phi}_{Bn} = \begin{cases} (N_R \dot{\phi}_{Tn} - V_d - i_{Bn} R)/N_T & \text{if } i_{Bn} = F_{1B}/N_T \\ 0 & \text{if } i_{Bn} < F_{1B}/N_T \end{cases}$$

$$\phi_{Bn} = \phi_{B(n-1)} + \Delta t_n \dot{\phi}_{Bn}$$



- (12)\* Print time-variable output,  $(t, \phi_T, \phi_R, \dot{\phi}_T, \dot{\phi}_R, \psi_{dT}, \psi_{dR}, F_T, F_R, i_F, i_B, i_{An}, \phi_B,$  and the number of iterations per  $\Delta t$ ) once every (say) 5  $\Delta t$ 's.
- (13) Compute flux changes:
- $$\Delta \phi_B = \phi_{Bn, final} + \phi_r$$
- $$\Delta \phi_T = \phi_{Tn, final} - \phi_{T0}$$
- $$\Delta \phi_R = \phi_{Rn, final} - \phi_{R0}$$
- (14) Compute flux gain:
- $$G = \Delta \phi_R / \Delta \phi_T$$
- (15) Print over-all output ( $\Delta \phi_T / 2 \phi_r, G, \Delta \phi_B / 2 \phi_r,$  total number of iterations, total number of  $\Delta t$ 's, total number of failures to converge, and total number of times  $f'_B$  has been used).

#### 4. COMPUTED AND EXPERIMENTAL RESULTS

##### a. CORE AND CIRCUIT PARAMETERS

A 5-bit core-diode shift register, Fig. 19, was built using the following components:

##### *Core*

Lockheed 145SC1 ferrite core ( $OD = 145$  mils,  $ID = 90$  mils,  $h = 70$  mils). The parameters of this core are the same as those of Core J-1 in Table I, p. 23, except that  $\phi_r = 30$  maxwells and  $\phi_s = 32.40$  maxwells.

##### *Circuit*

Number of turns:  $N_A = 4$ ;  $N_T = 10$ ;  $N_R = 4$

Loop resistance:  $R_\ell = 0.06$  ohm

Diode: Fairchild, FD 600 ,

$R_d = 0.850$  ohm ,

$V_d = 0.75$  volt .

---

\* If the objective is to compute only the flux gain and  $\Delta \phi_B$  versus  $\Delta \phi_T$ , with  $I_A$  as a parameter, then printing of the time variables, Step (12), should be eliminated.

#### Drive Current

Rise time:  $T_r \approx 2.5$  microseconds

Amplitude:  $I_A$  is variable

Pulse width: Approximately 30 microseconds

An empirical expression for the waveform of the drive current, in which  $t$  is in units of second, is as follows:

$$i_A(t) = \begin{cases} [1 - 0.6147(t \cdot 10^6 - 3)^2]I_A & \text{If } 2.458 \cdot 10^{-6} < t < 3 \cdot 10^{-6} \\ \min [0.1356(t \cdot 10^6)^2, 1]I_A & \text{otherwise} \end{cases} \quad (91)$$

Equation (91) is used to write PROCEDURE  $i_A(t)$  in Appendix B.

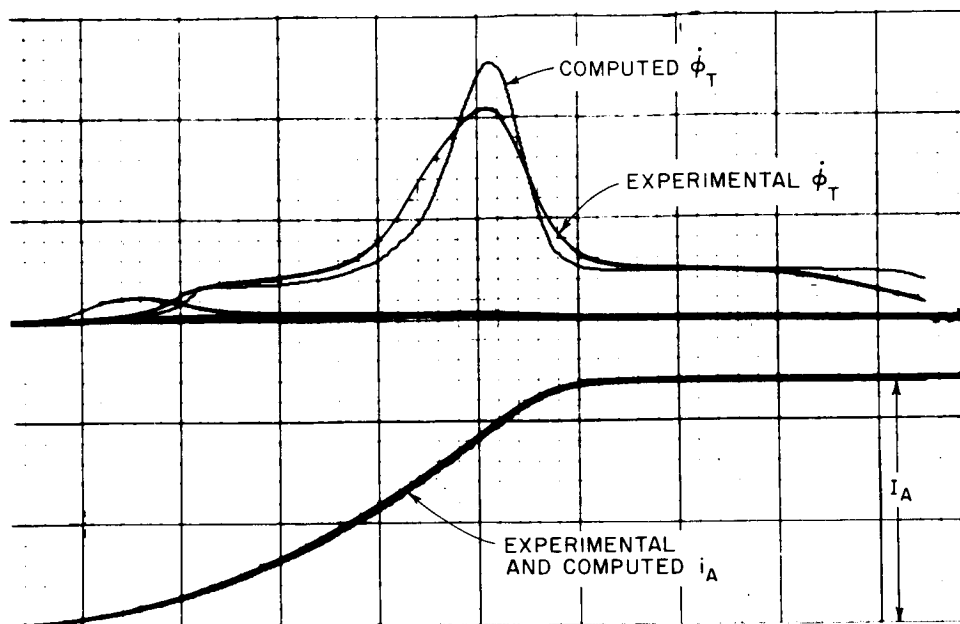
#### b. COMPARISON OF COMPUTED AND EXPERIMENTAL TIME VARIABLES

The computed time variables were plotted automatically, and are compared with experimental oscillograms for  $I_A = 1.18$  ampere in Fig. 21. These include  $\dot{\phi}(t)$ ,  $i_A(t)$ ,  $\dot{\phi}_R(t)$ ,  $\dot{\phi}_B(t)$ , and  $i_F(t)$ . The computed waveforms were plotted from part of the output of the computer program, Appendix E, in which the above core and circuit parameters were used. The computation was performed on a Burroughs B-5000 computer, and the automatic plotting was done on a CalComp, Model 570, plotter. Computation time was less than 3 minutes, including 70 seconds of compiling time (if automatic plotting was excluded, the overall computation time was reduced to one minute).

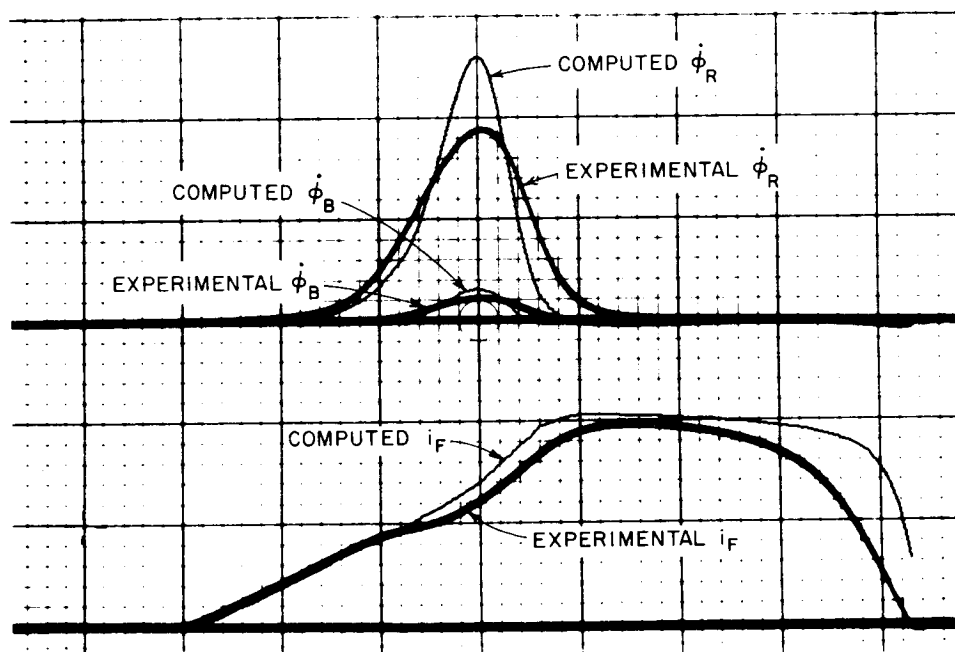
### 5. DISCUSSION

#### a. VALIDITY OF COMPUTATION

The agreement between the computed and the experimental waveforms of  $\dot{\phi}_T(t)$ ,  $\dot{\phi}_R(t)$ ,  $\dot{\phi}_B(t)$ , and  $i_F(t)$  is as expected. The peak values of the computed  $\dot{\phi}_T$  and  $\dot{\phi}_R$  are higher than the respective experimental values by about 18 percent. This difference is attributed to the values of  $\lambda$  and  $\rho_p$  used in the computation. These values had been obtained by switching an unloaded core with a step drive. As explained in Part C-4, ramp- $F$  switching is described better by lower values of  $\lambda$  and  $\rho_p$ .



(a)  $\dot{\phi}_T(t)$  AND  $i_A(t)$



(b)  $\dot{\phi}_R(t)$ ,  $\dot{\phi}_B(t)$ , AND  $i_F(t)$

RB-3696-230

FIG. 21 EXPERIMENTAL AND COMPUTED TIME VARIABLES IN A CORE-DIODE SHIFT REGISTER WITH A SINGLE ONE ( $I_A = 1.18$  ampere)

Time scale =  $0.5 \mu\text{sec}/\text{major div.}$ ;  $\dot{\phi}_R$  and  $\dot{\phi}_B$  scale =  $0.5 (\text{volt/turn})/\text{major div.}$ ;  
 $i_A$  scale =  $0.5 \text{ ampere}/\text{major div.}$ ;  $i_F$  scale =  $0.2 \text{ ampere}/\text{major div.}$ ;  
 $\dot{\phi}_T$  scale =  $0.25 (\text{volt/turn})/\text{major div.}$

b. VARIATION OF  $\phi$  VS.  $F$  DURING SWITCHING TIME

We can use another portion of the computation output in order to plot the variations of  $\phi_T(F_T)$  and  $\phi_R(F_R)$  during switching time, superimposed on the static  $\phi(F)$  curve. Such plots are shown in Fig. 22, in which consecutive numbers are added in order to represent time in a parametric form. Note, however, that since  $\Delta t$  is not fixed, the time intervals between *different* pairs of numbers on the  $\phi_T(F_T)$  and  $\phi_R(F_R)$  plots are not necessarily the same.

c. FLUX-GAIN CURVES

The computer program in Appendix E was modified slightly by eliminating the output printing of the time variables for the purpose of computing the flux-gain curves only. In this way, computation time was reduced, and only essential data were recorded. The resulting plots of computed flux-gain *vs.* normalized  $\Delta\phi_T$ , with  $I_A$  as a parameter, are shown in Fig. 23, where the computed points are marked by small circles. The computation for these plots was restricted to  $-\phi_r \leq \phi_{T0} \leq 0$ .

d. RANGE OF BISTABLE OPERATION

As was pointed out on pp. 70-71 of Report 1, the lower boundary of the drive-current range corresponds to a *maximum* point where  $G$  *vs.*  $\Delta\phi_T$  is tangent to the horizontal straight line  $G = 1$ . This maximum point is designated by the letter  $B$  in Fig. 23. It is thus predicted that  $I_A^{\min} = 0.565$  ampere, and that when a ONE drops to ZERO,  $\Delta\phi_T = \Delta\phi_R = 0.88 \cdot (2\phi_r) = 52.8$  maxwells. These predictions have been found to agree with experimental observation.

Recall that a single-ONE information pattern is assumed in the analysis. The flux change in Core  $B$ ,  $\Delta\phi_B$ , is thus an undesired ZERO level. Plots of computed  $\Delta\phi_B/2\phi_r$  *vs.*  $\Delta\phi_T/2\phi_r$ , with  $I_A$  as a parameter, are shown in Fig. 24, where computed points are indicated by small circles. Note that  $\Delta\phi_B = 0$  for  $I_A \leq 0.50$  ampere.

In Fig. 23, the points where the  $G$  *vs.*  $\Delta\phi_T/2\phi_r$  curves intersect the horizontal straight line  $G = 1$ , correspond to *stable* ONE states, and are marked by  $x$ 's. The value of  $\Delta\phi_T$  at each of these points is the amount of flux change representing a stable ONE. From the values of  $I_A$  and  $\Delta\phi_T/2\phi_r$  of each of these stable points, one can easily determine the corresponding points on the plots of  $\Delta\phi_B/2\phi_r$  *vs.*  $\Delta\phi_T/2\phi_r$ , as marked by  $x$ 's in Fig. 24.

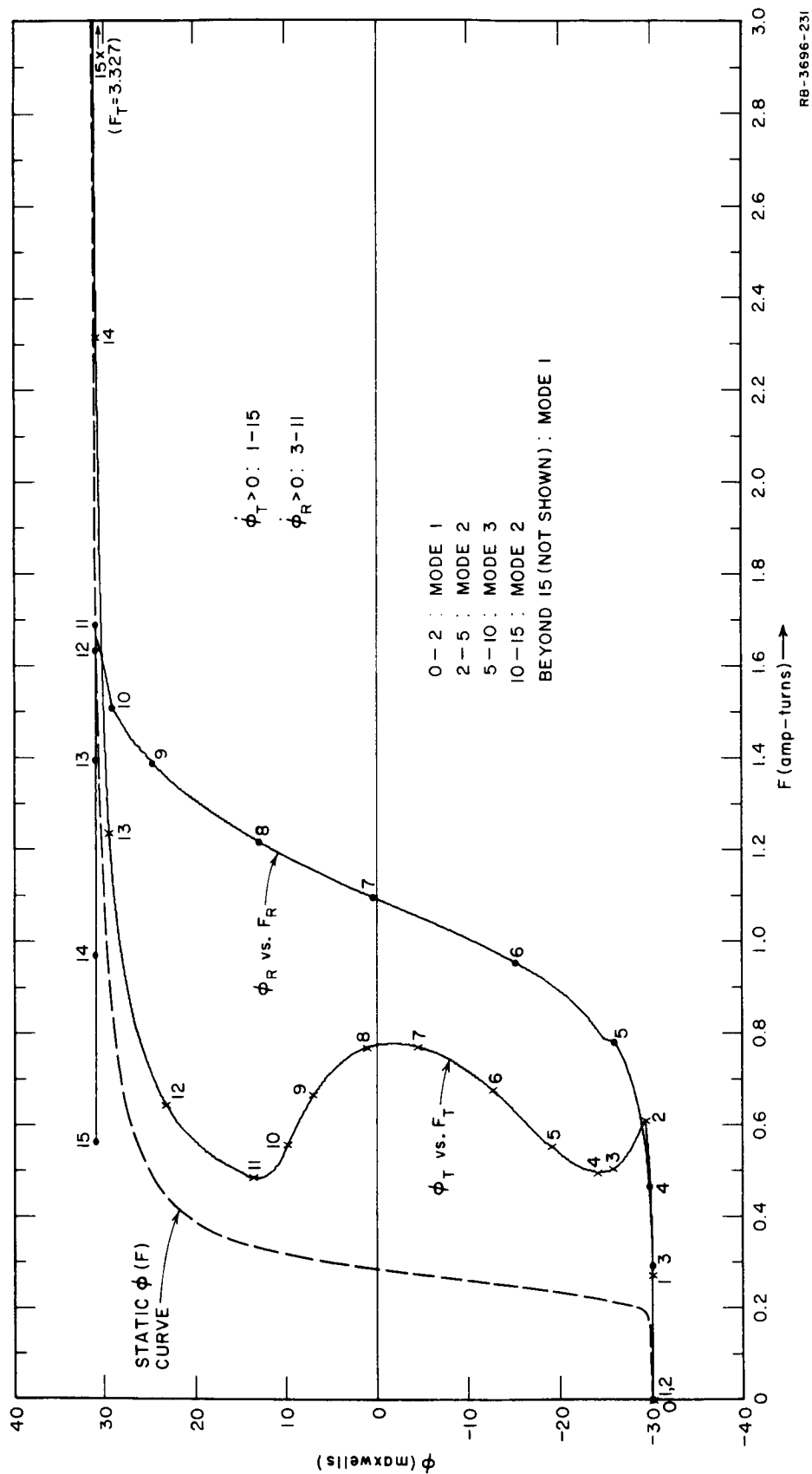
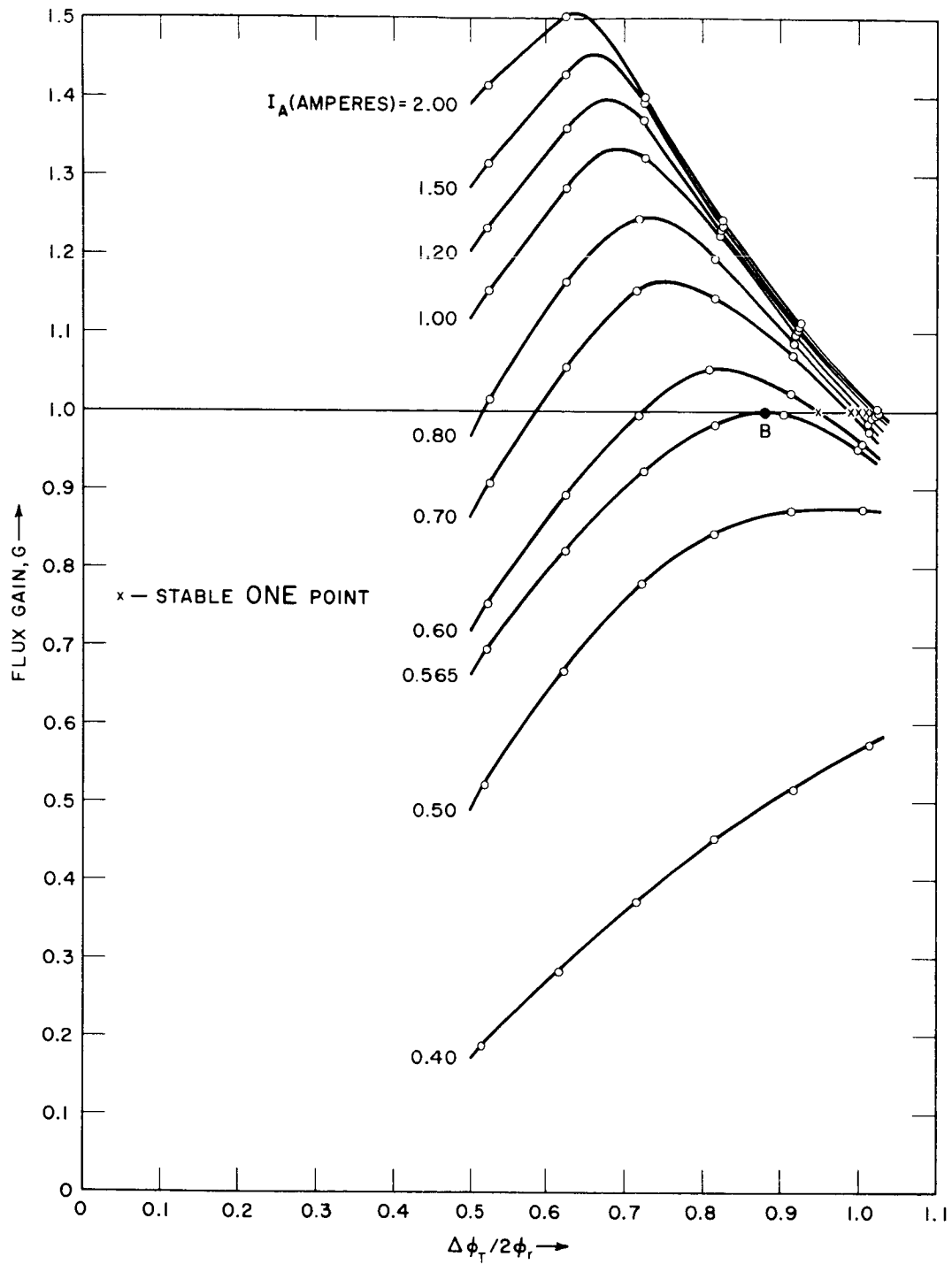
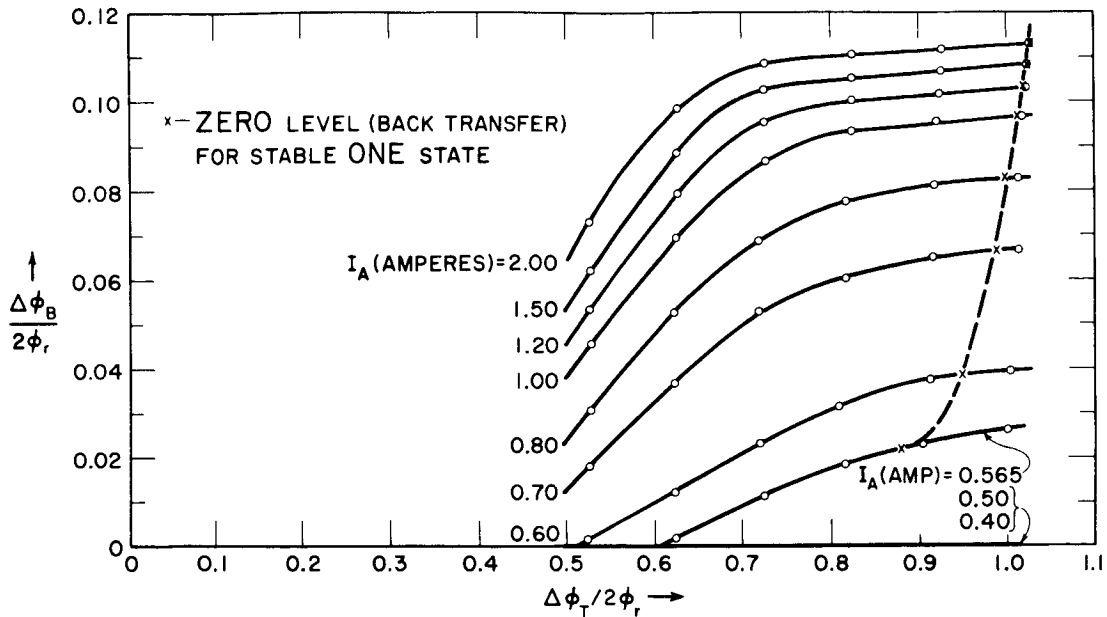


FIG. 22 VARIATIONS OF  $\phi_T(F_T)$  AND  $\phi_R(F_R)$  IN A CORE-DIODE SHIFT REGISTER  
(Corresponding to Fig. 21)



RC-3696-232

FIG. 23 FLUX-GAIN CURVES OF A CORE-DIODE SHIFT REGISTER WITH A SINGLE ONE



RB-3696-233

FIG. 24 BACK FLUX TRANSFER IN A CORE-DIODE SHIFT REGISTER WITH A SINGLE ONE

The value of  $\Delta\phi_B$  of each of these points is the amount of flux change representing the level of a stable ZERO due to back transfer. For example, if  $I_A$  varies from 0.6 ampere to 0.8 ampere to 2.0 ampere, then  $\Delta\phi$  representing a stable ONE varies from 95 to 100 to 102.6 percent of  $2\phi_r$ , and  $\Delta\phi$  representing a stable ZERO varies from 3.85 to 8.3 to 11.3 percent of  $2\phi_r$ , where  $2\phi_r = 60$  maxwells.

As can be seen from Fig. 69 on p. 71 of Report 1, a ZERO buildup to ONE corresponds to a *minimum* point where  $G$ . vs.  $\Delta\phi_T$  is tangent to the horizontal line  $G = 1$ . We have not computed this point because of the lack of proper models for switching from partially set states.

#### e. INFORMATION PATTERN

So far we have assumed a single-ONE information pattern in the shift register, which is the worst case that should be considered in order to compute the maximum  $I_A^{\min}$ . For computation of  $I_A^{\max}$ , which is beyond the scope of this report, a single-ZERO pattern should be considered.

Let us consider now the effects of a ONE transfer in each of the neighboring stages on the flux switching of the transmitter-receiver pair

under investigation. As shown in Fig. 20, the voltage  $N_T \dot{\phi}_R$  blocks the diode of the following stage regardless of whether a ZERO or a ONE is transferred in the following register stage. Hence, the analysis of a single-ONE case is also valid for the case in which a ONE is transferred in the following stage.

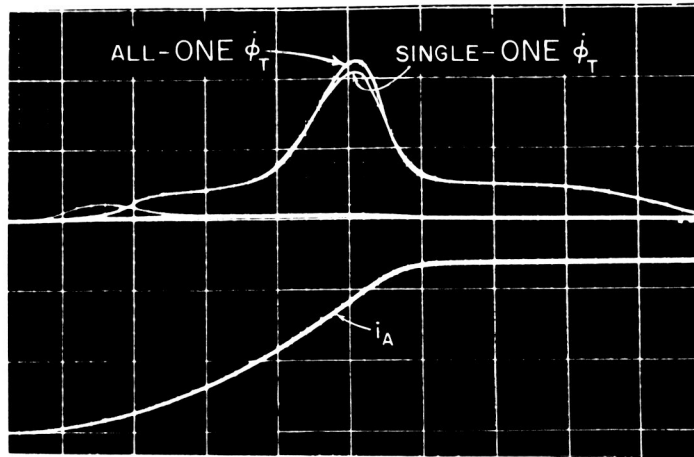
Now, suppose that Core B receives a ONE. The induced voltage,  $N_T \dot{\phi}_B$ , will similarly block the diode between Core B and Core T. In this case,  $i_B = 0$ , and Mode 3 does not exist. Although this case is easier to analyze than the single-ONE case, there is no practical need for analyzing it for the following reason. The back-loop current in the single-ONE case has been found to be negligible, i.e., varying from zero to around  $F_d^n/N_T$ . Hence, the flux transfer in the preceding stage has only a second-order effect on the flux switching in the stage under investigation.

In conclusion, the analysis and computation of the single-ONE case may be regarded as applicable to any other information pattern other than the all-ZERO case. In order to illustrate this point, experimental waveforms of  $\phi_T(t)$ ,  $i_A(t)$ ,  $\phi_R(t)$ , and  $i_F(t)$  in the single-ONE and all-ONE cases are compared in Fig. 25. Although representing two extreme cases of information pattern, these waveforms are quite close to each other.

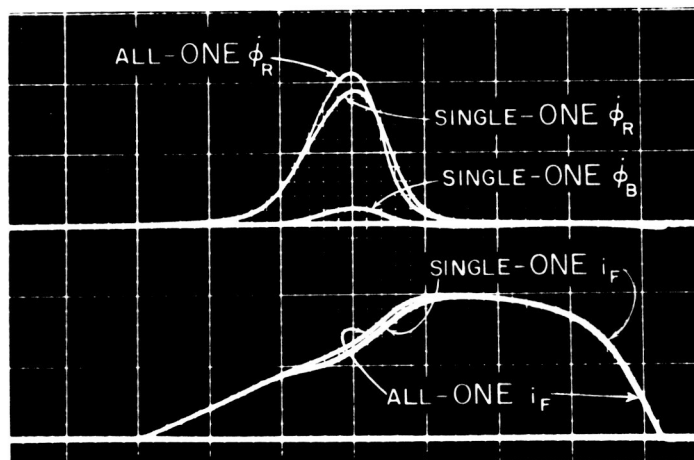
## 6. SUMMARY

A core-diode shift register, driven by a slow-rising current pulse of amplitude  $I_A$ , is analyzed for the case of a single-ONE information pattern by considering three cores: a transmitter (Core T), a receiver (Core R), and the receiver of a previous stage (Core B). Seven basic equations include the net  $F$  of each core (three equations),  $\phi(F, \phi)$  of Cores T and R (two differential equations, each based on the parabolic model for inelastic switching), and two loop equations. It is assumed that if Core B is switching,  $F_B$  is clamped to the static  $\phi(F)$  curve. Representing each diode by a voltage source and a resistance, three modes of operation are distinguished: in Mode 1, both diodes are blocked; in Mode 2, the back diode is blocked and the forward diode is conducting; in Mode 3, both diodes are conducting. Using the basic equations in each mode of operation, a computer program was written for computing the time variables during the switching time and also the flux-gain curves for different values of  $I_A$ . In addition to using the  $\phi(F, \phi)$  PROCEDURE for Cores T and R, Newton's equation  $x_j = x_{j-1} - [f_{(j)}/f'_{(j)}]$  is employed in an iterative solution of the forward loop equation,  $f = 0$ , during each  $\Delta t$ , where  $x$  is either the loop





(a)  $\dot{\phi}_T(t)$  AND  $i_A(t)$



(b)  $\dot{\phi}_R(t)$  AND  $i_F(t)$

RA-3696-234

FIG. 25 EXPERIMENTAL TIME VARIABLES IN A CORE-DIODE SHIFT REGISTER WITH SINGLE-ONE AND ALL-ONE INFORMATION PATTERNS

( $I_A = 1.18$  ampere)

Time scale =  $0.5 \mu\text{sec}/\text{major div.}$ ;  $\dot{\phi}_R$  and  $\dot{\phi}_B$  scale =  $0.5 (\text{volt/turn})/\text{major div.}$ ;

$i_A$  scale =  $0.5 \text{ ampere}/\text{major div.}$ ;  $i_F$  scale =  $0.2 \text{ ampere}/\text{major div.}$

$\dot{\phi}_T$  scale =  $0.25 (\text{volt/turn})/\text{major div.}$ ;

current  $i_F$  or  $\phi$ , whichever yields a faster convergence. Comparisons between experimental and computed  $\phi_T(t)$ ,  $\phi_R(t)$ ,  $\phi_B(t)$ , and  $i_F(t)$  waveforms are given in Fig. 21. The agreement, although quite good, can be improved by reducing the values of  $\lambda$  and  $\rho_p$  by about 30 percent. By repeating the computation of  $\Delta\phi$  of each core for various values of initial transmitter flux and drive-current amplitude, flux-gain curves and ZERO back flux transfer are computed and plotted in Figs. 23 and 24. It is concluded from these plots that if  $I_A$  is reduced to 0.565 ampere, a ONE, represented by 88% of  $2\phi_r$ , drops to ZERO. It is shown that the analysis of a single-ONE case is applicable to the case of an information pattern with any number of ONES.

## F. CONCLUSIONS

An attempt has been made in this section to achieve two objectives: First, to delineate improved flux switching models (Part A), and second, to describe the application of the improved parabolic model for inelastic switching to the calculation of flux switching and load currents in three magnetic circuits (Parts B through E).

From the comparison between the computed and the experimental data, there is no doubt that the original parabolic model [Eqs. (1), (2), and (3)] has been improved considerably by replacing Eq. (3) by Eq. (4). Such a replacement is also consistent with the definition of static  $\phi(F)$  curve in the sense that for a given positive  $F$  value, the flux level at the end of switching cannot exceed  $\phi_d$ . As it stands now, the modified parabolic model [Eqs. (1), (2), and (4)] can be used in computation of  $\phi(t)$  where the required accuracy is not high, e.g.,  $\pm 10$  percent. However, higher accuracy will be obtained for computation of  $\phi(t)$ , because time integration of  $\phi(t)$  tends to average out fluctuations of computed  $\phi(t)$  around experimental  $\phi(t)$ . This feature is important for the analysis and design of most of the magnetic circuits, because the operation of these circuits depends on the net flux change, rather than the details of the  $\phi(t)$  waveform.

It is clear that there is room for further improvements of the switching model in the following areas:

- (1) Determine how the switching parameters are affected by the shape of  $F(t)$ , e.g., a ramp  $F(t)$  and an exponentially decaying  $F(t)$ .

- (2) Study the elastic and inelastic initial  $\dot{\phi}$  spikes in more detail, using different values of amplitude and rise time of  $F$ , and include their contributions to the over-all  $\dot{\phi}$  in the switching model.
- (3) Include the effects of excessive core thickness on the over-all switching parameters.

All these model improvements are related to switching from a well-defined, remanent flux state in saturation. Models for switching from a partially set state are a separate topic and will be discussed in the next section.

The experiments described in this section have been performed using two cores whose material properties and relative dimensions were very different from each other. In view of the agreements between computed and experimental results, this fact adds to the validity of the modified parabolic switching models in general. However, there is a need to use additional types of core, with different material and geometry in order to evaluate the extent of applicability of this model.

Five years ago, the modified parabolic model might have been discarded as impractical. Today, as computer-programming languages have become so much simpler, the complexity of this model creates little difficulty. The practicality of this model has been demonstrated in this section. With the speed of modern computers going up and the cost of computation going down, application of complex and accurate switching models in numerical solutions for magnetic circuits becomes more practical every day. This is one reason why we should not hesitate to further improve the switching models, and write computer programs for other magnetic circuits.

As often reported in the available literature, magnetic circuit problems have been solved numerically by a computer, using various switching models. In most of these cases, however, neither the methods of numerical solution nor the computer programs have been included in the publication. In this report, both are given in detail so that anyone who is interested in using a computer for a numerical solution of a similar magnetic circuit problem, can do so with a minimum of effort.

Computer programs for three magnetic circuits have been included in this report: an unloaded core, a loaded core, and a core-diode shift register. Other than assignment of values for the switching parameters,

these programs are independent of the switching model, since the program for the latter is included in a separate PROCEDURE. As such, these programs will hardly be affected by any revisions in the switching model. Similar computer programs will be written for other types of magnetic circuits which include toroidal cores, multipath cores, or both.

### III FLUX SWITCHING FROM A PARTIALLY SET STATE

#### A. DESCRIPTION OF EXPERIMENTS

##### 1. INTRODUCTION

The parabolic switching model, with its numerous modifications, can adequately describe flux-switching when initiated from negative remanence by a rectangular pulse. However, when switching is initiated from a partially demagnetized state, or when the drive pulse is not rectangular, significant discrepancies exist. It is important to determine the details of these discrepancies, and examine the possibilities of either improving our present switching model, or obtaining a new model that takes account of the discrepancies. Switching from a partially demagnetized state and switching with a nonrectangular drive pulse are treated as a single problem because the discrepancies in both cases are believed to come from the same source. This will be discussed in Sec. III-E. However, most of the data of this report were taken for the case in which the initial state is partially demagnetized.

The literature contains relatively few references on this subject. A previous technical report<sup>7</sup> gave rather extensive experimental data on the properties of a partially set core, but it contained data on only one ferrite material, was restricted to a single polarity of test pulse, and left unanswered some questions of interpretation of the data that can now be partially answered. Therefore, the purpose of this section is to extend the experiments of Ref. 7 to other ferrite materials, to use both polarities of test pulse, and to further interpret these data and present some new ideas for future development of a switching model capable of describing such data.

A partially demagnetized condition can be reached by several different methods, such as imperfect clearing due to nonconstant cross-sectional area (tapered leg), thermal demagnetization, cyclic demagnetization, and partial switching from remanence by pulses of various shapes. For simplicity, only one method will be considered in this report--the same method used in Ref. 7. In this method a rectangular pulse (PARTIAL-SET pulse) is used to partially set the core, i.e., switch it from negative

remanence ( $\phi = -\phi_r$ ) to some partially set flux state. This partially set flux state can be identified by three parameters: the flux level,  $\phi_{ps}$ , the duration,  $T_{ps}$  (or alternatively, the amplitude  $F_{ps}$ ) of the PARTIAL-SET pulse used to obtain that flux level, and the period of time,  $T_b$ , between the end of this PARTIAL-SET pulse and the beginning of the following TEST pulse used to determine the characteristics of each partially set state. The problem, then, is to describe the switching properties as a function of the three parameters,  $\phi_{ps}$ ,  $T_{ps}$ , and  $T_b$ . The experiments were carried out for a moderate number of judiciously chosen partially set states. For each state, the switching properties were determined by applying a rectangular TEST pulse whose polarity and amplitude,  $F$ , were variable. Three basic types of response to the TEST pulse were measured: (1) the 700- $\mu$ sec  $\phi(F)$  curve; (2) the  $\dot{\phi}_p(F)$  curve; and (3) the  $\dot{\phi}(t)$  waveform. The experimental data will be presented and discussed under these three headings in Parts B, C, and D, respectively, and conclusions and further discussion will be given in Part E.

## 2. EXPERIMENTAL SET-UP

The experimental set-up is, for the most part the same as that used in Ref. 7. Brief descriptions will be given here for the convenience of the reader and to point out the differences where they do exist.

### a. CORE

The geometry chosen for these experiments is that of a toroid whose OD/ID ratio is slightly greater than unity, so that radial variations of  $B$  and  $H$  would be minimized. The value of  $OD/ID = 1.10$  was used, as a compromise between having radial variations of  $B$  and  $H$  on one hand, and difficulty in fabrication and an unusually high surface-to-volume ratio (which could, conceivably, affect the switching properties) on the other hand. The toroidal cores were ultrasonically cut from one-half-inch-diameter discs of commercially available ferrite material.

Two different ferrite materials were tested, Lockheed 0-6, and Indiana General 5209. Most of the data were taken on the 5209 material because the  $\dot{\phi}(t)$  waveforms of the 0-6 material were not simple  $\text{sech}^2$  functions, as was the case for the 5209 material (and also the Telemeter T-5 material of Ref. 7). One core of each material was tested. These two cores are

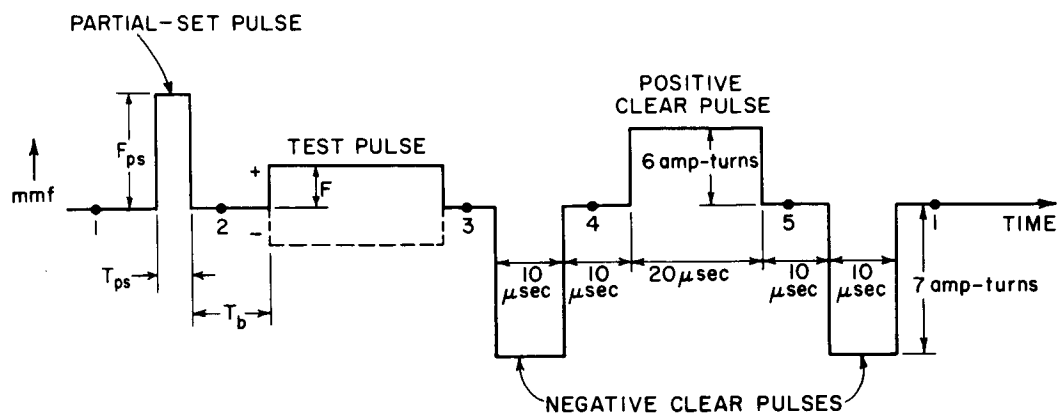
identified as Core I-3 for the Lockheed 0-6 material and I-4 for the Indiana General 5209 material. Since both cores were ultrasonically cut by the same tool, most of their dimensions are nearly identical. Those dimensions are given in Table IV.

Table IV  
DIMENSIONS OF CORES I-3 AND I-4

Outer radius, $r_o$	0.378 cm
Inner radius, $r_i$	0.343 cm
Average radius,	0.360 cm
$r_o/r_i$	1.10
$h$ (thickness along axis)	0.0767 cm (Core I-3)
	0.0848 cm (Core I-4)
$r_o - r_i$	0.035 cm

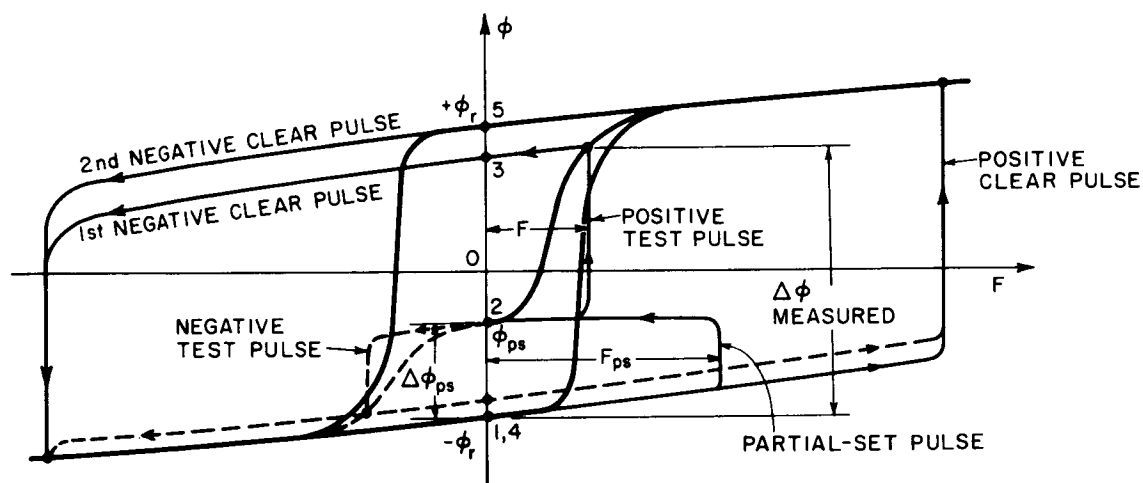
#### b. PULSE SEQUENCE

The pulse sequence used throughout the experiments on partial-setting is given in Fig. 26(a), together with the appropriate nomenclature. The corresponding paths of operation in the  $\phi(F)$  plane are shown in Fig. 26(b). The numbers 1 through 5 in Fig. 26(b) correlate with the numbers of Fig. 26(a). The PARTIAL-SET pulse switched the core from negative remanence ( $\phi = -\phi_r$ ) to the partially set state which was to be tested. This state is identified by the set of parameters  $\phi_{ps}$ ,  $T_{ps}$  and  $T_b$ . The following TEST pulse then switched the core to some new flux level to determine the characteristics of the initial, partially set state. The amplitude,  $F$ , of the TEST pulse was varied to switch the core at different rates and to different flux levels. The polarity of  $F$  could be either positive or negative. The first negative CLEAR pulse then switched the core back to  $-\phi_r$ . The last two CLEAR pulses, which switch the core to  $+\phi_r$  and then back to  $-\phi_r$  again, served to remove all traces of past history. A single CLEAR pulse has been found to be inadequate to completely remove the effects of a core's past history.<sup>7,9</sup> Hewitt and Overn<sup>9</sup> explain this effect by proposing that 360-degree domain walls are formed when a core is cleared from a partially set state. These 360-degree walls can then contribute to switching during the following cycle. Their experimental measurements, and subsequent measurements made in this laboratory, showed that the effects of past history can be removed by adding a CLEAR pulse of the same polarity as the pulse that partially set the core. This is the justification for the positive CLEAR pulse. This positive CLEAR pulse was preceded by a negative CLEAR pulse, so that a flux measurement could be made immediately after the TEST pulse, before any other flux changes were made. The flux switched by the TEST pulse could not be measured during the TEST pulse because the duration of the TEST pulse was sometimes long compared to the time constant of the integrator (150  $\mu$ sec). Switching during the first negative CLEAR pulse was relatively fast, so that integration was not a problem.



(a) PULSE SEQUENCE

RA-3696-236



(b) VARIATIONS OF  $\phi$  AND  $F$

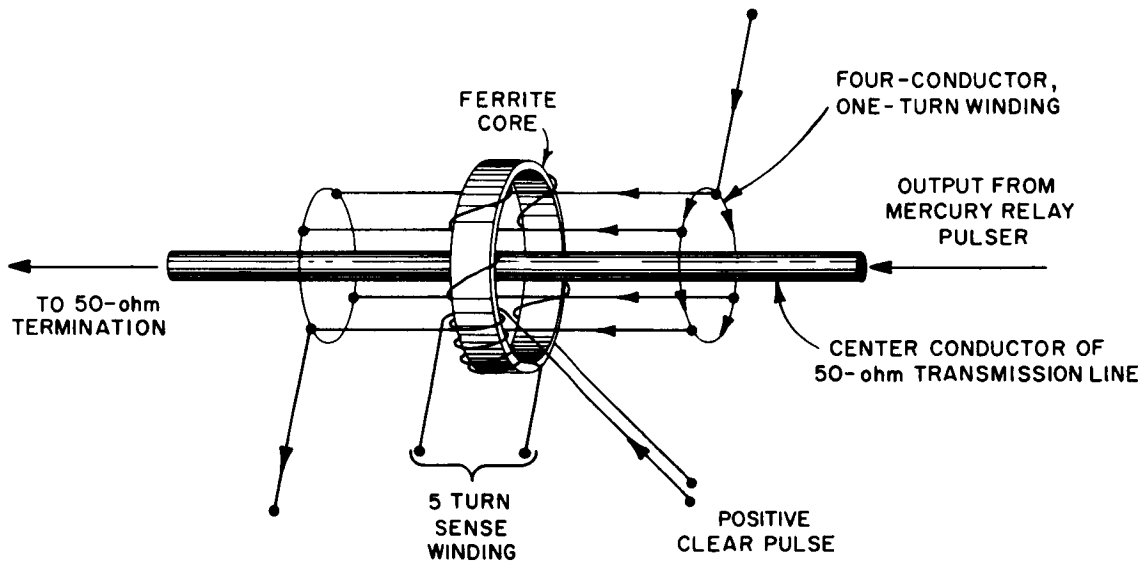
RA-3696-236A

FIG. 26 PARTIAL SWITCHING EXPERIMENT



c. COAXIAL CORE HOLDER AND WINDINGS

The core was mounted coaxially in a section of 50-ohm transmission line, so that fast-rise MMF pulses could be applied by sending a current pulse down the transmission line. The winding configuration was the same as used in Ref. 7, except for the number of turns in the CLEAR winding. This winding configuration is shown in Fig. 27 which is reproduced from Ref. 7. The CLEAR winding was changed from 5 turns to 10 turns to provide a more uniform  $H$  field around the circumference of the core. The four-conductor, one-turn winding was used for the TEST pulse in addition to either the positive or negative CLEAR pulses, depending upon the polarity of the TEST pulse.



RA-2697-115

FIG. 27 CONFIGURATION OF CORE AND WINDINGS  
Reproduced from Ref. 7

d. PULSERS

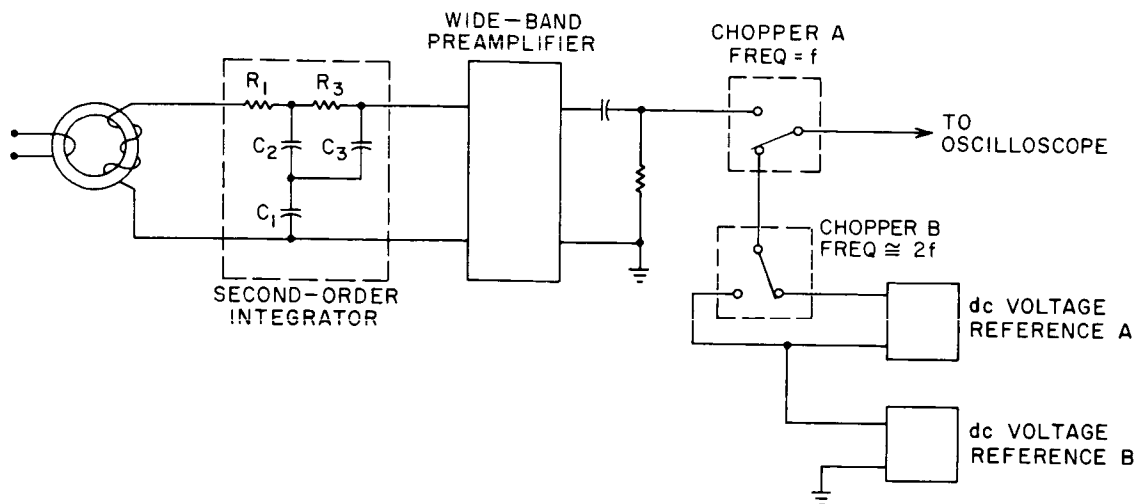
Three different pulsers were used for the experiments on partial switching. The first pulser, which supplied all three CLEAR pulses, consisted of conventional negative hard-tube drivers with a  $0.1\text{-}\mu\text{sec}$  rise time. The second pulser consisted of three positive transistor drivers in parallel. These three current drivers could all be driven by either a common input pulse or separate input pulses of different durations and at different times. The minimum rise-time of these drivers was about

50 nsec (nanoseconds), and the maximum amplitude was 1.3 amperes each. The maximum pulse width was about 700  $\mu$ sec. The third pulser was a mercury relay pulser with a rise-time of less than 0.7 nsec. This type of pulser<sup>10</sup> generates a pulse by discharging a certain length of transmission line into an impedance-matched load via a coaxial mercury relay. The length of the charged transmission line determines the pulse duration, and the voltage to which it is charged determines the pulse amplitude. This pulser had a maximum amplitude of 40 amperes, a pulse duration ranging from 1 nsec to 900 nsec, and a characteristic impedance of 50 ohms. It was used only for partial-set pulses of 900 nsec or less in duration. Longer partial-set pulses and all of the TEST pulses were supplied by one or more of the transistor drivers, which were connected to the four-conductor, one-turn winding. Since mercury relay pulsers characteristically have a lot of jitter, it was necessary to synchronize all of the other pulsers to the mercury relay pulser when it was used.

#### e. FLUX MEASUREMENT

The flux changes were measured by means of a special second-order integrator, two choppers, and two dc voltage references. The circuit diagram is shown in Fig. 28. This integrator is a different type of second-order integrator from the one described on page 133 of Report 2, and is discussed in greater detail in Ref. 7. In the integrator described in Report 2, the main signal and the error correction signal were summed external to the integrator. This addition is inconvenient when a chopper and a voltage reference are used to measure the switched flux. The integrator used here, and in Ref. 7 adds the error-correction signal internally to eliminate this difficulty.

In this integrator another capacitor,  $C_2$ , is added in series with the usual capacitor,  $C_1$ . The first-order integral is thus available at two places, across  $C_1$  and across  $C_2$ . The signal across  $C_2$  is then integrated again via  $R_3$  and  $C_3$  to obtain the first-order error-correction signal which appears across  $C_3$ . Since  $C_1$  and  $C_3$  are in series across the output terminals, the main signal and the error correction signal are thereby added algebraically. The combination of two choppers (at different frequencies) and two dc voltage references provides two reference lines on the oscilloscope display. One reference line (B) was used as a variable base line and the other used to measure the amplitude of the flux signal.



RA-3696-237

FIG. 28 CIRCUIT FOR MEASURING FLUX CHANGES

When the  $\dot{\phi}_p(F)$  and  $\dot{\phi}(t)$  data were taken, the period of time between the end of the TEST pulse and the beginning of the first CLEAR pulse was made much larger than the integrator time constant,  $R_1 C_1$  so that the integrator capacitors would be nearly discharged prior to the flux measurement. A small remanent charge does not matter, however, since the variable base line of voltage reference B can account for it. The measurement of the  $\phi(F)$  curves will be discussed in Part B.

#### f. TEMPERATURE

The experimental measurements were all made at a temperature of 29°C. The temperature was automatically maintained by means of a heating coil and thermistor probe imbedded in the outer conductor of the coaxial core holder. Ample time was allowed so that the core and its associated conductors would reach thermal equilibrium before any measurements were taken. These measurements should be extended to other temperatures.

### B. CURVES OF $\phi(F)$

#### 1. EXPERIMENT

Curves of  $\phi(F)$  were taken for each partially set state by using a 700- $\mu$ sec TEST pulse. These 700- $\mu$ sec  $\phi(F)$  curves are assumed to be close to the true static  $\phi(F)$  curves. A comparison was made in Ref. 7 between and 800- $\mu$ sec  $\phi(F)$  curve and a 17-msec  $\phi(F)$  curve for the ferrite T-5 material.

This comparison revealed only about 3 percent difference in  $F_c$  for the two cases. No such check has been made, however, for the materials used here.

The experimental 700- $\mu$ sec  $\phi(F)$  curves were measured by adjusting the TEST pulse to 700- $\mu$ sec and by adjusting the time interval between the end of the TEST pulse and the beginning of the first CLEAR pulse to about 0.5  $\mu$ sec. The flux change was integrated from just prior to the end of the TEST pulse to just after the end of the first CLEAR pulse [see Fig. 26(b)]. The experimental  $\phi(F)$  curves therefore represent peak, not remanent, flux values.

## 2. RESULTS

Only two  $\phi(F)$  curves were measured for Core I-3 (Lockheed 06 material) one for no partial setting, and one for  $\phi_{ps} = -(1/2)\phi_r$ ,  $T_{ps} = 900$  nsec, and  $T_b = 50$   $\mu$ sec (see Fig. 29). The no-partial-setting curve exhibits a vertical side for a flux change of over  $\phi_r$ . When  $F$  was adjusted to that part of the curve the core would switch relatively quickly on some cycles, exhibit a time delay before switching on other cycles, and on still other

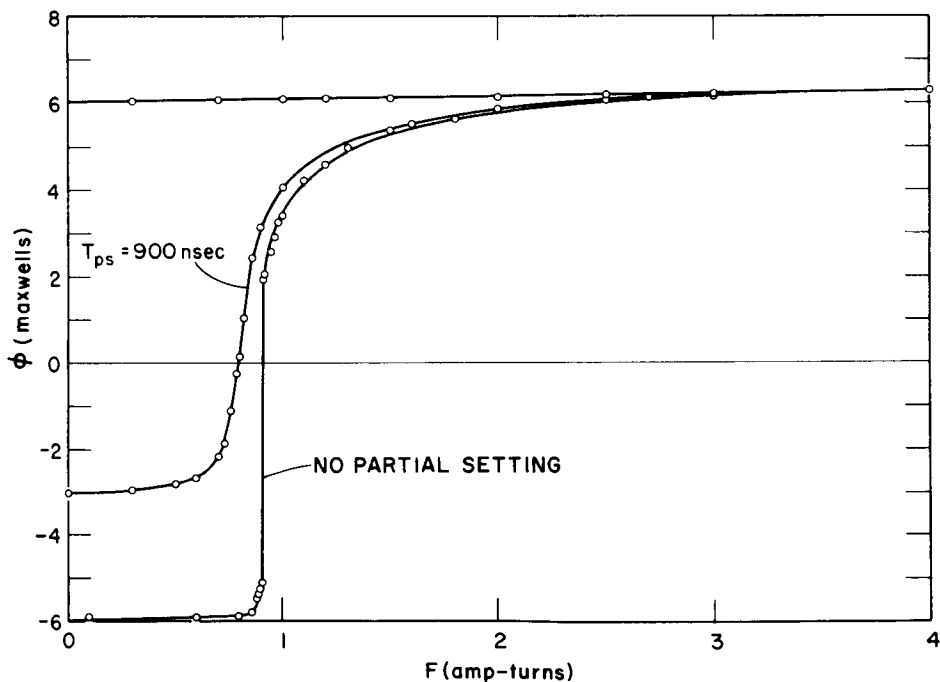


FIG. 29 700- $\mu$ sec  $\phi(F)$  CURVES OF CORE I-3

cycles, not switch at all. This appeared to be a random process. A  $\dot{\phi}(t)$  oscillogram will be included in Part D\* to illustrate this type of switching. Note that the vertical side does not appear on the partially set  $\phi(F)$  curve. The vertical side was observed to gradually shorten in  $\Delta\phi$  and eventually disappear as  $\phi_{ps}$  was increased from  $-\phi_r$  to  $-(1/2)\phi_r$ .

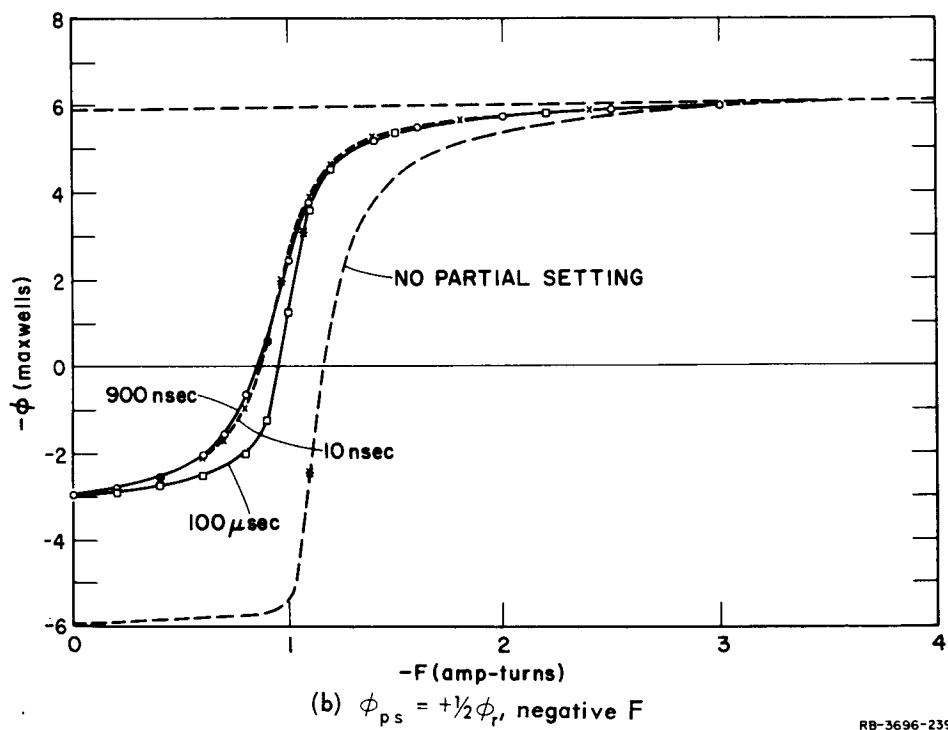
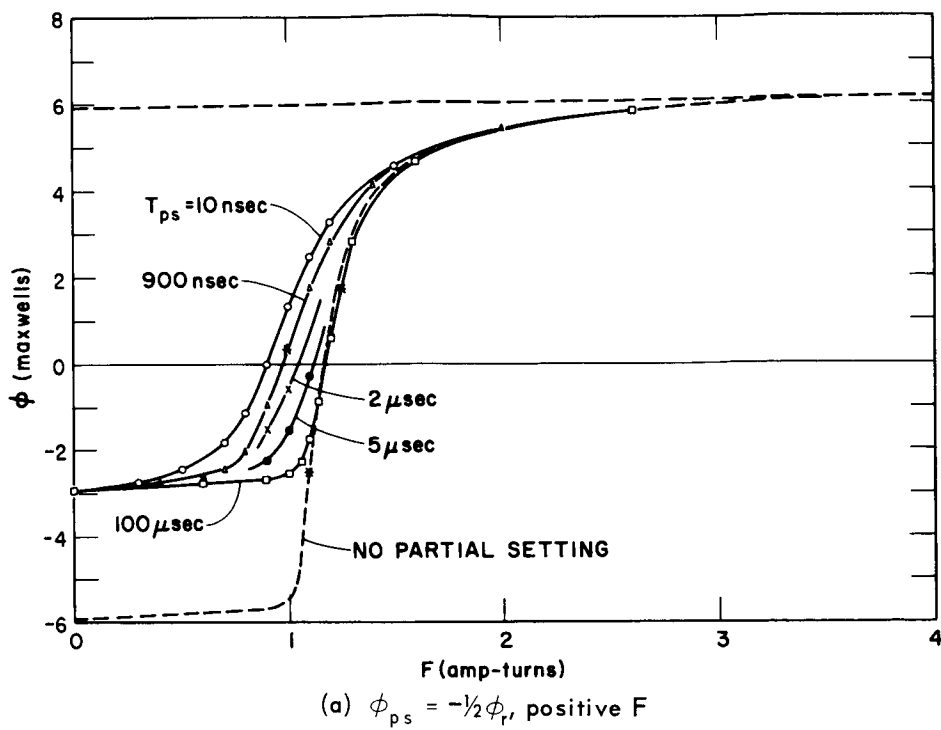
Six families of  $\phi(F)$  curves were taken for Core I-4, three for a positive TEST pulse, and three for a negative TEST pulse. These are shown in Fig. 30. Note that the curves for a negative TEST pulse are shown reversed for easy comparison. The parameter in each of these six families of curves was the duration  $T_{ps}$  of the PARTIAL-SET pulse, which varied from 10 nsec to 100  $\mu$ sec. The three values of  $\phi_{ps}$  used for each polarity of TEST pulse were  $-(1/2)\phi_r$ , 0, and  $+(1/2)\phi_r$ .

### 3. DISCUSSION

The vertical segment in the  $\phi(F)$  curve for Core I-3 is not shared by either Core E-6 (Ref. 7) or Core I-4. However the 900-nsec partial-set curve for Core I-3 is very similar to the 900-nsec curves for the other two cores. Note that the threshold is both considerably lowered and rounded by partial setting. The curves of Figs. 30(a), (c), and (e), that is, for  $+F$ , show a very similar lowering and rounding of the threshold for  $T_{ps} = 900$  nsec (similar to Cores I-3 and E-6). Note that for  $+F$  and slow partial setting ( $T_{ps}$  large), the threshold is neither lowered nor rounded, but that fast partial setting ( $T_{ps}$  small) lowers and rounds the threshold very much. This, too, is very similar to the results of Core E-6. Also, notice that the curves for slow partial setting cross the major  $\phi(F)$  curve. This was also observed on Core E-6. This might be partially explained by the fact that these  $\phi(F)$  curves are not truly static curves. However, the effects are somewhat too large to be entirely explained by this fact. Since no data for  $-F$  were taken on either Core E-6 (Ref. 7) or Core I-3, no comparisons can be made. We observe, however, that for Core I-4, the  $\phi(F)$  curves for  $-F$  are considerably different from the curves for  $+F$ . The biggest difference exists for slow partial setting (e.g.,  $T_{ps} = 100 \mu$ sec). For this case the threshold is lowered considerably for  $-F$ , but not for  $+F$ . Probably the major difference in the physical condition for  $+F$  and  $-F$  is the availability of favorable nucleation sites (points at which the nucleation of a domain is relatively easy). For a positive TEST pulse, these favorable sites already have nucleated positive

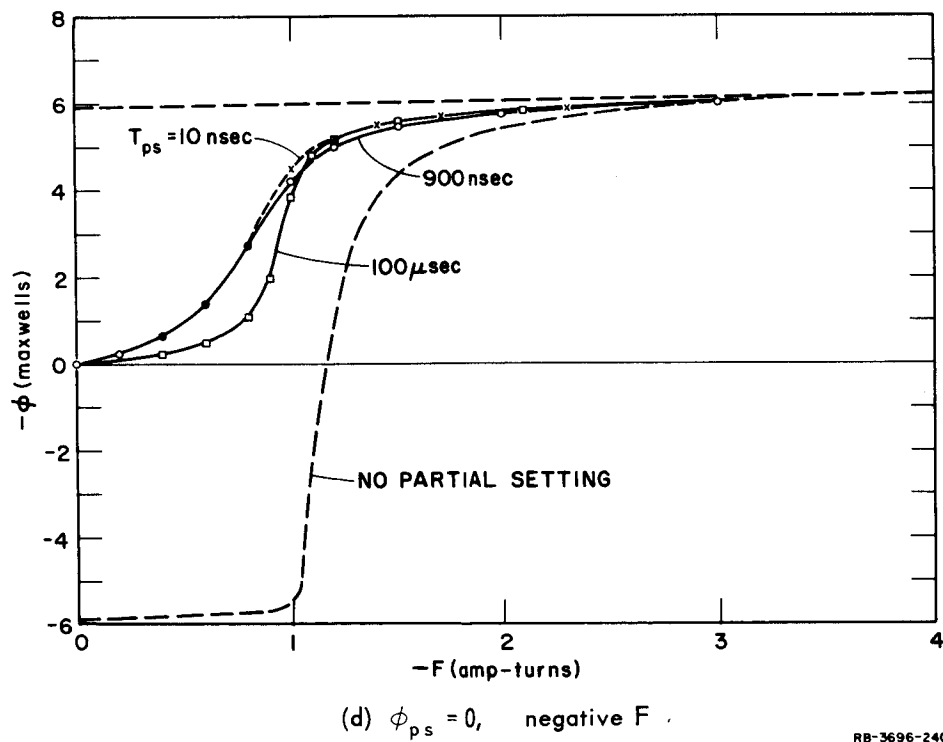
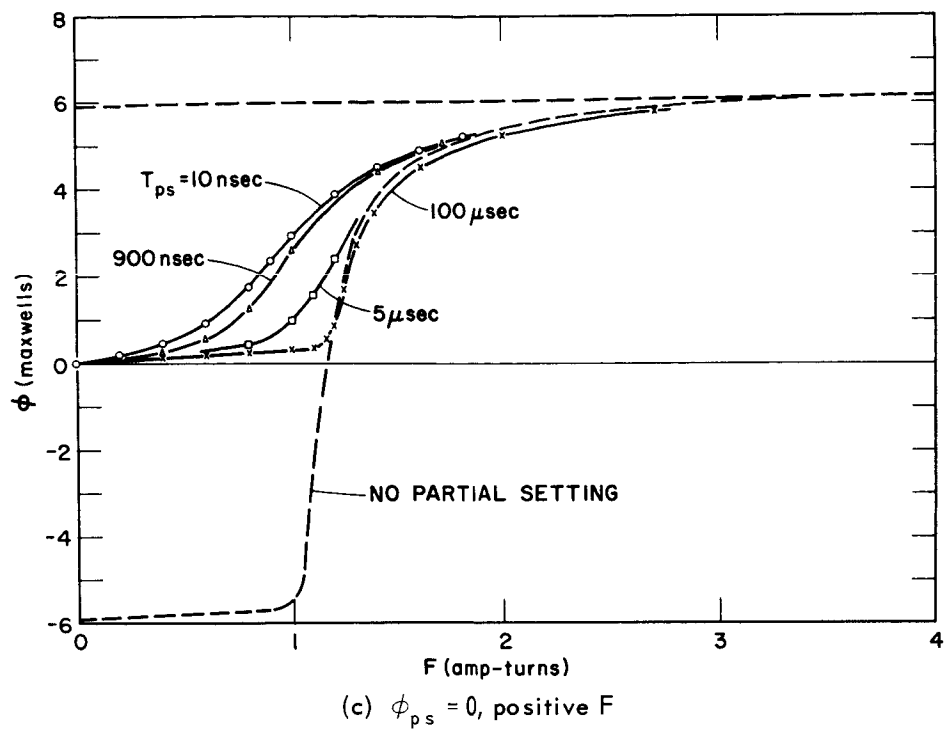
---

\* Figure 33



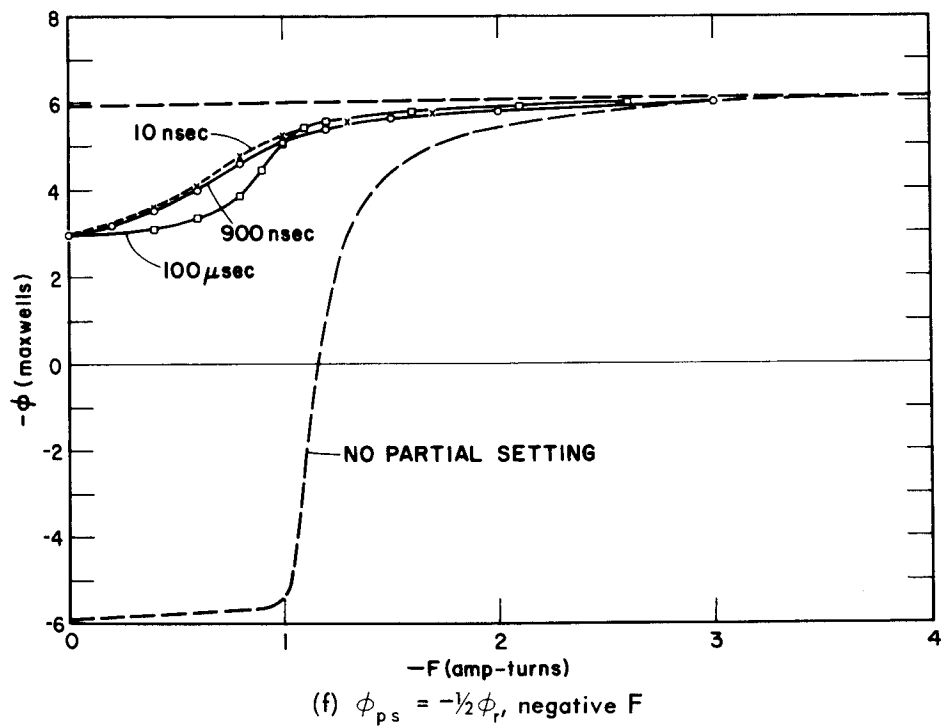
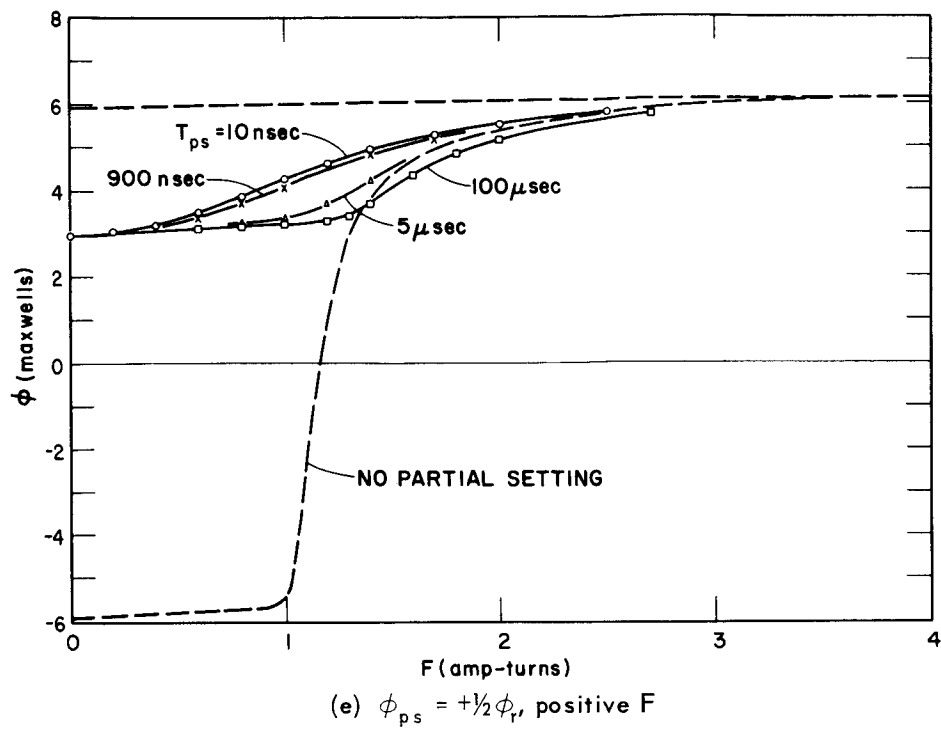
RB-3696-239

FIG. 30 700- $\mu$ sec  $\phi(F)$  CURVES OF CORE I-4



RB-3696-240

FIG. 30 Continued



RB-3696-241

FIG. 30 Concluded



domains and additional switching will occur by further growth of these domains. However, for a negative TEST pulse, negative domains can nucleate at these same favorable sites within the previously nucleated positive domains.<sup>11</sup> Thus, for a negative TEST pulse, the favorable nucleation sites are available during both the PARTIAL-SET pulse and the following TEST pulse; for a positive TEST pulse, they are available only during the PARTIAL-SET pulse. These differences are probably, in some way, responsible (e.g., via differences in the demagnetization fields) for the differences observed in the positive and negative  $\phi(F)$  curves, and also in the  $\dot{\phi}(t)$  waveforms and the  $\dot{\phi}_p(F)$  curves yet to be discussed.

The threshold of the  $\phi(F)$  curve is more rounded for  $-F$  curves than for the corresponding  $+F$  curves, but the  $-F$  curves have less wing, i.e., they saturate faster than the corresponding  $+F$  curves. Another unexpected result for the  $-F$  curves is the crossing of a curve for one value of  $T_{ps}$  with a curve for the same  $\phi_{ps}$  but a different  $T_{ps}$  [e.g., Fig. 30(d) and (f)]. The basic physics of most of these results is not known yet; however, additional discussion will be given in Part E after the other experimental results have been given.

### C. WAVEFORM OF $\dot{\phi}(t)$

#### 1. INTRODUCTION

One of our primary concerns in investigating the properties of switching from a partially set state is the  $\dot{\phi}(t)$  waveform for a constant drive pulse. We want to know first if the waveform (ignoring scale factors) is nearly independent of  $F$ , and second if this waveform can be described by a  $\text{sech}^2$  function, as it generally can for switching from  $-\phi_r$  (for a thin ring core). This information is needed to determine the possibilities of retaining the parabolic switching model, although somewhat modified, for switching from a partially set state. The  $\dot{\phi}(t)$  data of Ref. 7, which were only for a positive TEST pulse, showed that for Core E-6, the  $\dot{\phi}(t)$  could still be described by a  $\text{sech}^2$  function, but the parabolic model had to be modified to include a new parameter,  $\phi_c$ , which varies with  $T_{ps}$ ,  $\phi_{ps}$ ,  $T_b$ , and  $F$ .

Since  $\phi_c$  is important for describing the effects of partial setting, especially regarding  $\dot{\phi}(t)$ , it will now be discussed. The parabolic model has already been modified in Eq. (4) in Sect. II-A, to account for the limiting of flux switching in accordance with the static  $\phi(F)$  curve.



$$\dot{\phi} = \lambda(F - F_0'')^\nu \operatorname{sech}^2 \left\{ \frac{\lambda(F - F_0'')^\nu t}{\phi_c + \frac{1}{2}(\phi_s + \phi_d)} \right. \\ \left. + \tanh^{-1} \left[ \frac{\phi_0 + \phi_c + \frac{1}{2}(\phi_s - \phi_d)}{\phi_c + \frac{1}{2}(\phi_s + \phi_d)} \right] \right\} \quad (93)$$

where  $\phi_0$  is the initial value of  $\phi$  for the inelastic switching described by the parabolic model. Note that as  $\phi_c$  varies, with everything else except  $\dot{\phi}$  and  $t$  fixed, neither the total area under the  $\dot{\phi}(t)$  curve, nor  $\dot{\phi}_p$  changes, but  $t_p$  does change. Relatively little information is yet available as to the relationship of  $\phi_c$  to  $T_{ps}$ ,  $\phi_{ps}$ ,  $T_b$  and  $F$ , but some trends can be pointed out.

The objectives of this part of the report, then, are (1) to determine if similar  $\dot{\phi}(t)$  waveforms are obtained for Cores I-3 and I-4 as were obtained for Core E-6 in Ref. 7, (2) to determine what  $\dot{\phi}(t)$  waveforms are obtained for a negative TEST pulse, and (3) to consider  $\phi_c$  in somewhat greater detail than was done in Ref. 7. Part C-2 will present the  $\dot{\phi}(t)$  waveforms relative to a  $\operatorname{sech}^2$  function for both Core I-3 and Core I-4. Part C-3 will present data on the effect of varying  $T_{ps}$ , with  $\phi_{ps}$  and  $F$  held constant for both cores. Both Parts C-2 and C-3 will include the effects of a negative TEST pulse on Core I-4. Part C-4 will present data on the effects of varying  $\phi_{ps}$  with  $T_{ps}$  and  $F$  held constant for Core I-4. Part C-5 will summarize the results.

## 2. COMPARISON OF $\dot{\phi}(t)$ AND $\operatorname{SECH}^2$ FUNCTION

A comparison between the  $\dot{\phi}(t)$  and a  $\operatorname{sech}^2$  function was made by including a plot of a  $\operatorname{sech}^2$  function on the graticule of the oscilloscope camera. The  $\dot{\phi}(t)$  waveforms were examined during the TEST pulse. The flux switched by the PARTIAL-SET pulse was measured by momentarily removing the TEST pulse and measuring the flux switched by the first CLEAR pulse (see Fig. 26). The TEST pulse was made long enough so that switching would be completed by the end of the TEST pulse.

Two  $\dot{\phi}(t)$  waveforms for Core I-4 are compared to  $\operatorname{sech}^2$  functions in Fig. 32, one for a positive TEST pulse, and the other for a negative TEST

pulse. These two waveforms are for different partially set states and  $F$  values, but each was observed to be fairly representative of the polarity of the TEST pulse with which it was obtained. It should be mentioned that the same amount of flux is switched by the positive TEST pulse as by the negative TEST pulse only if the values of  $\phi_{ps}$  for the two cases are equal in magnitude and opposite in polarity [cf. Fig. 26(b)].

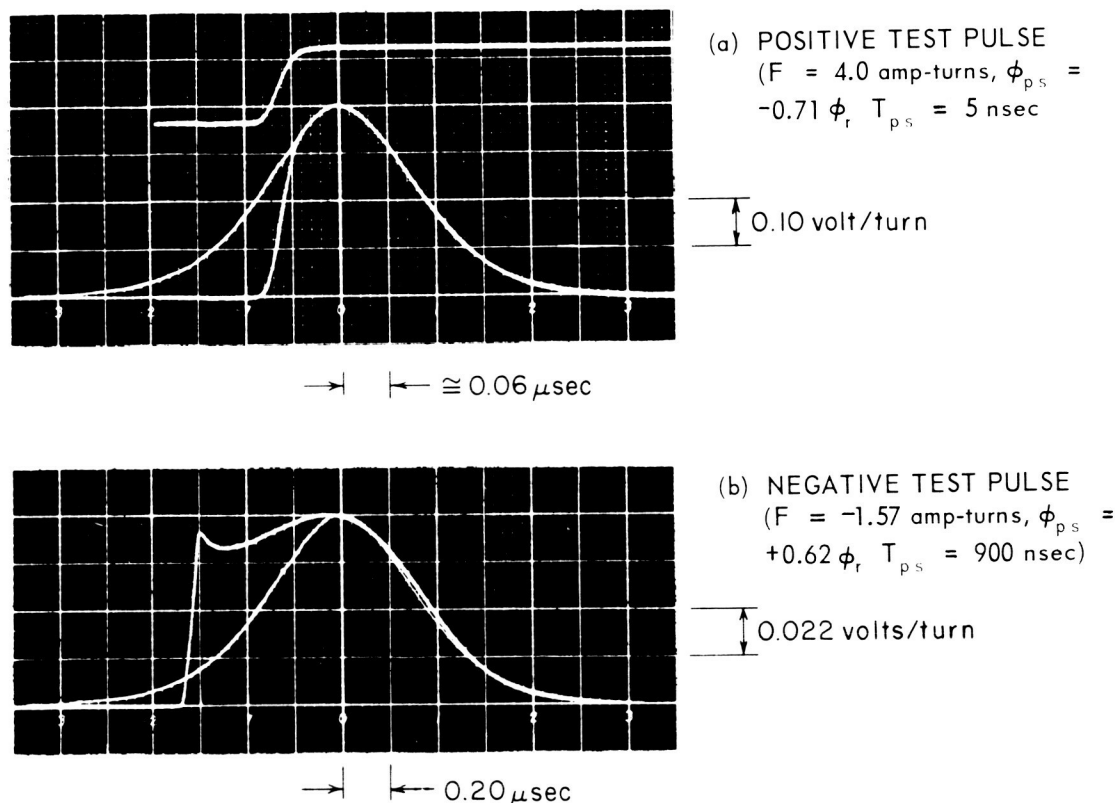
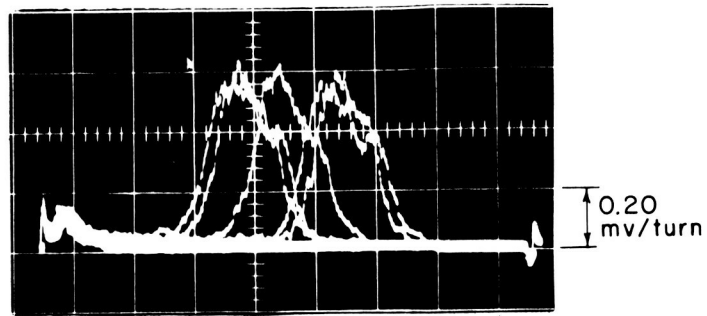


FIG. 32 COMPARISON OF  $\dot{\phi}(t)$  TO  $\text{SECH}^2$  FUNCTION  
 Core I-4,  $T_b = 50 \mu\text{sec}$

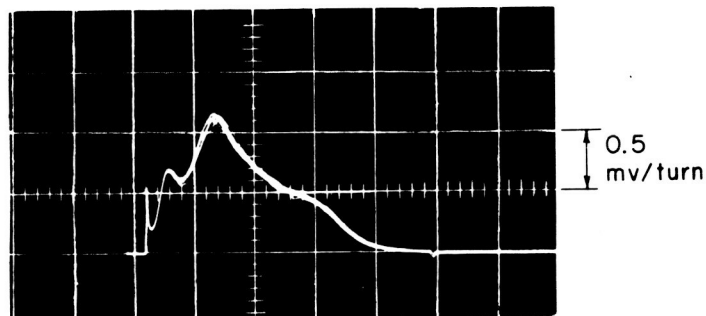
The  $\dot{\phi}(t)$  waveforms of Core I-4 for a positive TEST pulse are qualitatively very similar to those of Core E-6 (Ref. 7). This is encouraging because it implies that the parabolic model might be modified to describe switching in several ferrite materials. The  $\dot{\phi}(t)$  waveforms for a negative TEST pulse are not so simple [cf. Fig. 32(b)], because they are not very similar to  $\text{sech}^2$  functions although, as  $F$  was increased a somewhat greater similarity was obtained. It appears as if the tail of the initial spike, as discussed in Sect. II-A-2, accounts for a large percentage of the total flux switched. The 700- $\mu\text{sec}$   $\phi(-F)$  curves of Fig. 30 demonstrate that

the threshold is lower for a negative TEST pulse than for a positive one. It is possible that these results for a negative TEST pulse can be explained, at least in part, by the nucleation of negative domains within the positive domains of reversed magnetization<sup>11</sup> as was discussed in Part B-3. These negative domains would contribute to the total domain wall area ( $\lambda$  will be greater) and therefore cause faster switching than would be obtained for a comparable case with positive TEST pulse. The lower threshold observed in Figs. 30(b), (d), and (f) will also cause faster switching. This will be discussed further in Part D in connection with the  $\dot{\phi}_p(F)$  curves. The shape of the  $\dot{\phi}(t)$  waveform for a negative TEST pulse cannot easily be explained, however, since the detailed domain configuration, which results in a  $\text{sech}^2 \dot{\phi}(t)$  for a positive TEST pulse is not yet fully understood, even for the case in which switching is initiated from a remanent state ( $\pm\phi_r$ ). The above explanations for a negative TEST pulse must not be too readily accepted, because the anomalies of switching from partially set states with a positive TEST pulse requires explanations which are not consistent with the usual concepts of domain wall switching.<sup>7</sup> It may be that some physical mechanisms are involved which have not yet been seriously considered but which are capable of describing the anomalies for both positive and negative TEST pulse polarities.

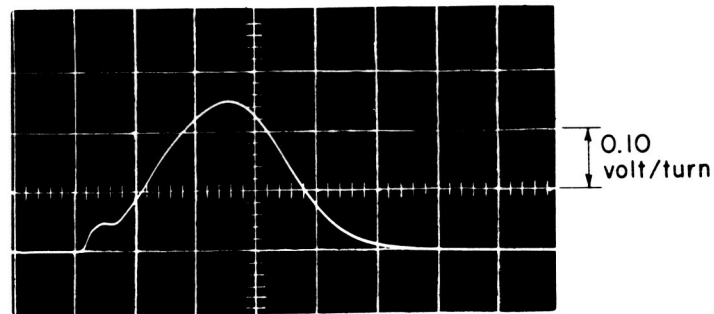
Waveforms of  $\dot{\phi}(t)$  for Core I-3 were much different from those of either Core I-4 or Core E-6 of Ref. 7. Even for no partial setting, the  $\dot{\phi}(t)$  waveforms could not be described by a single  $\text{sech}^2$  function. The  $\dot{\phi}(t)$  waveforms for three different values of  $F$  are shown in Fig. 33. The multiple exposure in Fig. 33(a) shows that switching is not exactly repeated for every cycle. Note that even for the highest  $F$  value the waveform cannot be accurately described by a  $\text{sech}^2$  function. It appears from Fig. 33(b) that the core is composed of two distinct materials. The complicated  $\dot{\phi}(t)$  waveforms of Core I-3 in Fig. 33 make it undesirable to use this core for studying the effects of partial setting. The added complexity would make it even more difficult to interpret the experimental results. Note that the shape of these  $\dot{\phi}(t)$  curves (Fig. 33) changes significantly as  $F$  changes. Thus, if this core is a composite of several ferrite materials, the individual components must differ by more than just  $\lambda$ . The  $\dot{\phi}(t)$  of Fig. 33(a) for  $F = 0.906$  amp-turn shows that the true static  $\phi(F)$  curve is re-entrant. At just over the threshold, *i.e.* Fig. 33(a), there is first a delay in switching, and then the core switches with a significant excess of MMF. The re-entrant shape does not show up in Fig. 29



(a)  $F = 0.906$  amp-turn  $\rightarrow$   $\leftarrow 100 \mu\text{sec}$



(b)  $F = 1.23$  amp-turns  $\rightarrow$   $\leftarrow 10 \mu\text{sec}$



(c)  $F = 4.00$  amp-turns  $\rightarrow$   $\leftarrow 0.2 \mu\text{sec}$

RA-3696-244

FIG. 33  $\dot{\phi}(t)$  OF CORE I-3  
No partial setting

because this  $\phi(F)$  curve was obtained with a constant current source. A constant current source results in a vertical section in the  $\phi(F)$  curve, over the re-entrant portion.

### 3. EFFECTS OF VARYING $T_{ps}$

The effects of  $T_{ps}$  on the  $\dot{\phi}(t)$  waveform were determined by photographing several  $\dot{\phi}(t)$  waveforms for different  $T_{ps}$  values, keeping the values of  $\phi_{ps}$ ,  $T_b$ , and  $F$  constant. The value of  $\phi_{ps}$  was held constant as  $T_{ps}$  was changed by adjusting  $F_{ps}$ . The value of  $T_b$  was made large compared to the relaxation time of  $\dot{\phi}(t)$ . These waveforms are shown superimposed for easy comparison. Both positive and negative polarities of the TEST pulse were used for Core I-4 and the results are given in Figs. 34(a) and (b). Only a positive TEST pulse was used for Core I-3 and these results are given in Fig. 35. It can be seen from Figs. 34(a) and 35 that, for a positive TEST pulse,  $\phi_c$  is strongly influenced by variations in  $T_{ps}$  (or  $F_{ps}$ ) as  $\phi_{ps}$  is held constant. This is evidenced by the fact that the initial value of  $\dot{\phi}$ , excluding the initial spike, varies roughly between 50 and 100 percent of  $\dot{\phi}_p$ . The initial value of  $\dot{\phi}$ ,  $\dot{\phi}_0$ , cannot be determined directly from  $\dot{\phi}(t)$  because of the presence of the initial spike. It can be estimated, however, by mentally fitting a  $\text{sech}^2$  function to the  $\dot{\phi}(t)$  waveform and finding the relative value of this function at  $t = 0$  (i.e., at the beginning of the TEST pulse). The ratio of  $\dot{\phi}_0$  to  $\dot{\phi}_p$  increases as  $\phi_c$  increases, providing that  $\phi_0$ ,  $\phi_s$ , and  $\phi_d$  are fixed and  $\phi_0$  is less than  $-\phi_c - (\phi_s - \phi_d)/2$ . A greater value of  $\phi_0$  corresponds to an experimental  $\dot{\phi}(t)$  which has no maximum other than the initial spike.

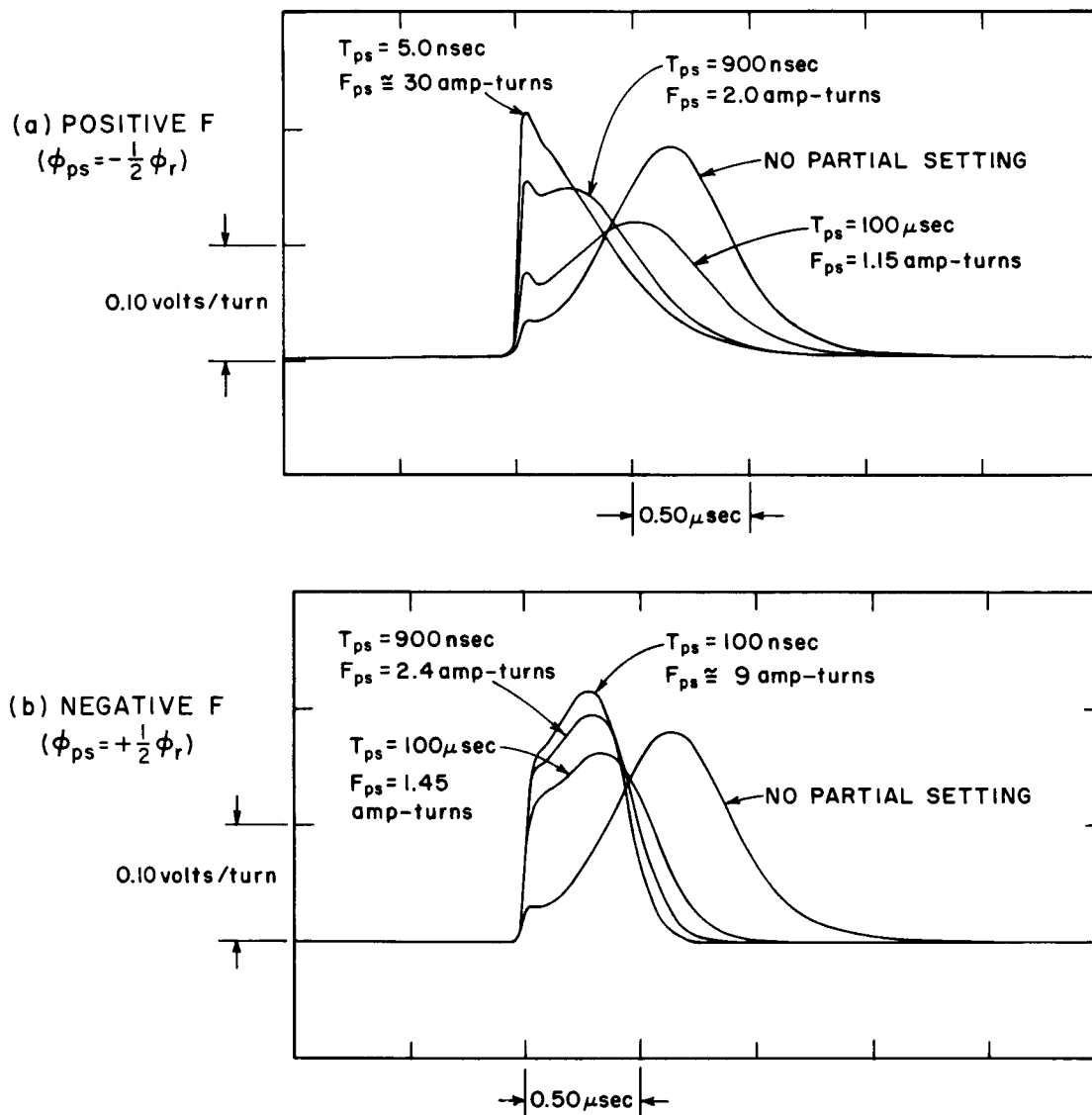
The value of  $\phi_c$  can be calculated from the ratio of  $\dot{\phi}_0$  to  $\dot{\phi}_p$  by use of Eq. (92) and by letting  $\dot{\phi}_p = (F - F_0'')^\nu$ , and  $\phi = \phi_0$ , i.e.,

$$\eta_0 \equiv \frac{\dot{\phi}_0}{\dot{\phi}_p} = 1 - \left( \frac{2\phi_0 + 2\phi_c + \phi_s - \phi_d}{\phi_s + 2\phi_c + \phi_d} \right)^2 \quad (94)$$

where

$$\phi_0 = \phi_{ps} + \Delta\phi' \quad (95)$$

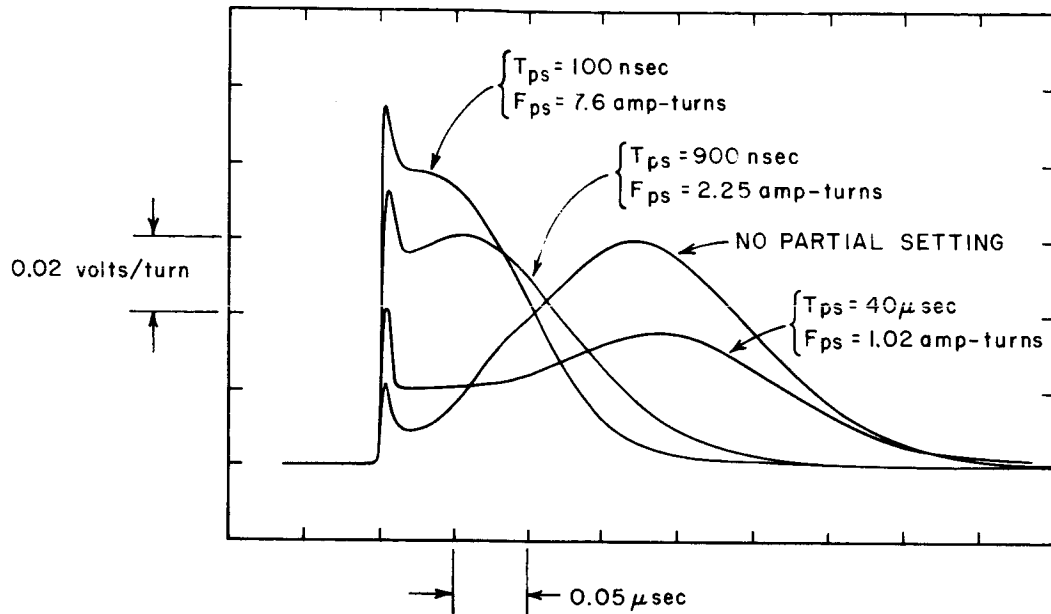
and  $\Delta\phi'$  is defined as the area of the  $\dot{\phi}(t)$  which is not included under the  $\text{sech}^2$  function (see Fig. 7 of Ref. 7).



RA-3696-245

FIG. 34 EFFECTS OF  $T_{ps}$  ON  $\dot{\phi}(t)$  OF CORE I-4  
 $F = 2.50 \text{ amp-turns}$ ,  $T_b = 50 \mu\text{sec}$





RA-3696-246

FIG. 35 EFFECTS OF  $T_{ps}$  ON  $\dot{\phi}(t)$  OF CORE I-3

$$\phi_{ps} = -\frac{1}{2}\phi_r, F = 2.00 \text{ amp-turns}, T_b = 50 \mu \text{sec}$$

Actual values of  $\phi_c$  were not determined as was done in Ref. 7; however, results are clearly similar—that is,  $\phi_c$  increases significantly as  $T_{ps}$  decreases from 100  $\mu$ sec to 100 nsec ( $F_{ps}$  increases).

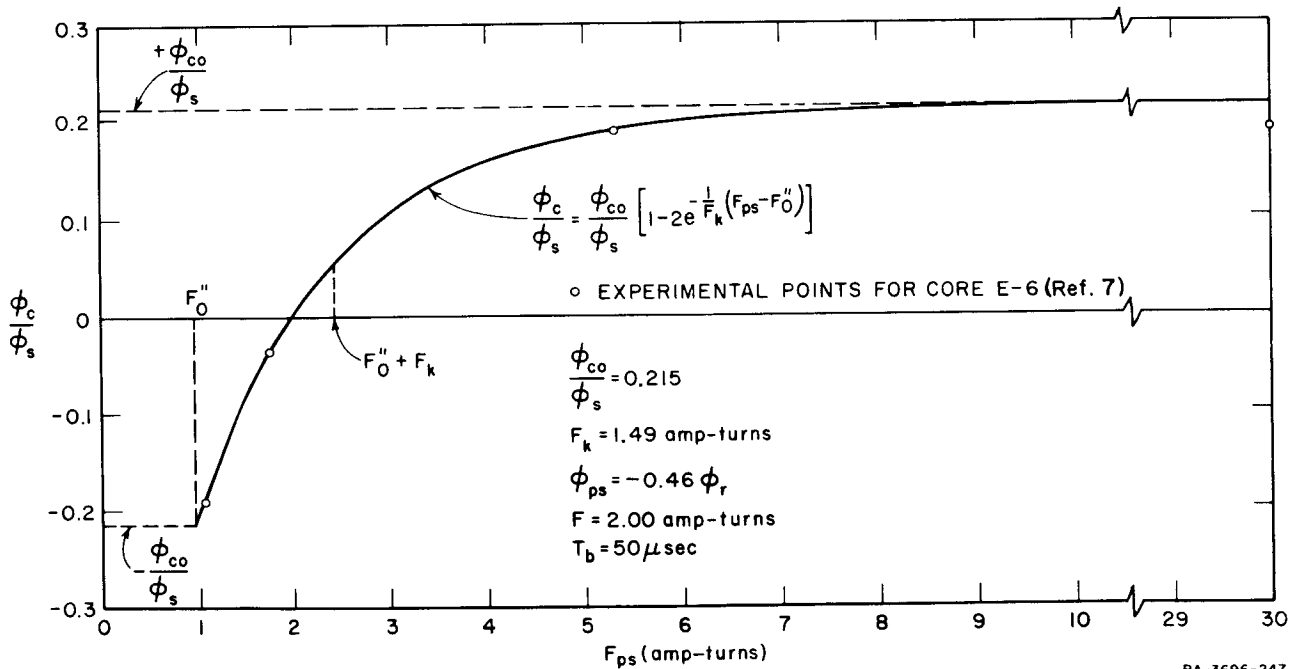
In the case of a negative TEST pulse, Fig. 34(b), it is not as easy to judge the variation of  $\phi_c$  because the waveform of  $\dot{\phi}(t)$  is not as accurately described by a  $\text{sech}^2$  function. The value of  $\dot{\phi}_p$  in this figure, as well as in Figs. 34(a) and 35, is clearly changing as  $T_{ps}$  varies. This is a result of variations in  $F_0''$  and  $\lambda$  and is the primary topic of Part D. It should be recalled that variations in  $\phi_c$  do not influence the value of  $\dot{\phi}_p$  [cf. Eq. (93)]. Changing  $\lambda$  or  $F_0''$  or both affects the value of  $\dot{\phi}_p$  by the same factor as it does the value of peaking time,  $t_p$ . Disregarding any such changes in Fig. 34(b) we see that not much other change is evident. Thus, it can be concluded that  $T_{ps}$  has little effect on  $\phi_c$  when the TEST pulse is negative (if such a quantity as  $\phi_c$  can be defined for a negative TEST pulse). This conclusion must be restricted to Core I-4; no data have been taken for a negative TEST pulse on the other cores (I-3 or E-6).

Values of  $\phi_c$  were calculated in Ref. 7 for Core E-6 for four different values of  $T_{ps}$ , but these  $\phi_c$  values were not plotted. It is, therefore,

worthwhile to include a graph of those values here. For reasons to be discussed in Part E, the values of  $\phi_c$  were plotted *vs.*  $F_{ps}$  rather than *vs.*  $T_{ps}$  ( $\phi_{ps}$  was held constant for these data). This graph is shown in Fig. 36, where the experimental data are represented by points. The solid curve was obtained by fitting an exponential to these points with the restriction that the value of  $\phi_c$  for  $F_{ps} = F_0''$  (i.e.,  $-\phi_{co}$ ) must be equal to the negative of the value for  $F_{ps} \rightarrow \infty$ . This restriction, which was consistent with the data, was made so that  $\phi_c$  could be described as a product of two functions, one having  $F_{ps}$  as an argument, and the other  $\phi_{ps}$ . This resulted in a simpler function. An exponential function was used merely as an example of the general type of function required to describe  $\phi_c$  *vs.*  $F_{ps}$ . The exponential function plotted in Fig. 36 is

$$\phi_c = \phi_{co} [1 - 2e^{-(1/F_k)(F_{ps} - F_0'')}]$$
 (96)

where  $\phi_{co}$  is some function of  $\phi_{ps}$  and  $F_k$  is some function of  $F$ . The value of  $F_k$  was determined empirically to be 1.49 amp-turns for the  $F$  value (2.00 amp-turns) used in taking the data of Fig. 36. The data of Fig. 36 was taken with  $T_b$  large compared to the relaxation time. If  $T_b$



RA-3696-247

FIG. 36  $\phi_c$  *vs.*  $F_{ps}$

is reduced to zero for  $F = F_{ps}$  then switching must reduce to that obtained for a constant MMF throughout switching. This means that  $\phi_c$  must be zero for  $T_b = 0$  and  $F_{ps} = F$ . In Fig. 36 it appears as if  $\phi_c = 0$  at  $F = F_{ps} = 2.00$  amp-turns, even though  $T_b \neq 0$ . Perhaps at small  $F_{ps}$  values,  $T_b$  has little effect upon  $\phi_c$ . It is interesting to assume, tentatively, that Eq. (96) is applicable for  $T_b = 0$  and apply the restriction  $\phi_c = 0$  for  $F_{ps} = F$ , so that  $F_k$  can be calculated as a function of  $F$  and  $F_0''$ . In doing this we obtain

$$F_k = \frac{F - F_0''}{\ln 2} \quad (97)$$

Substituting Eq. (97) into Eq. (96) results in

$$\phi_c = \phi_{c0} \left\{ 1 - 2^{[(F - F_{ps}) / (F - F_0'')] } \right\} \quad (98)$$

Equations (96), (97), and (98) have been obtained from data of Core E-6 and, therefore, cannot be assumed to be correct for other cores. However, some indication of the general trend of  $\phi_c$  vs.  $F_{ps}$  and  $F$  of Core I-4 can be gained by checking Eq. (98) with some of the data of Core I-4. These checks are not intended to prove the general validity of Eq. (98) but only to test its plausibility.

Note that Eq. (98) results in a positive  $\phi_c$  for  $F < F_{ps}$  and a negative  $\phi_c$  for  $F > F_{ps}$ . This effect can be checked for Core I-4 at  $F = 2.50$  amp-turns, and  $\phi_{ps} = -(1/2)\phi_r$  by estimating the ratio  $\dot{\phi}_0$  to  $\dot{\phi}_p$  in Fig. 34(a). Assuming that  $\Delta\phi'$  is about  $0.052 \phi_s$  (taken from the data of Ref. 7) and reading  $\phi_d$  for  $F = 2.5$  amp-turns from Fig. 30(a) as  $0.936 \phi_s$ , and  $\phi_r = 0.96 \phi_s$ , we obtain  $\phi_0 = \phi_{ps} + \Delta\phi' = -(1/2)(0.96 \phi_s) + 0.052 \phi_s = -0.43 \phi_s$ . Using these values in Eq. (94), and letting  $\phi_c = 0$ , results in a ratio of  $\dot{\phi}_0$  to  $\dot{\phi}_p$  0.83. In Fig. 34(a) we see that for  $F_{ps} = 1.15$  amp-turns  $< F$ , the ratio of  $\dot{\phi}_0$  to  $\dot{\phi}_p$  is certainly less than 0.83 and therefore  $\phi_c$  is negative, in agreement with Eq. (98). Likewise for  $F_{ps} \approx 30$  amp-turns  $> F$ ,  $\dot{\phi}_0 \approx \dot{\phi}_p$ , therefore  $\phi_c$  is positive, again in agreement with Eq. (98). In the intermediate case,  $F_{ps} = 2.0$  amp-turns,  $\dot{\phi}(t)$  has a ratio of  $\dot{\phi}_0$  to  $\dot{\phi}_p$  which is only slightly less than 0.83, thereby resulting in a value of  $\phi_c$  which is a little less than zero, also in agreement with Eq. (98). For these values Eq. (98) appears, at least, to give the correct trend for  $\phi_c$  vs.  $F_{ps}$ .

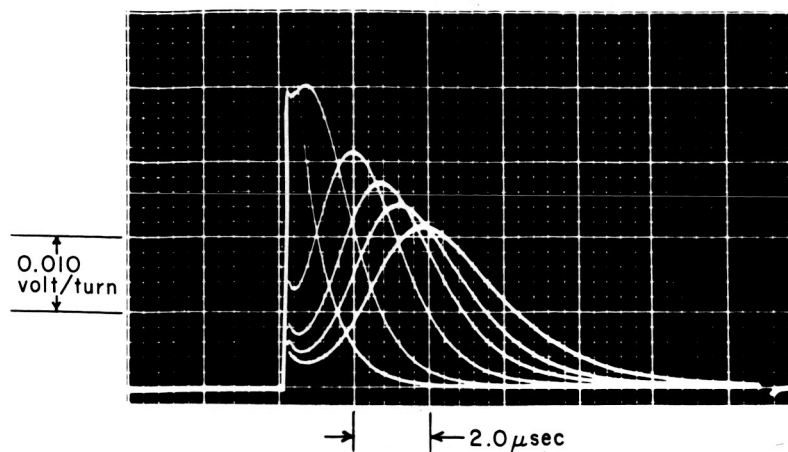
#### 4. EFFECTS OF VARYING $\phi_{ps}$

The effects of  $\phi_{ps}$  upon the  $\dot{\phi}(t)$  waveform were examined by photographing the  $\dot{\phi}(t)$  waveforms for several values of  $\phi_{ps}$ . The values of  $\phi_{ps}$  were obtained by varying  $F_{ps}$ . The value of  $T_{ps}$  was held fixed at 5 nsec, which is at the low end of the range of possible  $T_{ps}$  values. This value of  $T_{ps}$  was chosen because it resulted in the largest values of  $\phi_c$ . Three families of waveforms were obtained, corresponding to low, medium, and high values of  $F$  of the TEST pulse. These are given in Fig. 37(a), (b), and (c), respectively. It should be recalled that the rise time of the TEST pulse is about 50 nsec, because it influences the early part of the waveforms for the medium and high  $F$  values.

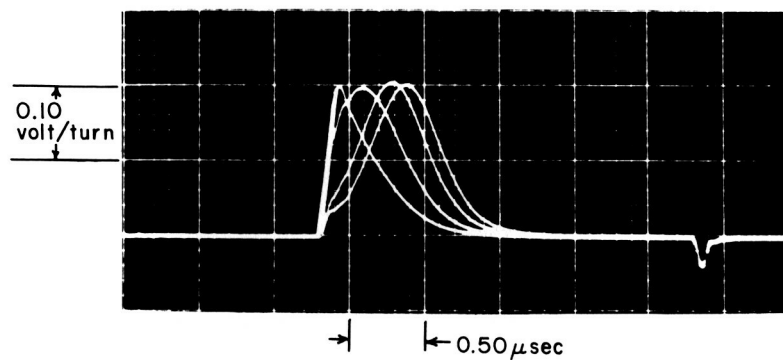
Note that at  $F = 1.50$  amp-turns, Fig. 37(a), increasing  $\phi_{ps}$  increases  $\dot{\phi}_p$ , whereas, for  $F = 4.00$  amp-turns, Fig. 37(c), increasing  $\phi_{ps}$  decreases  $\dot{\phi}_p$ . This implies a change in both  $\lambda$  and  $F_0''$  with  $\phi_{ps}$  and is discussed further in Part D in connection with the  $\dot{\phi}_p(F)$  data. Note also that the waveform does not appear to change (disregarding scale factors) when  $\phi_{ps}$  is increased except for the location of the beginning of the waveform relative to its peak.

The effects of  $\phi_{ps}$  upon  $\phi_c$  have not been carefully examined. When  $\phi_{ps}$  is varied,  $\phi_0$  also varies, and this causes a variation in the ratio of  $\dot{\phi}_0$  to  $\dot{\phi}_p$  even if  $\phi_c$  is constant [cf. Eq. (94)]. Thus, cursory observations of  $\dot{\phi}(t)$  waveforms for various values of  $\phi_{ps}$  are not sufficient to determine even qualitative variations in  $\phi_c$ . Instead,  $\Delta\phi'$  and  $\dot{\phi}_0$  must be measured so that  $\phi_0$  can be determined from Eq. (95) and  $\phi_c$  calculated from Eq. (94). It is reasonable to assume, however, that for a very small  $\Delta\phi_{ps}$ , varying  $F_{ps}$  will have little effect upon  $\phi_c$ , and that as  $\Delta\phi_{ps}$  increases the effects of  $F_{ps}$  upon  $\phi_c$  will increase. The value of  $\phi_c$  for no partial setting is probably nearly zero for all values of  $F$ , although, this has not been experimentally verified. Determination of the variation of  $\phi_c$  with  $F$  for no partial setting is complicated by the small variation of  $\phi_0$  with  $F$ , which is a subtle problem needing further investigation. It can be shown from Eq. (93) that the total flux switched is a function of  $\phi_0$  but not a function of  $\phi_c$ . These two quantities must not, therefore be confused with each other.

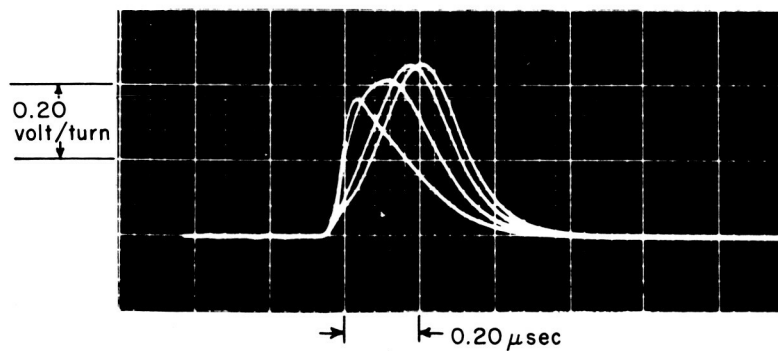
The quantity  $\phi_{c_0}$  of Eqs. (96) and (98) was said to be a function of  $\phi_{ps}$ . This function has not yet been determined. However, it is likely



- (a)  $F = 1.5$  amp-turns  
 $(\Delta\phi_{ps}/\phi_r = 0.031, 0.042, 0.055, 0.078, 0.202, 0.75)$



- (b)  $F = 2.6$  amp-turns  
 $(\Delta\phi_{ps}/\phi_r = 0.028, 0.055, 0.20, 0.74)$



- (c)  $F = 4.0$  amp-turns  
 $(\Delta\phi_{ps}/\phi_r = 0.028, 0.055, 0.20, 0.74)$

RA-3696-248

FIG. 37 EFFECTS OF  $\Delta\phi_{ps}$  ON  $\dot{\phi}(t)$

Core I-4,  $T_{ps} = 5.0$  nsec,  $T_b = 50$   $\mu$ sec,  $\Delta\phi_{ps} = \phi_{ps} + \phi_r$

that  $\phi$  increases monotonically from zero as  $\phi_{ps}$  increases from  $-\phi_r$  to zero. It is not yet known whether  $\phi_{co}$  continues to increase as  $\phi_{ps}$  exceeds zero or whether it begins to decrease when  $\phi_{ps}$  exceeds zero.

As another rough check of Eq. (98), consider the second to the left-most  $\dot{\phi}(t)$  waveform in Fig. 37(a). For this  $\dot{\phi}(t)$ ,  $\phi_{ps} = -0.80 \phi_r$ . An estimate of the ratio of  $\dot{\phi}_0$  to  $\dot{\phi}_p$  from this waveform is 0.90. Determining  $\phi_d$  to be  $0.70 \phi_s$  from Fig. 30(a),  $\phi_r$  to be  $0.96 \phi_s$ , and estimating  $\Delta\phi'$  to be  $0.03 \phi_s$  (less than the  $0.052 \phi_s$  used above because  $F$  is smaller here), we obtain  $\phi_0 = -0.74 \phi_s$ . Using these values in Eq. (94) and solving for  $\phi_c$  results in  $\phi_c = 0.24 \phi_s$ . In this case  $F_{ps}$  is equal to approximately 27 amp-turns which is much larger than the 1.50 amp-turn value of  $F$ . Since  $F \ll F_{ps}$ , Eq. (98) results in  $\phi_c = \phi_{co}$ , which is  $0.215 \phi_s$  for Core E-6 (Fig. 36). The 0.24 value is quite high considering the fact that  $\Delta\phi_{ps}$  is only  $0.20\phi_r$  for this calculation, whereas, in Fig. 36  $\Delta\phi_{ps}$  is  $1/2\phi_r$ . Perhaps  $\phi_{co}$  is significantly larger for Core I-4 than for Core E-6. However, the fact that  $\phi_c$  is strongly positive for  $F \ll F_{ps}$  is in qualitative agreement with Eq. (98).

The formulation and checks of Eq. (98) were only approximate. Therefore, this equation must not yet be taken as more than an approximate example of the relationship of  $\phi_c$  to  $F_{ps}$ ,  $\phi_{ps}$ , and  $F$ . Much more experimental work needs to be done to establish more rigorously these relationships, especially with regards to the effects of  $\phi_{ps}$ .

## 5. SUMMARY

The parabolic model of Sect. I-A was modified to include the parameter  $\phi_c$ . Experimental  $\dot{\phi}(t)$  waveforms for partially set states were compared to a  $\text{sech}^2$  function. It was found that the  $\dot{\phi}(t)$  for a positive TEST pulse was very similar to a  $\text{sech}^2$  function, as was also the case for Core E-6 of Ref. 7. Thus the parabolic model should prove to be useful if its parameters can be adequately determined as a function of the partially set state. The  $\dot{\phi}(t)$  for a negative TEST pulse was not accurately described by a  $\text{sech}^2$  function, especially not at low  $F$  values. The  $\dot{\phi}(t)$  of Core I-3 was not accurately described by a  $\text{sech}^2$  function even for no partial setting. It was found that the major effect of  $T_{ps}$  on the  $\dot{\phi}(t)$  waveform for a positive TEST pulse was to change  $\phi_c$ . This effect was very similar to that of Core E-6. No such effect was obtained for a negative TEST pulse. Data from Ref. 7 for Core E-6 was plotted and from this plot a function for  $\phi_c(F_{ps}, F)$  was obtained. A few rough checks of this equation from the data of Core I-4 indicated that this function seems reasonable.

The effects of  $\phi_{ps}$  on  $\dot{\phi}(t)$  were discussed and it was speculated that  $\phi_{ps}$  affects the coefficient  $\phi_{co}$  of the function for  $\phi_c(F_{ps}, F)$ .

#### D. CURVES OF $\dot{\phi}_p(F)$

##### 1. INTRODUCTION

Once the static  $\phi(F)$  curves and the  $\dot{\phi}(t)$  waveforms have been determined for each partially set state, it is important to determine how the speed of switching varies with the applied MMF,  $F$ . There are two common methods of determining this property: one is to measure  $\dot{\phi}_p$  vs.  $F$ , and the other is to measure  $1/\tau_s$  vs.  $F$ . The factors which need to be considered in deciding between these two methods were discussed in Ref. 7. It was decided, on the basis of these factors, that the method based upon  $\dot{\phi}_p$  vs.  $F$  would be used for this report. These  $\dot{\phi}_p(F)$  data were found to be decided, on the basis of these factors, that the method based upon  $\dot{\phi}_p$  vs.  $F$  would be used for this report. These  $\dot{\phi}_p(F)$  data were found to be describable by the function

$$\dot{\phi}_p = \lambda(F - F_0'')^\nu \quad (99)$$

as is usually the case for switching which is initiated from  $-\phi_r$  (for thin ring cores). This equation is consistent with Eq. (93). The variations of the quantities  $F_0''$ ,  $\lambda$ , and  $\nu$  as a function of  $\phi_{ps}$ ,  $T_{ps}$ , and  $T_b$  can then be examined. In the case of a negative TEST pulse,  $\dot{\phi}(t)$  can not be accurately described by a  $\text{sech}^2$  function alone. Therefore, the parabolic model is not capable of describing this switching. The values of  $F_0''$ ,  $\lambda$ , and  $\nu$  for this case do not, therefore, apply to Eqs. (92) and (93). However, they can be used to describe the  $\dot{\phi}_p(F)$  curves. The object of this part of the report is to study the effects of partial setting upon  $F_0''$ ,  $\lambda$ , and  $\nu$ .

The  $\dot{\phi}_p(F)$  data were taken by first establishing the desired partially set state and then measuring the peak  $\dot{\phi}$  during the TEST pulse as a function of the  $F$  of the TEST pulse. The flux level,  $\phi_{ps}$ , of the partially set state was determined by temporarily removing the TEST pulse and measuring the flux switched by the first CLEAR pulse. The effects of  $\phi_{ps}$ ,  $T_{ps}$ , and  $T_b$ , upon the  $\dot{\phi}_p(F)$  curve were determined by varying one of these quantities at a time while holding the other two fixed. For each partially set state, the data were plotted as  $\dot{\phi}_p$  vs.  $(F - F_0'')$  on log-log paper to determine  $F_0''$ ,  $\lambda$ , and  $\nu$ . A trial-and-error process was used to determine which value of  $F_0''$  resulted in a straight-line plot. The value of  $\nu$  was then determined as the slope of this line, and  $\lambda$  as the  $\dot{\phi}_p$  value for  $F - F_0'' = 1$  amp-turn.

Error bars in  $F''_0$ ,  $\lambda$ , and  $\nu$  were estimated by determining how much  $F''_0$  could be changed before a noticeable curvature showed up in the log-log plot of  $\dot{\phi}_p$  vs.  $(F - F''_0)$ . Once  $F''_0$ ,  $\lambda$  and  $\nu$  were determined, for each partially set state, these values were used to calculate the  $\dot{\phi}_p(F)$  curves which are shown as solid lines in all of the figures containing  $\dot{\phi}_p(F)$  data.

The  $\dot{\phi}_p(F)$  data were restricted to the cases in which  $\phi_{ps}$  was less than  $-0.3 \phi_r$ . For larger values of  $\phi_{ps}$ , and all except the largest values of  $T_{ps}$ , no major maximum in  $\dot{\phi}(t)$  was obtained. Even when  $\phi_{ps}$  and  $T_{ps}$  were near their limits the data could not be taken at the very low  $F$  values because the tail of the initial spike increased enough to obscure the major maximum in  $\dot{\phi}$ . As  $T_{ps}$  decreases, for a positive  $F$ ,  $\phi_c$  increases (cf. Fig. 36). As  $\phi_c$  increases, the argument of the  $\text{sech}^2$  function in Eq. (93) increases toward zero. If the argument becomes equal to or greater than zero, no maximum in  $\dot{\phi}(t)$  is obtained [cf. Eq. (93)]. Thus, for a given  $\phi_{ps}$ , and a positive  $F$ , as  $T_{ps}$  is decreased below a certain value, the major maximum in  $\dot{\phi}$  becomes obscured by the initial spike, or ceases to exist at all, and no, or very little,  $\dot{\phi}_p(F)$  data can be taken. For  $\phi_{ps} = -(1/2)\phi_r$ , this value of  $T_{ps}$  was somewhat less than 500 nsec for Core I-4. For a negative  $F$ , this problem is not nearly as serious, and  $\dot{\phi}_p(F)$  data can be taken for much smaller  $T_{ps}$  values. Most of the  $\dot{\phi}_p(F)$  data were taken on Core I-4.

In Part D-2 we consider the effects of  $T_{ps}$  upon the  $\dot{\phi}_p(F)$  curve, in Part D-3 we consider the effect of  $\phi_{ps}$ , and in Part D-4 we consider the effect of  $T_b$ . Part D-5 contains further, more general, discussion and conclusions.

## 2. EFFECTS OF VARYING $T_{ps}$

Curves of  $\dot{\phi}_p(F)$  for  $\phi_{ps} = -(1/2)\phi_r$ , with  $T_{ps}$  as a parameter, were taken with both a positive and a negative TEST pulse. Curves for  $T_{ps}$  values of 100  $\mu\text{sec}$ , 900 nsec, and 500 nsec, and a positive TEST pulse are given in Fig. 38. The  $\dot{\phi}_p(F)$  for no partial setting is included as a reference. The most important result of these data is that the slope of the curves for partial setting is much lower at a given  $F$  value than for no partial setting. This is very similar to the results of Core E-6 in Ref. 7. Only two  $\dot{\phi}_p(F)$  curves were taken for Core I-3, one for no partial setting, and one for  $T_{ps} = 900$  nsec. These curves are shown in Fig. 39. These curves show the same general characteristics as the corresponding curves for Cores I-4 and E-6.



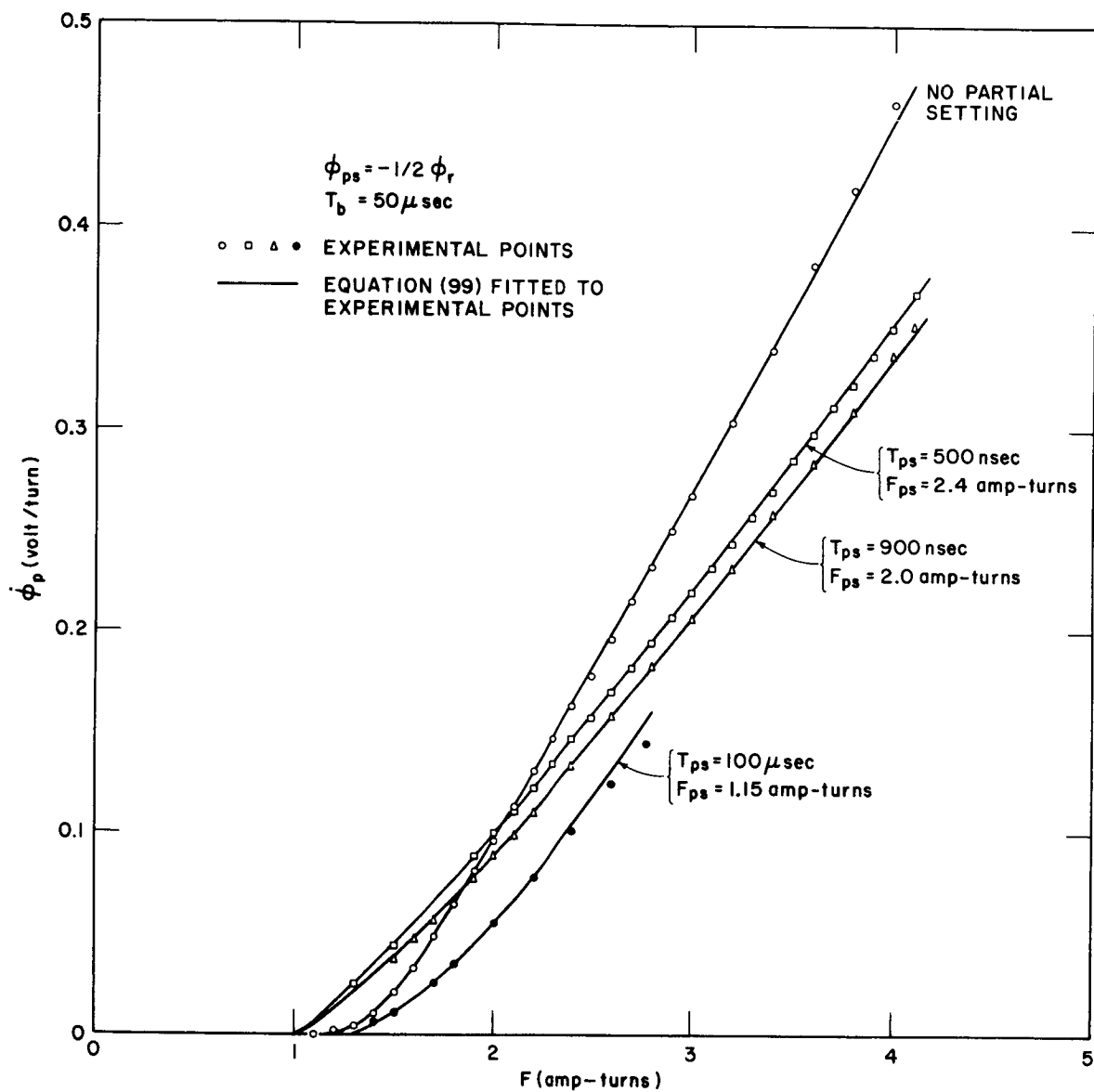
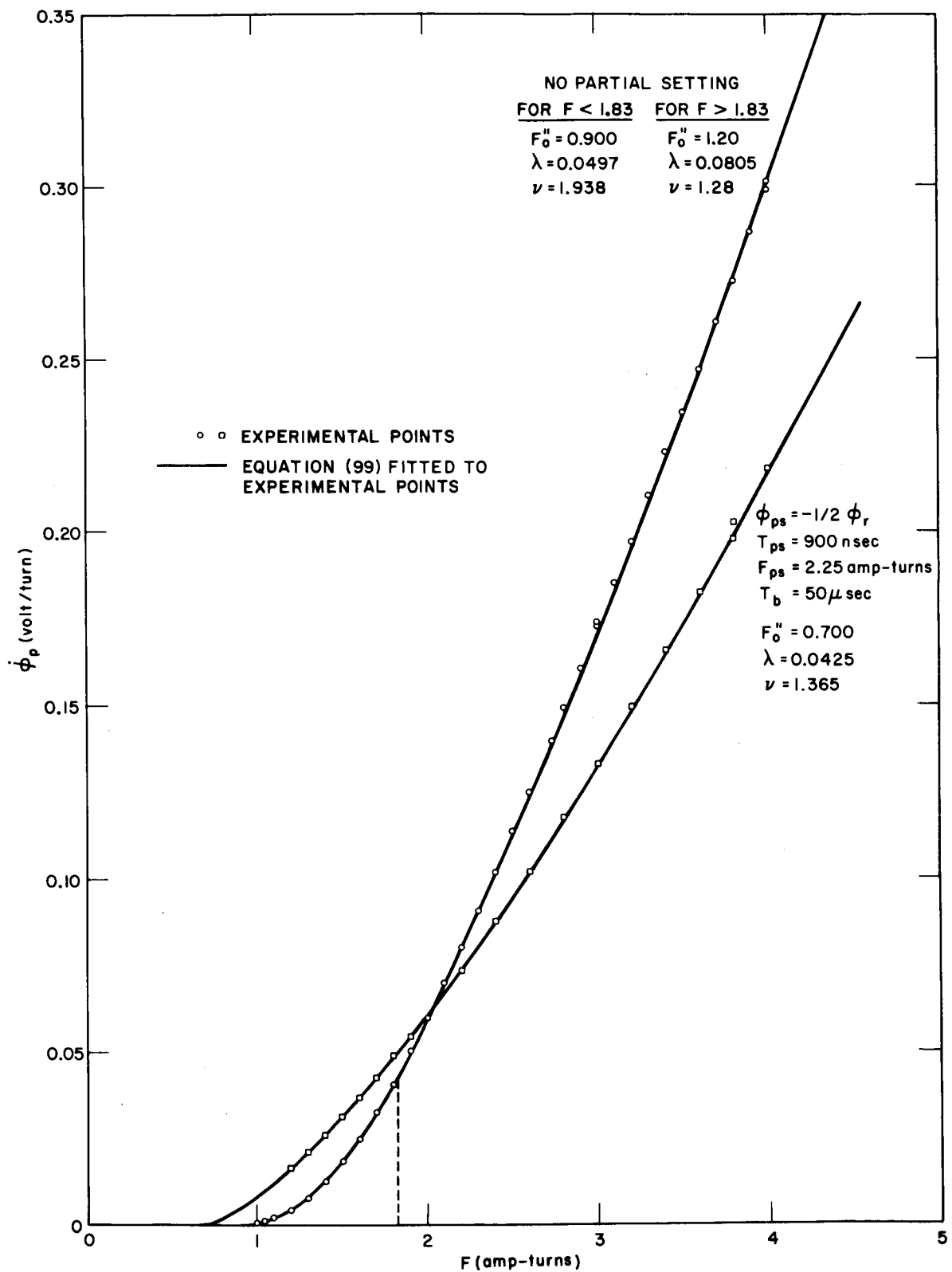


FIG. 38  $\dot{\phi}_p$  (+F) OF CORE I-4 WITH  $T_{ps}$  AS A PARAMETER



RB-3696-250

FIG. 39  $\dot{\phi}_p (+F)$  OF CORE I-3

The no partial setting curve in Fig. 38 exhibits a subtle change in curvature near  $F = 1.62$  amp-turns, which is not noticeable in the figure. However when  $\dot{\phi}_p$  is plotted *vs.*  $(F - F_0'')$  with log-log scales, the transition can be easily seen, and is illustrated in Fig. 40. The lower region, below  $F = 1.62$  amp-turns, can be described with  $F_0'' = 1.10$  amp-turns,  $\lambda = 0.146$ , and  $\nu = 2.14$ . The upper region can be described by either two linear segments, (not shown in Fig. 40) or a single curve having  $F_0'' = 1.35$ ,  $\lambda = 0.154$ , and  $\nu = 1.1$ . The amount of curvature above  $F = 1.62$  amp-turns is small enough, compared to the scatter of the data points, that it is difficult to judge which description is more accurate. The horizontal dashed line in Fig. 40, which is at  $F = 1.62$  amp-turns, indicates the transition between the two regions. This value was chosen so that the slopes of the two regions of  $\dot{\phi}_p(F)$  would be equal. The physical reasons for two different regions in the  $\dot{\phi}_p(F)$  curve are not known. It might be that there are two different mechanisms of switching, such as domain wall motion and noncoherent rotation or perhaps just some variations of domain wall switching. The  $\dot{\phi}_p(F)$  data of Core E-6 did not require more than one region to be described by Eq. (96) for a comparable range of  $F$ . However, the no-partial-setting  $\dot{\phi}_p(F)$  data of Core I-3 also required two regions with a transition at  $F = 1.83$  amp-turns. The values of  $F_0''$ ,  $\lambda$ , and  $\nu$  used for the solid curves of Fig. 38 are plotted *vs.*  $T_{ps}$  in Fig. 41 to illustrate general trends. The data are not accurate enough, nor complete enough, to determine exact functional relationships. However, for the following discussion, it is assumed that the curves drawn in Fig. 41 are indicative of the actual relationships between these quantities. The value of  $F_0''$ ,  $\lambda$ , and  $\nu$  for Core I-3 are given in Fig. 39 since there is only one  $\dot{\phi}_p(F)$  curve for a partially set state.

The 100- $\mu$ sec  $\dot{\phi}_p(F)$  curve in Fig. 38 deviates from the experimental points at the upper end. However, not enough data points were taken to determine the values of  $F_0''$ ,  $\lambda$ , and  $\nu$  above  $F = 2.5$  amp-turns.

Even though the  $\dot{\phi}_p(F)$  curves for Core I-4 appear to be qualitatively similar to the curves for Core E-6, the quantitative examination of  $F_0''$ ,  $\lambda$ , and  $\nu$ , as given in Fig. 41, points out several significant differences between these two cores. However, before these differences are discussed, it should be recalled that Core I-4 has an OD/ID ratio of 1.10 whereas Core E-6 of Ref. 7 had a ratio of only 1.06. The 1.10 ratio of Core I-4 might be large enough to begin influencing

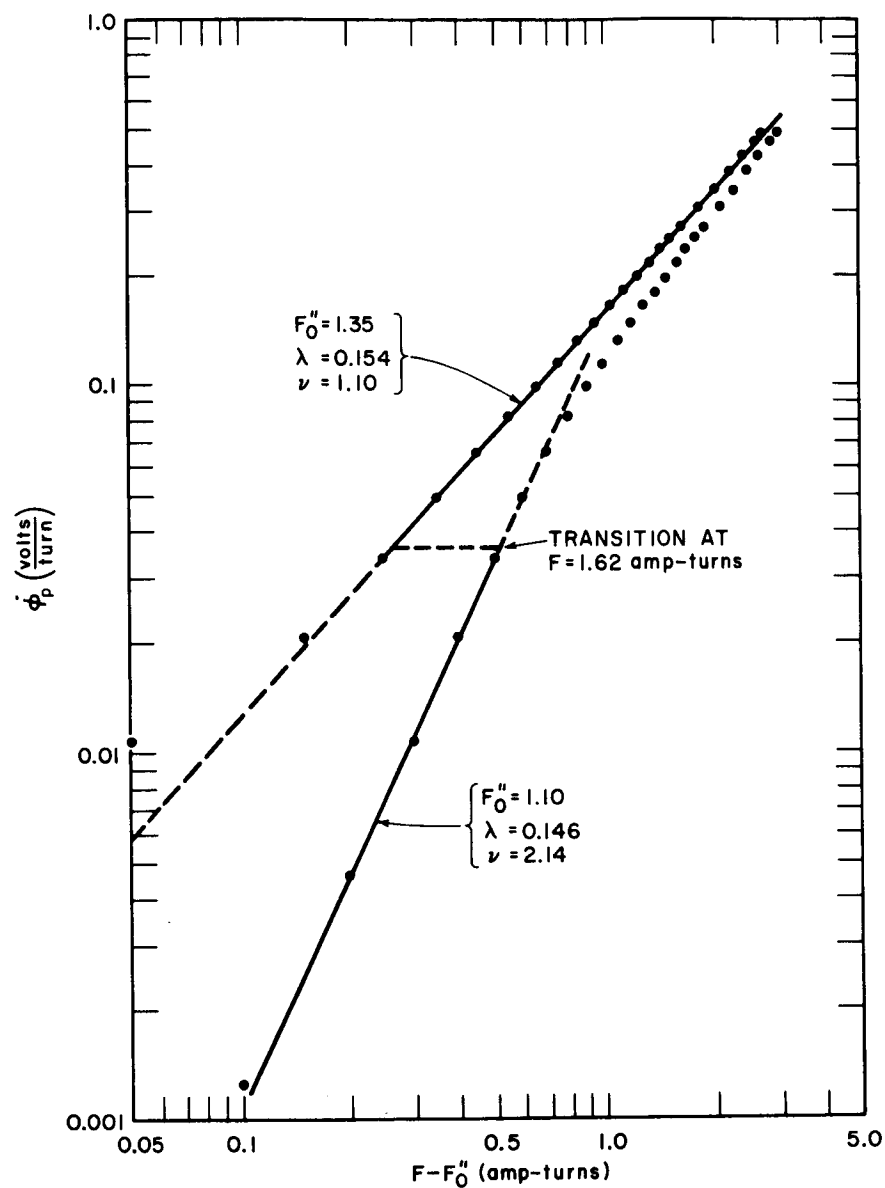
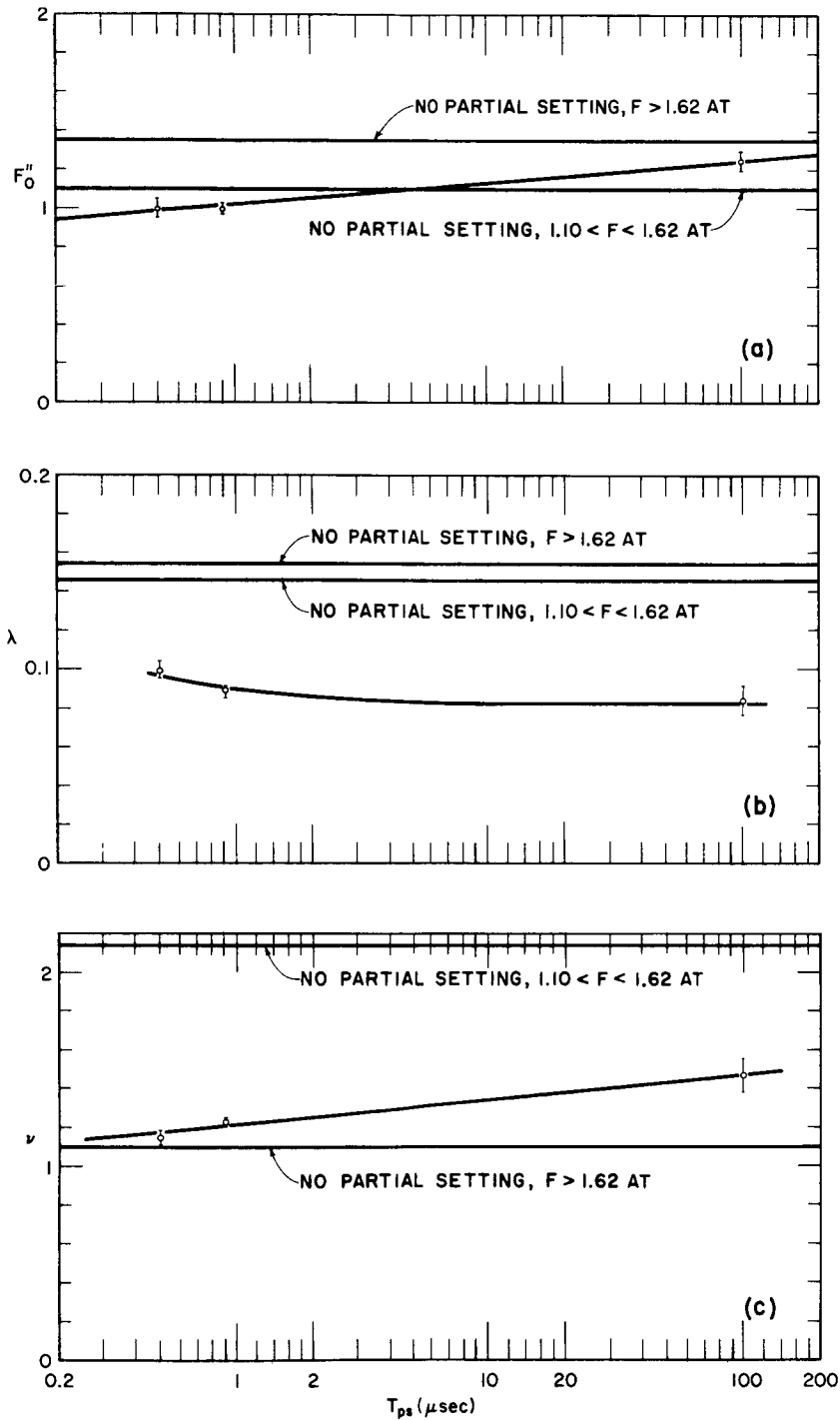


FIG. 40  $\log \dot{\phi}_p$  vs.  $\log (F - F_0'')$  OF CORE I-4  
No partial setting



RC-3696-252

FIG. 41  $F_0''$ ,  $\lambda$ , AND  $\nu$  vs.  $T_{ps}$  FOR A POSITIVE TEST PULSE  
Core I-4,  $\phi_{ps} = -\frac{1}{2}\phi_r$ ,  $T_b = 50 \mu\text{sec}$

the curvature in  $\dot{\phi}_p(F)$  by a small amount, but it is not likely that the difference in the OD/ID ratios can account for the difference in  $F''_0$ ,  $\lambda$ , and  $\nu$  to be discussed. There is also a possibility that core surface effects could produce some differences since the surface-to-volume ratio of Core E-6 is about 70 percent greater than of Core I-4. This possibility has not been investigated, but several experiments<sup>12</sup> have led us to believe that surface effects are probably not too important as long as both cores being compared have cut rather than molded surfaces (both Cores E-6 and I-4 were made by ultrasonic cutting). It is, therefore, assumed that any differences result from differences in the material property.

Figure 41(a) indicates that  $F''_0$  of Core I-4 decreases only moderately as  $T_{ps}$  is decreased. This is in contrast to Core E-6, for which  $F''_0$  (called  $F''_0$  in Ref. 7) decreased very little as  $T_{ps}$  decreased from 100  $\mu\text{sec}$  to 5  $\mu\text{sec}$ , but below  $T_{ps} = 1 \mu\text{sec}$ ,  $F''_0$  decreased quite rapidly. The  $F''_0$  vs.  $T_{ps}$  curve for Core E-6 extrapolated to zero at about  $T_{ps} = 0.4 \mu\text{sec}$ , whereas for Core I-4 the curve extrapolates to zero somewhere below 1 nsec.

It is interesting to note that these differences in Core E-6 and I-4 do not show up in the 700- $\mu\text{sec}$   $\phi(F)$  curves.

Cores E-6 and I-4 have very similar properties concerning the effect of  $T_{ps}$  upon  $\lambda$ . In both cores,  $\lambda$  (called  $K$  in Ref 7) was reduced by about 42 percent as a result of partial setting to  $\phi_{ps} = -(1/2)\phi_r$ , and was relatively independent of  $T_{ps}$  ( $\lambda$  is not much different for the two  $F$  regions for Core I-4). The only difference noted was that as  $T_{ps}$  was decreased from 1  $\mu\text{sec}$  to 0.5  $\mu\text{sec}$ , a slight increase in  $\lambda$  occurred for Core I-4, whereas a slight decrease occurred for Core E-6. In both cases, however, this change was comparable to the measurement inaccuracies, and may not necessarily represent a true property of the materials. Core I-3 shows some significant differences regarding  $\lambda$ . In the first place,  $\lambda$  for Core I-3 for no partial setting is 1.6 times larger for the upper  $F$  region of  $\dot{\phi}_p(F)$  than it is for the lower region (cf. Fig. 39). For Core I-4,  $\lambda$  of the upper and lower regions differed by a factor of only 1.05. The data of Fig. 39 show that partial setting to  $-(1/2)\phi_r$  reduced  $\lambda$  of the lower  $F$  region of Core I-3 by only 15 percent whereas it reduced  $\lambda$  of the upper region by 47 percent. The  $\dot{\phi}_p(F)$  data for Core I-3 for a 900- $\mu\text{sec}$  PARTIAL SET pulse did not have to be broken into two regions to be described by Eq. (99). The transition from a  $\dot{\phi}_p(F)$  curve of two regions

to one of one region will be illustrated when the effects of  $\phi_{ps}$  upon  $F''_0$ ,  $\lambda$ , and  $\nu$  are examined for Core I-4.

A comparison of the effects of  $T_{ps}$  upon  $\nu$  for Cores I-4 and E-6 reveals that for  $T_{ps}$  between 100  $\mu$ sec and 3  $\mu$ sec the  $\nu$  are practically equal, and that as  $T_{ps}$  decreases below 3  $\mu$ sec,  $\nu$  of Core E-6 begins to curve upward whereas  $\nu$  of Core I-4 continues downward.

The  $\dot{\phi}(t)$  waveform for a negative TEST pulse (Part C) exhibited a well defined maximum for  $\phi_{ps} = -(1/2)\phi_r$  even for very small values of  $T_{ps}$ . Therefore,  $\dot{\phi}_p(-F)$  curves could be taken for much smaller values of  $T_{ps}$ , for a comparable  $\phi_{ps}$ , than  $\dot{\phi}_p(F)$  curves for a positive TEST pulse. Curves of  $\dot{\phi}_p(-F)$  for  $T_{ps}$  values of 100  $\mu$ sec, 900 nsec, 500 nsec, and 100 nsec are given in Fig. 42. A curve was taken for  $T_{ps} = 20$  nsec but not included in Fig. 42 to prevent crowding. The value of  $\phi_{ps}$  for these curves was  $+(1/2)\phi_r$ , which is comparable (cf. Fig. 26) as far as total flux switched is concerned, to  $-(1/2)\phi_r$  for a positive TEST pulse. It should be recalled that  $\dot{\phi}(t)$  for a negative TEST pulse is not very well described by a  $\text{sech}^2$  function. Thus, the values of  $F''_0$ ,  $\lambda$ , and  $\nu$  determined from the  $\dot{\phi}_p(-F)$  curves of Fig. 42 cannot be used in the parabolic switching model except for rough approximations.

The major difference between the  $\dot{\phi}_p(-F)$  curves of Fig. 42 and the  $\dot{\phi}_p(+F)$  curves of Fig. 38 is the difference in the slopes of the curves. For a negative TEST pulse,  $\lambda$  is not lowered as much by partial setting as it was for a positive TEST pulse. This is consistent with the nucleation of negative domains within the previous positive domains, as was discussed in Parts B-3 and C-2. This is illustrated in Fig. 43, where  $F''_0$ ,  $\lambda$  and  $\nu$  for a negative TEST pulse are plotted vs.  $T_{ps}$ . Note also that  $\lambda$  increases somewhat as  $T_{ps}$  decreases.

The curvature shown for  $F''_0$  vs.  $T_{ps}$  in Fig. 43 is barely greater than the error bars so that it is debatable whether  $F''_0$  is constant with  $T_{ps}$  or variable as shown. The values of  $F''_0$  from this curve are given by asterisks on the  $\phi(-F)$  curves of Fig. 30(b). These values fall near the values of  $F_c$  as was also the case for a positive TEST pulse [Fig. 30(a)].

Since  $\lambda$  is not much reduced by partial setting, for a negative TEST pulse, and  $F''_0$  is reduced somewhat, the  $\dot{\phi}_p(F)$  curves of Fig. 42 fall mostly above the curve for no partial setting. In addition, the  $\dot{\phi}(t)$  curves for the same conditions indicated that some of the flux is switched by another mechanism (i.e., other than that described by the parabolic model

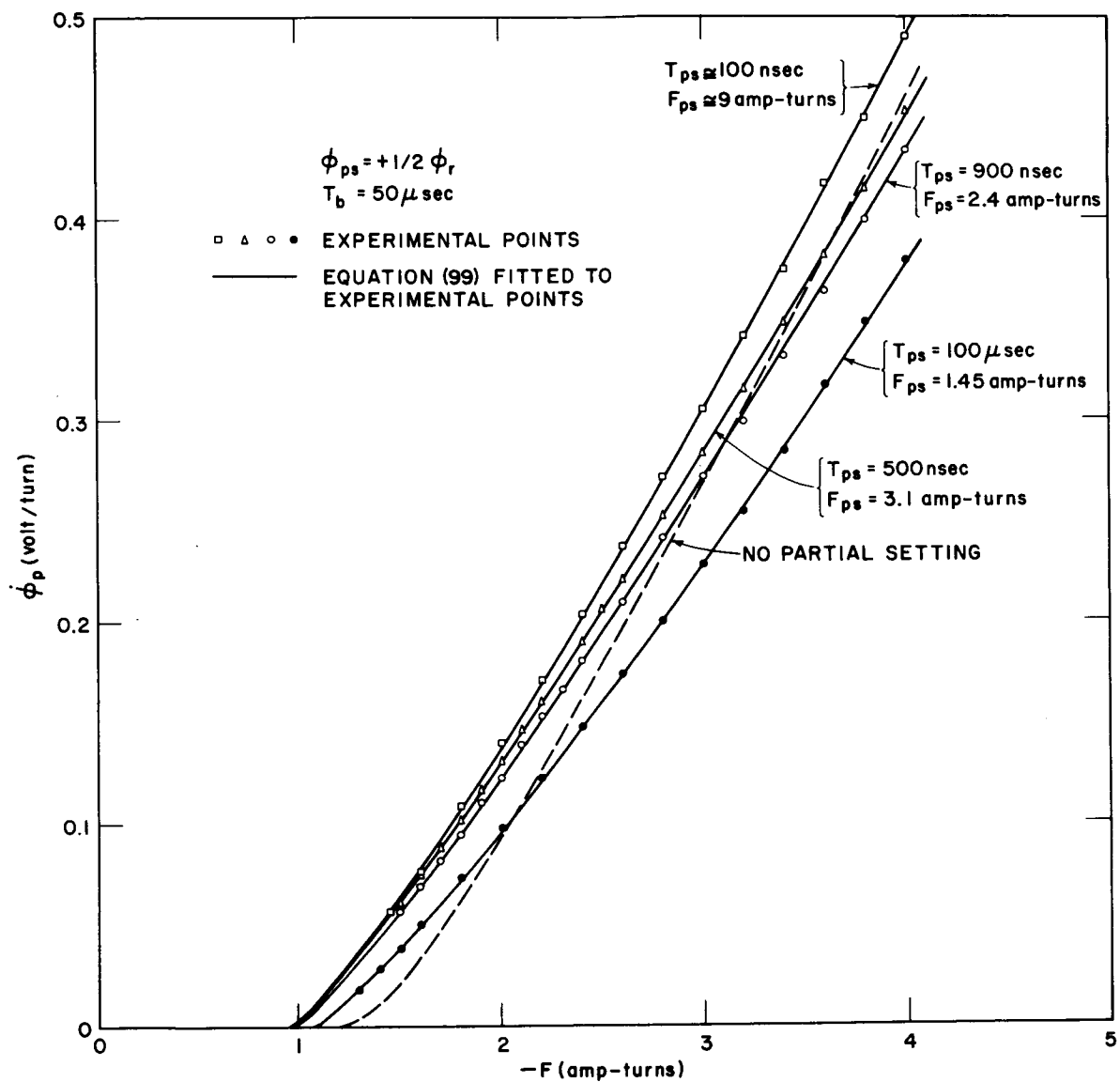
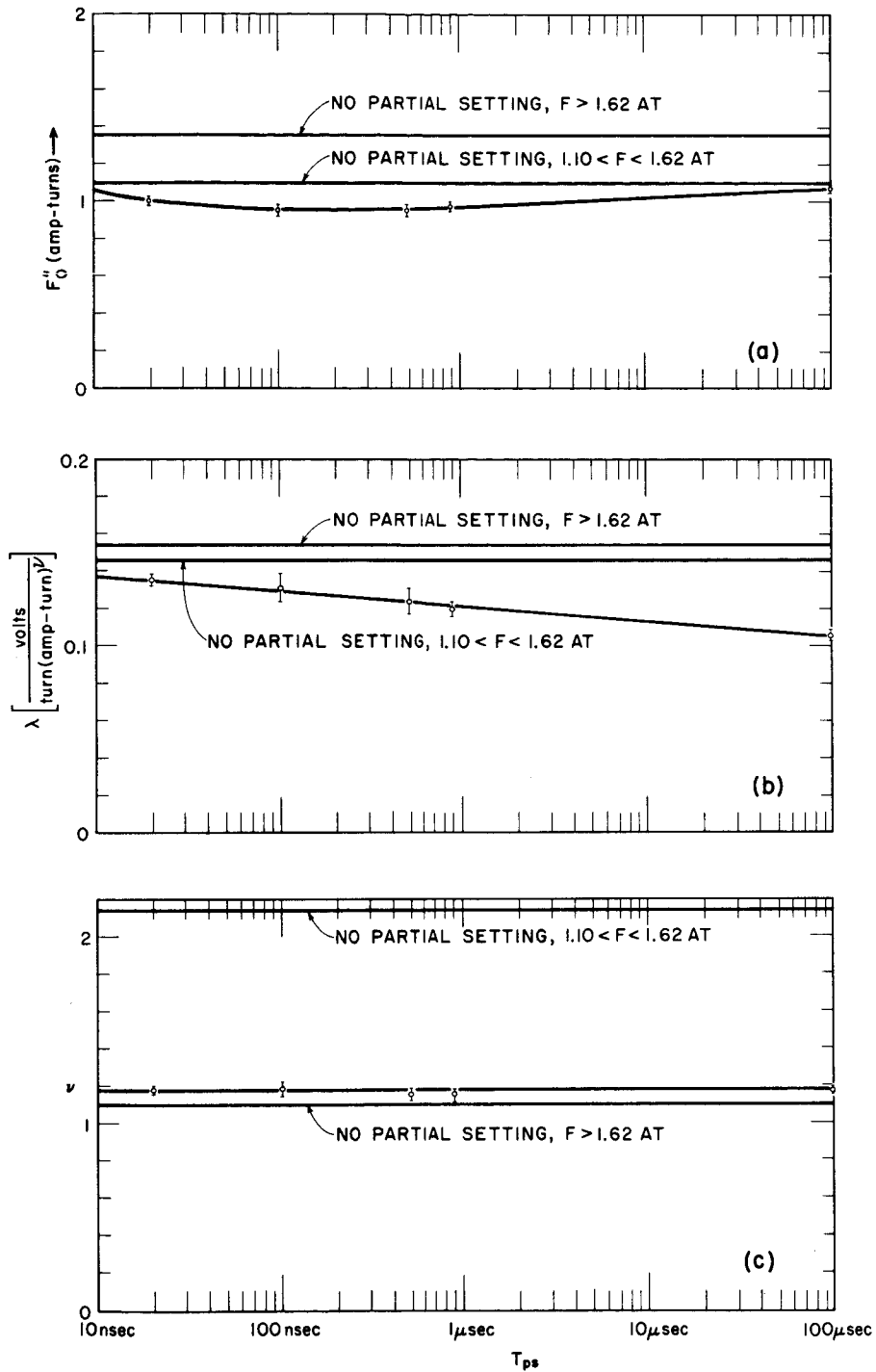


FIG. 42  $\dot{\phi}_p(-F)$  OF CORE I-4 WITH  $T_{ps}$  AS A PARAMETER





RC-3696-254

FIG. 43  $F_0''$ ,  $\lambda$ , AND  $\nu$  vs.  $T_{ps}$  FOR A NEGATIVE TEST PULSE  
Core I-4,  $\phi_{ps} = +\frac{1}{2}\phi_r$ ,  $T_b = 50 \mu$ sec

mechanism) prior to the peak in  $\dot{\phi}(t)$ . The net effect is that switching is considerably speeded up (switching time reduced) by this partial setting. For example, the 900-nsec  $\dot{\phi}(t)$  curve of Fig. 34(b) has reduced to 10 percent of its  $\dot{\phi}_p$  prior to the peak in  $\dot{\phi}(t)$  for no partial setting, whereas for the comparable case in Fig. 34(a), this 10 percent point occurs considerably later than the peak in  $\dot{\phi}(t)$  for no partial setting.

Figure 43(c) shows that  $\nu$  for a negative TEST pulse is practically independent of  $T_{ps}$ , and is nearly equal to the value for no partial setting for  $F < 1.62$  amp-turns.

### 3. EFFECTS OF VARYING $\phi_{ps}$

The effects of  $\phi_{ps}$  upon the  $\dot{\phi}_p(F)$  curve were determined by measuring the  $\dot{\phi}_p(F)$  for a number of different  $\phi_{ps}$  values but with  $T_{ps}$  and  $T_b$  held constant. These curves are given in Fig. 44 for Core I-4. The value of  $T_{ps}$  was 900 nsec for these curves. No such curves were taken for Core I-3 or for a negative TEST pulse for Core I-4. It is immediately seen in Fig. 44 that the slope of  $\dot{\phi}_p(F)$ , at a given  $F$  value, is decreasing monotonically with  $\phi_{ps}$ . This is shown more clearly in Fig. 45 where  $F_0''$ ,  $\lambda$ , and  $\nu$  are plotted *vs.*  $\phi_{ps}$ . This figure also demonstrates how the two regions in  $\dot{\phi}_p(F)$  coalesce as  $\phi_{ps}$  increases from  $-\phi_r$ . There seems to be a definite trend for these curves of  $F_0''$ ,  $\lambda$ , and  $\nu$  to flatten out as  $\phi_{ps}$  approaches zero. It is not known whether these curves continue to decrease slightly as  $\phi_{ps}$  exceeds zero or whether they turn upward. It is speculated in Part E that  $F_0''$  and  $\lambda$  curve upward as  $\phi_{ps}$  exceeds zero.

Corresponding families of  $\dot{\phi}_p(F)$  curves need be taken for other values of  $T_{ps}$  to determine if the functions for  $F_0''(\phi_{ps}, T_{ps})$ ,  $\lambda(\phi_{ps}, T_{ps})$ , and  $\nu(\phi_{ps}, T_{ps})$  can each be described as the product of two functions, one a function of  $\phi_{ps}$ , the other of  $T_{ps}$ .

### 4. EFFECT OF VARYING $T_b$

The effect of  $T_b$  (*cf.* Fig. 26) was determined by taking a  $\dot{\phi}_p(F)$  curve for  $T_b$  very small and comparing it to the corresponding  $\dot{\phi}_p(F)$  curve for a large  $T_b$ . Because the rise time of the TEST pulse (50 nsec) was much larger than the fall time of the PARTIAL SET pulse, (less than 0.7 nsec) it was impossible to reduce the duration between these pulses to zero. Therefore the  $\dot{\phi}_p(F)$  curves were taken for as small a value of  $T_b$  as

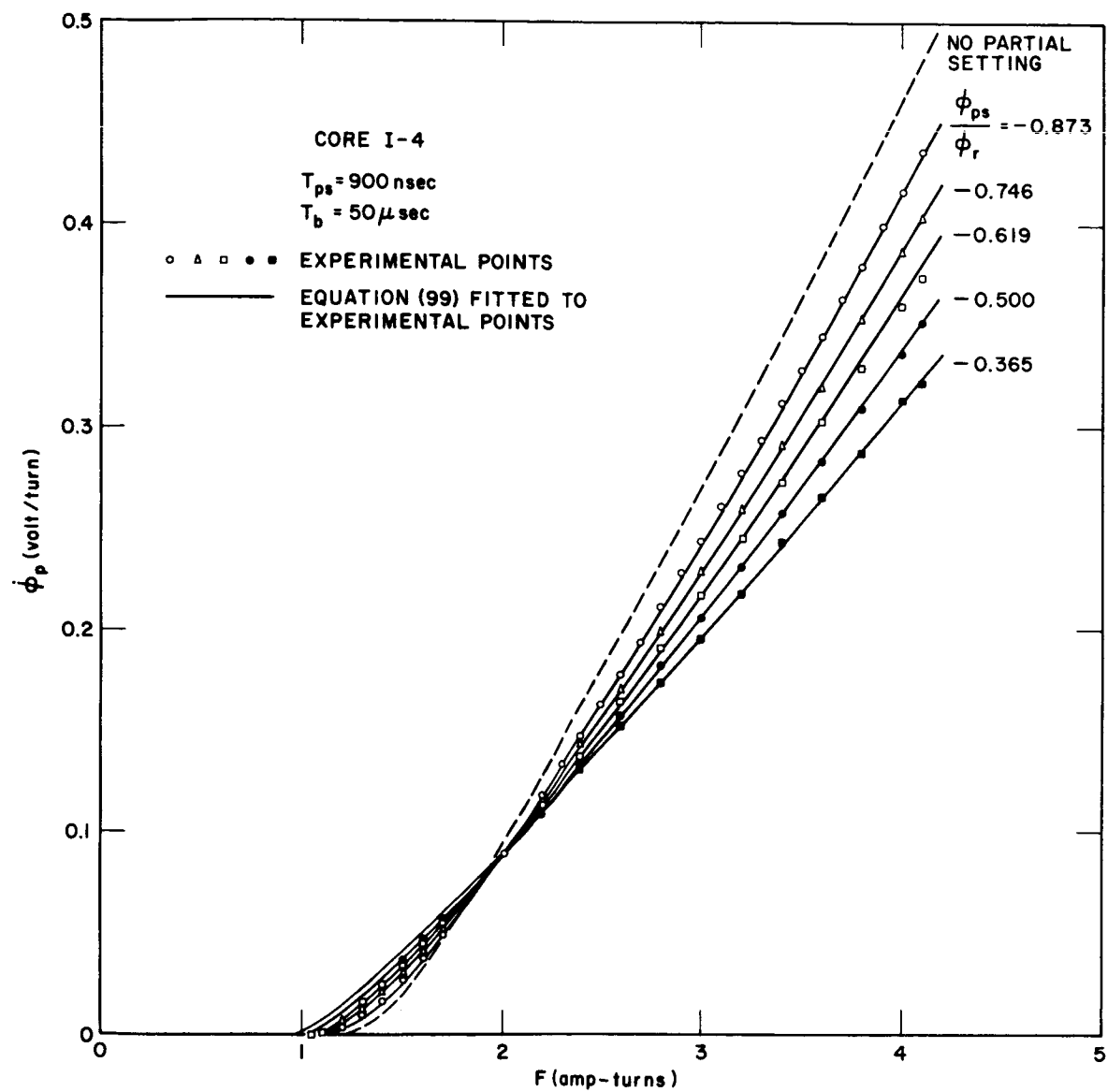
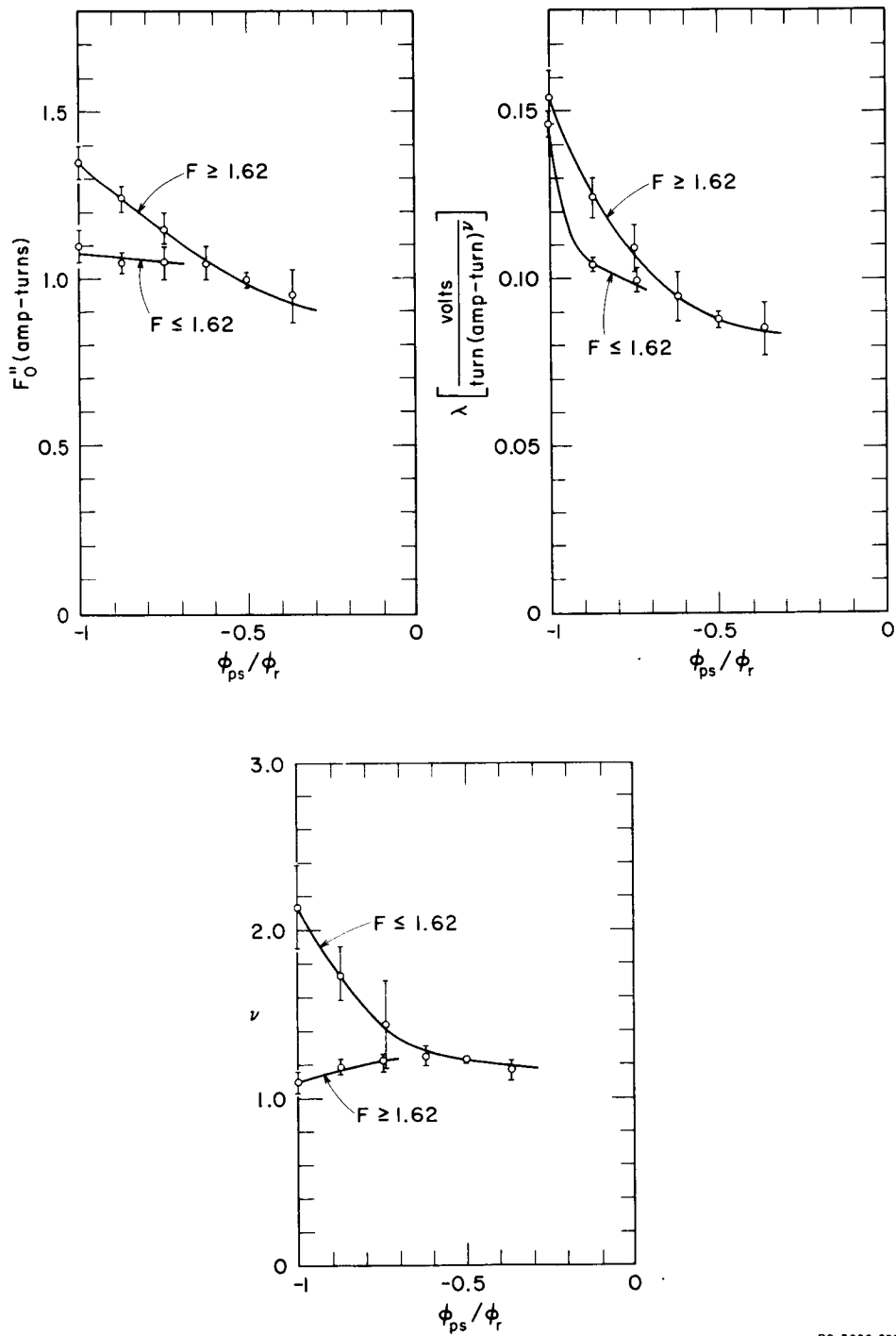


FIG. 44  $\dot{\phi}_p(+F)$  WITH  $\phi_{ps}$  AS A PARAMETER



RC-3696-256

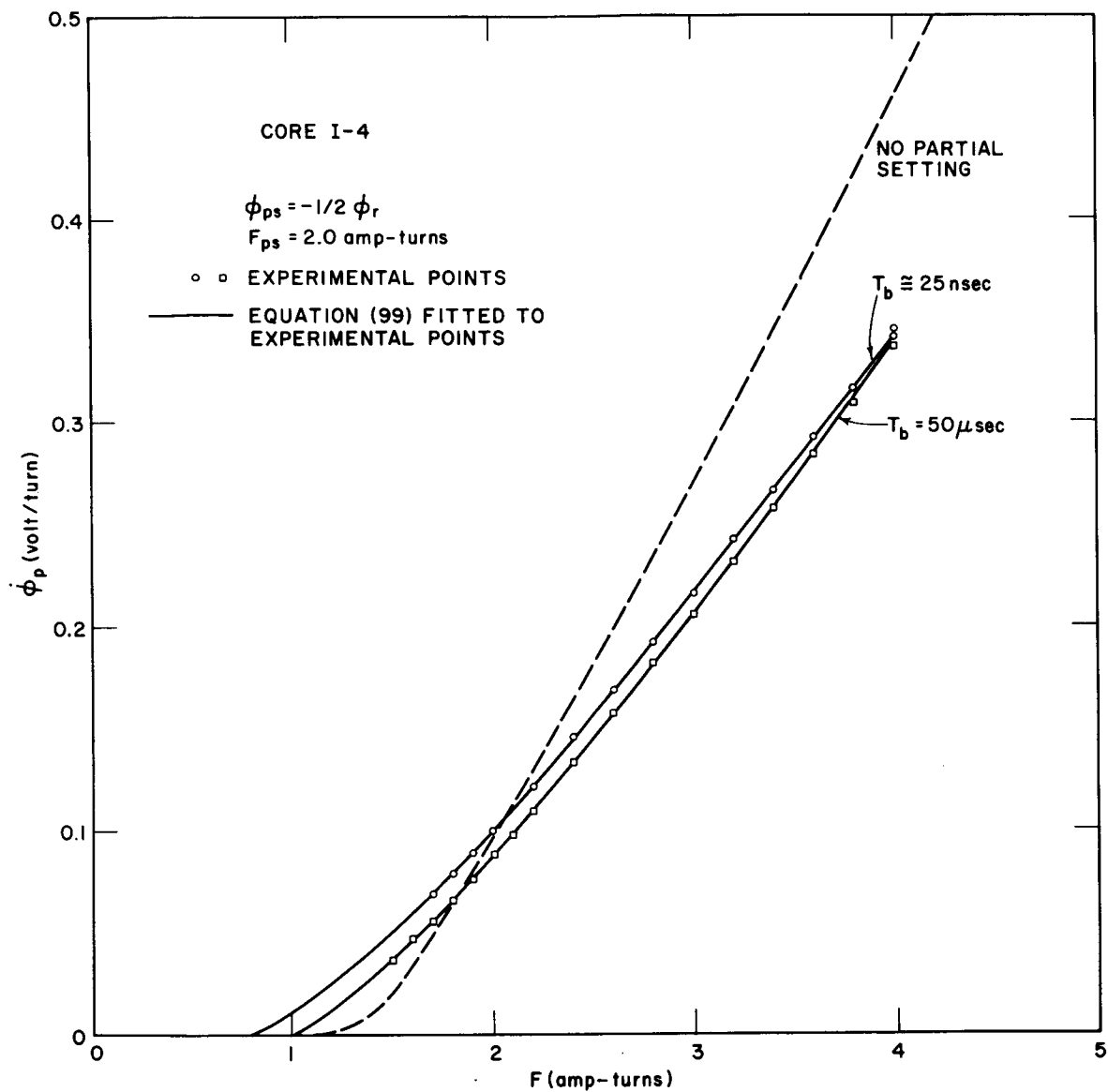
FIG. 45  $F_0''$ ,  $\lambda$ , AND  $\nu$  vs.,  $\phi_{ps}$   
Core I-4,  $T_{ps} = 900$  nsec,  $T_b = 50$   $\mu$ sec

possible. The value of  $T_b$  was measured as the time between the half-amplitude points of the pulses. Another problem in this experiment is the measurement of  $\phi_{ps}$ . Immediately following the termination of the PARTIAL-SET pulse some flux is unset elastically. Thus, the true value of  $\phi_{ps}$  should be measured at the instant when the TEST pulse exceeds the threshold. Instead, for simplicity, the value of  $\phi_{ps}$  was measured with the TEST pulse removed (flux change was measured via the first CLEAR pulse). Then  $T_{ps}$  and  $F_{ps}$  were held fixed as the TEST pulse was replaced and  $T_b$  adjusted to its minimum value. This means that the two  $\dot{\phi}_p(F)$  curves to be compared are not actually taken for exactly the same value of  $\phi_{ps}$ .

It is assumed (cf. Ref. 7) that the relaxation effects following the PARTIAL SET pulse correspond to the decaying tail in  $\dot{\phi}(t)$ . This assumption is supported by the observation that as  $T_b$  is decreased, with  $T_{ps}$  and  $F_{ps}$  held constant, no change in  $\dot{\phi}(t)$  during the TEST pulse is noted until the front edge of the TEST pulse begins to overlap with the decaying tail in  $\dot{\phi}(t)$  immediately following the PARTIAL SET pulse. This decaying tail can have a time constant ( $\tau_r$ ) of the order of several tenths of a microsecond. As long as  $T_b$  is several times  $\tau_r$ ,  $\dot{\phi}(t)$  is not affected by changes in  $T_b$ .

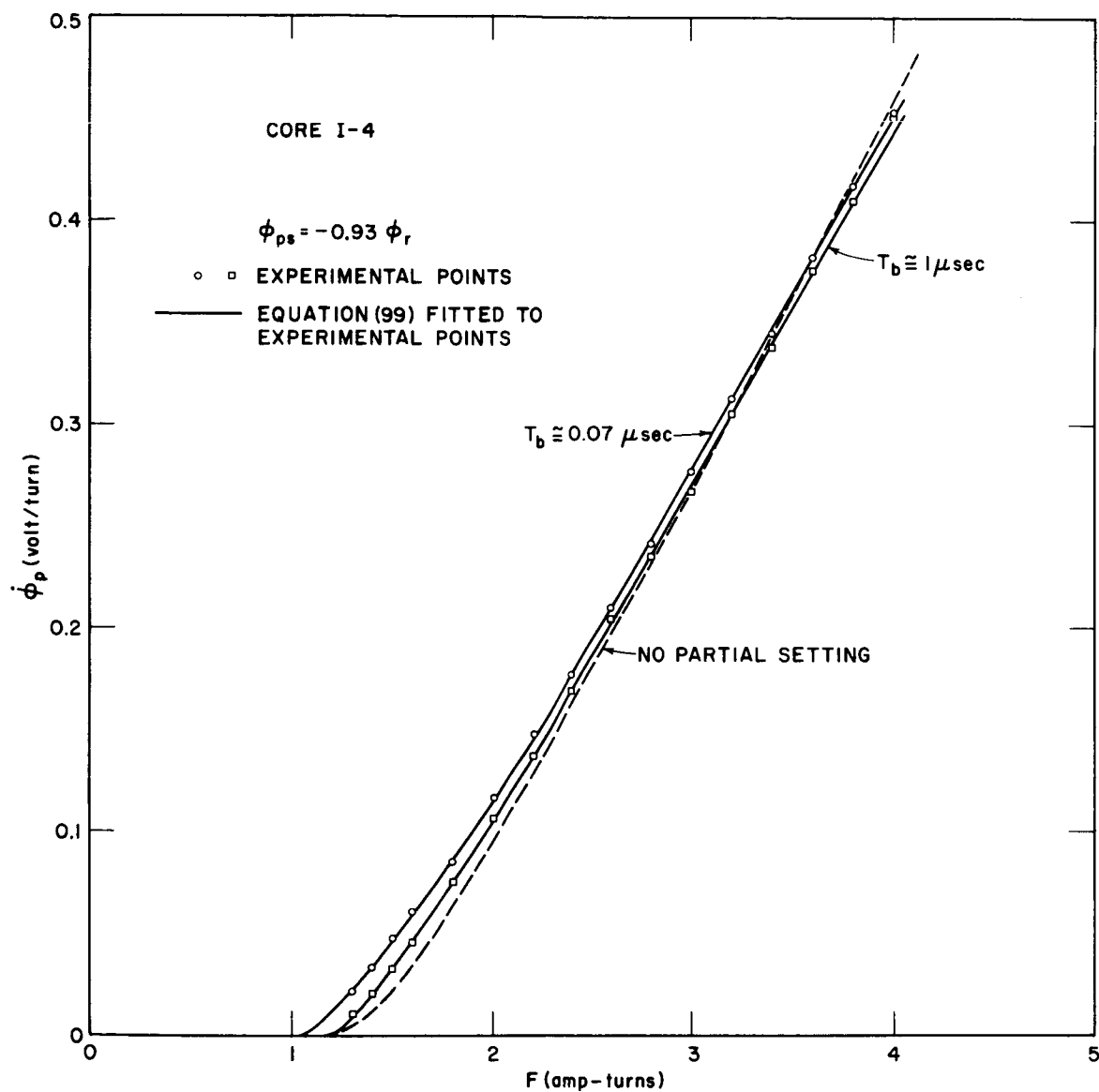
The  $\dot{\phi}_p(F)$  curves for small  $T_b$  were taken by using the mercury relay pulser for the PARTIAL-SET pulse. Typically, reflections of the order of several percent follow this pulse and therefore result in some error in the  $\dot{\phi}_p(F)$  measurements. Therefore, the effects of  $T_b$  should not be taken too quantitatively. They are included to give indications of the qualitative changes which result as  $T_b$  is decreased to zero.

Two  $\dot{\phi}_p(F)$  curves were taken for small values of  $T_b$ . The first one, given in Fig. 46(a), was  $T_{ps} = 900$  nsec,  $\phi_{ps} = -(1/2)\phi_r$  and  $T_b = 25$  nsec. The second one, given in Fig. 46(b), was for  $T_{ps} = 5$  nsec,  $\phi_{ps} = -0.93 \phi_r$ , and  $T_b = 70$  nsec. Notice that in both cases the effect of reducing  $T_b$  is to reduce both  $F_0''$  and  $\lambda$ . This is also the effect produced by increasing  $\phi_{ps}$  (see Fig. 45). Thus, some of the effect of  $T_b$  is probably a result of a change in  $\phi_{ps}$  due to the interruption of the elastic switching at the end of the PARTIAL-SET pulse. However, notice that the crossing point of the  $\dot{\phi}_p(F)$  curves in Fig. 44, which is for a 900-nsec PARTIAL-SET pulse, is at about  $F = 2$  amp-turns, whereas the curves of Fig. 46(a), also for a 900-nsec PARTIAL-SET pulse, have a crossing point beyond  $F = 4$  amp-turns. This means that  $F_0''$  is reduced more, relative to the reduction in  $\lambda$ , in



RB-3696-257

FIG. 46 EFFECT OF  $T_b$  ON  $\dot{\phi}_p(F)$   
 (a)  $T_{ps} = 900$  nsec



RB-3696-257A

FIG. 46 Concluded  
(b)  $T_{ps} = 5 \text{ nsec}$

Fig. 46(a) than in Fig. 44. Reducing  $T_b$ , with  $\phi_{ps}$  actually maintained constant, must therefore result in either a reduction of  $F_0''$ , or an increase of  $\lambda$ , or both. Shahan and Gutwin<sup>13</sup> found that decreasing  $T_b$  decreases the threshold of the  $\phi(F)$  curves for a number of materials. Thus,  $F_0''$  probably decreases with a decrease in  $T_b$ . In either case, reducing  $T_b$  for a fixed  $\phi_{ps}$  increases the switching speed if  $F$  is less than 4 amp-turns. The magnitude of these effects will increase somewhat as  $T_b$  is further reduced; however, there does not seem to be a very large effect as was anticipated for  $T_{ps} = 5$  nsec. Tancrell<sup>14</sup> reports a reduction in threshold for some materials when a very small amount of flux is partially set with a large amplitude pulse of 30 nsec duration and a small  $T_b$ . Figure 46(b) illustrates such an effect; however, the reduction in threshold, for  $T_b = 70$  nsec, is not enough to allow the logic scheme proposed by Tancrell to operate at very fast speeds for the ferrite material used here. Similar data have not been taken for a negative TEST pulse.

## 5. SUMMARY

The  $\dot{\phi}_p(F)$  curve of Core I-4 for no partial setting is accurately described by the function  $\dot{\phi}_p = \lambda(F - F_0'')^\nu$ , providing that it is broken into two regions each having a different set of values for  $F_0''$ ,  $\lambda$ , and  $\nu$ . Curves of  $\dot{\phi}_p(F)$  were taken with  $T_{ps}$  as a parameter for both positive and negative polarities of the TEST pulse. These curves can be described by the above  $\dot{\phi}_p(F)$  equation with only one set of values for  $F_0''$ ,  $\lambda$ , and  $\nu$ . For a positive TEST pulse it was found that  $F_0''$  increases approximately linearly with  $\log T_{ps}$ , but with a relatively low slope. This contrasts with the data of Core E-6 (Ref. 7) for which  $F_0''$  increases rapidly as  $T_{ps}$  increases from 0.5  $\mu$ sec to 1  $\mu$ sec, levels off between 1 and 5  $\mu$ sec, and increases very little for  $T_{ps}$  greater than 5  $\mu$ sec. The value of  $\lambda$  is reduced by about 42 percent by partial setting to  $-(1/2)\phi_r$  and is relatively independent of  $T_{ps}$ . This is very similar to the data of Core E-6. The value of  $\nu$  increases somewhat as  $T_{ps}$  increases. The  $\dot{\phi}_p(F)$  curves for a negative TEST pulse exhibit an  $F_0''$  which is nearly independent of  $T_{ps}$ , a  $\lambda$  which is not reduced as much as for a positive TEST pulse, and is more dependent upon  $T_{ps}$  (it decreases somewhat as  $T_{ps}$  increases) and a  $\nu$  which is constant.

The effects of  $\phi_{ps}$  on the  $\dot{\phi}_p(F)$  curves were determined for  $T_{ps} = 900$  nsec for a positive TEST pulse. It was found that the two regions in the  $\dot{\phi}_p(F)$  curves gradually reduce to one region as  $\phi_{ps}$  increases from  $-\phi_r$  to  $-(1/2)\phi_r$ . The values of  $F_0''$  and  $\lambda$  for both regions



in  $\dot{\phi}_p(F)$  decrease as  $\phi_{ps}$  increases from  $-\phi_r$  to  $-(1/2)\phi_r$ . The value of  $\nu$  for the lower- $F$  region decreases, and for the upper- $F$  region increases; as  $\phi_{ps}$  increases over the same range. The effects of  $T_b$  on  $\dot{\phi}_p(F)$  for  $T_{ps} = 5$  nsec,  $\Delta\phi_{ps} = 0.07\phi_r$  and for  $T_{ps} = 900$  nsec,  $\Delta\phi_{ps} = -(1/2)\phi_r$ , were found to be relatively small. It was concluded from this  $T_b$  data that, as  $T_b$  decreases, for  $\phi_{ps}$  constant, either  $F''_0$  decreases, or  $\lambda$  increases, or both.

## E. DISCUSSION AND CONCLUSIONS

There are many partial setting effects which alter the switching of a square-loop ferrite core. The most outstanding of these effects is that  $\lambda$  is reduced considerably by partial setting, but is hardly affected by the duration  $T_{ps}$  of the PARTIAL-SET pulse. The effort expended in trying to find a physical reason for this large reduction in  $\lambda$  was unsuccessful. However, in the process a hypothetical experiment was considered which showed that the concepts of switching originally held, and common to the literature of the field, cannot be entirely correct. This can be illustrated by the following example.

Consider the case in which a step MMF of amplitude  $F_{ps}$  is applied to a core which is initially at  $-\phi_r$  (see Fig. 47). Let  $t_1$  be the time when the core has switched to  $\phi = -(1/2)\phi_r$ . Assume that the switching from  $t = 0$  to  $t = t_1$  can be described accurately by the parabolic model given in Eq. (92) with certain known values of the parameters  $F''_0$ ,  $\lambda$ ,  $\nu$ ,  $\phi_c$ ,  $\phi_0$ , and with a known function for  $\phi_d(F)$ . If switching is continued beyond  $t_1$  with the same MMF,  $F_{ps}$ , then the values of these same parameters will be adequate to describe this switching. However, the results of this report, and of Ref. 7, have shown that if a step change in MMF is made at  $t = t_1$ , the same values of these parameters can not correctly describe the remaining switching, but new, significantly different, values can. This new set of values will describe switching correctly [not only  $\dot{\phi}_p$  but the entire  $\dot{\phi}(t)$  with the exception of the initial spike] for any reasonable  $F$  value, including  $F_{ps}$ , as long as  $F$  is constant. When  $F = F_{ps}$ ,

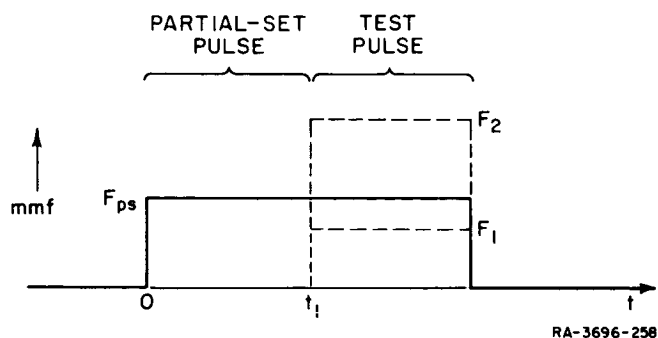


FIG. 47  $F(t)$  FOR  $T_b = 0$

there are two sets of values for these parameters which will give the correct  $\dot{\phi}(t)$ . This corresponds to the crossing point of two  $\dot{\phi}_p(F)$  curves, one for no partial setting, and the other for the given partially set state (i.e.,  $\phi_{ps} = -(1/2)\phi_r$ ,  $T_{ps} = t_1$ , and  $T_b = 0$ ). It must be concluded, however, that only the new set of values of the parameters represents the actual switching for  $t$  greater than  $t_1$  because of their generality for any  $F$  value, i.e., the old set of values give the correct result for  $F = F_{ps}$  only by the coincidence that the error in  $F_0''$  and  $\nu$  cancels the error in  $\lambda$ . Assume for example, that an incorrect value is used for  $F_0''$  in Eq. (92), but that this error is canceled by choosing an appropriate value for  $\lambda$ . A subsequent change in  $F$  will destroy this cancellation. The new set of parameters will correctly describe switching only if no further change is made in the MMF. These considerations lead us to the following conclusion. At any instant during the switching, with a constant applied MMF, the actual values of all of the parameters are the values that would be determined if at that instant in time the core is considered to be partially set. This partially set state is identified by the flux which has been switched,  $\Delta\phi_{ps}$  (where  $\phi_{ps} = -\phi_r + \Delta\phi_{ps}$ ), the time that the core has been switching,  $T_{ps}$ , and by  $T_b = 0$ . Using these values of  $\phi_{ps}$ ,  $T_{ps}$ , and  $T_b$  the true values of the parameters (e.g.,  $F_0''$ ,  $\lambda$ ) can be determined from data similar to those of Sec. III of this report, but for  $T_b = 0$ . These new values of the parameters are appropriate only to the instant of time for which they were determined. As switching progresses for a constant-drive MMF, the values of these parameters continue to change. These values can be determined for any particular partially set state only because of the error cancellation in  $F_0''$ ,  $\nu$ , and  $\lambda$  which occurs when the drive MMF is maintained constant. Note that for  $F = F_{ps}$ ,  $\phi_c = 0$  according to Eq. (96).

Consider, again, the case in which a step change in MMF is made during switching, as shown in Fig. 47. Assume that functions have been determined for the parameters (including  $\phi_d$ ) with  $\phi_{ps}$ ,  $F_{ps}$ , and  $F$  as arguments and with  $T_b = 0$ . Switching can then be described for the entire switching process by using the model of Eq. (92) and by making a step change in the values of the parameters at  $t = t_1$ . Now consider the case in which an additional step change in  $F$  is made during the switching process at a time  $t = t_2$  (not shown in Fig. 47). The description of the switching beyond  $t = t_2$  requires another step change in the values of the parameters at  $t = t_2$ . The new value of  $\phi_{ps}$  at  $t = t_2$  is available from the description of the previous switching. However,  $F_{ps}$  is not now defined because

the partially set flux at  $t = t_2$  has not been switched by a single value of  $F$  as was the case at  $t = t_1$ . Thus, the functions which give the switching parameters as a function of  $\phi_{ps}$ ,  $F_{ps}$ , and  $F$ , do not apply. This problem can be overcome if a flux averaged value is used for  $F_{ps}$ , i.e.,

$$F_{ps} = \frac{1}{\phi_{ps} + \phi_0} \int_{\phi=\phi_0}^{\phi_{ps}} F d\phi, \quad (100)$$

where  $\phi_0$  is the initial value of  $\phi$  at  $t = 0$  and  $\phi_{ps}$  is the final value of  $\phi$  at  $t = t_2$ . Using this value for  $F_{ps}$ , the new values of the switching parameters can be determined and  $\phi(t)$  and  $\dot{\phi}(t)$  can be calculated for  $t > t_2$ . This same process can be extended for any additional number of steps.

Note that in this process the parameters are still treated as being constant when  $F$  is constant. If  $F$  is varying in time then this process is not directly applicable. However, it appears as if a new model can be developed which is capable of describing switching for any  $F(t)$  function. This model would be written as

$$\dot{\phi} = \lambda(F - F_0'')^\nu \left\{ 1 - \left( \frac{\phi + \phi_c}{\phi_s + \phi_c} \right)^2 \right\} \quad (101)$$

where

$$F_0'' = F_0''(\phi, F_{ps})$$

$$\lambda = \lambda(\phi)$$

$$\nu = \nu(\phi, F_{ps})$$

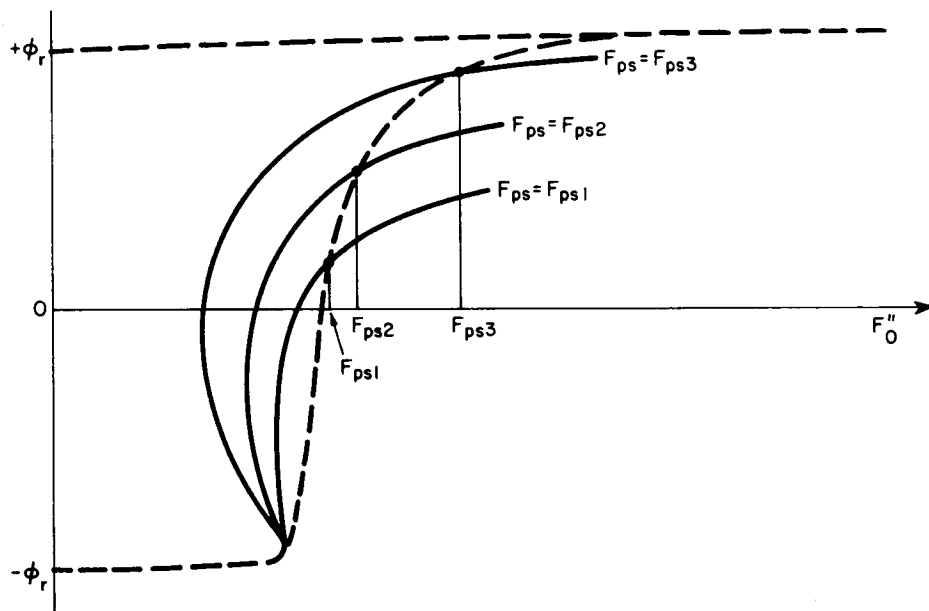
$$\phi_c = \phi_c(\phi, F_{ps}, F)$$

and

$$F_{ps} = \frac{1}{\phi + \phi_0} \int_{\phi=\phi_0}^{\phi} F d\phi'. \quad (102)$$

The function for  $\phi_c$  can probably be obtained from Eq. (98).

At first sight this appears to be a very complex model; however, the functions for  $\lambda$ , and  $\nu$  can probably be approximated by relatively simple functions. Note also that the function  $\phi_d(F)$  is no longer needed, since its purpose is fulfilled by the (somewhat more complicated) function  $F_0''(\phi, F_{ps})$ ; i.e., switching will terminate when  $F_0''$  is equal to  $F$ . A crude sketch of this function is shown in Fig. 48 to illustrate this effect. The static  $\phi(F)$  curve is included as a dotted curve for reference. Consider the case in which  $F$  is constant. Then  $F_{ps} = F$  from Eq. (102). The curves of Fig. 48 cross the static  $\phi(F)$  curve when  $F_0''$  is equal to  $F_{ps}$ . At that  $\phi$  and time,  $(F - F_0'')$  is equal to zero, and switching will terminate. Note that for a fixed  $\phi$ ,  $F_0''$  decreases as  $F_{ps}$  increases, in agreement with Fig. 41(a). Also, for a fixed  $F_{ps}$ ,  $F_0''$  decreases as  $\phi$  is increased from  $-\phi_r$  to  $-(1/2)\phi_r$ , in agreement with Fig. 45(a). Actually,  $F_{ps}$  is not constant in Fig. 45(a) but  $T_{ps}$  is. However,  $F_0''$  would also decrease if  $F_{ps}$  is held constant and  $\phi_{ps}$  increased by increasing  $T_{ps}$ .



RA-3696-259

FIG. 48 A SKETCH OF  $F_0''(\phi, F_{ps})$

The partially set state has been described in Eq. (101) and (102) by  $F_{ps}$  rather than by  $T_{ps}$ , because  $F_{ps}$  is easier to define and is probably a more fundamental quantity. In the case of ferrite materials which require two regions to describe the  $\phi_p(F)$  curve, it will be necessary to replace each of the functions for  $F_0''$ ,  $\lambda$ , and  $\nu$  of Eq. (101) by two equivalent functions, one for each region of  $F$ . The transition point,  $F_B$ , must also be known.

It is interesting to note that this model is capable of giving an asymmetric  $\dot{\phi}(\phi)$  at low values of  $F$ . This was considered in Report 2 (pp. 55, 56) except that the static  $\phi(F)$  curve was used to approximate  $F_0''(\phi)$ , and partial setting was not considered.

In the case in which  $F(t)$  is monotonically increasing during switching, Eq. (102) will give  $F_{ps} < F$ . This will result in a decrease in  $\dot{\phi}_p$ , i.e.,  $\dot{\phi}_p$  will be lower than if  $\lambda$ ,  $F_0''$ , and  $\nu$  were assumed to be constant during switching as was done in Sec. II. This is true because  $\dot{\phi}_p(F)$  for  $T_b = 0$  has a lower  $\lambda$  and  $F_0''$  and therefore crosses the  $\dot{\phi}_p(F)$  curve for no partial setting at  $F = F_{ps}$  (e.g., Ref. 7, Fig. 18). This lowering of  $\dot{\phi}_p$  was observed in Sec. II. Likewise, for  $F(t)$  monotonically decreasing during switching, Eq. (102) will give  $F_{ps} > F$  and  $\dot{\phi}_p$  will be increased. This has not yet been experimentally verified.

Now consider the problem of the large decrease in  $\lambda$ . The question to ask is not why does partial setting reduce  $\lambda$ , but why does  $\lambda$  decrease during the first part of switching. The physical reasons for the decrease of  $\lambda$  are still not known, nor are the changes in  $F_0''$ ,  $\nu$ , and  $\phi_c$ , but the phenomenological behavior is somewhat clarified by realizing that these parameters must be continuously changing during switching (except  $\phi_c$  when the MMF is constant).

The parameter  $\lambda$ , when related to the parameters of the switching model described by Menyuk and Goodenough<sup>15</sup>, can be considered to contain four basic material parameters. These are (1) the viscous damping coefficient,  $\beta$ , for domain wall motion, (2) the saturation magnetization,  $M_s$ , (3) the density of domain nucleations, and (4) the quantity  $\langle \cos \theta \rangle$  which accounts for the statistical variation in the directions of the easy axes of the individual ferrite crystallites. It is not known which, if any, of these are responsible for the variation in  $\lambda$ . It is possible that the empirical parabolic switching model cannot be so clearly related to any previous theoretical model. If the viscous damping coefficient  $\beta$  is entirely responsible for the variation in  $\lambda$  then the average domain wall velocity may be constant during switching (for a constant applied MMF). The domain wall velocity is usually considered to be directly proportional to  $(H - H_0)$  and inversely proportional to  $\beta$ , where  $H_0$  is related to  $F_0''$ . Thus, changes in  $\lambda$  and  $F_0''$  during switching do not necessarily imply that the average domain wall velocity is also varying during switching.

Future experiments should include more extensive data for  $T_b = 0$  and for switching by  $F(t)$  drives of various shapes so that this suggested switching model can be verified and actual functions obtained and verified for  $F_0''$ ,  $\lambda$ ,  $\nu$ , and  $\phi_c$  as a function of  $\phi_{ps}$ ,  $F_{ps}$ , and  $F$ .

Switching for a negative TEST pulse is more complicated and requires further investigation of the  $\dot{\phi}(t)$  waveforms before a quantitative model can be developed. Further development of the initial spike model of Sec. II may prove to be useful for this case.

In most respects it can be concluded that the effects of partial setting are similar for Core I-4 (Indiana General 5209 material) and for Core E-6 (Telemeter T-5 material) of Ref. 7. The small amount of data for Core I-3 (Lockheed 06 material) also exhibited similar properties.

In general, the basic physics of partial switching, or even switching for a constant-MMF drive, are not at all well understood. However, the properties of partial switching are beginning to be understood phenomenologically and considerable progress has been made in the development of appropriate switching models. Considerable investigation remains to be done before all of the effects of partial setting have been revealed and described by practical switching models. In the meantime, the data presented can be used for qualitative explanations of the operation of magnetic circuits involving switching from partially set states.

*APPENDIX A*

**COMPUTER PROGRAM FOR PROCEDURE  $\dot{\phi}(F, \phi, \phi_d, \dot{\phi}')$**

## APPENDIX A

### COMPUTER PROGRAM FOR PROCEDURE $\dot{\phi}(F, \phi, \phi_d, \dot{\phi}')$

Language: ALGOL 60.

Program Description: Computes  $\dot{\phi}$ ,  $\phi_d$ , and  $\dot{\phi}'$  for given values of  $F$  and  $\phi$ .  
(Core parameters are declared and assigned values in the main program.)

Identifiers:\*

(1) Analytical identifiers

<u>Identifier</u>	<u>Symbol</u>	<u>Identifier</u>	<u>Symbol</u>
F	$F$	PHI	$\phi$
FB	$F_B$	PHID	$\phi_d$
F0	$F_0$	PHIDOT	$\dot{\phi}$
F0PP	$F''_0$	PHIDOTP	$\dot{\phi}_p$
F12	$F_{12}$	PHIDOTPPRIME	$\dot{\phi}'_p$
F23	$F_{23}$	PHIDOTPRIME	$\dot{\phi}'$
HA	$H_a$	PHIDPRIME	$\phi'_d$
HN	$H_n$	PHIR	$\phi_r$
HQ	$H_q$	PHIS	$\phi_s$
LAMBDA	$\lambda$	ROP	$\rho_p$
LI	$l_i$	V1	$V_1$
LO	$l_o$	V2	$V_2$
NU	$\nu$		

(2) Auxiliary identifiers

<u>Identifier</u>	<u>Description</u>
DONE	Boolean variable
OK	Label (address in program)

---

\*Listed in alphabetic order.



Program:

REAL PROCEDURE PHIDOT(F, PHI, PHID, PHIDOTPRIME);	PHIDOT01
COMMENT THIS PROCEDURE COMPUTES PHIDOT, PHID, AND PHIDOTPRIME	PHIDOT02
FOR GIVEN VALUES OF F AND PHI. CORE PARAMETERS, WHICH MUST BE	PHIDOT03
SUPPLIED FROM OUTSIDE THE PROCEDURE, ARE:	PHIDOT04
LI, LO, PHIR, PHIS, HA, HQ, HN, LAMBDA, FOPP, NU, ROP, FO, FB ;	PHIDOT05
REAL F, PHI, PHID, PHIDOTPRIME;	PHIDOT06
BEGIN	PHIDOT07
REAL PHIDPRIME, PHIDOTP, PHIDOTPPRIME ;	PHIDOT08
OWN REAL F12, F23, V1, V2 ;	PHIDOT09
LABEL OK;	PHIDOT10
OWN BOOLEAN DONE;	PHIDOT11
COMMENT COMPUTE F12, F23, V1, AND V2 ONLY ONCE ;	PHIDOT12
IF DONE THEN GO TO OK;	PHIDOT13
DONE = TRUE;	PHIDOT14
F12 = HQ*LI ;	PHIDOT15
F23 = HQ*LO ;	PHIDOT16
V1 = (PHIS-PHIR)/((LO-LI)*HA);	PHIDOT17
V2 = (PHIS+PHIR)*HQ/((LO-LI)*HN);	PHIDOT18
OK;	PHIDOT19
COMMENT COMPUTE PHID AND PHIDPRIME VS. F ;	PHIDOT20
IF F ≤ F12 THEN	PHIDOT21
BEGIN	PHIDOT22
PHID = V1*F*LN((F-HA*LO)/(F-HA*LI))-PHIR;	PHIDOT23
PHIDPRIME = V1*(LN((F-HA*LO)/(F-HA*LI))+F*(1/(F-HA*LO)	PHIDOT24
-1/(F-HA*LI)))	PHIDOT25
END;	PHIDOT26
IF F12 < F AND F ≤ F23 THEN	PHIDOT27
BEGIN	PHIDOT28
PHID = V2*(F/HQ-LI+F*(1/HN-1/HQ)*LN((1-HN/HQ)/(1-HN*LI/F)))	PHIDOT29
-PHIR;	PHIDOT30
PHIDPRIME = V2*(1/HQ+(1/HN-1/HQ)*(LN(F*(1-HN/HQ)/(F-HN*LI))	PHIDOT31
-HN*LI/(F-HN*LI)))	PHIDOT32
END;	PHIDOT33
IF F23 < F THEN	PHIDOT34
BEGIN	PHIDOT35
PHID = V2*(LO-LI+F*(1/HN-1/HQ)*LN((F-HN*LO)/(F-HN*LI)))	PHIDOT36
-PHIR;	PHIDOT37
PHIDPRIME = V2*(1/HN-1/HQ)*(LN((F-HN*LO)/(F-HN*LI))	PHIDOT38
+F*HN*(LO-LI)/((F-HN*LO)*(F-HN*LI)))	PHIDOT39
END;	PHIDOT40
COMMENT COMPUTE PHIDOTP AND PHIDOTPPRIME VS. F ;	PHIDOT41
IF F ≤ FOPP THEN	PHIDOT42
BEGIN	PHIDOT43
PHIDOTP = 0;	PHIDOT44
PHIDOTPPRIME = 0	PHIDOT45
END;	PHIDOT46
IF FOPP < F AND F ≤ FB THEN	PHIDOT47
BEGIN	PHIDOT48
PHIDOTP = LAMBDA*(F-FOPP)*NU;	PHIDOT49
PHIDOTPPRIME = LAMBDA*NU*(F-FOPP)*(NU-1)	PHIDOT50
END;	PHIDOT51
IF FB < F THEN	PHIDOT52
BEGIN	PHIDOT53
PHIDOTP = ROP*(F-FO);	PHIDOT54
PHIDOTPPRIME = ROP	PHIDOT55
END;	PHIDOT56
COMMENT COMPUTE PHIDOT AND PHIDOTPRIME ;	PHIDOT57
PHIDOT = IF PHID-PHI > 0.001*PHIR THEN PHIDOTP*(1-((2*PHI+PHIS	PHIDOT58
-PHID)/(PHIS+PHID))*2) ELSE 0 ;	PHIDOT59
PHIDOTPRIME = (1-((2*PHI+PHIS-PHID)/(PHIS+PHID))*2)*PHIDOTPPRIME	PHIDOT60
+4*PHIDOTP*(2*PHI+PHIS-PHID)*(PHI+PHIS)*PHIDPRIME/(PHIS+PHID)*3	PHIDOT61
END PHIDOT;	PHIDOT62

Remarks: \*

Lines PHIDOT03-PHIDOT05: The switching parameters are declared and assigned values in the main program for two reasons: first, in order to be able to use the same PROCEDURE for different types of core or for different legs of a multipath core; second, because some of these parameters are needed in the main program, e.g., for computing  $\tau_s$ , Eq. (46) or (47), and  $t_0$ , Eq. (45).

Lines PHIDOT12-PHIDOT19. Since the parameters  $F_{12}$ ,  $F_{23}$ ,  $V_1$ , and  $V_2$  are independent of  $F$  and  $\phi$ , there is no need to compute their values more than once, *if only one type of core is used in the main program*. Initially, the Boolean variable DONE is FALSE by default, so that these parameters will be computed only during the first execution of the PROCEDURE. *If two or more types of toroidal core (or at least one type of multipath core) are used in the main program, Line PHIDOT13 should be deleted.* In order to avoid confusion, one might also delete Lines PHIDOT10 through PHIDOT14 and Line PHIDOT19 altogether from the  $\dot{\phi}(F, \phi)$  PROCEDURE.

Lines PHIDOT58-PHIDOT59. Switching computation is arbitrarily truncated when  $\phi$  approaches  $\phi_d$  to within 0.1 percent of  $\phi_r$ , which is about 0.05 percent of the maximum amount of flux switching.

---

\*Remarks are addressed according to line numbers, which are listed on the right-hand column of the program.

*APPENDIX B*

**COMPUTER PROGRAMS FOR PROCEDURES**

**MIN (A,B), MAX (A,B), MIN 3 (A,B,C), AND IA(T)**

## APPENDIX B

### COMPUTER PROGRAMS FOR PROCEDURES

MIN(A,B), MAX(A,B), MIN3(A, B, C), AND IA(T)

1. PROCEDURE MIN(A,B)

Language: ALGOL 60.

Program Description: Takes the value of either A or B, whichever is smaller.

Program:

REAL PROCEDURE MIN(A,B);	MIN	01
VALUE A,B; REAL A,B;	MIN	02
BEGIN MIN ← IF A < B THEN A ELSE B END MIN ;	MIN	03

2. PROCEDURE MAX(A,B)

Language: ALGOL 60.

Program Description: Takes the value of either A or B, whichever is larger

Program:

REAL PROCEDURE MAX(A,B);	MAX	01
VALUE A,B; REAL A,B;	MAX	02
BEGIN MAX ← IF A > B THEN A ELSE B END MAX ;	MAX	03

3. PROCEDURE MIN3(A, B, C)

Language: ALGOL 60.

Program Description: Takes the value of either A or B or C,  
whichever is smallest.

Program:

REAL PROCEDURE MIN3(A,B,C) ;	MIN3	01
VALUE A,B,C; REAL A,B,C; BEGIN	MIN3	02
MIN3: IF A < B AND A < C THEN A ELSE IF B < C THEN B ELSE C	MIN3	03
END MIN3 ;	MIN3	04

4. PROCEDURE IA(T)

Language: ALGOL 60.

Program Description: Computes  $i_A$  as a function of time.

Program:

REAL PROCEDURE IA(T) ;	IA(T)	01
REAL T ;	IA(T)	02
BEGIN	IA(T)	03
IA ← IF 2.4580-6 < T AND T < 30-6 THEN CAPIA*(1-0.6147*(T*106-3)*2)	IA(T)	04
ELSE CAPIA*MIN(0.1356012*T*2,1)	IA(T)	05
END IA ;	IA(T)	06

*APPENDIX C*

**COMPUTER PROGRAM FOR UNLOADED-CORE FLUX SWITCHING**

## APPENDIX C

### COMPUTER PROGRAM FOR UNLOADED-CORE FLUX SWITCHING

Language: ALGOL 60.

Program Description: Computes  $i_D$ ,  $\dot{\phi}$ ,  $\phi$ ,  $\phi_d$ , and  $F$  versus  $t$  for given core and drive parameters.

Identifiers:

#### (1) Analytical identifiers

<u>Identifier</u>	<u>Symbol</u>	<u>Identifier</u>	<u>Symbol</u>
CAPID	$I_D$	NU	$\nu$
DELT	$\Delta t$	PHIC	$\phi$
DPHDTDFC	$\dot{\phi}'$	PHIC1	$\phi_{n-1}$
F	$F$	PHIC2	$\phi_{n-2}$
FB	$F_B$	PHIDC	$\phi_d$
F0	$F_0$	PHIDOTC	$\dot{\phi}$
FOPP	$F_0''$	PHIDOTC1	$\dot{\phi}_{n-1}$
HA	$H_a$	PHIR	$\phi_r$
HN	$H_n$	PHIS	$\phi_s$
HQ	$H_q$	ROP	$\rho_p$
ID	$i_D$	T	$t$
LAMBDA	$\lambda$	TAUS	$\tau_s$
LI	$l_i$	TF	$T_f$
LO	$l_o$	TH	$T_h$
ND	$N_D$	TR	$T_r$

#### (2) Auxiliary identifiers

<u>Identifier</u>	<u>Description</u>
CIRCUITPARAMETERH	Format for the list CIRCUITPARAMETERL.
CIRCUITPARAMETERL	List of drive parameters ( $T_r$ , $I_D$ , and $N_D$ ).
CIRCUITPARAMETERS	List of drive parameters (same as above) for input-data cards.

<u>Identifier</u>	<u>Description</u>
CORENAME	Core name, e.g. E-6 or J-1.
COREPARAMETERH	Format for the list COREPARAMETERL.
COREPARAMETERL	List of core parameters (Core name, $l_i$ , $l_o$ , $\phi_r$ , $\phi_s$ , $H_a$ , $H_q$ , $H_n$ , $\lambda$ , $F_0''$ , $\nu$ , $\rho_p$ , $F_0$ , and $F_B$ ).
COREPARAMETERS	List of core parameters (same as above) for input-data cards.
COUNT	Index number of $n$ th $\Delta t$ during switching.
CTS	Index number of $j$ th iteration for each $n$ th $\Delta t$ .
C0	$\phi_{n(j=1)} - \phi_{n(j=0)}$ .
DELPHIC	$\phi_{n(j)} - \phi_{n(j-1)}$ .
GUESS	Label of location where initial approximation of $\phi$ is made for each $n$ th $\Delta t$ .
K	Index number of $n$ th $\Delta t$ for which output results are plotted automatically
LINES	Index number of printed line.
LOOP	Label of location from where iterative computation is repeated for each $n$ th $\Delta t$ .
OUTPUTFORMAT	Format for the list OUTPUTVARIABLES.
OUTPUTHEADING	Format for output column heading.
OUTPUTVARIABLES	List of results ( $t$ , $i_D$ , $\dot{\phi}$ , $\phi$ , $\phi_d$ , $F$ , and $j_{max}$ ).
QUIT	Label of location where computation terminates.
START	Label of location where computation starts for given core and circuit parameters.
SWITCHING	Label of location where computation starts for each $n$ th $\Delta t$ .
THETA9	$[\phi_{n(j=9)} - \phi_{n(j=8)}] / [\phi_{n(j=1)} - \phi_{n(j=0)}]$ .
XSCALE	Time scale, used in automatic plotting of $\dot{\phi}(t)$ .
YSCALE	$\dot{\phi}$ scale, used in automatic plotting of results.

Program:

UNLOADED CORE	001
BEGIN	002
COMMENT DECLARE CORE PARAMETERS, DRIVE PARAMETERS, VARIABLES, AND	003
AUXILIARY IDENTIFIERS ;	004
REAL LI, LO, PHIR, PHIS, HA, HQ, HN, LAMBDA, FOPP, NU, ROP, F0, FB ;	005
REAL TR, CAPID, TAUS, TH, TF ;	006
REAL T, DELT, PHIC, PHIC1, PHIC2, PHIDOTC, PHIDOTC1, ID, F,	007
DELPHIC, C0, THETA9, PHIDC, DPHDTC, XSCALE, YSCALE ;	008
INTEGER LINES, COUNT, CTS, ND, K ;	009
ALPHA CORENAME ;	010
LABEL START, SWITCHING, GUESS, LOOP, QUIT ;	011
COMMENT DECLARE INPUT/OUTPUT ;	012
FILE IN CR 0(2,10) ; FILE OUT F1 1(2,15) ;	013
LIST COREPARAMETERS(CORENAME, LI, LO, PHIR, PHIS, HA, HQ, HN, LAMBDA,	014
FOPP, NU, ROP, F0, FB) ;	015



LIST COREPARAMETERL(CORENAME,LI×103,LO×103,PHIR×108,PHIS×108,HA,HQ,HN,	016
LAMBDA,FOPP,NU,ROP,F0,FB) ;	017
LIST CIRCUITPARAMETERS(TR,CAPID,ND) ;	018
LIST CIRCUITPARAMETERL(TR×106,CAPID,ND) ;	019
LIST OUTPUTVARIABLES(T×106,ID,PHIDOTC,PHIC×108,PHIDC×108,F,CTS) ;	020
FORMAT COREPARAMETERH("CORE ",A6,X4,"LI=",F8.3,X4,"LO=",F8.3,X4,"PHIR=",	021
F8.3,X4,"PHIS=",F8.3,X4,"HA=",F8.3,X4,"HQ=",F8.3,X4,"HN=",F8.3,X15,	022
"LAMBDA=",F8.5,X4,"FOPP=",F8.3,X4,"NU=",F8.3,X4,"ROP=",F8.3,X4,"F0="	023
,F8.3,X4,"FB=",F8.3/) ;	024
FORMAT CIRCUITPARAMETERH("DRIVE PARAMETERS",X8,"TR=",F8.3,X4,"CAPID=",	025
F8.4,X4,"ND=",I2/) ;	026
FORMAT OUTPUTHEADING(/ X6,"T",X11,"ID",X7,"PHIDOTC",X7,"PHIC",X7,"PHIDC"	027
,X9,"F",X9,"CTS"/) ;	028
FORMAT OUTPUTFORMAT(F9.3,F12.3,F12.5,2F12.2,F12.3,I10) ;	029
COMMENT PROCEDURES USED BY THIS PROGRAM ARE MIN AND PHIDOT ;	030

<p>PROCEDURE PHIDOT (F,φ), APPENDIX A</p> <p>PROCEDURE MIN (A,B), APPENDIX B</p>
--

COMMENT READ INPUT-DATA CARDS AND PRINT HEADINGS ;	031
READ(CR/,COREPARAMETERS) ;	032
START:	033
READ(CR/,CIRCUITPARAMETERS) [QUIT] ;	034
WRITE(F1[PAGE]) ;	035
WRITE(F1,COREPARAMETERH,COREPARAMETERL) ;	036
WRITE(F1,CIRCUITPARAMETERH,CIRCUITPARAMETERL) ;	037
WRITE(F1,OUTPUTHEADING) ;	038
LINEs + 5 ; COUNT + K + 0 ;	039
COMMENT INITIALIZE VARIABLES AND PARAMETERS ;	040
PHIC2 + PHIC1 + -PHIR ; PHIDOTC1 + 0 ;	041
TAUS + IF TR ≤ 10-7 THEN PHIR/(0.3×ROP×(ND×CAPID-FOPP)) ELSE	042
SQRT(PHIR×TR/(0.15×ROP×ND×CAPID)) ;	043
DELT + TAUS/500 ;	044
T + TR×FOPP/(ND×CAPID) ;	045
COMMENT COMPUTE VARIABLES DURING SWITCHING TIME ;	046
SWITCHING:	047
T + T + DELT ;	048
COUNT + COUNT + 1 ;	049
ID + CAPID×MIN(T/TR,1) ;	050
F + ND×ID ;	051
CTS + 0 ;	052
GUESS:	053
PHIC + PHIC2 + 2×DELT×PHIDOTC1 ;	054
LOOP:	055
CTS + CTS + 1 ;	056
PHIDOTC + PHIDOT(F,PHIC,PHIDC,DPHDTDFC) ;	057
DELPHIC + PHIC1 + DELT×(PHIDOTC+PHIDOTC1)/2 - PHIC ;	058
PHIC + PHIC + DELPHIC ;	059
IF CTS = 1 THEN C0 + DELPHIC ;	060
IF CTS = 9 THEN BEGIN THETA9 + DELPHIC/C0; IF 0.9 <	061
ABS(THETA9) THEN GO TO GUESS ; DELPHIC + 0 END ;	062
IF ABS(DELPHIC) > 0.02×PHIR×DELT/TAUS AND CTS ≠ 10	063
THEN GO TO LOOP ;	064
PHIC2 + PHIC1 ; PHIC1 + PHIC ; PHIDOTC1 + PHIDOTC ;	065
COMMENT PRINT OUTPUT ;	066
IF COUNT MOD 25 = 0 THEN	067
BEGIN	068
K + K + 1 ;	069
IF LINEs MOD 50 = 0 THEN	070
BEGIN	071
WRITE(F1[PAGE]) ;	072
WRITE(F1,OUTPUTHEADING)	073
END ;	074

WRITE(F1,OUTPUTFORMAT,OUTPUTVARIABLES);	075
LINES = LINES + 1	076
END ;	077
IF PHIDOTC $\neq$ 0 THEN GO TO SWITCHING ;	078
GO TO START ;	079
QUIT:	080
END.	081

A sample of input data:

---

"E-6", 22.190-3, 23.540-3, 3.450-8, 3.7260-8, 230.0, 35.0, 30.0,  
 0.069, 0.95, 1.31, 0.112, 1.45, 3.0,  
 0.050-6, 1.1, 1,

---

Remarks:

Lines 018 - 019. For a trapezoidal or triangular drive, add  $T_h$  and  $T_f$ , Eq. (49).

Line 030. Additional PROCEDURES (447 cards altogether) were used for automatic plotting of the results.

Line 044.  $\Delta t$  may be increased to  $\tau_s/50$  with negligible effect on accuracy (cf. Fig. 13).

Line 045. Since computation cannot proceed unless  $\dot{\phi} \neq 0$  (cf. Line 078), initial  $t$  cannot be smaller than  $t_0$ . If, for some reason, it is required to start computation earlier, the condition in Line 078 must be changed.

Line 050. Following Eq. (48), the expression corresponds to step or ramp drive; for trapezoidal [Eq. (49)], triangular, or any other drive, the expression for  $i_D$  should be modified.

Lines 061 - 064. If  $|\theta_9| > 0.9$ , it is assumed that convergence has not been achieved. By going back to GUESS,  $\phi$  is reset to the initial value. Values computed next are retained by getting out of the loop, because by now  $j = 10$ .

Line 063. Convergence specification.

Line 065. These substitutions correspond to increasing  $n$  by 1.

Line 067. Output is printed once every 25  $\Delta t$ 's.

Line 070 - 074. No more than 50 lines per page are printed.

Input data. The first two lines include the core parameters of Core E-6. The last line includes the drive parameters of the first case in Table II, p. 24 ( $F_D = 1.1$  amp-turn).

*APPENDIX D*

**COMPUTER PROGRAM FOR LOADED-CORE FLUX SWITCHING**

# APPENDIX D

## COMPUTER PROGRAM FOR LOADED-CORE FLUX SWITCHING

Language: ALGOL 60.

Program Description: Computes  $i_D$ ,  $\dot{\phi}$ ,  $\phi$ ,  $\phi_d$ ,  $F$ ,  $\dot{q}$ , and  $e_d + \dot{q} R_d$  versus  $t$  for given core, circuit, and drive parameters.

Identifiers:

### (1) Analytical identifiers

<u>Identifier</u>	<u>Symbol</u>	<u>Identifier</u>	<u>Symbol</u>
C	$C$	NU	$\nu$
CAPID	$I_D$	PHIC	$\phi$
DELQD	$\Delta \dot{q}$	PHIC1	$\phi_{n-1}$
DELT	$\Delta t$	PHIC2	$\phi_{n-2}$
DPHDTDFC	$\dot{\phi}'$	PHIDC	$\phi_d$
ED	$e_d$	PHIDOTC	$\dot{\phi}$
EK	$E_k$	PHIDOTC1	$\dot{\phi}_{n-1}$
F	$F$	PHIR	$\phi_r$
FB	$F_B$	PHIS	$\phi_s$
FJ	$f_{n(j)}$	Q	$q$
FJPR	$f'_{n(j)}$	Q1	$q_{n-1}$
F0	$F_0$	QD	$\dot{q}$
FOPP	$F''_0$	QD1	$\dot{q}_{n-1}$
HA	$H_a$	QD2	$\dot{q}_{n-2}$
HN	$H_n$	QDD	$\ddot{q}$
HQ	$H_q$	QDD1	$\ddot{q}_{n-1}$
ID	$i_D$	R	$R$
I0	$I_0$	RD	$R_d$
L	$L$	RL	$R_L$
LAMBDA	$\lambda$	ROP	$\rho_p$
LI	$l_i$	T	$t$
LO	$l_o$	TAUS	$\tau_s$
NC	$N_c$	TR	$T_r$
ND	$N_D$		

(2) Auxiliary identifiers

<u>Identifier</u>	<u>Description</u>
CIRCUITPARAMETERH	Format for the list CIRCUITPARAMETERL.
CIRCUITPARAMETERL	List of circuit parameters ( $N_c$ , $R_L$ , $L$ , $C$ , $R_d$ , $I_0$ , $E_k$ , $I_D$ , $N_D$ , and $T_r$ ).
CIRCUITPARAMETERS	List of circuit parameters (same as above) for input-data cards.
CORENAME	Core name, e.g. J-1.
COREPARAMETERH	Format for the list COREPARAMETERL.
COREPARAMETERL	List of core parameters (Core name, $l_i$ , $l_o$ , $\phi_r$ , $\phi_s$ , $H_a$ , $H_q$ , $H_n$ , $\lambda$ , $F_0''$ , $\nu$ , $\rho_p$ , $F_0$ , and $F_B$ ).
COREPARAMETERS	List of core parameters (same as above) for input-data cards.
COUNT	Index number of $n$ th $\Delta t$ during switching.
CTS	Index number of $j$ th iteration for each $n$ th $\Delta t$ .
GUESS	Label of location where initial approximation of $\phi$ is made for each $n$ th $\Delta t$ .
K	Index number of automatically plotted set of output.
LINES	Index number of printed line
LOOP	Label of location from where iterative computation is repeated for each $n$ th $\Delta t$ .
OUTPUTFORMAT	Format for the list OUTPUTVARIABLES.
OUTPUTHEADING	Format for output column heading.
OUTPUTVARIABLES	List of results ( $t$ , $i_D$ , $\dot{\phi}$ , $\phi$ , $\phi_d$ , $F$ , $\dot{q}$ , $e_d + \dot{q} R_d$ , $j_{\max}$ ).
P	$1/\ddot{q}_j$ if $\ddot{q}_j \neq 0$ , zero otherwise.
P1	$1/(\dot{q}_{j-1} - \dot{q}_{n-1})$ if $\dot{q}_{j-1} \neq \dot{q}_{n-1}$ , zero otherwise.
QUIT	Label of location where computation terminates
S	$1/C$ if $C$ is finite, zero otherwise.
START	Label of location where computation starts for given core and circuit parameters.
SWITCHING	Label of location where computation starts for each $n$ th $\Delta t$ .
XSCALE	Time scale, used in automatic plotting of resulting waveforms.
YSCALE	$\dot{\phi}$ scale, used in automatic plotting of $\dot{\phi}(t)$ .
ZSCALE	$\dot{q}$ scale, used in automatic plotting of $\dot{q}(t)$ .

Program:

LOADED CORE	001
BEGIN	002
COMMENT DECLARE CORE PARAMETERS, CIRCUIT PARAMETERS, VARIABLES, AND	003
AUXILIARY IDENTIFIERS ;	004
REAL LI, LO, PHIR, PHIS, HA, HQ, HN, LAMBDA, FOPP, NU, ROP, FO, FB ;	005
REAL RL, L, C, RD, IO, TR, CAPID, EK, TAUS, R, S, P, P1 ;	006
REAL T, DELT, PHIC, PHIC1, PHIC2, PHIDOTC, PHIDOTC1, ID, F, Q, Q1, QD,	007
QD1, QD2, QDD, QDD1, DELQD, PHIDC, DPHDTDFC,	008
ED, FJ, FJPR, XSCALE, YSCALE, ZSCALE ;	009
INTEGER LINES, CTS, COUNT, NC, ND, K ;	010
ALPHA CORENAME ;	011
LABEL START, SWITCHING, GUESS, LOOP, QUIT ;	012
COMMENT DECLARE INPUT/OUTPUT ;	013
FILE IN CR 0(2,10) ; FILE OUT F1 1(2,15) ;	014
LIST COREPARAMETERS(CORENAME, LI, LO, PHIR, PHIS, HA, HQ, HN, LAMBDA,	015
FOPP, NU, ROP, FO, FB) ;	016
LIST COREPARAMETERL(CORENAME, LI×1Q3, LO×1Q3, PHIR×1Q8, PHIS×1Q8, HA, HQ, HN,	017
LAMBDA, FOPP, NU, ROP, FO, FB) ;	018
LIST CIRCUITPARAMETERS(NC, RL, L, C, RD, IO, EK, CAPID, ND, TR) ;	019
LIST CIRCUITPARAMETERL(NC, RL, L×1Q6, C×1Q6, RD, IO×1Q6, EK, CAPID, ND, TR×1Q6) ;	020
LIST OUTPUTVARIABLES(T×1Q6, ID, PHIDOTC, PHIC×1Q8, PHIDC×1Q8, F, QD, ED+QD×RD,	021
CTS) ;	022
FORMAT COREPARAMETERH("CORE ", A6, X4, "LI=", F8.3, X4, "LO=", F8.3, X4, "PHIR=",	023
F8.3, X4, "PHIS=", F8.3, X4, "HA=", F8.3, X4, "HQ=", F8.3, X4, "HN=", F8.3, X4, "LAMBDA=",	024
F8.5, X4, "FOPP=", F8.3, X4, "NU=", F8.3, X4, "ROP=", F8.3, X4, "FO=",	025
F8.3, X4, "FB=", F8.3, X4) ;	026
FORMAT CIRCUITPARAMETERH("CIRCUIT", X8, "NC=", I2, X4, "RL=", F8.3, X4, "L=",	027
F8.3, X4, "C=", F8.3, X4, "RD=", F8.3, X4, "IO=", F8.3, X4, "EK=", F8.5,	028
"PARAMETERS", X5, "CAPID=", F8.3, X4, "ND=", I2, X4, "TR=", F8.3, X4) ;	029
FORMAT OUTPUTHEADING(/ X6, "T", X11, "ID", X7, "PHIDOTC", X7, "PHIC", X7, "PHIDC"	030
, X9, "F", X11, "QD", X10, "VD", X9, "CTS"/) ;	031
FORMAT OUTPUTFORMAT(F9.3, 2F12.3, 2F12.2, 3F12.3, I10) ;	032
COMMENT PROCEDURES USED BY THIS PROGRAM ARE MIN, MAX, AND PHIDOT ;	033

PROCEDURE PHIDOT ( $F, \phi$ ), APPENDIX A  
 PROCEDUREs MIN (A,B) and MAX (A,B), APPENDIX B

COMMENT READ INPUT-DATA CARDS AND PRINT HEADINGS ;	034
READ(CR,/, COREPARAMETERS) ;	035
START:	036
READ(CR,/, CIRCUITPARAMETERS) [QUIT] ;	037
WRITE(F1, PAGE) ;	038
WRITE(F1, COREPARAMETERH, COREPARAMETERL) ;	039
WRITE(F1, CIRCUITPARAMETERH, CIRCUITPARAMETERL) ;	040
WRITE(F1, OUTPUTHEADING) ;	041
LINES = 6 ; COUNT = 0 ;	042
K = 0 ;	043
COMMENT INITIALIZE VARIABLES AND PARAMETERS ;	044
PHIC2 = PHIC1 = -PHIR ; QD2 = QD1 = QDD1 = Q1 = PHIDOTC1 = 0 ;	045
S = IF C < 1Q10 THEN 1/C ELSE 0 ; R = RL + RD ;	046
TAUS = IF TR ≤ 1Q-7 THEN 2×PHIR/(0.3×ROP×(ND×CAPID-FOPP)) ELSE	047
SQRT(PHIR×TR/(0.15×ROP×ND×CAPID)) ;	048
DELT = TAUS/200 ;	049
T = TR×FOPP/(ND×CAPID) ;	050

COMMENT COMPUTE VARIABLES DURING SWITCHING TIME ;	051
SWITCHING:	052
T = T + DELT ;	053
COUNT = COUNT + 1 ;	054
ID = CAPID*MIN(T/TR,1) ;	055
CTS = 0 ;	056
GUESS:	057
PHIC = PHIC2 + 2*DELT*PHIDOTC1 ;	058
QD = QD2 + 2*DELT*QDD1 ;	059
IF IO < 1Q10 THEN QD = MAX(QD,0) ;	060
Q = Q1 + DELT*(QD+QD1)/2 ;	061
LOOP:	062
CTS = CTS + 1 ;	063
IF CTS = 9 THEN GO TO GUESS;	064
F = ND*ID - NC*QD ;	065
PHIDOTC = PHIDOT(F,PHIC,PHIOC,DPHOTOFC) ;	066
ED = EK*LN(QD/IO + 1) ;	067
QDD = (QD-QD1)/DELT ;	068
PHIC = PHIC1 + DELT*(PHIDOTC+PHIDOTC1)/2 ;	069
IF CTS < 10 THEN	070
BEGIN	071
FJ = R*QD - NC*PHIDOTC + ED + S*Q + L*QDD ;	072
IF QDD ≠ 0 THEN P = 1 / QDD ELSE P = 0 ;	073
IF QD=QD1 THEN P1=0 ELSE P1=1/(QD-QD1);	074
FJPR = R + DPHOTOFC*NC*2 + EK/(QD+IO) + S*QD*P	075
+L*P1*(QDD-QDD1) ;	076
DELQD = -FJ/FJPR ;	077
QD = QD + DELQD ;	078
IF IO < 1Q10 THEN QD = MAX(QD,0) ;	079
IF CTS ≥ 5 THEN QD = QD - 0.5 * DELQD ;	080
Q = Q1 + DELT*(QD+QD1)/2 ;	081
IF ABS(DELQD) > 0.0010*ABS(QD)	082
THEN GO TO LOOP	083
END ;	084
PHIC2 = PHIC1 ; PHIC1 = PHIC ; PHIDOTC1 = PHIDOTC ;	085
QD2 = QD1 ; QD1 = QD ; Q1 = Q ; QDD1 = QDD ;	086
COMMENT PRINT OUTPUT ;	087
IF COUNT MOD 10 = 0 THEN	088
BEGIN	089
IF LINES MOD 50 = 0 THEN	090
BEGIN	091
WRITE(F1[PAGE]) ;	092
WRITE(F1,OUTPUTHEADING)	093
END ;	094
WRITE(F1,OUTPUTFORMAT,OUTPUTVARIABLES);	095
LINES = LINES + 1	096
END ;	097
IF PHIDOTC ≠ 0 THEN GO TO SWITCHING ;	098
GO TO START ;	099
QUIT:	100
END.	101

A sample of input data:

"J-1   ",7.18E-3,11.58E-3,31.0E-8,33.48E-8,250.0,26.0,22.50,1.64,  
0.27,1.43,2.27,0.55,1.20,  
2,0.131,0.38E-6,0.253E-6,0.74,2.7E-6,0.0833,1.80,1,0.10E-6,

Remarks:

Line 019. If a diode is not included in the load, we shall arbitrarily let  $R_d = 0$ ,  $I_0 = 10^{20}$ , and  $E_k = 0$ .

Line 033. Automatic plotting requires additional PROCEDURES.

Line 046. The use of  $S$  instead of  $1/C$  is designed to allow for the inclusion of a load with no capacitance, i.e.,  $S = 0$  for  $C \rightarrow \infty$ .

Lines 047-049. Since  $\tau_s$  is estimated from the no-load expression of either Eq. (46) or Eq. (47), the actual computed  $\tau_s$  will be considerably longer. Hence, increasing  $\Delta t$  to, say,  $\tau_s/50$  may have a negligible effect on the accuracy.

Lines 060 and 078. If a diode is included in the load,  $I_0 < 10^{20}$  (see remark to Line 019), and thus  $\dot{q} \geq 0$ .

Lines 066 and 071. If a diode is not included in the load,  $E_k = 0$  and  $R_d = 0$  (see remark to Line 019), and thus  $e_d = 0$ , and  $R = R_L$ .

Lines 072-075. The expression in Lines 074 and 075 stands for Eq. (70), in which the substitutions  $1/C = S$ ,  $1/\ddot{q}_{n(j)} = P$ , and  $[\dot{q}_{n(j-1)} - \dot{q}_{n-1}] = P_1$  are made in order to prevent an arithmetic overflow in case either  $C \rightarrow \infty$  (no capacitor in the load), or  $\ddot{q}_{n(j)} = 0$ , or  $\dot{q}_{n(j-1)} = \dot{q}_{n-1}$ .

Line 079. If convergence has not been reached within four iterations, computational oscillations are assumed, and Eq. (58) is replaced by Eq. (58a).

Line 081. Convergence specification.

Line 082. If convergence has not been reached within eight iterations, divergence is assumed, and the initial approximation plus a single correction up to Line 068 is restored.

Lines 085-086. These substitutions correspond to increasing  $n$  by 1.

Lines 088. Output is printed once every 10  $\Delta t$ 's.

Lines 090-094. No more than 50 lines per page are printed.

Input-data. The parameters of Core J-1 are given in the first two lines. The last line includes the circuit parameters of the sixth case in Table III (step drive, R-L-C-Diode load), p. 40.



*APPENDIX E*

**COMPUTER PROGRAM FOR CORE-DIODE SHIFT REGISTER**

# APPENDIX E

## COMPUTER PROGRAM FOR CORE-DIODE SHIFT REGISTER

Language: ALGOL 60.

Program Description: Computes  $\phi_T$ ,  $\phi_R$ ,  $\dot{\phi}_T$ ,  $\dot{\phi}_R$ ,  $\phi_{dT}$ ,  $\phi_{dR}$ ,  $F_T$ ,  $F_R$ ,  $i_F$ ,  $i_B$ ,  $i_A$ , and  $\dot{\phi}_B$  versus  $t$ ; computes  $G$  and  $\Delta\phi_B/2\phi_r$  versus  $\Delta\phi_T/2\phi_r$ .

Identifiers:

### (1) Analytical identifiers

<u>Identifier</u>	<u>Symbol</u>	<u>Identifier</u>	<u>Symbol</u>
CAPIA	$I_A$	IAN	$i_{An}$
DEL	$\Delta i_F / \Delta t$	IB	$i_B$
DELIB	$\Delta i_B$	IFC	$i_F$
DELIF	$\Delta i_F$	IFN	$i_{Fn(0)}$
DELPHIB	$\Delta \phi_B$	LAMBDA	$\lambda$
DELPHIDOTT	$\Delta \dot{\phi}_T$	LI	$l_i$
DELPHIR	$\Delta \phi_R$	LO	$l_o$
DELPHIT	$\Delta \phi_T$	NA	$N_a$
DELT	$\Delta t$	NR	$N_R$
DPHDTDFR	$\dot{\phi}_R'$	NT	$N_T$
DPHDTDFT	$\dot{\phi}_T'$	NU	$\nu$
F	$F$	PHIB	$\phi_B$
FB	$F_B$	PHIDOTB	$\dot{\phi}_B$
FPRA	$f_A'$	PHIDOTR	$\dot{\phi}_R$
FPRB	$f_B'$	PHIDOTT	$\dot{\phi}_T$
FR	$F_R$	PHIDR	$\phi_{dR}$
FT	$F_T$	PHIDT	$\phi_{dT}$
F0	$F_0$	PHIR	$\phi_r$
F0PP	$F_0''$	PHIRC	$\phi_R$
F1B	$F_{1B}$	PHIRCO	$\phi_{R0}$
G	$G$	PHIRN	$\phi_{Rn(0)}$
HA	$H_a$	PHIS	$\phi_s$
HN	$H_n$	PHIT	$\phi_T$
HQ	$H_q$	PHITN	$\phi_{Tn(0)}$

<u>Identifier</u>	<u>Symbol</u>	<u>Identifier</u>	<u>Symbol</u>
PHIT0	$\phi_{T0}$	T	$t$
R	$R$	TAUS	$\tau_s$
RD	$R_d$	TF	$T_f$
RL	$R_L$	TH	$T_h$
ROP	$\rho_p$	TR	$T_r$
		VD	$V_d$

(2) Auxiliary identifiers

<u>Identifier</u>	<u>Description</u>
CF	Equal to zero if convergence has been achieved; otherwise, equal to 1.
CFS	Total number of convergence failures throughout switching time.
COUNT	Index number of $n$ th $\Delta t$ during switching.
CT	Index number of $j$ th iteration for each $n$ th $\Delta t$ .
CTM	Number of times Condition (2), p. 62, is not satisfied in Mode 2.
CTP	Number of times $(R/N_T)  df/d\dot{\phi}_T $ is larger than $ df/di_F $ for each $n$ th $\Delta t$ .
CTPS	Summation of CTP during switching time.
CTS	Total number of iterations during switching time, i.e., $\sum CT$ .
EXIT	Label of location where switching terminates.
FHEAD	Format for heading of time-variable output.
FMG	Format for the list OUG.
FMH	Format for $I_A$ and $\phi_{T0}$ heading.
FMT	Format for the list OUTLIST.
GHEAD	Format for heading of over-all flux changes and flux gain.
HEDF	Index number of printed line.
MODE	Label of location where mode of operation is selected.
MODE 1	Label of location where Mode 1 begins.
MODE 2	Label of location where Mode 2 begins.
MODE 3	Label of location where Mode 3 begins.
OUN	List of over-all output ( $\Delta\phi_T/2\phi_r$ , $G$ , $\Delta\phi_B/2\phi_r$ , CTS, COUNT, CFS, and CTPS).

Identifier	Description
OUTH	List of core and circuit parameters ( $l_i, l_o, \phi_r, \phi_s, H_a, H_q, H_n, F_0, F_B, F_0, \rho_p, \nu, \lambda, T_r, T_h, T_f, N_A, N_T, N_R, R_L, R_d$ , and $V_d$ ).
OUTLIST	List of time-variable output ( $t, \phi_T, \phi_R, \dot{\phi}_T, \dot{\phi}_R, \phi_{dT}, \phi_{dR}, F_T, F_R, i_F, i_B, i_A, \dot{\phi}_B$ , and $j_{\max}$ ).
TEST	Label for location where $\dot{\phi}_B$ and $\phi_B$ are computed, and a decision is made as to whether convergence has been achieved.

Program;

BEGIN	001
COMMENT COMPUTATION OF T, PHIT, PHIRC, PHIDOTT, PHIDOTR, PHIDT, PHIDR,	002
FT, FR, IF, IB, IA(T), PHIDOTB, DELPHIT/2PHIR, G, AND DELPHIB/2PHIR	003
IN A CORE-DIODE SHIFT REGISTER ;	004
COMMENT DECLARATION OF CORE PARAMETERS ;	005
REAL LI,LO,PHIR,PHIS,HA,HQ,HN,FOPP,FB,F0,ROP,NU,LAMBDA,F1B ;	006
COMMENT DECLARATION OF CIRCUIT PARAMETERS ;	007
REAL TR,TH,TF,RL,RD,VD,R,CAPIA,TAUS;	008
INTEGER NA, NT, NR ;	009
COMMENT DECLARATION OF VARIABLES;	010
REAL T,DELT,PHIRCO,PHITO,PHIT,PHIRC,PHIDOTT,PHIDOTR,PHITN,PHIRN,IAN,	011
F,FPRA,FPRB,DEL,FR,FT,DELPHIDOTT,IFN, PHIB, PHIDOTB, DELPHIB,	012
PHIDT,PHIDR,DPHIDOTT,DPHIDOTR,DELPHIT,DELPHIR,IFC,IB,DELIF,DELIB,G;	013
INTEGER COUNT,CT,CTS,HEDF,CF,CFS,CTM,CTP,CTPS ;	014
LABEL SWITCHING, MODE, MODE1, MODE2, MODE3, TEST,EXIT;	015
COMMENT DECLARATION OF OUTPUT LISTS AND FORMATS;	016
FILE OUT PRINTER 1(4,15);	017
LIST OUTH(1000*LI,1000*LO,100*PHIR,100*PHIS,HA,HQ,HN,FOPP,FB,F0,ROP,	018
NU,LAMBDA,100*TR,100*TH,100*TF,NA,NT,NR,RL,RD,VD) ;	019
LIST OUTLIST(T*100,PHIT*100,PHIRC*100,PHIDOTT,PHIDOTR,PHIDT*100,	020
PHIDR*100,FT,FR,IFC,IB,IAN,PHIDOTB,CT);	021
LIST OUG(DELPHIT/(2*PHIR),G,DELPHIB/(2*PHIR),CTS,COUNT,CFS,CTPS) ;	022
FORMAT FMTH(X40,"CORE PARAMETERS"/"LI=",F7.3,X6,"LO=",F7.3,X6,	023
"PHIR=",F7.3,X6,"PHIS=",F7.3,X6,"HA=",F7.3,X6,"HQ=",F7.3,X6,"HN=",	024
F7.3/"FOPP=",F7.3,X6,"FB=",F7.3,X6,"F0=",F7.3,X6,"ROP=",F7.3,X6,	025
"NU=",F7.3,X6,"LAMBDA=",F7.3/X40,"CIRCUIT PARAMETERS"/"TR=",F7.3,	026
X5,"TH=",F7.3,X5,"TF=",F7.3,X5,"NA=",I2,X5,"NT=",I2,X5,"NR=",I2,X5,	027
"RL=",F7.3,X5,"RD=",F7.3,X5,"VD=",F7.3 ) ;	028
FORMAT FMH(X40,"IA=",F5.2," PHITO=",F6.2/);	029
FORMAT FHEAD( " T PHIT PHIRC PHIDOTT PHIDOTR PHIDT",	030
" PHIDR FT FR IF", " IB IA(T) ",	031
"PHIDOTB CT"/) ;	032
FORMAT FMT(F6.4,2F9.2,2F9.4,2F9.2,6F9.4,I5);	033
FORMAT GHEAD(// "DELPHIT/2PHIR G DELPHIB/2PHIR "	034
"CTS COUNT CFS CTPS") ;	035
FORMAT FMG(/,3F11.4,X4 ,3I10,I9/);	036
COMMENT THIS PROGRAM USES THE PROCEDURES MIN, MAX, IA(T), PHIDOT ;	037

PROCEDURE PHIDOT ( $F, \phi$ ), APPENDIX A

PROCEDURES MIN (A,B), MAX (A,B), and IA(T), APPENDIX B

COMMENT INITIALIZE CORE PARAMETERS;	038
LI + 7.18Q-3; LO + 11.58Q-3; PHIR + 30.0Q-8; PHIS + 1.08*PHIR;	039
HA + 250; HQ + 26.0; HN + 22.5; FOPP + 0.27; FB + 1.20;	040
F0 + 0.55; ROP + 2.27; NU + (FB-FOPP)/(FB-F0); LAMBDA + ROP/(NU*	041
(FB-FOPP)*(NU-1)); F1B + 0.25 ;	042
COMMENT INITIALIZE CIRCUIT PARAMETERS;	043
RD + 0.85; VD + 0.75; RL + 0.06; PHIRC+ -PHIR;	044
TR + 2Q-6; TH + 5Q-6; TF + 2Q-6; NA + 4; NT + 10; NR + 4; R + RL+RD;	045
COMMENT START COMPUTATION;	046
FOR CAPIA + 1.18 DO BEGIN	047
IF NA*CAPIA > FOPP THEN	048
FOR PHIT0 + -PHIR DO BEGIN	049
COMMENT PRINT HEADING ;	050
WRITE(PRINTER,PAGE);	051
WRITE(PRINTER,FMTH,OUTH);	052
WRITE(PRINTER,FMH,CAPIA,PHIT0*1Q8);	053
WRITE(PRINTER,FHEAD);	054
HEDF + 11; CTS + CFS + CTPS + 0 ;	055
COUNT + -1; PHIT + PHIT0; PHIB + PHIRC+PHIRC0;	056
PHIDOTT + PHIDOTR + IFC + IB + DELIF + 0 ;	057
TAUS + (PHIR-PHIT0)*(NT*2/(R+0.6*ROP*NR*2)+NR*2/R+1.67/ROP)/(NA	058
*CAPIA-F0+NT*(VD-0.6*ROP*NR*F0)/(R+0.6*ROP*NR*2)+VD*NR/R);	059
T + SQRT(7.375*FOPP/(NA*CAPIA))*1Q-6 ;	060
COMMENT COMPUTATION FOR SWITCHING TIME ;	061
SWITCHING:	062
DELT + IF PHIDOTT = 0 THEN TAUS/200 ELSE 0.005*MIN(TAUS,(	063
PHIR-PHIT0)/ABS(PHIDOTT));	064
T + T +DELT; CTM+ 0;	065
PHITN + PHIT ; PHIRN + PHIRC ; IAN + IA(T); IFN+IFC;	066
MODE:	067
IFC + IFN + DEL * DELT ;	068
CT + CTP + 0; CTM + CTM+1;	069
IF CTM = 6 THEN GO TO TEST ;	070
IF PHIDOTT ≤ VD/NT THEN GO TO MODE1;	071
IF VD/NT < PHIDOTT AND PHIDOTT ≤ VD/NR THEN GO TO MODE2;	072
IF VD/NR < PHIDOTT THEN GO TO MODE3;	073
MODE1:	074
DELIF + IFC + IB + FR + 0; FT + NA*IAN;	075
PHIDOTT + PHIDOT(FT,PHIT,PHIDT,DPHDTDFT);	076
PHIDOTR + PHIDOT(FR,PHIRC,PHIDR,DPHDTDFR);	077
PHIT + PHITN+PHIDOTT*DELT;	078
PHIRC + PHIRN ;	079
CT + 1;	080
IF PHIDOTT = 0 AND PHIT > 0 THEN GO TO EXIT;	081
IF PHIDOTT > VD/NT THEN	082
BEGIN CT + 0; GO TO MODE2 END;	083
GO TO TEST;	084
MODE2:	085
IF CT ≥ 5 THEN IFC + IFC - 0.5* DELIF ;	086
CT + CT+1;	087
IB + 0; FT + NA*IAN-NT*IFC; FR + NR*IFC;	088
PHIDOTT + PHIDOT(FT,PHIT,PHIDT,DPHDTDFT);	089
PHIDOTR + PHIDOT(FR,PHIRC,PHIDR,DPHDTDFR);	090
PHIT + PHITN+PHIDOTT*DELT;	091
PHIRC + PHIRN+PHIDOTR*DELT;	092
IF PHIDOTT = 0 AND PHIT > 0 THEN GO TO EXIT;	093
F + NT*PHIDOTT-NR*PHIDOTR-R*IFC-VD;	094
FPRA + -(NT*2*DPHDTDFT+NR*2*DPHDTDFR+R);	095
IF FT ≤ FOPP THEN FPRB + 1Q20 ELSE	096
FPRB + NT +(R+NR*2*DPHDTDFR)/(NT*DPHDTDFT) ;	097

IF ABS(FPRA) < (R/NT)*ABS(FPRB) THEN	098
BEGIN	099
CTP = CTP+1 ;	100
DELPHIDOTT = -F/FPRB ;	101
PHIDOTT = PHIDOTT + DELPHIDOTT ;	102
DELIF = NT * DELPHIDOTT/R ;	103
IFC = (NT*PHIDOTT-NR*PHIDOTR-VD)/R ;	104
IF ABS(DELPHIDOTT) > 0.001*ABS(PHIDOTT) AND CT < 20	105
THEN GO TO MODE2	106
END	107
ELSE	108
BEGIN	109
DELIF = -F/FPRA ;	110
IFC = IFC + DELIF ;	111
IF ABS(DELIF) > 0.001*ABS(IFC) AND CT < 20	112
THEN GO TO MODE2	113
END ;	114
IF VD/NT ≥ PHIDOTT OR PHIDOTT > VD/NR THEN	115
BEGIN IFC = IFN; CT = CTP + 0; GO TO MODE END;	116
GO TO TEST;	117
MODE3:	118
IF CT ≥ 5 THEN IFC = IFC - 0.5* DELIF ;	119
CT = CT+1;	120
FR = NR*IFC;	121
PHIDOTR = PHIDOT(FR,PHIRC,PHIDR,DPHOTOFR);	122
DELIB = MAX(0,MIN((NR*PHIDOTT-VD)/R,F1B/NT))-IB;	123
IF CT < 5 THEN IB = IB+DELIB ELSE IB = IB+0.5*DELIB;	124
FT = MAXIAN -NT*IFC -NR*IB ;	125
PHIDOTT = PHIDOT(FT,PHIT,PHIDT,DPHOTOFT);	126
PHIT = PHIT+PHIDOTT*DELT;	127
PHIRC = PHIRN+PHIDOTR*DELT;	128
IF PHIDOTT = 0 AND PHIT > 0 THEN GO TO EXIT;	129
F = NT*PHIDOTT-NR*PHIDOTR-R*IFC-VD;	130
FPRA = IF IB = F1B/NT THEN -(NT*2*DPHOTOFT+NR*2*DPHOTOFR	131
+R) ELSE -((NT*2+NR*2+NR*4*DPHOTOFR/R)*DPHOTOFT+NR*2	132
*DPHOTOFR+R);	133
IF FT ≤ FOPP THEN FPRB = 1Q20 ELSE	134
FPRB = IF IB = F1B/NT THEN NT*(R+NR*2*DPHOTOFR)/(NT*	135
DPHOTOFT) ELSE NT*NT*(R+NR*2*DPHOTOFR)/(DPHOTOFT*(NT*	136
+NR*2+NR*4*DPHOTOFR/R));	137
IF ABS(FPRA) < (R/NT)*ABS(FPRB) THEN	138
BEGIN	139
CTP = CTP+1 ;	140
DELPHIDOTT = -F/FPRB ;	141
PHIDOTT = PHIDOTT + DELPHIDOTT ;	142
DELIF = NT * DELPHIDOTT/R ;	143
IFC = (NT*PHIDOTT-NR*PHIDOTR-VD)/R ;	144
IF ABS(DELPHIDOTT) > 0.001*ABS(PHIDOTT) AND CT < 20	145
THEN GO TO MODE3	146
END	147
ELSE	148
BEGIN	149
DELIF = -F/FPRA ;	150
IFC = IFC + DELIF ;	151
IF ABS(DELIF) > 0.001*ABS(IFC) AND CT < 20	152
THEN GO TO MODE3	153
END ;	154
IF VD/NR ≥ PHIDOTT THEN	155
BEGIN IFC = IFN; CT = CTP + 0; GO TO MODE2 END;	156
GO TO TEST;	157

TEST:	158
PHIDOTB + IF IB = F1B/NT THEN (NR*PHIDOTT-VD-IB*R)/NT	159
ELSE 0 ;	160
PHIB + PHIB + PHIDOTB*DELT ;	161
IF CT ≥ 20 OR CTM = 6 THEN	162
BEGIN CF + CF + 1 ; CFS + CFS + 1 END ;	163
COUNT + COUNT+1 ;	164
IF COUNT MOD 5 = 0 THEN	165
BEGIN WRITE(PRINTER,FMT,OUTLIST) ; HEDF + HEDF+1 ;	166
END ;	167
IF HEDF MOD 50 = 0 THEN	168
BEGIN	169
WRITE(PRINTER,PAGE) ;	170
WRITE(PRINTER,FHEAD) ;	171
HEDF + HEDF+2 ;	172
END ;	173
CF + 0 ;	174
CTS + CTS + CT ;	175
CTPS + CTPS + CTP ;	176
DEL + (IFC-IFN)/DELT ;	177
GO TO SWITCHING ;	178
EXIT:	179
DELPHIB + PHIB + PHIR ;	180
DELPHIT + PHIT-PHITO ;	181
DELPHIR + PHIRC-PHIRCO ;	182
G + DELPHIR/DELPHIT ;	183
WRITE(PRINTER,GHEAD) ;	184
WRITE(PRINTER,FMG,OUTG) ;	185
END	186
END	187
END.	188

#### Remarks:

Lines 008, 019 and 045. The parameters,  $T_r$ ,  $T_h$ , and  $T_f$ , are used for a trapezoidal drive current, Fig. 6(d). They have not been used for the results shown in Figs. 21 through 24.

Lines 041-042. In this case, the core parameters  $\nu$  and  $\lambda$  are computed from Eqs. (24) and (25) after assurance that the resulting computed  $\phi_p(F)$  curve agrees with the experimental data.

Line 042. The value  $F_{1B} = 0.25$  amp-turn is taken from experimental static  $\phi(F)$  curve (cf. Fig. 17).

Line 047 and 049. For the computation of the flux-gain curves, Fig. 23, and  $\Delta\phi_B$ , Fig. 24, additional values of  $I_A$  and  $\phi_{T0}$  were used.

Line 060. The initial time is obtained by equating  $i_A(t)$ , Eq. (91), to  $F_0''/N_A$ .

Line 070. After six returns to MODE, it is assumed that convergence has not been achieved, and the computation proceeds to the next  $\Delta t$ .

Lines 086 and 119. If convergence has not been reached within five iterations, computational oscillations are assumed, and Eq. (58) is replaced by Eq. (58a).

Lines 096 and 101; 134 and 141. If  $F_T \leq F_0''$ ,  $\dot{\phi}_T = \Delta \dot{\phi}_T = 0$ . This is obtained effectively by arbitrarily letting  $f_B' = 10^{20}$ .

Lines 116 and 156. If Condition (2), p. 62, has not been satisfied,  $i_{F(j)}$  is reset to the initial value,  $i_{F(0)}$ .

Lines 112 and 145. Convergence specification.

Lines 162-163. Criteria for registering convergence failure.

Lines 165-173. Time-variable output is printed once every 5  $\Delta t$ 's, no more than 50 lines per page. If only  $G$  and  $\Delta \phi_B / 2 \phi_r$  vs.  $\Delta \phi_T / 2 \phi_r$  are computed, these lines should be deleted.



## REFERENCES

1. D. Nitzan, "Flux Switching in Multipath Cores," Report 1, for Jet Propulsion Laboratory, Contract 950095 under NASw-6, SRI Project 3696, Stanford Research Institute, Menlo Park, California (November 1961).
2. D. Nitzan and V. W. Hesterman, "Flux Switching in Multipath Cores," Report 2, for Jet Propulsion Laboratory, Contract 950095 under NASw-6, SRI Project 3696, Stanford Research Institute, Menlo Park, California (November 1962).
3. "An Introduction to ALGOL 60 for the B5000 Information Processing System," Bulletin 5000-21001-D, Burroughs Corporation, Detroit 32, Michigan (Revised December 1961).
4. "Extended ALGOL Reference Manual for the Burroughs B5000," Bulletin 5000-21012, November 1962, Burroughs Corporation, Detroit 32, Michigan (Revised August 1963).
5. W. E. Milne, *Numerical Solution of Differential Equations*, (John Wiley & Sons Inc., New York, 1953) chapter 2.
6. W. Shockley, *Electrons and Holes in Semiconductors*, (D. Van Nostrand Company, Inc., New York, 1950) chapter 4.
7. V. W. Hesterman, "Flux-Switching Properties of a Partially Set Core," Tech. Report 5, Contract Nonr 2712(00), SRI Project 2697, Stanford Research Institute, Menlo Park, California (November 1963).
8. R. W. McKay and K. C. Smith, "Effect of Previous History on Switching Rates in Ferrites," *J. Appl. Phys.* 31, Supplement, pp. 133S-134S (May 1960).
9. F. G. Hewitt and W. M. Overn, "History Effect of Time-Limited Excitation," *J. Appl. Phys.* 34, pp. 1117-1118, Part 2 (April 1963).
10. I. A. D. Lewis and F. H. Wells, *Millimicrosecond Pulse Techniques*, pp. 115-122, 2nd ed. (Pergamon Press, New York, New York, 1959).
11. S. R. Ray, "Model of Partial Switching in Polycrystalline Ferromagnetics," Proc. Intermag. Conf., Washington, D. C., IEEE (April 1963).
12. V. W. Hesterman, "Evaluation of Flux-Switching Models for Magnetic Devices," Tech. Report 2, Contract Nonr 2712(00), SRI Project 2697, Stanford Research Institute, Menlo Park, California (September 1961).
13. V. T. Shahan and O. A. Gutwin, "Threshold Properties of Partially Switched Ferrite Cores," *J. Appl. Phys.* 33, Supplement, pp. 1049-1050 (March 1962).
14. Roger H. Tancrell, "Impulse Selection for Core Logic," *J. Appl. Phys.* 32, Supplement, pp. 40S-41S (March 1961).
15. N. Menyuk and J. B. Goodenough, "Magnetic Materials for Digital-Computer Components. I. A Theory of Flux Reversal in Polycrystalline Ferromagnetics," *J. Appl. Phys.* 26, pp. 8-18 (January 1955).

## **INDEX**

## INDEX

- ALGOL 60, 16
  - computer program:
    - core-diode shift register, 157-163
    - loaded core, 149-153
    - PROCEDURE for:
      - drive current, 140
      - maximum of (A,B), 139
      - minimum of (A,B), 139
      - minimum of (A,B,C), 140
    - $\phi(F, \phi)$ , 133-135
    - unloaded core, 143-146
    - PROCEDURE, use of, 16
- Amplitude of pulses, 84
- Analysis:
  - core-diode shift register, 57-60
    - assumptions, 57-80
    - basic equations, 58-60
    - diode model, 57
    - equivalent circuit, 58
    - information pattern effect, 74-75
- Anomalies of switching, 97
- Area under  $\phi(t)$ , 95, 99
- Asterisks on  $\phi(F)$  curves, 115
- Asymmetric  $\phi(\phi)$ , 129
- Average of  $F_{ps}$  over flux, 127
  
- Back transfer of spurious  $\Delta\phi$  in core-diode shift register, 58-60, 67-68, 70-71, 74-75
  
- Cancellation of error:
  - second-order integrator, 86
  - $\lambda$  and  $F_0$ , 126
- Capacitive load:
  - effect on switching, 54
  - experiment, 39-40
- Capacitor in integrator, 86-87
- Characteristic impedance of transmission line, 86
- Chopper, 86-87
- Circuit:
  - core-diode shift register, 56
  - equivalent circuit of, 58
  - flux measurement, 87
  - loaded core, 39
- Clear pulse, 83-84, 88, 95
- Clearing, 83
  - incomplete, 81
- Coalesce, two regions in  $\phi_p(F)$ , 118
- Coaxial:
  - core holder, 85, 87
  - mercury relay, 86
- Coercive, MMF, 6-7, 115
  
- Computation, core diode shift register:
  - computer program outline, 63-68
    - approximate switching time, 63
    - back spurious flux transfer, 67-68
    - flux gain, 68
    - Mode 1, 64-65
    - Mode 2, 65-66
    - Mode 3, 66-67
  - method of, 60-63
  - mode switching, 62
  - Newton's method, 61-62
- Computation, loaded-core switching:
  - basic equations, 41
  - computer program outline, 45-46
  - computed vs. experimental, 46-54
    - step drive, 48-49, 52
    - ramp drive, 50-51, 53
  - convergence, 42, 45
  - method of, 41-43
  - sequence of, 43-45
- Computation, unloaded-core switching:
  - computer program outline, 28-29
  - initial  $\phi$  spikes, Core E-6, 29-30
  - sequence of, 27-28
  - $\phi$  of Core E-6, 29-31, 35-37
  - $\phi$  of Core J-1, 29, 32, 35-36
- Computation,  $\phi(F, \phi)$  PROCEDURE, 18-20
  - outline, 20-21
  - $\phi_d$  and  $\phi'_d$ , 19-20
  - $\phi_p$  and  $\phi'_p$ , 20
  - $\phi$  and  $\phi'$ , 20
- Computer program:
  - core-diode shift register, 63-68, 157-163
  - loaded core, 45-46, 149-153
  - unloaded core, 28-29, 143-146
  - $\phi(F, \phi)$  PROCEDURE, 20-21, 133-135
- Constant current source, 99
- Convergence in computation:
  - core-diode shift register, 61-63
  - loaded core, 42, 45-46
  - unloaded core, 28
- Core:
  - cutting of ultrasonically, 82, 83, 114
  - differences between E-6 and I-4, 114
  - dimensions, 83
  - geometry, 82, 85, 114
  - holder, coaxial, 85, 87
  - material, 81, 82-83
  - parameters, 23
    - used in  $\phi(F, \phi)$  PROCEDURE, 17-18
  - thickness effect, 12-15
- Core-diode shift register--see Shift register, core-diode
- Core E-6:
  - dimensions, 23
  - ramp-F switching, 31

# INDEX

- Core E-6--Continued
  - step- $F$  switching:
    - discussion, 33
    - results, 30
    - $\phi(F)$ , 34
  - switching parameters, 23
  - trapezoidal- $F$  switching, 31
  - triangular- $F$  switching, 31
- Core J-1:
  - dimensions, 23
  - switching loaded:
    - experiment, 39-40
    - experimental vs. computed, 46-54
    - ramp drive, 50-51, 53
    - step drive, 48-49, 52
  - switching unloaded:
    - experiment, 22, 24
    - experimental vs. computed, 32
- Crossing:
  - 700  $\mu$ sec  $\phi(F)$  curves, 89, 93, 128
  - $\dot{\phi}_p(F)$  curves, 121, 126, 129
- Crystallites, 129
- Current:
  - drive, 22, 24, 27
  - driver, 85
  - load--see Load current
  - loop, backward, 58-60,
  - loop, forward, 58-62, 70
- Cutting cores ultrasonically, 82-83, 114
- Cyclic demagnetization, 81
- Damping coefficient, 129
- Decaying tail in  $\phi(t)$ , 121
- Decrease in  $\lambda$ , 114-115, 129
- Delay in switching, 97
- Demagnetization:
  - fields, 93
  - partial, 81
- Density of domain nucleation, 129
- Diameter of cores, 83
- Differential equations, numerical solutions of, 25, 41-43
- Dimensions:
  - Core E-6 (thin ring), 23
  - Core I-3 (thin ring), 83
  - Core I-4 (thin ring), 83
  - Core J-1 (commercial toroid), 23
- Diode, forward characteristic of, 41, 57
- Disc, ferrite, 82
- Discharge, capacitor, 54, 87
- Discharging transmission line, 86
- Discrepancies in switching model, 81
- Domain:
  - nucleation, 89, 129
  - walls, 12, 97
    - area, 97
    - motion, 111, 129
    - 360°, 83
- Drive current (or MMF)
  - expression, 27
  - unloaded core, 22, 24
  - waveforms, 22, 24
- Drivers, current, 85-86
- Duration:
  - of pulses, 84
  - TEST pulse, 95
- Easy axes, 129
- Elastic flux change, 121
- Equivalent circuit, core-diode shift register, 58
- Error:
  - bars, 108
  - cancellation for  $\lambda$  and  $F''_0$ , 126
  - correction in integrator, 86-87
  - in  $\dot{\phi}_p(F)$  for small  $T_b$ , 121
- Experiment:
  - core-diode shift register, 68-70
  - loaded core (Core J-1), 39-40
  - set up, 82
  - unloaded core:
    - Core E-6, 30-31
    - Core J-1, 32
- Fall time of PARTIAL-SET pulse, 118
- Ferrite:
  - disc, 82
  - materials, 81-82, 96, 128
- Flux:
  - averaged value of  $F_{ps}$ , 127
  - elastic change, 121
  - limiting of switching, 93
  - measurement, 83, 86, 88, 95, 107, 121
    - circuit, 87
  - peak, 88
  - remanent, 88
- Flux gain, 56, 60, 68, 71, 73-74
- Flux switching:
  - beginning time (step- $F$  and ramp- $F$ ), 26
  - core-diode shift register--see Shift register, core-diode
  - inelastic, 5-9
    - limitations of old  $\eta(\phi)$  model, 5-6
    - modified model, 6-9
  - initial  $\dot{\phi}$  spikes, 6-7, 10-11, 96, 99
    - computation of, 29, 130
    - computed vs. experimental, 30
    - elastic, 10-11
    - inelastic, 11-12
  - loaded core--see Loaded core switching
  - unloaded core--see Unloaded core switching
- Flux transfer in core-diode shift register, 55-56
- Gain, flux--see Flux gain
- Geometry of cores, 82, 83, 85, 114

# INDEX

- Half-amplitude points, 121
- History, effects of, 83
- Holder for core, coaxial, 85, 87
- Impedance of transmission line, 86
- Incomplete clearing, 81, 83
- Indiana General 5209 material, 82-83, 130
- Inductive load:
  - convergence, 42-43
  - effect on switching, 54
  - experiment, 30-40
- Inelastic switching, 5-9
- Information in a core-diode shift register
  - effect on analysis, 74-75
  - transfer, 55-56
- Initial value of:
  - $\phi$ , 95, 99, 104, 127
  - $\dot{\phi}$ , 99, 103
- Initial  $\dot{\phi}$  spike, 6-7, 10-12, 96, 99, 108, 125, 130
  - computation of, 29-30, 33-34
  - elastic, 10-11, 29-30
  - inelastic, 11-12, 29-30
  - parameter values, 29
- Inner diameter of core, 83
  - ratio to outer diameter, 82, 83
- Integration of  $\dot{\phi}$ , 87, 88
- Integrator, second-order, 83, 86, 87
- Interruption of switching, 121
- Jitter in pulses, 86
- Leg element:
  - length, 12
  - static  $\phi(F)$ , 14
  - switching, computations of, 14-15
  - switching parameters, 13-14
- Loaded core switching:
  - analysis, 41
  - computations:
    - basic equations, 41
    - method of, 41-43
    - sequence of, 43-45
  - computed  $\phi(F)$ :
    - ramp drive, 53
    - step drive, 52
  - computed vs. experimental  $\dot{\phi}$  and  $i_L$ :
    - ramp drive, 50-51
    - step drive, 48-49
  - computer program outline, 45-46
  - experiment, 39-40
  - experimental results, 48-51
  - inductive vs. capacitive load, 54
- Load current
  - differentiation with respect to, 43
  - experimental vs. computed, 48-51
- Lockheed 06 material, 82, 88, 130
- Log-log plots of  $\dot{\phi}_p(F)$ , 107, 111, 112
- Loop currents in core-diode shift register--see Shift register, core-diode, loop currents
- Lowering of  $\lambda$ , 114-115, 129
  - see parameter, variation of
- Magnetization, saturation, 129
- Materials, ferrite, 81, 82, 124, 128
  - parameters, 129
  - two distinct, 97
- Material parameters, 15, 23, 129
- Maximum ADVANCE current in core-diode shift register, 56
- Maximum in  $\dot{\phi}(t)$ , 107, 115
- Measurement of flux, 83, 86, 88, 95, 107, 121
  - circuit, 87
  - curves of  $\phi(F)$ , 84, 86, 87-88
  - $\Delta\phi_{ps}$ , 84, 104, 126
- Mechanism of switching, 111, 115
- Mercury relay pulser, 85, 86
- Minimum ADVANCE current in core-diode shift register, 56, 71, 74
- Mode of operation in core-diode shift register:
  - analysis, 59-60
  - computation, 62
  - computer program:
    - Mode 1, 64-65, 160
    - Mode 2, 65-66, 160-161
    - Mode 3, 66-67, 161
- Modifications of parabolic switching model, 8, 81, 93, 94, 127, 130
- Negative:
  - domains, 93, 97, 115
  - $F$  effects, 89
  - remenance, 83,
- Newton's method for solving  $f(x) = 0$ :
  - basic relation, 42
  - core-diode shift register computation, 61-62, 65-67
  - loaded-core computation, 43
  - modified relation, 42
- No-load switching--see Unloaded core switching
- Noncoherent rotation, 111
- Nonconstant MMF, 125-127, 129, 130
  - parameters--see Variation of parameters
- Nonrectangular drive pulses, 81, 130
- Nucleation of domains, 89, 97
- Number of turns in drive windings, 85
- Numerical solution of differential equations:
  - core-diode shift register, 61
  - effect of  $\Delta t/t_s$ , 35-39
  - loaded core switching, 41-43
  - unloaded core switching, 25

# INDEX

## ONE in core-diode shift register:

- dropout, 56
- effect on neighboring stages, 74-75
- stable magnitudes, 71, 73-74
- transfer, 55-56

## Operation of core-diode shift register, 55-57

- Outer diameter of core, 83
- ratio to inner diameter, 82, 83, 111, 114

## Outline for computer programs, 20-21, 28-29, 45-46, 63-68

## Outside to inside (OD/ID) ratio:

- Core E-6, 23
- Core I-3, 83
- Core I-4, 83
- Core J-1, 23
- effect on  $\dot{\phi}$ , 34-35

## Parabolic model for inelastic $\dot{\phi}$ , 5-9, 93-94, 127 for $\phi_c$ , 93-94

### Parameters:

- core--see Core parameters
- initial  $\dot{\phi}$  spikes, 10-12, 29
- material--see Material parameters
- partially set state, 82
- switching--see Switching parameters
- variations of 107, 111, 126, 130
- $F''_0$ , 97, 101, 104, 107, 113-115, 117-118, 120-121, 124-129
- $F_{ps}$ , 102-104, 127
- $T_b$ , 118
- $T_{ps}$ , 99, 107, 108, 111, 113-118
- $\lambda$ , 97, 101, 104, 107, 113-115, 117-118, 120-121, 124-129
- $\nu$ , 107, 113, 115, 117-118, 120, 125-129
- $\phi_c$ , 93-95, 99-107, 108, 125-127
- $\phi_{ps}$ , 82, 93, 102, 104, 118, 121, 124-127, 130

## PARTIAL-SET pulse, 84

## Partially demagnetized state, 81

## Partially set state, 82, 83

## Past history effects, 83

## Peak $\dot{\phi}$ , 5

- computation of in  $\dot{\phi}(F, \phi)$  PROCEDURE, 20

## Peaking time, 95, 101

## Polarity of TEST pulse, 81, 82, 84

## PROCEDURE, 16-17

- $i_A(t)$ , 69, 140
- Max (A,B), 139
- Min (A,B), 139
- Min 3(A,B,C), 140
- $\dot{\phi}(F, \phi)$ :
  - computation steps, 18-20
  - $\phi_d$  and  $\phi'_d$ , 19-20
  - $\phi_p$  and  $\phi'_p$ , 20
  - $\phi$  and  $\phi'$ , 20
  - core parameters, 17-18
  - input-output, 16-17
  - outline, 20-21

## Program, computer--see Computer program

## Pulse:

- duration, 86
- sequence, 83-84

## Pulsers, 85-86

## Radial variations of $H$ , 82

## Radius of cores, 83

## Ramp drive, loaded core, 50-51

## Ramp- $F$ , unloaded core:

- computed vs. experimental:
  - Core E-6, 31, 36
  - Core J-1, 32, 36
- switching parameters, 35-36
- switching time, approximate, 26

## Random switching, 89, 97-98

## Range of ADVANCE current in core-diode shift register, 56-57, 71, 74

## Ratio:

- outer-to-inner radius of cores, 82, 83, 111, 114
- surface-to-volume of cores, 82, 114
- $\dot{\phi}_0$  to  $\dot{\phi}_p$ , 99

## Receiver in core-diode shift register:

- basic switching equation, 59
- computed flux switching, 70, 72
- receiving information, 55-56

## Re-entrant $\phi(F)$ curve, Core I-3, 97-98

## Reference, voltage, 86, 87

## Reflections in transmission line, 121

## Regions in $\dot{\phi}(F)$ , 111, 114, 124

- coalescence, 118, 124

## Relaxation time of $\dot{\phi}(t)$ , 99, 102, 121

## Rise time of pulses, 85, 86

- TEST pulse, 104, 118

## Rotation, noncoherent, 111

## Saturation magnetization, 129

## Sech<sup>2</sup> function for $\dot{\phi}(t)$ , 82, 97, 99, 106

- graticule of camera, 95
- parabolic model of, 93-96, -126, 127, 129

## Second-order integrator, 86, 87

## Sequence of computation:

- core-diode shift register, 64-68
- loaded core switching, 43-45
- unloaded core switching, 27-28
- $\dot{\phi}(F, \phi)$  PROCEDURE, 18-20

## Sequence of pulses, 83, 84

## Sense winding, 85

## Shape of $\dot{\phi}(t)$ , 93, 96-97

## Shift register, core-diode:

- analysis of, 57-60
- assumptions, 57-58
- basic equations, 58-59
- equivalent circuit, 58
- information pattern, effect of, 74-75

# INDEX

- Shift register, core-diode--*continued* -
  - modes of operation, 59-60
  - slow switching assumption, 58-59
  - computation:
    - back flux transfer, 67-68
    - conditions, 62
    - convergence, 62
    - flux gain, 68
    - method of, 60-63
    - mode switching, 62
    - Newton's method, 62
    - steps, 64-68
  - computed and experimental time variables, 68-70
  - computed results:
    - back  $\Delta\phi$  transfer, 71, 74
    - flux-gain curves, 71, 73
    - range of ADVANCE current, 71-74
    - stable ONES and ZEROS, 71, 73-74
    - $\phi(F)$  of transmitter and receiver, 71-72
  - computer program, outline, 63-68
  - back flux transfer, 67-68
  - flux gain, 68
  - mode switching, 64
  - Mode 1, 64-65
  - Mode 2, 65-66
  - Mode 3, 66-67
  - switching time, approximate, 63
  - time element, 64
  - flux gain, 56, 60
  - information pattern, effect of, 74-75
  - loop currents, 58-59, 70
  - maximum ADVANCE current, 56, 57
  - minimum ADVANCE current, 56, 71, 74
  - ONE dropout, 56
  - operation, 55-57
  - range of ADVANCE current, 56-57
  - rise time of ADVANCE current, effect of, 57
  - transfer of information, 55-56
  - ZERO buildup, 56, 57
- Slope of  $\dot{\phi}_p(F)$  curves, 108, 115
- Speed of switching, 107, 124
- S-shape  $\phi(F)$ , 47, 52-53
- Static  $\phi(F)$  curve, 7-8, 87, 89
  - computation of, 19-20
  - of leg element, 14
- Static  $-\phi(F)$ -limited parabolic model, 6-9
- Statistical variation of  $\cos \theta$ , 129
- Step- $F$ :
  - during switching, 125-127
  - experiment, 6-7, 22-24
  - experimental vs. computed:
    - Core E-6, 30, 33
    - Core J-1, 32
- Step drive loaded core, 39-40, 48-49
- Surface of core, 114
- Surface-to-volume ratio, 82, 111, 114
- Switching flux--see Flux switching
- Switching models, further improvements, 77-78, 81, 93
  - physical, 129
- Switching parameters:
  - Core E-6, 23
  - Core J-1, 23
  - effect of decaying  $F$  on, 54
  - effect of ramp- $F$  on, 35-36
  - inelastic, 5
  - initial, 10-12
  - elastic, 10
  - inelastic, 11-12
  - leg element, 13-14
- Switching speed, 107, 118, 124
- Switching time, 107, 118
- Switching time, approximate:
  - core-diode shift register, 63
  - unloaded core:
    - ramp  $F$ , 26
    - step  $F$ , 26
- Synchronization of pulses, 86
- Tail in  $\dot{\phi}(t)$ , 121.
- Tapered leg, 81
- Telemeter T-5 material, 23, 82, 87, 130
- Temperature:
  - control of, 87
  - experiment, 23, 87
- Termination:
  - switching, of, 93, 128
  - transmission line of, 85
- TEST pulse, 82-84
- Thermistor, 87
- Thick core (or leg):
  - division into leg elements, 12-13
  - computation of  $\dot{\phi}$ , 12-15
- Thin-ring cores, 107
- Threshold MMF, lowering and rounding of, 89
- Time element  $\Delta t$  in numerical solution, 26
  - core-diode shift register, 60-61
  - effect of, 35-39
- Toroidal geometry, 82
- Transfer of information in a core-diode shift register, 55-56
- Transition between regions in  $\dot{\phi}_p(F)$ , 111, 112, 128
- Transmission line, 85, 86
- Transmitter in core-diode shift register:
  - basic equations, 59
  - computed flux switching, 70, 72
  - flux state transfer, 55-56
  - flux switching effect:
    - back  $\Delta\phi$  transfer, 74
    - flux gain, 73
  - reference, change of, 58
- Turns in winding, number of, 85
- Ultrasonic cutting, 82, 83, 114
- Uniform  $H$  field, 85
- Unloaded core switching:
  - computation:
    - method of, 25
    - sequence of, 27-28
    - switching start, 26
  - computed  $\phi(F)$ :
    - ramp  $F$ , 37
    - step  $F$ , 34

## INDEX

### Unloaded core switching--*continued*

- computed *vs.* experimental  $\dot{\phi}$ 
  - Core E-6, 30-31, 36
  - Core J-1, 32, 36
- computer program outline, 28-29
- drive, 24
- effect of  $OD/ID$ , 34-35
- effect of  $\Delta t$ , 35-39
- experiment, 22, 24
- ramp- $F$  switching parameters, 35-37

### Variation in:

- domain wall velocity, 129
- $F$ , --*see* Constant MMF
- parameters--*see* Parameters, variation of
- $t_p$ , 95, 101
- $\eta_0$ , 99

Velocity of domain walls, 129

Vertical section in  $\phi(F)$ , 99

Voltage reference, 86, 87

Waveform, drive MMF, 22, 24

Waveforms of  $\phi(t)$ , 93-106

Windings, 40, 68, 85

### ZERO in core-diode shift register:

- back transfer, 71, 74
- buildup to ONE, 56
  - means against, 57
- stable magnitudes, 71, 73-74